

**PROJECT TRIDENT  
TECHNICAL REPORT**

# **ACOUSTIC SCATTERING IN THE OCEAN**

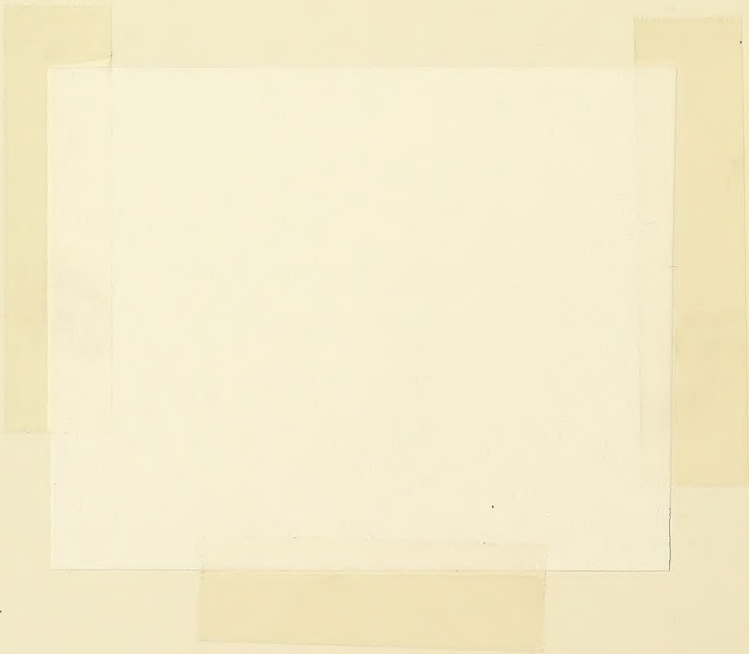
**ARTHUR D. LITTLE, INC.**

35 ACORN PARK CAMBRIDGE, MASSACHUSETTS

**DEPARTMENT OF THE NAVY  
BUREAU OF SHIPS**

**N0bsr-81564 S-7001-0307**

**AUGUST 1963**



MBL/WHOI



0 0301 0036076 4

PROJECT TRIDENT  
TECHNICAL REPORT

**ACOUSTIC SCATTERING  
IN THE OCEAN**

BY  
R. F. MEYER  
B. W. ROMBERG

ARTHUR D. LITTLE, INC.

35 ACORN PARK CAMBRIDGE, MASSACHUSETTS

DEPARTMENT OF THE NAVY  
BUREAU OF SHIPS

N0bsr-81564 S-7001-0307

AUGUST 1963





PREFACE

This report was prepared by Arthur D. Little, Inc., as part of its effort on Project TRIDENT, under Contract NObsr-81564 with the Bureau of Ships, Department of the Navy.



# TABLE OF CONTENTS

	<u>Page</u>
List of Figures	vii
List of Tables	xiii
FOREWORD	xv
I. INTRODUCTION	I-1
A. PURPOSE AND SCOPE	I-1
B. APPROACH	I-1
C. GENERAL CONCLUSIONS	I-2
II. SUMMARY	II-1
A. BASIC PRINCIPLES	II-1
B. SCATTERING BY STRONG INHOMOGENEITIES	II-4
C. SCATTERING BY WEAK INHOMOGENEITIES	II-7
III. STRONG INHOMOGENEITIES	III-1
A. SCATTERING OF SOUND FROM A FLUID SPHERE	III-1
B. SCATTERING FROM AIR BUBBLES	III-14
C. SCATTERING BY MARINE ORGANISMS	III-62
D. SCATTERING FROM THE SEA SURFACE	III-68
IV. WEAK INHOMOGENEITIES	IV-1
A. THE WAVE EQUATION FOR AN INHOMOGENEOUS MEDIUM	IV-1
B. SCATTERING FROM AN ISOLATED INHOMOGENEITY	IV-10

TABLE OF CONTENTS (Continued)

	<u>Page</u>
IV. WEAK INHOMOGENEITIES (Continued)	
C. THE WEAK INHOMOGENEITIES OF THE OCEAN	IV-17
D. SIGNAL FLUCTUATION AND CORRELATION RESULTING FROM THE OCEAN MICRO- STRUCTURE	IV-35
APPENDIX A - SOME SOLUTIONS OF THE WAVE EQUATION	A-1
APPENDIX B - THE MULTIPLE SCATTERING OF WAVES	B-1
APPENDIX C - NOTATION	C-1
BIBLIOGRAPHY	R-1
PROJECT TRIDENT TECHNICAL REPORTS	1
DISTRIBUTION LIST	1



# LIST OF FIGURES

<u>Figure No.</u>		<u>Page</u>
II-1	Scattering of a Plane Wave by a Sinusoidal Surface	II-6
II-2	Scattering by the Ocean Micro-Structure	II-10
II-3	Low Frequency Scattering Model	II-15
II-4	High Frequency Scattering Model for the Interference Range	II-15
II-5	High Frequency Scattering Model for the Focusing Range	II-15
II-6	Coefficient of Variation as a Function of Range	II-16
II-7	Fluctuation Measurements Made by ORL	II-16
III-1	Rayleigh Scattering from Small Fluid Spheres in the Backward Direction (After Anderson)	III-10
III-2	The Reflectivity $R$ as a Function of the Relative Sound Velocity $h$ and Acoustic Radius $Ka$ (After Anderson)	III-11
III-3	The Reflectivity $R$ as a Function of the Relative Density $g$ and the Acoustic Radius $Ka$ (After Anderson)	III-11
III-4	The Reflectivity $R$ as a Function of the Acoustic Radius $Ka$ (After Anderson)	III-12
III-5	Scattering Power as a Function of the Acoustic Radius $Ka$ (After Anderson)	III-13
III-6	Directivity of Scattering for $Ka \sim 1$ (After Anderson)	III-13
III-7	Air Bubble Resonant Frequency as a Function of Bubble Radius	III-22
III-8	Damping Constant for Four Typical Bubble Sizes as a Function of Frequency	III-24

LIST OF FIGURES (Continued)

<u>Figure No.</u>		<u>Page</u>
III-9	Theoretical and Experimental Values of the Damping Constant at Resonance	III-26
III-10	$\Delta = \left( \frac{f_o^2}{f^2} - 1 \right)^2 / \delta^2$ as a Function of Incident Frequency for Four Typical Bubble Sizes	III-27
III-11	Ratio of Scattering Cross Sections to Geometric Cross Sections	III-31
III-12	Ratio of Extinction Cross Sections to Geometric Cross Sections	III-32
III-13	Attenuation and Phase Velocity in Screens With Uniform Bubble Sizes (After Meyer and Skudrzyk)	III-41
III-14	Theoretical Attenuation Through a Bubble Screen With a Distribution of Bubble Sizes (After Meyer and Skudrzyk)	III-42
III-15	Observed Attenuation Through Bubble Screens With a Distribution of Bubble Sizes (After Meyer and Skudrzyk)	III-43
III-16	Statistical Characteristics of Bubble Sizes in Continuous Flow and Pulsed Screens (After Carstensen and Foldy)	III-46
III-17	Attenuation and Reflection From Pulsed and Continuous Flow Bubble Screens (After Carstensen and Foldy)	III-47
III-18	Transmission Measurements Through Continuous Flow Screens (After Laird and Kendig)	III-48
III-19	Theoretical and Observed Attenuations (After Laird and Kendig)	III-49
III-20	Distribution of the Number of Bubbles and Fractional Volume as a Function of Bubble Radius (After Laird and Kendig)	III-49

LIST OF FIGURES (Continued)

<u>Figure No.</u>		<u>Page</u>
III-21	Theoretical Phase Velocity (After Laird and Kendig)	III-51
III-22	Distribution of Fractional Volume for Various Bubble Sizes (After Fox, Curley and Larson)	III-51
III-23	Phase Velocity and Attenuation Through a Screen Having the Bubble Distribution of Figure III-22 (After Fox, Curley and Larson)	III-52
III-24	Attenuation and Phase Shift Through Single and Double Lattice Screens at Normal Incidence	III-54
III-25	Reflection of Normally Incident Sound From a Single Lattice Screen (After MacPherson)	III-57
III-26	Phase Velocity in Air-Water Mixtures (After Silberman)	III-57
III-27	Phase Velocity and Attenuation as Functions of Frequency at Various Concentrations and Bubble Sizes	III-58
III-28	Variation of Volume Scattering Cross Sections (After Hersey and Backus)	III-68
III-29	Schematic Diagram of a Plane Wave Incident on a Corrugated Surface	III-72
III-30	Theoretical and Experimental Scattering Directions (After Leporskii)	III-93
III-31	Experimental and Theoretical Magnitudes of $A_0$ for Surface A	III-94
III-32	Experimental and Theoretical Magnitudes of $A_0$ for Surface B	III-95
III-33	Experimental and Theoretical Magnitudes of $A_0$ for Surface A	III-96
III-34	Experimental and Theoretical Magnitudes of $A_0$ for Surface B	III-97

LIST OF FIGURES (Continued)

<u>Figure No.</u>		<u>Page</u>
III-35	Experimental and Theoretical Magnitudes of $A_{-1}$ for Surface A	III-98
III-36	Experimental and Theoretical Magnitudes of $A_{-1}$ for Surface B	III-99
III-37	Experimental and Theoretical Magnitudes of $A_{-1}$ for Surface A	III-100
III-38	Experimental and Theoretical Magnitudes of $A_{-1}$ for Surface B	III-101
III-39	Comparison of Theoretical (Brekhovskikh) and Experimental Scattering Patterns (After Leporskii)	III-102
III-40	Comparison of Theoretical and Experimental Scattering Magnitudes for the Lysanov Theory (After Leporskii)	III-103
III-41	Theoretical and Experimental Scattering Patterns for the Lysanov Model (After Leporskii)	III-103
III-42	Ratio of I at $\gamma \neq 0$ to I at $\gamma = 0$	III-116
III-43	Sketch of Limiting Sound Ray Bending	III-118
III-44	Sea Surface Scattering Loss in Specular Direction for Emitting Ray in Isothermal Layer	III-122
IV-1	The Geometry of Scattering	IV-4
IV-2	Scattering Coordinates	IV-11
IV-3	Directivity Pattern as a Function of $\Gamma a$ (After Skudrzyk)	IV-16
IV-4	Computed Daily Variations of the Mean Temperature of the Sea (After Skudrzyk)	IV-18
IV-5	Microthermal Variations at Various Depths (After Urlick and Searfoss)	IV-19



LIST OF FIGURES (Continued)

<u>Figure No.</u>		<u>Page</u>
IV-6	Patch Diameter vs Depth (After Skudrzyk)	IV-20
IV-7	Probability Distribution of Two-Point Temperature Difference	IV-21
IV-8	Temperature Fluctuations and Associated Correlation Function (After Liebermann)	IV-23
IV-9	Schematic Representation of Physically Realistic Spectrum (Log-Log Scale)	IV-30
IV-10	Horizontal Temperature Structure Functions as Measured in the Sea	IV-32
IV-11	Comparison of Experimental Correlation Functions With a Correlation Function Corresponding to a Kolmogoroff Spectrum	IV-34
IV-12	Coefficient of Variation as a Function of Range	IV-40
IV-13	Geometry for High Frequency Scattering	IV-44
IV-14	The Transverse Autocorrelation for the Case of Small $D$ ( $D \ll 1$ ): 1. The autocorrelation coefficient of the amplitude fluctuations; 2. The autocorrelation coefficient of the phase fluctuations, identical with the autocorrelation coefficient of the refractive index fluctuations (After Chernov)	IV-47
IV-15	The Transverse Autocorrelation for the Case of Large $D$ ( $D = 10$ ): 1. The autocorrelation coefficient of the amplitude fluctuations; 2. The autocorrelation coefficient of the refractive index fluctuations; 3. The autocorrelation of the phase fluctuations. (After Chernov)	IV-48
IV-16	Correlation Coefficient as a Function of the Distance Between the Hydrophones	IV-49



LIST OF TABLES

<u>Table No.</u>		<u>Page</u>
III-1	Three Models of Air Bubble Scattering	III-20
III-2	Scattering and Extinction Cross Sections of Air Bubbles	III-30
III-3	Reflection Coefficients $A_n$ for the Surface $S(x) = 0.15 \cos 3.08x$ and Incident Angle $\theta$	III-80
III-4	Comparison of Numerical and Analytical Integration of I at $\gamma = 0$	III-115
IV-1	Scattering Strengths and Directivity Patterns of Spherically Symmetric Scatterers	IV-15
IV-2	Ocean Micro-Structure Correlation Functions and Associated Spectra	IV-33
IV-3	Theoretical Scattering for Two Types of Correlation Function	IV-38
IV-4	Theoretical Amplitude and Phase Fluctuations	IV-45





## FOREWORD

The work on acoustic scattering from the small inhomogeneities of the ocean suffers from a lack of cohesion. There are many diverse and apparently unrelated papers and experimental results which are nowhere treated from a common point of view or even in a consistent notation.

As a result, this survey of the field has become a compromise between a compendium of miscellaneous material, a critique of the current state of knowledge, and a textbook. We have tried to incorporate the more mathematical material in the body of the report, since much of the progress in this field has been essentially mathematical. If the reader is primarily interested in obtaining a physical understanding of the subject, however, he should feel free to skim the mathematical detail unabashedly. We hope that the text contains sufficient continuity without the mathematics.

The authors wish to acknowledge here the very helpful survey by E. Skudrzyk covering the scattering by weak inhomogeneities. This is one substantial portion of the subject matter which we found to be well summarized.



## I. INTRODUCTION

### A. PURPOSE AND SCOPE

The purpose of this report is to survey our current understanding of the effect of small random inhomogeneities on the propagation of acoustic waves in the ocean. The inhomogeneities of interest to us are small in comparison to the over-all dimensions of the medium: small compared to the ocean depth or the depth of the principal ocean layers and small compared to the length of the path of propagation. In particular, we have in mind such inhomogeneities as air bubbles, marine organisms, surface roughness (as opposed to large-scale inhomogeneities such as sea mounts) and the innumerable local fluctuations of temperature, density and salinity which are commonly referred to as the ocean micro-structure. In practice we invariably encounter very large numbers of inhomogeneities, located at random throughout the medium. Furthermore, some of the inhomogeneities are of an indistinct or irregular shape. This is particularly true of the patchy thermal structure and the irregular surface and bottom.

The small inhomogeneities of the ocean affect a propagating sound wave in a number of ways. To the extent that the inhomogeneities cause back-scattering of the sound, they have the effect of attenuating the propagating wave in the forward direction. Furthermore, the back-scattering causes the sound to reverberate so that a pulse emitted over a short period of time is received during a much extended interval. Finally, the slow variation in the propagation constants of the medium causes the modulation of the phase and amplitude of the propagating signal, which results on the one hand in fading, and on the other in the incoherence of the signal as received by two different observers. The scope of this report is, therefore, to outline the theoretical models which have been developed to account for the above phenomena, and to compare the predictions of the theory with the often scanty experimental data.

We hope that the report may serve as a self-contained introduction to the acoustic effects of small random inhomogeneities for those connected with underwater sound propagation but not specialized in this particular field. At the same time, we intend the report to pinpoint some of the strengths and deficiencies in the present state of knowledge and to suggest topics in this general area deserving of further research.

### B. APPROACH

We distinguish in our approach between strong and weak inhomogeneities. A strong inhomogeneity corresponds to a radical change of the propagating characteristics of the medium, e.g., an air bubble, a fish, or the transition from

water to air at the surface. A weak inhomogeneity, on the other hand, corresponds to a slight change of the propagation characteristics of the medium, and is typified by the small but ubiquitous fluctuations of temperature, salinity, density and velocity.

All the theoretical methods employed to attack wave propagation in an inhomogeneous medium must take recourse to a number of mathematical and physical approximations in order to handle an otherwise too formidable problem. Thus, the analysis is generally confined to one type of inhomogeneity at a time, and ignores any interaction between different kinds of inhomogeneities. In the case of strong inhomogeneities, the approximation is usually to regularize the geometry of the individual scatterers. For example, air bubbles and marine organisms are taken to be spherical in shape, and ocean surface waves might even be regarded as sinusoidal. For weak inhomogeneities, on the other hand, a convenient approximation scheme is furnished by the fact that the changes in the relative propagation characteristics are very small compared to unity, so that the magnitude of these relative changes can be used as a small parameter in a perturbation theory.

It is therefore natural to divide the subject matter of this report into two parts: strong inhomogeneities; and weak inhomogeneities. The notation used is summarized in Appendix C.

### C. GENERAL CONCLUSIONS

The inhomogeneities of the ocean affect a passing sound wave in a manner which can be qualitatively understood by the theory outlined in this report. Quantitative predictions are still somewhat less accurate than we would expect possible when our present understanding of the scattering mechanisms is incorporated fully in the scattering calculations.

The theoretical investigations to date have attempted to cope with the formidable mathematical problems encountered by making numerous analytical approximations. We believe that the time is ripe to place much greater emphasis on numerical computation based directly on our physical understanding of the scattering process without the many rough analytical approximations required for a completely theoretical development. Especially in the areas of scattering by the surface (Section IIID) and by the micro-structure of the index of refraction (Chapter IV) we would expect that an imaginative program of numerical calculation would be able to improve considerably our current ability to predict sound scattering in the ocean.

We recommend, therefore, that some study be devoted to the design of efficient numerical procedures for carrying out these calculations, having as its ultimate objective a computer program capable of tracing the long-distance propagation of a sound wave subject to surface and volume scattering.



## II. SUMMARY

### A. BASIC PRINCIPLES

There are a few basic notions of wave propagation (such as incident and scattered wave, single and multiple scattering) which pervade this report. We wish to outline these ideas briefly before summarizing the separate chapters on strong and weak inhomogeneities.

Throughout the report we are concerned with fields of pressure ( $p$ ) or of velocity potential ( $\varphi$ ) caused by the insonification of an inhomogeneous medium. The mental picture with which we approach the analysis is invariably the following:

1. Instead of insonifying the inhomogeneous medium, we insonify a corresponding homogeneous medium by placing in it a source of acoustic energy. The resulting field is generally referred to as the incident or exciting field ( $p_{inc}$ ,  $\varphi_{inc}$ ).

2. The insonification of an inhomogeneous medium by a corresponding source will cause a different total field ( $p$ ,  $\varphi$ ). The difference between the two fields is called the scattered field:

$$p = p_{inc} + p_{sc}, \quad \varphi = \varphi_{inc} + \varphi_{sc}$$

The next step in the analysis is usually to consider a single isolated inhomogeneity in a perfect medium subjected to the exciting field  $\varphi_{inc}$ . The scattered field resulting from the inhomogeneity can generally be thought of as caused by the surface or the volume (or both) of the scatterer acting as a secondary source. In other words, the local values of the total field ( $p$  or  $\varphi$ ) at the surface or throughout the scatterer cause the scatterer to emit its scattered wave.

The scattered wave is therefore a functional of the total field:

$$\varphi_{sc} = L \{ \varphi \}$$

In most of the cases which concern us, the functional  $L$  is linear in the sense that a linear combination of two fields corresponds to the same linear combination of the two individually scattered fields. The precise description of the

functional results from a detailed model of the scatterer.\* The total field must therefore satisfy the functional equation:

$$\varphi = \varphi_{\text{inc}} + L \left\{ \varphi \right\} \quad (\text{II-1})$$

It is usually not possible to find the exact solution to this equation, i.e., to obtain that field  $\varphi$  which results when a given exciting field  $\varphi_{\text{inc}}$  is scattered by a known inhomogeneity characterized by  $L$ . Instead, a sequence of approximate solutions is obtained by a simple iterative scheme. If the effect of inhomogeneities were negligible, it would be adequate to take  $\varphi_{\text{inc}}$  as the total field. Suppose therefore that we choose  $\varphi^{(0)} = \varphi_{\text{inc}}$  as the initial approximation. We may then hopefully improve this approximation by substituting in (I-1) and obtain a first order approximation

$$\varphi^{(1)} = \varphi_{\text{inc}} + L \left\{ \varphi_{\text{inc}} \right\}$$

We may repeat this procedure any number of times, obtaining, in general, a  $k^{\text{th}}$  order approximation which is:

$$\varphi^{(k)} = (1 + L + L^2 + \dots + L^k) \left\{ \varphi_{\text{inc}} \right\}$$

The meaning of the different terms in this expression is the following. The first order correction to the initial approximation (choosing the exciting field as the total field) is the direct effect of every portion of the scatterer in scattering the incident field. However, this first order scattered wave gets scattered repeatedly, thus causing successively higher orders of scattering. In all cases with which we are concerned, the first order scattering approximation is an adequate description of scattering from a single inhomogeneity, since we are only interested in the far field.

---

\*It might appear more natural to regard the scattered field as a functional of the incident field rather than of the total field, e.g.,  $\varphi_{\text{sc}} = T \left\{ \varphi_{\text{inc}} \right\}$ . In practice, however, one usually finds the functional  $L$  more readily than the functional  $T$ . Furthermore, knowledge of  $T$  would not permit as easy a formulation of the problem of simultaneous scattering from many scatterers as is obtained above by the use of the functional  $L$ .

Consider now an ensemble of very many scatterers--distinct scatterers such as air bubbles or indistinct scatterers such as thermal patches. Suppose that the  $i^{\text{th}}$  scatterer is characterized by a scattering functional  $L_i$ . This scattering functional describes how the scattered field due to the  $i^{\text{th}}$  scatterer may be derived from the total field in the vicinity of the  $i^{\text{th}}$  scatterer. A field  $\varphi_{\text{inc}}$  incident on this ensemble of scatterers causes a total field  $\varphi$  which has a scattered component consisting of the sum of the individual scattered fields:

$$\varphi_{\text{sc}} = \sum_i L_i \{ \varphi \}$$

The total field, therefore, satisfies the functional equation

$$\varphi = \varphi_{\text{inc}} + \left( \sum_i L_i \right) \{ \varphi \} \quad (\text{II-2})$$

Suppose we proceeded to solve this equation by the same successive approximation scheme introduced for the single scatterer. Choosing the incident field again as the zeroth order approximation, we obtain a first approximation of the total field

$$\varphi^{(1)} = \varphi_{\text{inc}} + \left( \sum_i L_i \right) \{ \varphi_{\text{inc}} \}$$

The first order correction term is therefore just the sum of the first order scattered fields from the individual scatterers. This approximation is called, for self-evident reasons, the single scattering approximation. If we proceed to the second order approximation, we find a second order correction term whose physical meaning is that of the sum of all ways of scattering the incident field twice:

$$\varphi^{(2)} = \varphi_{\text{inc}} + \left( \sum_i L_i \right) \{ \varphi \}_{\text{inc}} + \left( \sum_{i,j} L_i L_j \right) \{ \varphi_{\text{inc}} \}$$

In other words, in addition to the direct scattering from each individual scatterer, the second order approximation also takes into account scattering from all pairs of scatterers. The next higher approximation would contain an additional term from all triplets of scatterers, etc. Usually the single scattering approximation suffices. Sometimes we can demonstrate the precise conditions under which the

second or higher order scattering terms become negligible. Since single scattering is invariably adequate for the far field of any one of the small inhomogeneities of interest to us, the question as to whether single scattering suffices for a collection of scatterers depends primarily on the number of scatterers involved. For very large scattering volumes, it may occasionally prove necessary to include multiple scattering effects.

## B. SCATTERING BY STRONG INHOMOGENEITIES

Chapter III covers the scattering from air bubbles, marine organisms and the ocean surface. The chapter commences with a study of the scattering from a fluid sphere (different from water) immersed in an infinite ocean. The purpose of this investigation is to give a feeling for the dependence of the scattering properties of an object on the parameters of the scattering object. It is found that the most important parameters are the relative size of the object and its relative compressibility. More precisely, the qualitative features of the scattering are determined by the size of the scatterer relative to the wavelength of the sound and by the compressibility of the scatterer relative to that of the surrounding water. We find that for scatterers small compared to a wavelength the scattering consists basically of isotropic and dipole radiation. If the scattering fluid is very compressible (e.g., a gas), the small fluid sphere pulsates predominantly with a breathing motion which gives rise to isotropic radiation. If, on the other hand, the sphere is very hard compared to the water, the principal motion of the sphere is that of rigid body oscillation (a sloshing motion) which causes the scattered radiation field to correspond to a dipole field.

When the scattering fluid sphere is no longer small compared to a wavelength the scattering becomes highly directional. No simple analytical results describe the scattered field, and we must be content to examine some numerical results. In general, however, the scattering from a medium or large object (always comparing the size of the object to the wavelength of the incident sound) becomes very much dependent on the shape of the object, and the idealization of the object as a sphere is no longer appropriate.

Next, in Section III-B we delve into a more detailed treatment of scattering from air bubbles. Since air bubbles are very compressible, the scattering from a single air bubble is essentially isotropic. We may liken the pulsating motion of the air bubble to the oscillation of a mass on a spring. Hence, we would expect a resonant behavior to occur when the inertial and compressibility effects are matched. This is indeed what happens, and the resonant frequency of air bubbles can easily be predicted.

Not only does the air bubble remove energy from the incident wave to produce the isotropic scattered wave, but it also dissipates a certain amount of energy due to viscosity, heat conduction, and surface tension. All this energy is removed from the incident wave, and we can make theoretical estimates of the resulting extinction cross section for a single bubble.

Numerous experiments have been conducted to compare the resonant and dissipative behavior of single bubbles with the theoretical predictions. The theoretical frequencies have been found to check exceedingly well with experimental results. The dissipative properties of single air bubbles check less well with the theory, and there is substantial difference between the results obtained in different experiments. Nonetheless, on the average, the theory seems to predict the experimental results.

In most portions of the ocean, air bubbles (including the gas swim bladders of fish, which behave like air bubbles) are sufficiently widely spaced that the single scattering approximation is adequate. However, regions with a higher concentration of air bubbles do occur (for example, in fresh wakes) and require a treatment incorporating the effect of multiple scattering. These bubble-water mixtures exhibit a cooperative behavior which makes them act macroscopically as a homogeneous medium with a sound velocity different from that of pure water and with substantial attenuation of the sound intensity. The theory of these bubbly mixtures is presented, and compared with the available experimental data. A substantial number of experiments have been performed, but all under controlled laboratory conditions rather than in the ocean. In view of the experimental difficulties encountered in producing bubble screens of uniform properties, the agreement between theory and experiment is quite good.

Section III-C treats scattering from marine organisms; these are idealized either as a sphere of a different fluid or else as a sphere of different fluid contained in an elastic shell (e.g., crustaceans). Obviously, the spherical model does some violence to reality, but one might hope that the model would suffice to explain the main features of scattering from a collection of organisms all of somewhat different shapes. Unfortunately, the experimental evidence from marine organisms is inadequate to draw conclusions about the theoretical calculations.

One interesting aspect of the ocean which might be explainable in terms of the behavior of marine organisms is the so-called deep scattering layer. It appears that the properties of this layer, which change with time of day, can be attributed to scattering from fish with gas bladders. The plausibility of different hypotheses regarding the contraction and expansion of these swim bladders as the fish change depth are discussed in the light of the resonant frequencies that would result.



Scattering from the surface of the ocean poses a very different problem. The spectrum of the ocean surface covers a large range of wavelengths. Ordinary ocean waves range in order of magnitude between wavelengths of one meter to those of 100 meters. Small ripples may be of the order of one centimeter, and tidal waves may be as long as 1000 kilometers. The ocean surface is a stochastic function, varying both in space and in time. A realistic description of this surface involves the space-time spectrum, and the interaction between the spatial and temporal components cannot be ignored. As is well known, surface waves of different lengths propagate at different speeds.

To obtain an understanding of scattering from this surface, one usually studies a very much simplified model. In fact, the most widely used idealization is the reflection of a plane wave from a stationary sinusoidal surface, a problem first posed by Lord Rayleigh. Figure II-1 shows a plane wave propagating towards the sinusoidal surface.

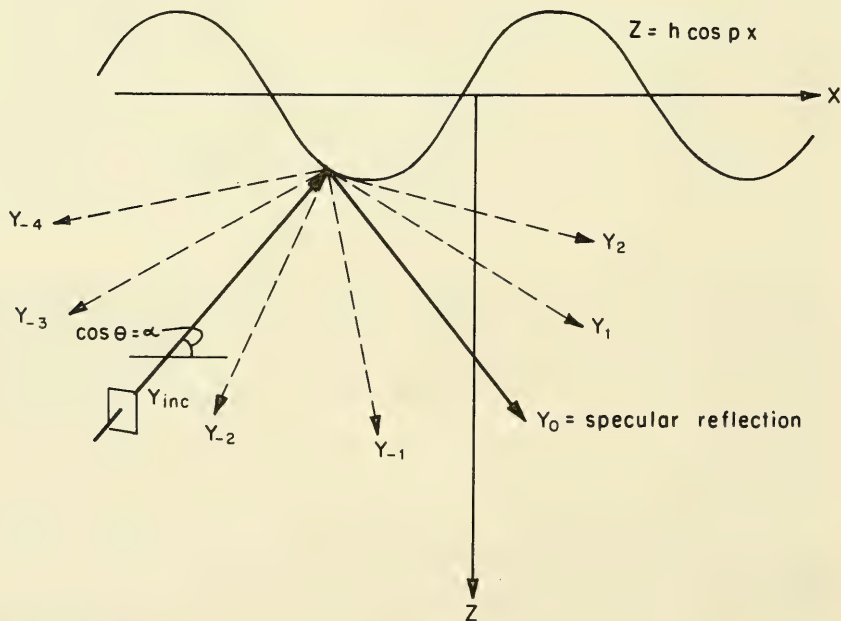


FIGURE II-1 SCATTERING OF A PLANE WAVE BY A SINUSOIDAL SURFACE

$$z = h \cos px$$

and inclined to this surface at an angle  $\theta$  whose cosine is equal to  $\alpha$ . It can be proven that the scattered wave will consist of the so-called specular reflection term whose angle of inclination has a  $\cos \theta = -\alpha$ , plus successively higher orders of scattering. The successively higher orders of scattering are inclined to the surface at an angle  $\cos \theta = -\alpha \pm \frac{mp}{k}$ , where  $k$  is the wave number of the incoming wave and  $m$  runs through the positive integers (1, 2, ...). If the surface were completely flat ( $p = 0$ ), the entire scattered wave would consist of the specular reflection alone. Several approximation methods have been devised to obtain the amplitude of the higher order components of scattering, but all appear to be limited to ranges of surface height and surface wavelength much smaller than the incident wavelength. Most cases of interest in the ocean are not in this category, and the theory therefore gives, at best, a qualitative explanation. It turns out that the higher order scattered terms are important for incident waves near normal incidence. If the incident wave makes a small angle with the horizontal, i.e., for grazing angles  $\theta \ll 1$ , the specular term dominates. This general conclusion appears to apply also under actual ocean conditions.

If the movement of the surface wave is taken into account, the signal received will no longer be a reflected version of the incident wave, but will become phase-modulated since the path length to the receiver is changing in time.

Some recent work by Marsh examines scattering from the surface based on a more realistic spatial spectrum of the surface. His work, and some extensions of it are reported here. This treatment, too, is limited by the condition that the height of the surface wave must not be too large compared to the wavelength of the incident sound. Nonetheless, for fairly low sea states and low frequency sound, the theory permits the calculation of the attenuation due to surface reflection. The scanty data available from ocean experiments seems to confirm the theoretical predictions. It should be pointed out that this is an important area in which good experimental results under ocean conditions are very sorely lacking. Scattering from the bottom is not treated in this report.

### C. SCATTERING BY WEAK INHOMOGENEITIES

Chapter IV treats scattering by the weak inhomogeneities which result principally through the turbulent breaking up of the layered structure of the ocean. As a consequence of the turbulence, the sound velocity, density, etc., of the ocean medium fluctuates in space and in time. Of these, the fluctuations in sound velocity are the most important, so that the main aspects of the propagation of sound are still governed by the wave equation

$$\nabla^2 \varphi = \frac{1}{c^2} \frac{\partial^2 \varphi}{\partial t^2}$$



However, the velocity of sound  $c$  is now a space - time dependent quantity which differs slightly from its average value  $c_0$

$$\frac{c_0}{c} = (1 + \nu(\underline{x}, t))$$

Here  $\nu$  is the fluctuating part of the index of refraction,  $c_0/c$ , and is much less than unity. The usual approximation scheme for weak inhomogeneities is to regard  $\nu$  as very small, and to ignore all effects which are quadratic or higher order in  $\nu$ .

The time fluctuations of the index of refraction are very slow compared to the passage time of sound waves. From the point of view of propagating sound waves, therefore, the medium has a spatial structure which is stationary. In the course of time this micro-structure changes slowly, causing corresponding slow changes in the amplitude and phase of the transmitted sound. In a theoretical analysis, therefore, we may confine ourselves to the problem of sound propagation through a stationary medium whose micro-structure is any one of the many detailed micro-structures which occur in sequence in the course of time. The expected values to be measured in an experiment are then obtained by taking an average over the ensemble of possible micro-structures.

The sound field consists again of an incident and a scattered wave

$$\varphi = \varphi_{\text{inc}} + \varphi_{\text{sc}}$$

The scattered wave is now a functional of the detailed micro-structure  $\nu$ ; in fact, the functional must be linear if we keep only first order terms:

$$\varphi_{\text{sc}} = \varphi_{\text{sc}} \left\{ \nu(\underline{x}) \right\}$$

We desire to determine the mean square fluctuations of the amplitude and phase of  $\varphi$ . These correspond to the variances of the slow fluctuations of amplitude and phase to be expected in the received signal due to slow changes in the structure of the medium. We therefore wish to evaluate averages over the ensemble of possible micro-structures which are of the form:

$$\left| \varphi_{\text{sc}} \right|^2 = \left\langle \left| \varphi_{\text{sc}} \left\{ \nu \right\} \right|^2 \right\rangle_{\text{ensemble of } \nu\text{'s}} \quad (\text{II-3})$$

The theoretical problems encountered in this task are twofold:

1. It is necessary to characterize the ensemble of micro-structures which represent the slowly changing details of the medium.
2. We must find some means for evaluating explicitly the averages of the field over this ensemble.

The micro-structure of the ocean consists essentially of patches whose local sound velocity is somewhat higher or lower than the average. The most appropriate way of characterizing this structure is by giving the spectrum of the index of refraction. This spectrum is a measure of the relative number of patches of any given size. From a knowledge of the spectrum we may derive such measurable properties of the medium as the correlation function of the index of refraction at two different points, or the mean square difference of the index of refraction at two separate points. Until the last few years, it was usual to employ an empirical spectral correlation function which had little theoretical justification but made it convenient to evaluate the averages over the ensemble required under step 2 above. Recently, some of the work has begun to make use of our knowledge of the turbulent mechanism which generates the ocean micro-structure, thus basing the scattering theory on spectra which are physically justified.

The evaluation of averages over the ensemble leads to analytical difficulties which usually require mathematical approximation. Giving a physical meaning to the results, we may distinguish two cases, as shown in Figure II-2. Consider a number of neighboring patches with an effective radius  $R$  scattering an incident wave of wave number  $k$ . For any one patch, the magnitude of the scattered wave is small compared to the incident wave. Furthermore, if the wavelength of the incident wave ( $\frac{2\pi}{k}$ ) is much less than the size of the scatterer  $R$ , the scattered wave can be shown to be highly collimated (see Section IV-B). In this case, the scattered wave consists either of a slightly divergent shadow zone or a slightly convergent zone of somewhat higher intensity, depending on whether the local index of refraction is larger or smaller than unity. Thus the scattered beam is essentially in the shape of a cone subtending a conical angle which may be shown to be of the order of  $\frac{1}{kR}$ . It is clear that this angle will be very much smaller than unity as long as the incoming wavelength satisfies the condition  $kR \gg 1$  mentioned above. Otherwise, if the incoming wavelength becomes of the same order of magnitude or greater than the size of the scatterer, the scattered sound has an omnidirectional nature. We see from Figure II-2 that if the frequency of the incident sound is sufficiently high, the "focusing" distance of the patch for a parallel beam of sound would be of the order of  $L_0 \approx kR^2$ . For a range  $L$  substantially less than  $L_0$  the principal effect of the inhomogeneities is therefore the focusing or defocusing of the sound. On the other hand, for a range  $L$  much larger than  $L_0$  the scattered waves from the different inhomogeneities overlap, and interference effects dominate. This range is therefore called the interference range.

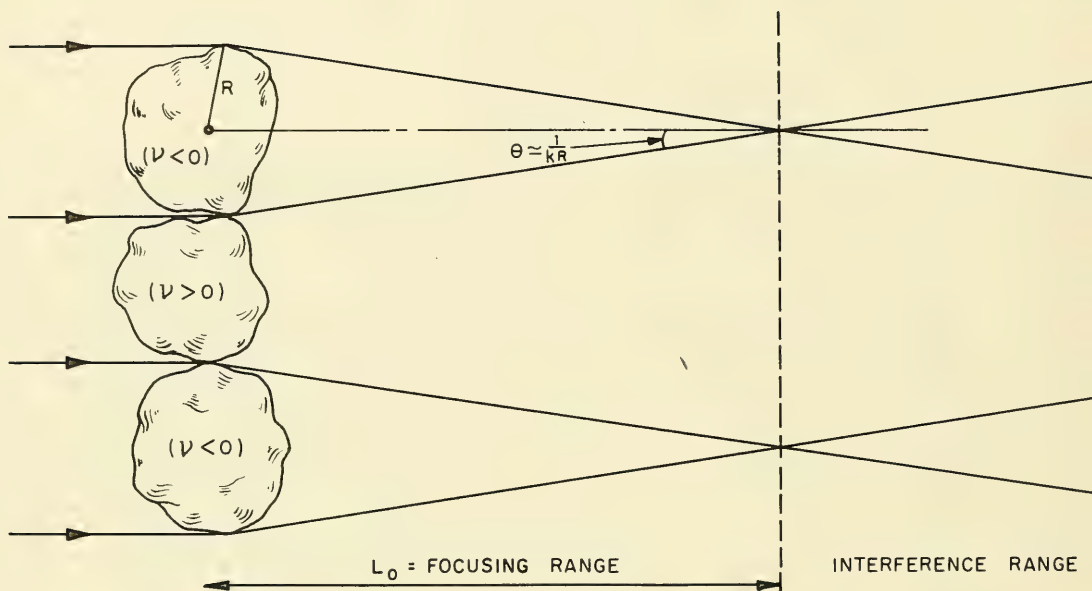


FIGURE II-2 SCATTERING BY THE OCEAN MICRO-STRUCTURE

Inside the focusing range we might expect an analysis in terms of ray acoustics to be adequate, since the scattered waves are all in phase. Rays are focused or defocused by individual inhomogeneities but do not interfere with one another. Beyond this range, wave acoustics become necessary. In Chapter IV we treat the general scattering formulation and obtain both the ray and interference results as limiting expressions. An excellent treatment based on ray acoustics alone and applicable in the focusing range may be found in Chernov, Part I.

The scattering from a single weak inhomogeneity is examined in Section IV-B. It is shown that the scattered pressure field is indeed highly directional when  $kR \gg 1$ . The ratio of the scattered to the incident pressure in the forward direction, i.e., in the direction of propagation of the incident plane wave, is shown to be

$$\left| \frac{p_{sc}}{p_{inc}} \right| \sim \frac{k^2 \tau |\nu|}{L} \quad (\text{II-4})$$

where  $L$  is the range (the distance from the scatterer at which we observe the field), and  $\tau$  is the scatterer's volume (proportional to  $R^3$ ). The constant of proportionality depends a bit on the shape of the scatterer but is generally of the order of magnitude of unity. One could almost arrive at (II-4) by the following very simple dimensional argument. The linearity of (II-4) in  $|\nu|$  is the result of using  $|\nu|$  as the parameter of smallness and ignoring all terms of second or higher order. The scattered sound is in the nature of a directional spherical wave, and the field should, therefore, decay as  $\frac{1}{L}$ . It is not unreasonable that the total scattering should be proportional to the volume of the scatterer. The only remaining parameter which can enter the expression is the wave number  $k$  characterizing the incident wave, and if the resulting expression (II-4) is to be dimensionless (as the ratio of two pressures must be) the wave number must enter quadratically.

On the basis of this result for a single scatterer, we may derive, in a very heuristic fashion, the principal conclusions of Section IV-D for a large collection of scattering patches. In the following, we shall present these intuitive arguments, aimed at determining the order of magnitude of the ratio of scattered to incident power. It should be clearly understood that these arguments are to be regarded only as an after-the-fact explanation of results obtained by somewhat more rigorous methods in the body of this report.

Consider first the case of low frequency sound, i.e., sound whose wavelength is much greater than the radius of the typical scatterer ( $kR < 1$ ). In this case, the scattered pressure from a single inhomogeneity will be omnidirectional, and the ratio of the scattered pressure to the incident pressure is given by (II-4) in every direction. Suppose we were to insonify by a plane wave a half space of an inhomogeneous medium packed densely with inhomogeneities all of radius  $R$ , as shown in Figure II-3. We wish to determine the ratio of the scattered pressure to the incident pressure a distance  $L$  inside the inhomogeneous medium. To this end we divide the inhomogeneous medium into slabs, each slab one scatterer thick (i.e., a slab thickness of  $2R$ ). Consider now the scattered pressure due to the scattering from a single slab. Clearly this pressure is independent of the distance behind the slab at which it is observed. It can, therefore, depend only on the properties of the individual scatterer ( $|\nu|$  and  $R$ ) and on the wave number of the incident sound  $k$ . Since each of the inhomogeneities of the slab has a scattering strength proportional to  $|\nu|$  the whole slab should have a scattering strength which is also proportional to  $|\nu|$ . Similarly, since the ratio of scattered to incident pressure for the single scatterer is proportional to the square of the frequency of the incoming sound, one would expect the same behavior for the slab. As a result, one is led at once by a dimensional argument to the expression

$$\left| \frac{p_{sc}}{p_{inc}} \right| \sim |\nu| k^2 R^2 \quad (II-5)$$

In a distance  $L$  the incident sound is scattered by  $\frac{L}{2R}$  such slabs. The scattered sound arriving at the observer from the different slabs is uncorrelated since its phase depends on the detailed constitution of each slab. Therefore, the power observed by the observer is the sum of the scattered powers from each of the slabs.\* It is common practice in underwater acoustics to deal with the square root of the ratio of scattered power to incident power; this is called the coefficient of variation. Its meaning is clearly that of the ratio of a typical scattered pressure amplitude to the amplitude of the incident wave. According to the above considerations, the coefficient of variation will be the product of the square root of the number of slabs and the scattering strength from each individual slab (i.e., powers add):

$$\frac{V}{P} = \frac{P_{sc}}{P_{inc}} \sim \sqrt{\frac{L}{2R}} \quad |v| \quad k^2 R^2 = |v| \quad k^2 R^{3/2} L^{1/2} \quad (\text{II-6})$$

Thus, we see that the scattered pressure a distance  $L$  inside the inhomogeneous medium will be proportional to the square root of  $L$ .

So much for the low frequency situation. At the other extreme, when the frequency of the incoming sound is high, the scattering from an individual scatterer will be very directional and we must therefore distinguish two cases corresponding to an observer inside the focusing range and an observer in the interference range.

Let us consider first the behavior to be expected in the interference range, i.e.,  $L \gg kR^2$ . Since we are considering the high frequency range ( $kR \gg 1$ ), the scattering of a single inhomogeneity is confined to a cone with half-angle  $\frac{1}{kR}$ . Therefore, an observer located a distance  $L$  inside the medium observes the scattered fields from those inhomogeneities which are located in a cone of half-angle  $\frac{1}{kR}$  with its apex at the observer. (See Figure II-4.) We again slice this cone into disks of thickness  $2R$ . A circular disk a distance  $L$  from the observer will have a surface area proportional to  $\left(\frac{L}{kR}\right)^2$ . The number

---

\*The argument that, in the case of a number of uncorrelated scattered pressures, the sum of the individual powers add, may be made more appealing to the statistically oriented by thinking of the pressure as a stochastic variable. The scattered pressure is a stochastic variable with zero mean; the scattered power is just the variance of the variable and hence the argument that the variance of a sum of such uncorrelated variables has a variance which is the sum of the individual variances becomes obvious.



of scattering inhomogeneities in this disk will therefore be proportional to  $\frac{L^2}{k^2 R^4}$ . The power scattered by the disk will again be the sum of the power scattered by the individual scatterers in the disk which, using (II-4) for the individual scatterer, yields:

$$\text{power scattered by disk} \sim \left( \frac{L^2}{k^2 R^4} \right) \left( \frac{|v|^2 R^6 k^4}{L^2} \right) = |v|^2 R^2 k^2 \quad (\text{II-7})$$

There are again  $\frac{L}{2R}$  disks, and the total coefficient of variation (the square root of the power ratio) therefore becomes:

$$v_p \sim \sqrt{\frac{L}{2R}} |v| Rk \sim |v| k \sqrt{RL} \quad (\text{II-8})$$

We observe that the coefficient of variation is again proportional to the square root of the range, but that the dependence on the frequency of the incoming sound and the size of the scatterer is quite different from that in the low frequency case.

Finally, we turn to the near (focusing) range for high frequency scattering. The physical situation is depicted in Figure II-5. The scattered pressure received by an observer is now due to a portion of each of  $\frac{L}{2R}$  single scatterers lined up in a row. Only part of the total volume of each of the scatterers contributes to the sound received by the observer. In fact, the contributing scattering volume for a scatterer a distance  $L$  from the observer is now given by:

$$\tau(L) \approx 2R \left( \frac{L}{kR} \right)^2 \sim \frac{L^2}{k^2 R} \quad (\text{II-9})$$

The power received by the observer is again the sum of the individual scattered powers from these portions of the single file of scatterers; therefore, the coefficient of variation becomes:

$$v_p \sim \sqrt{\frac{L}{2R}} \left( \frac{k^2 \tau(L) |v|}{L} \right) \sim \frac{L^{3/2} |v|}{R^{3/2}} \quad (\text{II-10})$$

Inside the focusing range, therefore, the scattered power is independent of the frequency of the incoming sound and increases as the three-halves power of the range. This is the result that would be obtained by a ray-acoustics analysis for the standard deviation of the phase of the received signal.



The general behavior derived above has been substantiated pretty well by experimental evidence. As an example, we show in Figure II-6 some measurements of the coefficient of variation, which exhibit the dependence as the square root of the range to be expected outside the focusing range. There is quite a wide scatter about the curve, and this is typical for any ocean measurements of scattering phenomena.

In conclusion, we show in Figure II-7 some measurements of the coefficient of variation made by the Ordnance Research Laboratory both for a signal traveling along the direct path and for the same signal traveling along the surface-reflected path. The coefficient of variation along the direct path increases effectively as the square root of the range. At short ranges, the surface-reflected path has a much greater coefficient of variation (i.e., a much greater percentage of scattered power). This is due to the effect, which we discussed earlier, of relatively high diffuse scattering from a corrugated surface near normal incidence. As the range gets longer and the angle of incidence becomes smaller, the higher order non-specular terms of reflection become less important. Finally, for very small grazing angles, the power scattered by the inhomogeneities of the surface become negligible, and the coefficient of variation along the surface-reflected path approaches that along the direct path.

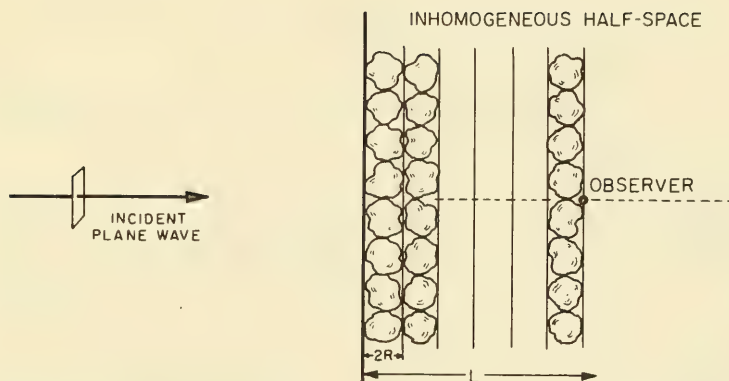


FIGURE II-3 LOW FREQUENCY SCATTERING MODEL

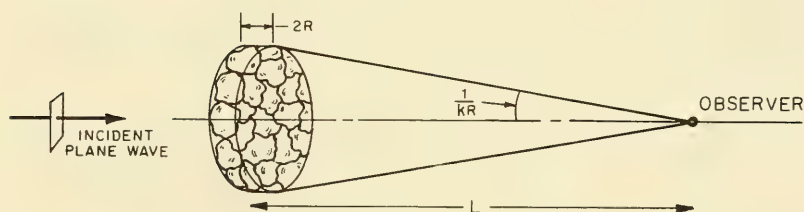


FIGURE II-4 HIGH FREQUENCY SCATTERING MODEL FOR THE INTERFERENCE RANGE

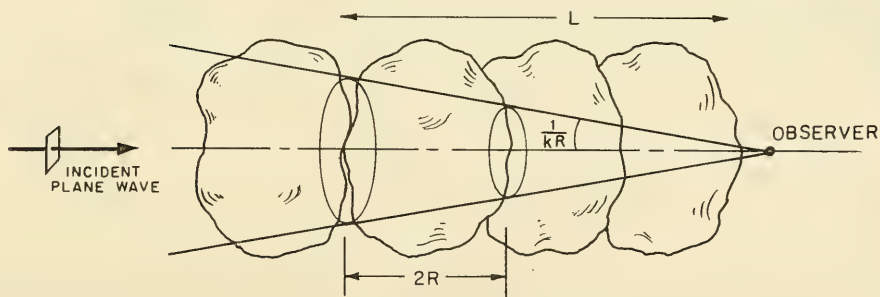


FIGURE II-5 HIGH FREQUENCY SCATTERING MODEL FOR THE FOCUSING RANGE

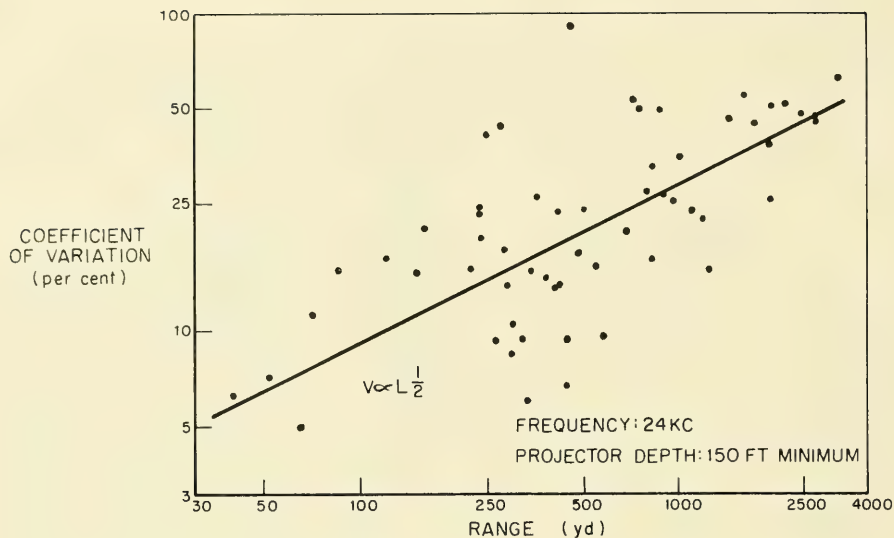


FIGURE II-6 COEFFICIENT OF VARIATION AS A FUNCTION OF RANGE

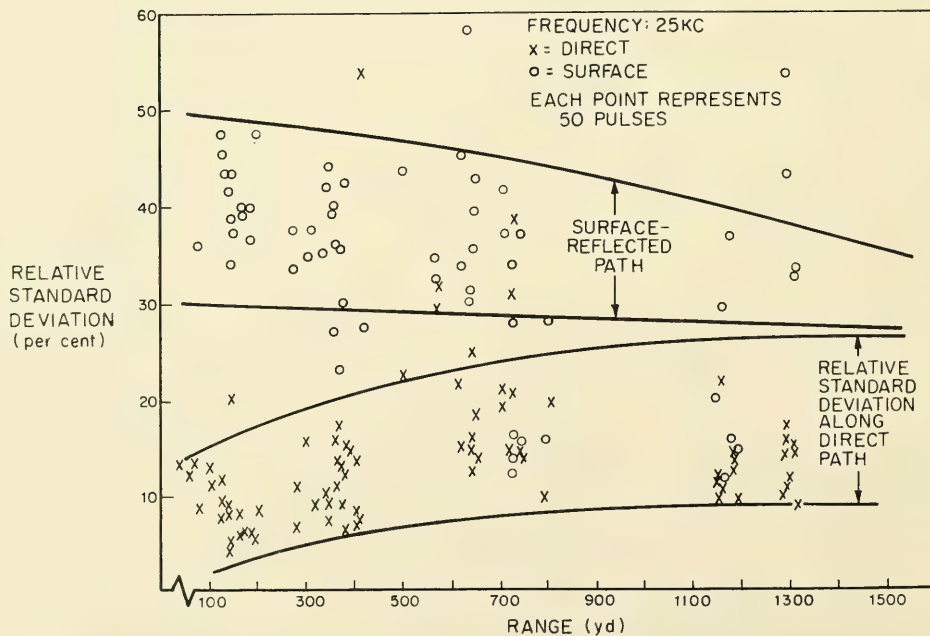


FIGURE II-7 FLUCTUATION MEASUREMENTS MADE BY ORL

### III. STRONG INHOMOGENEITIES

#### A. SCATTERING OF SOUND FROM A FLUID SPHERE

Before we examine the actual strong inhomogeneities of the ocean, we would like to specify the equations of sound propagation in water and study the very idealized model of a plane sound wave scattering from a fluid sphere. This will help to give us some insight into the effect of the scatterer's physical properties (size, hardness, density) on the characteristics of the resulting scattered sound (scattered power, directivity).

The passage of an acoustic wave through ocean water changes slightly the local state of the pressure, density and water velocity. We shall designate the unperturbed state by  $(p_0, \rho_0, \underline{u}_0)$  and denote the incremental fluctuations of pressure, density and velocity caused by the sound wave by  $(p, \rho, \underline{u})$ . The latter are in general functions of position  $\underline{x}$  and time  $t$ , e.g.,  $p = p(\underline{x}, t)$ . Throughout this chapter the unperturbed state variables  $(p_0, \rho_0, \underline{u}_0)$  will be regarded as constant in the region of space filled with water, i.e., outside the strong inhomogeneities. In fact, the unperturbed velocity  $\underline{u}_0$  is invariably set to zero; all analysis is performed in a frame of reference in which the unperturbed water is stagnant.

The equations of motion of the medium for acoustic (very small) disturbances are well known and consist of an equation of mass conservation (continuity) and three equations of momentum conservation:

$$\rho_t + \rho_0 u_{j,j} = 0 \text{ (mass conservation)} \quad (\text{III-1})$$

$$\rho_0 u_{j,t} + p_{,j} = 0, \quad j = 1, 2, 3 \text{ (momentum conservation)} \quad (\text{III-2})$$

In addition to these equations of motion, there is an equation of state which relates the local pressure in the medium to the local density.\* Since the square of the local sound velocity,  $c_0^2$ , is just the derivative of the pressure with respect to the density (at constant entropy), and since  $p$  and  $\rho$  are small variations of the unperturbed values  $p_0$  and  $\rho_0$ , we may write at once:

$$p = c_0^2 \rho \text{ (equation of state)} \quad (\text{III-3})$$

---

\*All motions are of sufficiently low amplitude and frequency that strictly adiabatic compression and expansion occurs when a sound wave passes.

Equations III-1 through III-3 govern the wave motion. A little manipulation of these shows that  $p$ ,  $\rho$  and  $\underline{u}$  all satisfy the ordinary wave equation. For example, we may obtain the wave equation for  $p$  by taking the partial derivative of (III-1) with respect to  $t$ , and then substituting for  $\rho$  from (III-3) and for  $\rho_0 u_{j,t}$  from (III-2). This yields:

$$\frac{1}{c_0^2} p_{,tt} - p_{,jj} = 0 \quad (\text{III-4})$$

We shall usually start with (III-4) as the basic equation of motion, and use (III-2) and (III-3) to derive  $\underline{u}$  and  $\rho$  from  $p$ .

The time dependence of the acoustic variables will almost always be harmonic. We shall therefore introduce state variables which are functions of position  $\underline{x}$  only, according to:

$$p(\underline{x}, t) = p(\underline{x}) e^{-i\omega t}, \quad \rho(\underline{x}, t) = \rho(\underline{x}) e^{-i\omega t}, \quad \underline{u}(\underline{x}, t) = \underline{u}(\underline{x}) e^{-i\omega t} \quad (\text{III-5})$$

It should be noted that the physical values of  $p$ ,  $\rho$  and  $\underline{u}$  are given by the real parts of (III-5). The resulting space-dependent state variables satisfy the analogous equations of motion:

$$-i\omega\rho + \rho_0 u_{j,j} = 0 \quad (\text{III-1a})$$

$$-i\omega\rho_0 u_j + p_{,j} = 0 \quad (\text{III-2a})$$

$$p = c_0^2 \rho \quad (\text{III-3a})$$

$$\frac{\omega^2}{c_0^2} p + p_{,jj} = k^2 p + p_{,jj} = 0 \quad (\text{where } k = \frac{\omega}{c_0} = \text{wave number}) \quad (\text{III-4a})$$

A word should be said about the flow of energy associated with the wave motion of  $p$ ,  $\rho$  and  $\underline{u}$ . The amount of work done across unit area of the  $j^{\text{th}}$  coordinate plane\* in a time interval  $dt$  is\*\*:

$$\delta W_j = \left[ \text{Re } p(\underline{x}, t) \right] \left[ \text{Re } u_j(\underline{x}, t) \right] dt$$

---

\*The coordinate plane with normal in the  $x_j$  direction.

\*\*Re preceding a complex number means "Real Part of"; Im is "Imaginary Part of."

In the case of harmonic time dependence,  $e^{-i\omega t}$ , we may compute the rate of energy flow (i.e., work done) across unit surface of a coordinate plane by averaging the above over one cycle in time:

$$I_j = \frac{\omega}{2\pi} \int_0^{2\pi/\omega} dt \left[ \operatorname{Re} p \right] \left[ \operatorname{Re} u_j \right]$$

If we carry out the integration over time, using (III-5), and express  $\underline{u}$  in terms of  $p$  by means of (III-2a), we find (using an asterisk to denote complex conjugate):

$$I_j = \operatorname{Re} \frac{1}{2} p(\underline{x}) u_j^*(\underline{x}) = \frac{1}{2\rho_o c_o} \operatorname{Im} p^*(\underline{x}) \frac{\partial}{\partial (kx_j)} p(\underline{x}) \quad (\text{III-6})$$

The simplest solution of (III-4) is the plane wave. For a plane wave propagating with wave number vector  $\underline{k}$  (i.e., propagating in the direction of  $\underline{k}$  with wave number  $k = |\underline{k}| = \frac{\omega}{c_o}$ ), we may write:

$$p(\underline{x}, t) = p e^{i \underline{k} \cdot \underline{x} - i\omega t} \quad (\text{III-7a})$$

These are, for different values of  $\underline{k}$ , all the different possible "separable" solutions in Cartesian coordinates. The energy flux in the direction of propagation (i.e.,  $\underline{k}$ ) is seen from (III-6) to be  $\frac{p^2}{2\rho_o c_o}$ .

If we ask for the separable (i.e., product form) solutions in spherical coordinates, we obtain another very useful set of solutions. Specifically, let  $r$  be the radial coordinate ( $r = |\underline{x}|$ ),  $\theta$  be the polar angle, and  $\phi$  the azimuthal angle. Normally, we deal with problems whose solution is independent of  $\phi$ , in that we treat scattering of waves incident along the polar axis on objects with complete  $\phi$  symmetry. We may then take as a complete set of wave functions:<sup>(1)</sup>

$$\left. \begin{aligned} p_m(\underline{x}, t) &= P_m(\cos \theta) j_m(kr) e^{-i\omega t} \\ p_m(\underline{x}, t) &= P_m(\cos \theta) n_m(kr) e^{-i\omega t} \end{aligned} \right\} m = 0, 1, \dots, \infty \quad (\text{III-7b})$$

---

1. P. M. Morse, "Vibration and Sound."



where  $P_m$  is the  $m^{\text{th}}$  order Legendre polynomial, and the radial functions  $j_m$  and  $n_m$  are related to the Bessel functions according to:

$$j_m(kr) = \sqrt{\frac{\pi}{2kr}} J_{(m+1/2)}(kr); \quad n_m(kr) = \sqrt{\frac{\pi}{2kr}} N_{(m+1/2)}(kr) \quad (\text{III-7c})$$

It should be noted that, for large  $kr$ ,  $j_m$  behaves like  $\frac{\cos(kr)}{kr}$  and  $n_m$  like  $\frac{\sin(kr)}{kr}$ .

We can now proceed to tackle the scattering of a plane wave (III-7a) incident on a fluid sphere consisting of a different material and imbedded in an infinite space of water.\* Let the density and sound velocity inside the fluid sphere be given by  $\rho_o'$  and  $c_o'$ . Any sound wave inside the fluid sphere will have to satisfy acoustic equations just like (III-1a) through (III-4a) but with  $\rho_o$  and  $c_o$  replaced by  $\rho_o'$  and  $c_o'$ . Suppose the incident plane wave is approaching along the polar axis and has pressure amplitude  $p_{\text{inc}}$ :

$$p_{\text{inc}}(\underline{x}, t) = p_{\text{inc}} e^{ikr \cos \theta - i\omega t} \quad (\text{III-8})$$

This incident wave causes both a scattered wave,  $p_{\text{sc}}$ , outside the sphere and an internal wave,  $p'$ , inside the sphere. The total acoustic pressure outside the fluid sphere is therefore  $p_{\text{inc}} + p_{\text{sc}}$ .

Each of the three pressure distributions  $p_{\text{inc}}$ ,  $p_{\text{sc}}$  and  $p'$  may be expressed in terms of the elementary wave functions (III-7b) since there is complete  $\phi$  symmetry. In particular, the scattered wave must be strictly an outgoing wave, and since the  $r$  dependence must be like  $\frac{e^{ikr}}{kr}$  for large  $(kr)$ , is therefore of the form:

$$p_{\text{sc}}(\underline{x}, t) = \sum_{m=0}^{\infty} A_m P_m(\cos \theta) \left[ j_m(kr) + i n_m(kr) \right] e^{-i\omega t} \quad (\text{III-9a})$$

---

\*Our treatment will follow Anderson, Ref. III-2.

The wave internal to the fluid sphere must remain finite at the origin; therefore, it must be expressible in terms of  $j_m$  alone:

$$p'(\underline{x}, t) = \sum_{m=0}^{\infty} B_m P_m(\cos \theta) j_m(k'r) e^{-i\omega t} \quad (\text{III-9b})$$

Note that  $k' = \frac{\omega}{c_0}$  is the appropriate wave number inside the fluid sphere corresponding to an angular frequency  $\omega$ . Finally, the incident plane wave may be expanded in spherical harmonics as:

$$p_{\text{inc}}(x, t) = p_{\text{inc}} \sum_{m=0}^{\infty} (-i)^m (2m+1) P_m(\cos \theta) j_m(kr) e^{-i\omega t} \quad (\text{III-9c})$$

It remains to apply the appropriate boundary conditions on the surface of the sphere. These are that both the pressure and the normal component of velocity must be continuous across the boundary. If the sphere has radius  $a$ , continuity of pressure requires:

$$p_{\text{inc}}(a) + p_{\text{sc}}(a) = p'(a) \quad (\text{III-10a})$$

The continuity of the normal velocity at the boundary is equivalent to the continuity of the normal (i.e., radial) derivative of the pressure, as may be seen from (III-2a). Hence, we have as the second boundary condition:

$$\frac{\partial}{\partial r} p_{\text{inc}}(a) + \frac{\partial}{\partial r} p_{\text{sc}}(a) = \frac{\partial}{\partial r} p'(a) \quad (\text{III-10b})$$

We substitute (III-9a) - (III-9c) into (III-10a) and (III-10b) and separate\* terms for each value of  $m$ . From the resulting pairs of simultaneous equations, we solve for  $A_m$  and find:

$$A_m = - \frac{p_{\text{inc}} (-1)^m (2m+1)}{1 + i C_m} \quad (\text{III-11})$$

---

\*This is permissible, because the Legendre polynomials are orthogonal.

where

$$C_m = \frac{\alpha_m(k'a)n_m(ka) - gh\beta_m(ka)j_m(k'a)}{\alpha_m(ka)j_m(ka) - gh\alpha_m(ka)j_m(k'a)} \quad (\text{III-11a})$$

and

$$\alpha_m(kr) = (2m+1) \frac{\partial}{\partial(kr)} j_m(kr); \quad \beta_m(kr) = (2m+1) \frac{\partial}{\partial(kr)} n_m(kr); \quad (\text{III-11b})$$

$$g = \frac{\rho'_0}{\rho_0}; \quad h = \frac{c'_0}{c_0}$$

The resulting expression for  $p_{sc}$  is, of course, hopelessly complicated. However, we are interested only in the far field, for which the asymptotic form of  $j_m + i n_m$  applies (showing the character of an outgoing spherical wave):

$$(-i)^m [j_m(kr) + i n_m(kr)] \approx (-i)^m \frac{e^{i kr}}{i kr} \text{ for } k r \gg 1 \quad (\text{III-12})$$

If we substitute (III-11) and (III-12) in (III-9a), we find for the far field scattered sound the expression:

$$p_{sc}(\underline{x}, t) \approx p_{inc} \frac{i e^{i kr - i \omega t}}{kr} \sum_{m=0}^{\infty} P_m(\cos \theta) \frac{(-1)^m (2m+1)}{1 + i C_m} \quad (\text{III-13})$$

The sum in (III-13) has the effect of a directivity factor; it indicates the dependence of the amplitude of the spreading wave on the polar angle  $\theta$ . For small values of  $ka$  and  $k'a$ , i.e., for a sphere with a circumference small compared to the wavelength of the sound in either medium, the coefficients  $C_m$  may be approximated quite conveniently by using the first term in the series expansions of  $j_m$  and  $n_m$  (in the case of  $j_0$  we need the first two terms to be able to compute  $\alpha_0$ ):

$$j_m(ka) \approx \frac{(ka)^m}{1 \cdot 1 \cdot 3 \cdots (2m+1)}, \quad m \geq 1;$$

$$n_m(ka) \approx \frac{-1 \cdot 1 \cdot 3 \cdots (2m+1)}{(ka)^{m+1}}, \quad m \geq 0;$$

$$j_0(ka) \approx 1 - \frac{(ka)^2}{6}$$

Substituting these in (III-11a), we obtain for the  $C_m$ :

$$C_0 \approx \frac{3gh^2}{(ka)^3 (1-gh)^2} ;$$

$$C_m \approx \frac{-1}{(ka)^{2m+1}} \frac{[m+g(m+1)] [(2m+1)(1 \cdot 3 \cdot \cdot (2m-1))]^2}{m(1-g)} , m \geq 1$$
(III-14)

Returning now to the sum in (III-13), we observe that for  $ka \ll 1$  and  $k'a \ll 1$ , the first two terms in the sum ( $m = 0$  and  $m = 1$ ) are of order  $(ka)^3$ . All the other terms are of higher order in  $ka$ ; in fact, successive terms increase in order by  $(ka)^2$ . For small  $ka$ , therefore, the first two terms of (III-13) should suffice. Using (III-14) to compute approximations for  $C_0$  and  $C_1$ , and recognizing that  $P_0 = 1$ ,  $P_1(\cos \theta) = \cos \theta$ , we obtain:

$$p_{sc}(x,t) \approx \frac{a e^{ikr-i\omega t}}{r} p_{inc}(ka)^2 \left[ \frac{1-gh^2}{3gh^2} + \frac{1-g}{1+2g} \cos \theta \right] \quad (III-15)$$

Fortunately, (III-15) may be given a relatively simple physical interpretation if we take the vantage point of the sphere. Since the sphere is very small compared to a wavelength, the passing sound wave has the effect of slowly raising and lowering the pressure in the entire vicinity of the sphere. In response, the sphere will expand and contract uniformly, as if it were breathing. However, since the mechanical properties of the fluid sphere are different from those of the surrounding water, the fluid sphere will expand and contract with a different amplitude from that which would be experienced by an equivalent sphere of water. The result is the emission of a pure spherical sound wave, corresponding to the first term in the square brackets of (III-15).

If  $gh^2 = 1$ , the mechanical impedance of the fluid sphere becomes identical with that of an equivalent sphere of water, since the impedance of a fluid sphere to a "breathing" mode of motion\* is

$$\frac{3 \rho'_0 c_0'^2}{ia\omega}$$

And indeed, the breathing mode in (III-15) vanishes when  $gh^2 = 1$ .

The second term in (III-15) corresponds to a "sloshing" type of motion, due to the pressure differential across the sphere. The pressure across the sphere is not quite constant, and the resultant force on the sphere causes it to oscillate as a rigid body along the polar axis. Since the density of the fluid sphere differs from that of the surrounding water, the amplitude of the resulting motion of the sphere will be different from what a corresponding sphere of water would experience subject to the same pressure gradient. As a consequence, the fluid sphere will oscillate as a rigid body relative to the surrounding water in the direction of the incoming wave. The normal velocity of this motion at the surface of the sphere depends on  $\theta$  as  $\cos \theta$ ; the pressure wave that is emitted will therefore be of the form

$\frac{e^{ikr-i\omega t}}{r} \cos \theta$ , which corresponds to the second term in (III-15). Note also that this term vanishes, as it should, when  $g = 1$ , i.e., when the mass densities of the fluid and of the water are the same.

A number of qualitative conclusions may be drawn from (III-15).

1. If  $gh^2 < 1$ , i.e., the fluid sphere is much more compressible than water, the breathing term completely dominates the sloshing term and isotropic scattering results.

---

\*This may be seen as follows. The overpressure in the fluid sphere is related to the "overdensity" according to (III-2a), i.e.,  $p = c_0'^2 \rho$ . The change in volume resulting from a normal velocity at the boundary relates the "overdensity" to the boundary velocity according to

$$\rho_t = - \frac{3 \rho'_0}{a} u = -i\omega \rho$$

for harmonic motion. Substituting one in the other yields  $p = \frac{3 \rho'_0 c_0'^2}{ia\omega} u$

as the linear relation between the harmonic driving velocity and the resulting harmonic pressure. The constant of proportionality is the mechanical impedance, where we make the analogy with electric networks by associating "velocity" with "current" and "pressure" with "voltage."

2. The breathing mode also dominates if the fluid has approximately the same density as water ( $g \approx 1$ ). Note that this condition is necessary (at least on the average) if the scatterer is to remain suspended in the water.
3. If the sphere is very hard ( $gh^2 \gg 1$ ), the sloshing mode will dominate.

The arguments leading to a breathing and a sloshing mode may be applied quite generally to the first two terms of (III-13), even in the case where  $ka$  is not very small. The first term is an outgoing spherical wave corresponding to a breathing motion, and the second term has the  $\cos \theta$  dependence associated with rigid body harmonic oscillation along the polar axis. The higher order terms ( $m \geq 2$ ) correspond to non-spherical deformations of the sphere and not-quite-rigid-body motions due to the finite size of the sphere.

In order to gain some insight in the general case (III-13), we must resort to numerical calculation. The properties of the scattering sphere which interest us most are the directivity of the scattering and the fraction of the incident power which is scattered. Both of these may be studied by comparison with uniform scattering from a perfectly reflecting sphere (commonly called geometrical scattering). In this case, the total energy intercepted by a sphere of radius  $a$  from an incident plane wave of pressure amplitude  $p_{inc}$  is considered to be scattered uniformly through a solid angle of  $4\pi$ . The pressure amplitude of the geometrically scattered wave at a distance  $r$  from the sphere may be written as

$$|p_{unif}| = \left[ \frac{\pi a^2}{4\pi r^2} \right]^{1/2} p_{inc} = \frac{a}{2r} p_{inc}$$

Using this as a standard, a reflectivity factor can be defined for large  $r$  by using (III-13):

$$R_\theta = \frac{|p_{sc}|}{|p_{unif}|} = \frac{2}{ka} \left| \sum_{m=0}^{\infty} P_m(\cos \theta) (-1)^m \frac{(2m+1)}{(1+iC_m)} \right| \quad (III-16)$$

This determines the directivity of the scattering. The total power scattered by the sphere (in comparison to geometrical scattering) is also of interest. Since the total power in a geometrically scattered wave is just that arriving at the sphere through a cylinder of radius  $a$ , the ratio of total scattered power to geometrically scattered power is

$$\Pi = \frac{1}{\pi a^2 p_{inc}} \int_S |p_{sc}|^2 dS$$

where  $S$  is a large sphere.



Using the orthogonality of the Legendre functions over the surface  $S$ , we find from (III-13):

$$\Pi = \frac{4}{k^2 a^2} \sum_{m=0}^{\infty} \frac{(2m+1)}{(1 + C_m^2)} \quad (\text{III-17})$$

The quantity  $\Pi$  is a measure of the fraction of incident power diverted from the original wave by the scatterer. The product  $(\Pi \cdot A)$  gives the total scattering cross section of a sphere whose geometric section is  $A$  units. Because of the complexity of the terms, it is not possible to do much further analysis with the mathematical expressions. However, Anderson has computed values of  $R_{\theta=0}$  (backward scattering) and  $\Pi$  for many cases. Figure III-1 shows the value of  $R/(ka)^2$  for various choices of relative density and sound velocity when  $ka < 1$ , and corresponds to (III-15).

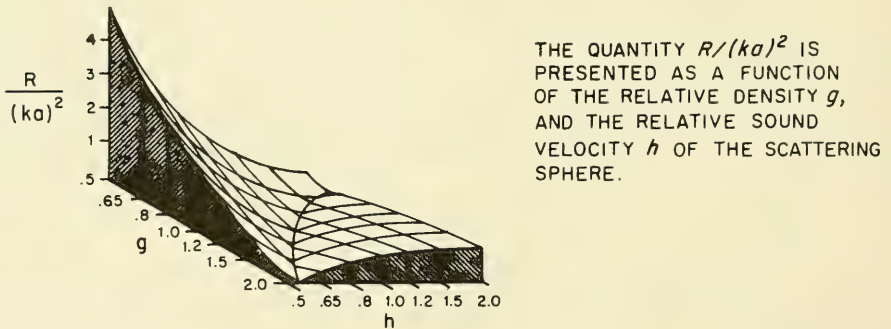


FIGURE III-1 RAYLEIGH SCATTERING FROM SMALL FLUID SPHERES IN THE BACKWARD DIRECTION (AFTER ANDERSON)

As  $g$  and  $h$  both become small,  $R$  increases to  $\frac{2}{3gh^2}$ . This happens when both the density and the speed of sound decrease in the scattering sphere. As  $g$  and  $h$  become large, the situation compares to an incompressible fixed sphere and  $R = \frac{5}{6} (ka)^2$ .

As the value of  $ka$  approaches 1.0, the simple Rayleigh solution (III-15) no longer holds and more terms of the series solution must be considered. In this region, which may be termed the critical region, some of the general characteristics of the backscattering in the Rayleigh region are still apparent. Figures III-2a and III-2b show the dependence of  $R$  on the relative sound velocity  $h$  and acoustic radius ( $ka$ ), while Figures III-3a and III-3b show the dependence of  $R$  on the relative density  $g$  and acoustic radius. Comparing the figures, the most striking difference is the presence of large slopes for the small values of  $h$  compared with the gradual rate of change of  $R$  with the relative density  $g$ . The difference between the dependence of  $R$  on  $h$  and  $g$  seems to become even more pronounced in this region than in the Rayleigh region, particularly for the larger values of ( $ka$ ).

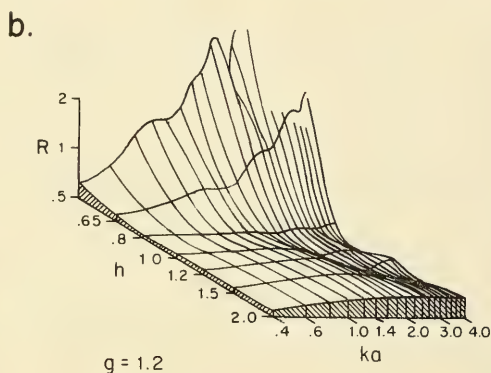
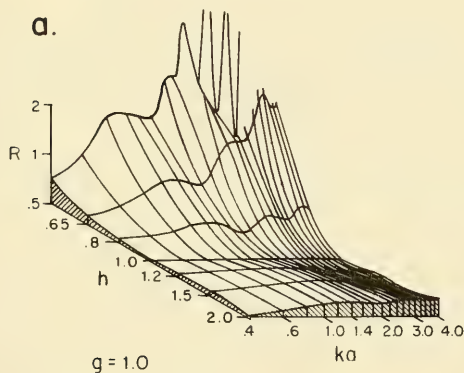


FIGURE III-2 THE REFLECTIVITY  $R$  AS A FUNCTION OF THE RELATIVE SOUND VELOCITY  $h$  AND ACOUSTIC RADIUS  $ka$  (AFTER ANDERSON)

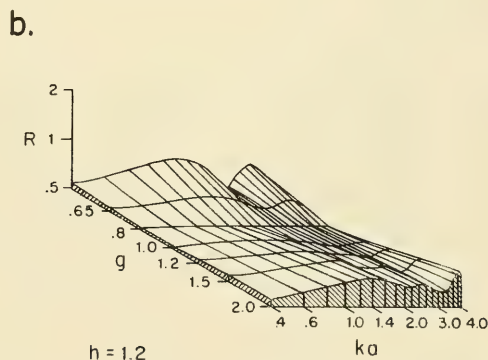
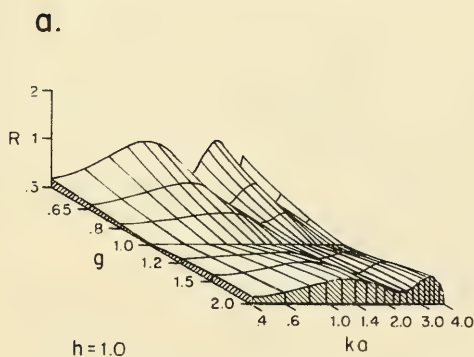


FIGURE III-3 THE REFLECTIVITY  $R$  AS A FUNCTION OF THE RELATIVE DENSITY  $g$  AND THE ACOUSTIC RADIUS  $ka$  (AFTER ANDERSON)

Values of  $R$  as a function of  $ka$  for other fluid spheres are shown in Figure III-4. Figure III-5 shows the corresponding values of  $\Pi$ .

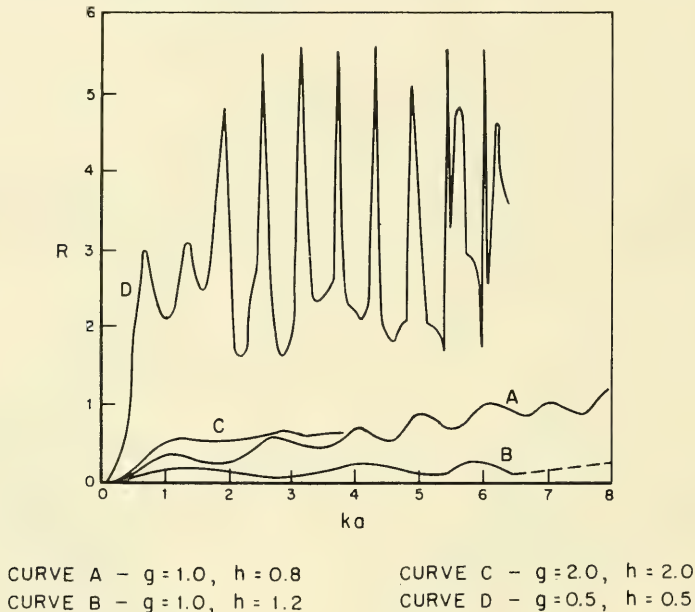
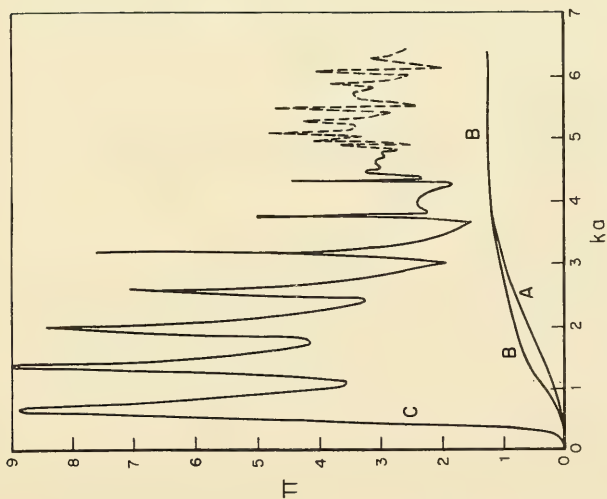


FIGURE III-4      THE REFLECTIVITY  $R$  AS A FUNCTION OF THE ACOUSTIC RADIUS  $ka$  (AFTER ANDERSON)

The effect of scattering in other than the backward direction is illustrated in Figure III-6 for a number of spheres with  $g = 1$ . As might be expected, these semi-transparent spheres scatter chiefly in the forward direction--this is due to the effect of refraction, which makes the spheres act as lenses. In general these patterns possess lobes, the number of lobes increasing with increasing  $ka$  and with decreasing  $h$ . It should be recalled that the quantity  $R_\theta$  does not give directly the diffraction pattern due to a spherical obstacle; it represents only the pressure amplitude in the spherically scattered wave and must be combined with the incident plane wave to give the true diffraction pattern.



CURVE A -  $g = 2.0$ ,  $h = 2.0$   
 CURVE B - RIGID SPHERE  
 CURVE D -  $g = 0.5$ ,  $h = 0.5$

THE DASHED LINE OF CURVE C DENOTES A REGION WHERE THE NUMBER OF POINTS CALCULATED WAS NOT SUFFICIENT TO DRAW A RELIABLE CURVE.

FIGURE III-5 SCATTERING POWER AS A FUNCTION OF THE ACOUSTIC RADIUS  $ka$  (AFTER ANDERSON)

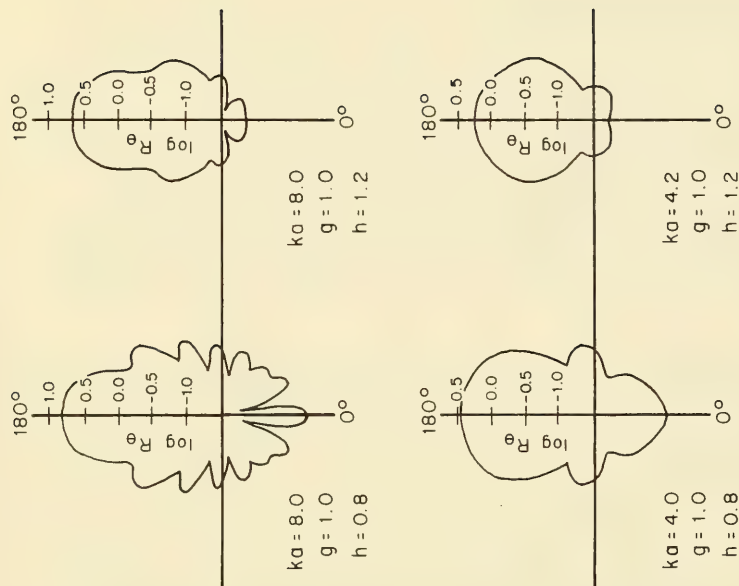


FIGURE III-6 DIRECTIVITY OF SCATTERING FOR  $ka \sim 1$  (AFTER ANDERSON)

## B. SCATTERING FROM AIR BUBBLES

Small air bubbles may be found throughout the ocean, and appear very often in conjunction with other scatterers. For example, they occur immediately below the surface of the ocean, due to the breaking of surface waves or the incidence of spray or rain on the surface; they are generated in the wake or turbulent boundary layers of ships; they may even take the form of gas bladders in fish. Typical air bubbles are quite small, usually less than one centimeter in diameter even though an occasional piscine bladder may be somewhat larger. The density of air bubbles is normally quite low, but their effect on the scattering of acoustic waves is far greater than one would expect from their low fractional volume.

We may obtain a general idea of the effect of air bubbles on sound waves through the analysis of the previous section. Consider the air bubble simply as a small sphere of air surrounded by an infinite expanse of water. We are concerned primarily with sound of 100 cps to 10,000 cps, in other words, sound with a wavelength in water of between 15 centimeters and 15 meters. Since the air bubbles are very small compared to the wavelength, we are indeed in a situation analyzed in the preceding section for the case  $ka \ll 1$ .

From that analysis emerged Equation III-15, which showed that the scattering of a plane wave from a small fluid sphere consists of "breathing" and a "sloshing" mode. For the case of air in the ocean, just below the surface, the two parameters  $g$  and  $h$  (the ratios of the densities and sound velocities of air and water) are given approximately by  $g = \rho'_0 / \rho_0 = 1.3 \times 10^{-3}$ ,  $h = c'_0 / c_0 = 0.2$ . In this case, therefore, the relative compressibility  $gh^2$  is so small ( $0.52 \times 10^{-4}$ ) that the breathing mode will completely dominate. The resulting scattered wave is isotropic, and its amplitude at the surface of the bubble is  $\frac{(ka)^2}{3gh^2} p_{inc}$  as given by (III-15). From this it would appear that the scattering strength of the bubble increases quadratically with the frequency of the incident sound. This is indeed true for sufficiently small  $ka$ , but not for the entire range  $ka \ll 1$ . If  $ka$  becomes of the same order of magnitude as  $3gh^2$ , so that the amplitude of the scattered wave would appear to be approximately the same as that of the incident wave, we must consider a more careful approximation of the breathing mode. According to (III-13), a plane incident wave of the form given in (III-8) will produce a spherically scattered "breathing" mode wave:

$$p_{sc}(r,t) = \frac{i p_{inc}}{1+i C_0} \frac{e^{ikr-i\omega t}}{kr} = \frac{p_{inc}}{C_0 - i} \frac{e^{ikr-i\omega t}}{kr} \quad (III-18)$$

The coefficient  $C_0$  can be found from (III-11a) to any desired degree of accuracy, since the spherical Bessel functions of order zero are given in terms of the simple trigonometric functions:

$$j_0(ka) = \frac{\sin ka}{ka}, \quad n_0(ka) = -\frac{\cos ka}{ka}$$

We can therefore develop  $C_0$  in a power series in  $ka$ , and if we keep all terms up to and including  $(ka)^3$ , we find for the coefficient of (III-18):

$$\frac{1}{C_0 - i} = \frac{(ka)^3}{3} \frac{\left[ (1 - gh^2) + \left( \frac{gh^2}{2} + \frac{g}{6} - \frac{1}{6} - \frac{1}{6h^2} \right) (ka)^2 + O\left((ka)^4\right) \right]}{\left[ gh^2 + \left( \frac{gh^2}{2} - \frac{1}{6}g - \frac{1}{3} \right) (ka)^2 - i(1 - gh^2) \frac{(ka)^3}{3} + O\left((ka)^4\right) \right]} \quad (\text{III-19})$$

For sufficiently small  $ka$ , all but the zero order terms may be ignored, and we find that the scattered amplitude behaves indeed as the square of the frequency. This is the approximation equivalent to (III-15). We notice, however, that as  $ka$  increases (though remaining much less than 1), the second order term in the denominator approaches the zeroth order term when  $(ka)^2$  approaches  $3gh^2$ , since the coefficient of the second term  $\frac{gh^2}{2} - (1/6)g - 1/3$  is essentially  $-1/3$  for the combination of air and water. Let us therefore investigate (III-19) more carefully in the neighborhood of  $(ka)^2 = 3gh^2 \approx 1.50 \times 10^{-4}$ . In this neighborhood, the value of the numerator remains essentially unity, since all other terms are of the order of magnitude of  $gh^2$ . The denominator must be kept to third order in  $ka$  since the zeroth and second order terms can be made to cancel. In this way we obtain the approximation:

$$\frac{1}{C_0 - i} \approx \frac{(ka)^3}{3} \frac{1}{\left[ gh^2 - \frac{1}{3}(ka)^2 - i \frac{(ka)^3}{3} \right]} \quad \text{for } (ka)^2 \approx 3gh^2 \quad (\text{III-20})$$

If we examine the magnitude of the scattering strength, we find that the scattered wave passes through resonance when  $(ka)^2$  is  $3gh^2$ . In other words,  $\left| \frac{1}{C_0 - i} \right|$  passes through a maximum. This may be seen most easily by observing that the square modulus of the coefficient is bounded by unity and reaches its upper bound at the point of resonance:



$$\left| \frac{1}{C_0 - i} \right|^2 = \frac{(1/9) (ka)^6}{\left[ (1/9) (ka)^6 + gh^2 - \frac{1}{3} (ka)^2 \right]^2} \leq 1$$

The bubbles therefore have a resonant wave number  $k_0$  (or resonant frequencies  $f_0$ ) such that  $k_0 = \frac{2\pi f_0}{c_0} = \frac{\omega_0}{c_0}$ . If we write the scattered wave as  $p_{sc}(r, t) = p_{sc} \frac{e^{+ikr - i\omega t}}{r}$ , then the amplitude of this wave can be expressed in terms of the resonant wave number or the resonant angular frequency as:

$$p_{sc} = \frac{ap_{inc} (ka)^2}{(k_0 a)^2 - (ka)^2 - i(ka)^3} = \frac{ap_{inc}}{\left(\frac{\omega_0}{\omega}\right)^2 - 1 - i\omega \left(\frac{a}{c_0}\right)} \quad (\text{III-21})$$

The resonant angular frequency may be given in terms of the physical variables describing the situation according to:

$$\omega_0^2 = k_0^2 c_0^2 = 3gh^2 \frac{c_0^2}{a^2} \frac{3\rho'_0 c_0'^2}{\rho_0 a^2} = \frac{3\gamma p_0}{\rho_0 a^2} \quad (\text{III-22})$$

At resonance, (III-21) becomes purely imaginary so that the scattered wave is  $90^\circ$  out of phase with the incident wave. It will be shown later that the imaginary term in the denominator corresponds to the energy that is removed from the incident wave and, in fact, is radiated out to infinity as the scattered wave. The real part of the denominator of (III-21) corresponds to the exchange of energy between the bubble and the incident wave. During part of each cycle the bubble is compressed and stores up energy which it returns during the remainder of the cycle. Thus, in this model there is no dissipative mechanism within the bubble itself; the only way it can remove energy from the incident wave is by radiating this energy in the form of an outgoing scattered wave.

### Mechanical Analogue

This behavior of the bubble is often compared to a simple mechanical analogue. Consider a mass  $M$  attached to a spring with spring constant  $K$  moving with a displacement  $x(t)$  in and out of a dashpot which offers a resistance force  $D \dot{x}$  proportional to the velocity of the mass. If this configuration is subjected to an harmonic exciting force  $F e^{-i\omega t}$ , the equation of motion becomes that of the damped harmonic oscillator:

$$M \ddot{x} + K x + D \dot{x} = F e^{-i\omega t}$$

It has as its solution:

$$x = \frac{F e^{-i\omega t}}{K - M \omega^2 - i D \omega} = \frac{(F/K) e^{-i\omega t}}{1 - \frac{\omega^2}{\omega_0^2} - \frac{D}{K} \omega} \quad \text{where } \omega_0^2 = \frac{K}{M} \quad (\text{III-23})$$

We note the correspondence in the form of the resulting motion with (III-21). The only difference is the replacement of (the resistance term)  $\frac{\omega_0^2}{\omega^2} - 1$  by the term

$1 - \frac{\omega^2}{\omega_0^2}$ . However, for  $\omega$  near  $\omega_0$ , i.e., near resonance, these two terms are

approximately equal. Because of the damping term introduced by the dashpot, we frequently refer to the imaginary term in the denominator as the damping constant

$$\delta = \frac{\omega D}{K} = \frac{\omega a}{c_0}.$$

### Equivalent Physical Model

The expression for the scattering amplitude (III-21) which was deduced from the general analysis of the preceding section could equally well have been obtained from a more direct physical model of the bubble. Since only the breathing mode contributes substantially to the scattered wave, it suffices to regard the incident sound pressure as spatially uniform near the bubble and varying in time as  $e^{i\omega t}$ . In other words, spatial gradients in the incident pressure field may be ignored when we do a strict breathing mode analysis. Thus, the incident wave

$p_{\text{inc}} e^{-i\omega t}$  causes a scattered wave  $p_{\text{sc}} \frac{e^{+ikr-i\omega t}}{r}$  and an interior wave (also uniform throughout the bubble)  $p' e^{-i\omega t}$ . The pressure at the boundary of the bubble must be continuous, and this requires that:

$$p_{\text{inc}} + \frac{p_{\text{sc}}}{a} e^{ika} = p' \quad (\text{III-24})$$

Thus, we have one relation between the three amplitudes  $p_{inc}$ ,  $p_{sc}$  and  $p'$ . A second relation may be obtained from the equation of motion of the water just outside the bubble boundary. Consider (III-2a) in radial coordinates, with  $u_r$  as the radial component of the velocity:

$$i \omega \rho_o u_r = p_{,r} \quad (III-25)$$

Since the incident wave does not depend on  $r$ , the gradient of the pressure on the bubble surface may be obtained entirely from the scattered wave:

$$p_{,r}(r=a) = p_{sc,r}(r=a) = p_{sc} \left( ik - \frac{1}{a} \right) \frac{e^{ika-i\omega t}}{a} \quad (III-26)$$

It remains to evaluate the radial velocity  $u_r$  in terms of  $p'$  by analyzing the thermodynamics of the interior of the bubble. For a perfect gas undergoing adiabatic compression, the volume  $V$  is related to the total pressure  $p = p_o + p'$  according to  $p \sim V^{-\gamma}$  where  $\gamma$  is approximately 1.4. The volume for a bubble with radius  $a + da$  is given by  $V = 4/3 \pi (a+da)^3 \simeq V_o \left( 1 + 3 \frac{da}{a} \right)$  where  $V_o$  is the unperturbed bubble volume  $\frac{4}{3} \pi a^3$ . It follows that pressure changes inside the bubble are related to changes of bubble radius according to:

$$\frac{dp}{p} = - \frac{\gamma dV}{V} = - 3 \gamma \frac{da}{a} \quad (III-27)$$

The acoustic fluctuations  $dp = p'$  and  $da$  are very small compared to the stagnation values  $p_o$  and  $a$ . Since  $\frac{da}{dt}$  is just the radial velocity  $u_r$  of the bubble surface, we can rewrite (III-27) to first order in the acoustic quantities as:

$$\frac{1}{p_o} \frac{dp'}{dt} = - \frac{3 \gamma}{a} u_r = - \frac{i \omega}{p_o} p' \quad (III-28)$$

We substitute (III-28) and (III-26) in (III-25) and obtain a relation between the amplitude of the scattered wave and the amplitude of the interior bubble pressure:

$$\frac{\omega^2 \rho_o a}{3 \gamma p_o} p' = p_{sc} (1 - ika) \frac{e^{ika}}{a^2} \quad (\text{III-29})$$

From (III-24) and (III-29), we can solve for  $p_{sc}$  in terms of  $p_{inc}$  and obtain the same result as (III-21) if we use the identifications of (III-22). This simple physical model and the associated mathematical approximations are therefore equivalent to the approximations of the breathing mode of a fluid sphere leading to (III-21).

In the above analysis we have ignored the effect of dissipation; the only loss of energy from the incident wave has been due to the radiation of the scattered wave. If we introduce heat conduction inside the bubble and viscosity in the water, and enclose the bubble in an elastic membrane which corresponds to the surface tension of the water, we can still carry through the calculations that lead to (III-21), using the same type of analysis shown in (III-24) and (III-29). Such a procedure has been carried out by Spitzer\* and results in a more complicated expression for the scattered amplitude. Nonetheless the expression has the same essential features exhibited by the simple models of a damped oscillator or a dissipation-free bubble. We show all three models for easy comparison in Table III-1, and catalog them for future reference as:

Model I - damped harmonic oscillator

Model II - dissipation-free bubble

Model III - bubble with conduction, viscosity and surface tension

We wish next to compare these three models with each other and with the available experimental data. If we compare the resonant frequencies predicted by Models II and III, we find that the effect of the dissipative mechanisms included in Model III is small for frequencies below 20,000 cps. The two curves for the resonant frequency are shown in Figure III-7 together with some data from a number of experiments which are in generally good agreement with the theoretical predictions. The anomalous results reported by Exner and Hampe were apparently caused by dust particles in the water. It is not surprising that the resonant frequency predicted for Models II and III should turn out to be so similar. After all, resonance comes about through the matching of the inertial properties of the system (i.e., the mass of the bubble and a portion of the surrounding water) and the compressibility of the system.

---

\*L. Spitzer, Ref. III-38.

TABLE III-1  
THREE MODELS OF AIR BUBBLE SCATTERING

	Model I	Model II	Model III
Underlying Conditions	Mass M oscillating with displacement $x(t) = Ae^{-i\omega t}$ as a result of forcing motion $F e^{-i\omega t}$ , spring force $Kx$ , and damping force $D\dot{x}$	Air bubble radius $a$ emitting scattered wave $p_{sc} e^{ikr-i\omega t}$ in response to incident plane wave $p_{inc} e^{ikx-i\omega t}$ when $ka \ll 1$	Same as Model II, but indicating effects of heat conduction in bubble, viscosity of water and surface tensions around bubble
Scattering Amplitude	$p_{sc} = \frac{(F/X)}{1 - (\omega/\omega_o)^2 - i\delta_I}$	$p_{sc} = \frac{p_{inc} a}{(\omega_o/\omega)^2 - 1 - i\delta_{II}}$	$p_{sc} = \frac{p_{inc} a}{(\omega_o/\omega)^2 - 1 - i\delta_{III}}$
Resonant Frequency	$\omega_o = \sqrt{\frac{K}{M}}$	$\omega_o = \frac{1}{a} \sqrt{\frac{3\gamma p_o}{\rho_o}}$	$\omega_o = \frac{1}{a} \sqrt{\frac{3\gamma x p_o}{\rho_o}}$ where $x = \frac{1}{\alpha} \left\{ 1 + \frac{2T}{ap_o} \left( 1 - \frac{\alpha}{3\gamma} \right) \right\}$
Damping Constant	$\delta_I = \frac{\omega D}{K}$	$\delta_{II} = \frac{\omega a}{c_o}$	$\delta_{III} = \frac{\beta}{\alpha} \left( \frac{\omega_o}{\omega} \right)^2 \left( 1 + \frac{2T}{ap_o} \right) + \frac{4\mu}{\omega a^2} + \frac{\omega a}{c_o}$

TABLE III-1 (Continued)

Notes:

The constants in Model III are given by:

$$\alpha = 1 + \frac{3(\gamma - 1)}{g} \left\{ \frac{\sin h}{\cos hg} - \frac{\sin g}{\cos g} \right\}; \quad \beta = \frac{3(\gamma - 1)}{2} \left\{ g \frac{\sin h}{\cos h} \frac{g}{g} + \frac{\sin g}{\cos g} - 2 \right\}$$

$$\text{where: } g = \sqrt{\frac{2\rho_o' C_p w a^2}{q}}$$

$C_p$  = specific heat of air = .24 cal/gm

$q$  = conductivity of air =  $5.6 \times 10^{-5}$  cal/cm sec

$T$  = surface tension = 75 dynes/cm

$\mu$  = coefficient of viscosity in water = 0.01 poise

approximate  
values  
at sea level



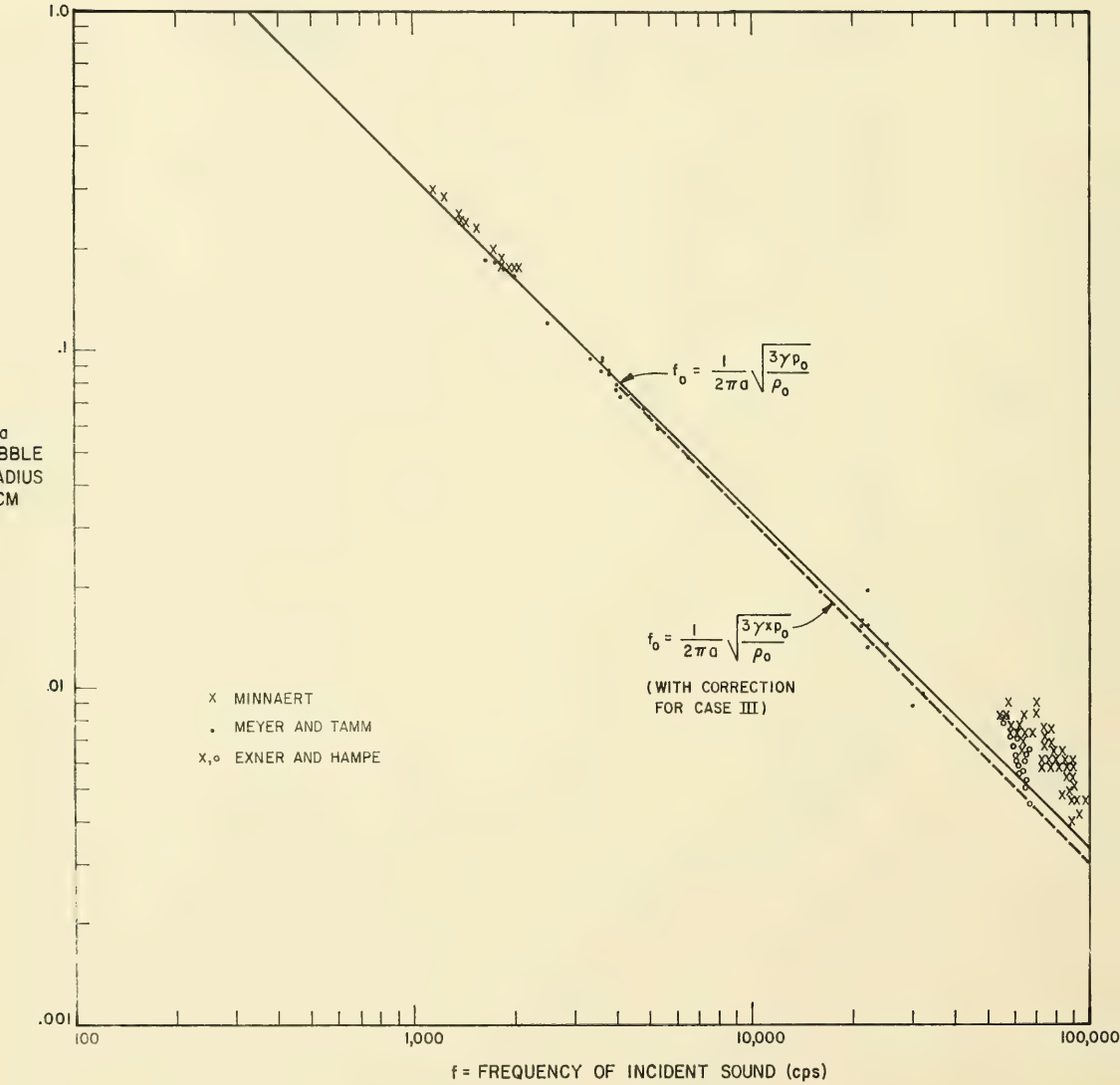


FIGURE III-7 AIR BUBBLE RESONANT FREQUENCY AS A FUNCTION OF BUBBLE RADIUS

We note that in the range of frequencies from 100 to 10,000 cps, the bubbles which are resonant will have radii between 0.03 cm and 3 cm. This coincides with the range of bubble size most commonly found in the ocean. It is apparent from Figure III-7 that within this range of frequencies, the expression

$$f_o = \frac{1}{2\pi a} \sqrt{\frac{3\gamma p_o}{\rho_o}} \quad \text{is a very good prediction of the resonant frequency.}$$

The damping constant  $\delta$ , on the other hand, may be expected to depend very heavily on the dissipative mechanism. We show in Figure III-8 how the damping constant  $\delta$  varies as a function of frequency for four typical bubbles. These curves were computed according to Model III for the bubbles whose radii and corresponding resonant frequencies (at sea level) are indicated below.

<u>a = Radius (cm)</u>	<u>f<sub>o</sub> = Resonant Frequencies (cps)</u>
1.0	326
0.1	3,240
0.01	31,000
0.001	260,000

We have shown on each curve the frequency at which the bubble is resonant. Near these resonant frequencies the dissipative and radiative mechanisms combine to produce a minimum value of  $\delta$ . In other words, the contribution of the dissipative mechanism to  $\delta$  decreases with increasing frequencies. The contribution of the radiative mechanism to  $\delta$  increases with increasing frequencies, and both contributions are important in the neighborhood of the resonant frequency since they conspire to produce a minimum in that range.

The damping constant has been studied extensively under a wide range of frequencies and by means of several different experimental techniques. One commonly used technique involves measuring the amplitude of the scattered wave for various frequencies of the incident wave. The logarithmic decrement is then given by

$$\Delta = \pi \frac{\Delta f}{f_o}$$

where  $f_o$  is the resonant frequency (maximum amplitude) and  $\Delta f$  is the difference of the two frequencies at each of which the response is one half of its maximum. In the literature, experimental results are expressed in terms of either  $\Delta$  or  $\delta$ ; in this report all values are converted to  $\delta$ .

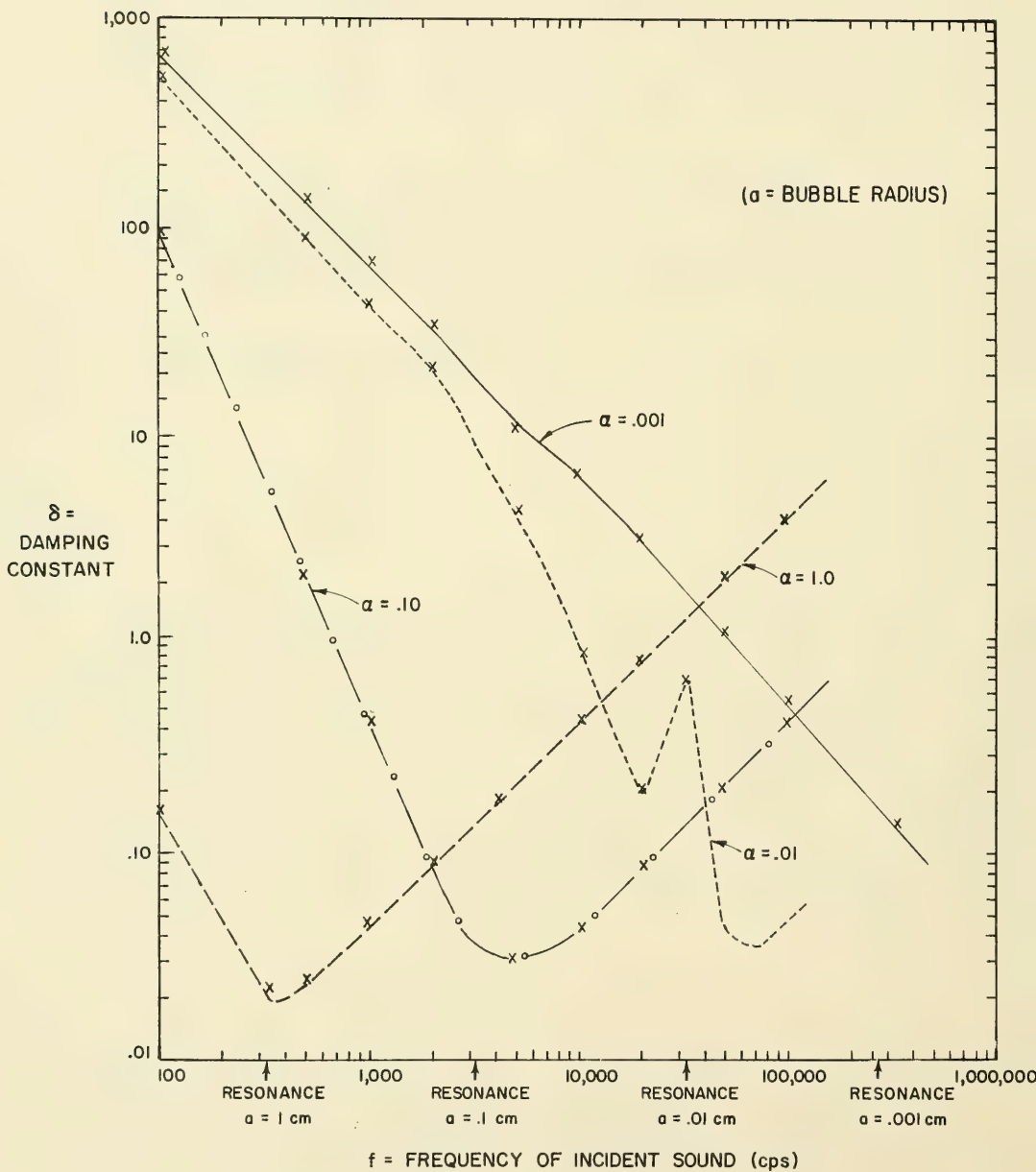


FIGURE III-8

DAMPING CONSTANT FOR FOUR TYPICAL BUBBLE SIZES  
 AS A FUNCTION OF FREQUENCY

Figure III-9 shows the experimental results for  $\delta$  at resonance as determined by several authors as well as the corresponding theoretical values obtained from Model III. The contributions to  $\delta$  due to viscous damping, radiation damping, and heat conduction damping are shown separately. Allowing for different experimental techniques and limits of error, the results generally confirm the theory. Exner and Hampe seem to have done the best and most extensive experimental work, and their results are probably the most accurate. Unfortunately, this work was done at very high frequencies. Lauer's work and Exner's work at low and intermediate frequencies, respectively, though done under less carefully controlled conditions, also agree with the theory in these ranges.

The only serious disagreement with the theory is in the work done by Meyer and Tamm, Carstensen and Foldy, and Fox, Curley and Larsen. In all cases the authors found values for the damping constant which were larger than those predicted by the theory. Fox, Curley and Larsen's single observation at 65,200 cps is about five times that predicted by theory. Carstensen and Foldy, and Meyer and Tamm report values of  $\delta$  for low and intermediate frequencies which are roughly two to three times the theoretical values.

These differences should not be considered as contradictions of the theory. The higher values were generally obtained indirectly in the course of attenuation studies and were needed to account properly for the observed attenuation. The theory is otherwise well supported; therefore, it seems that some significant factors were not considered when working backwards from the attenuation experiments.

In order to see how the variation in  $\delta^2$  compares with that of  $\left(\frac{f_o^2}{f^2} - 1\right)^2$ , we have plotted in Figure III-10 the ratio

$$\Delta = \left(\frac{f_o^2}{f^2} - 1\right)^2 / \delta^2$$

as a function of  $f$  for  $a = 1.0, 0.10, 0.01$  and  $0.001$  cm. One would like to be able to conclude that in the neighborhood of  $f = f_o$  the value of  $\left(\frac{f_o^2}{f^2} - 1\right)^2$  varies much more rapidly than  $\delta^2$ , i.e., that  $\delta^2$  may be considered relatively constant in the neighborhood of the resonant frequency. Outside this neighborhood,  $\delta^2$  is not very important. In later calculations of cross sections, we would then be able to view  $\delta$  as being constant over the full range of frequencies. Unfortunately, the horizontal nature of the curves in the neighborhood of the resonant frequency precludes this possibility.

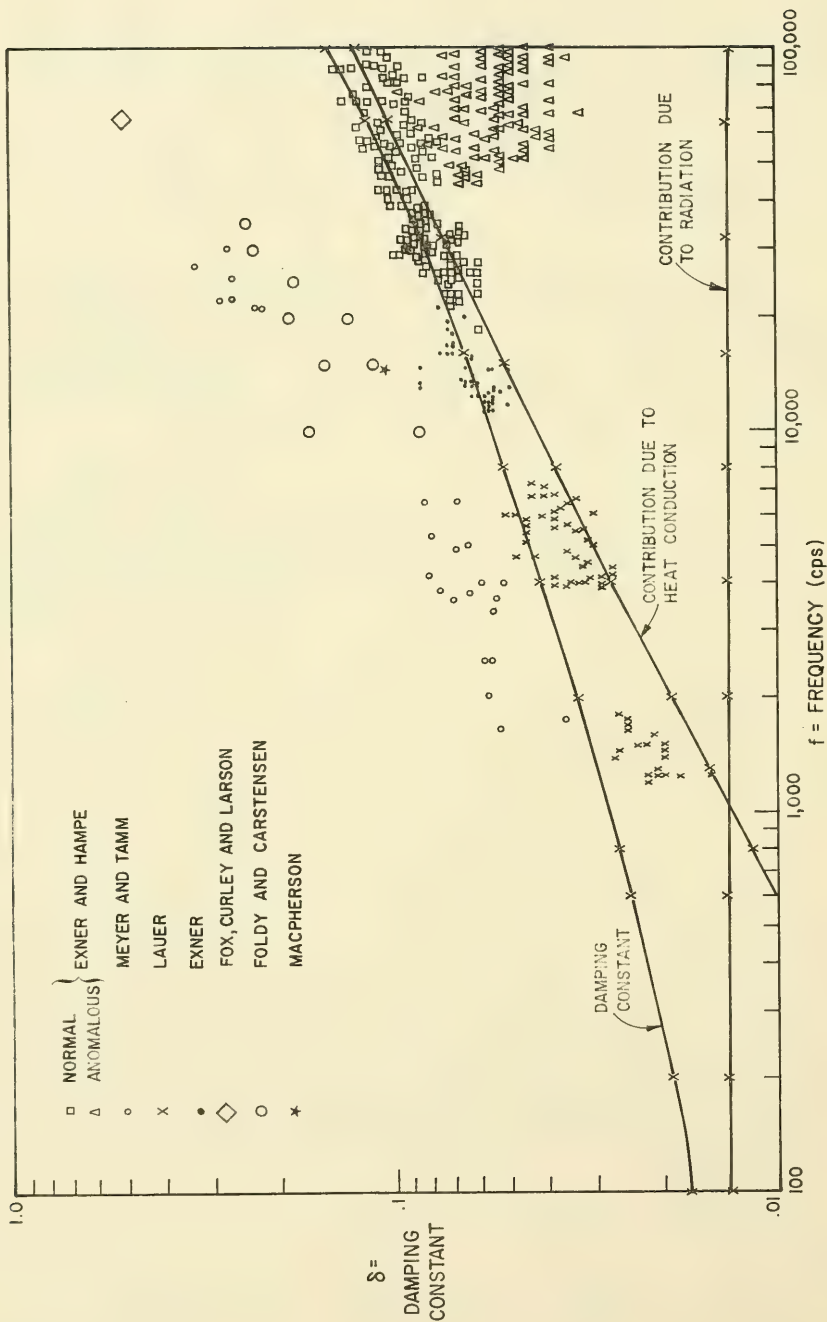


FIGURE III-9 THEORETICAL AND EXPERIMENTAL VALUES OF THE DAMPING CONSTANT AT RESONANCE

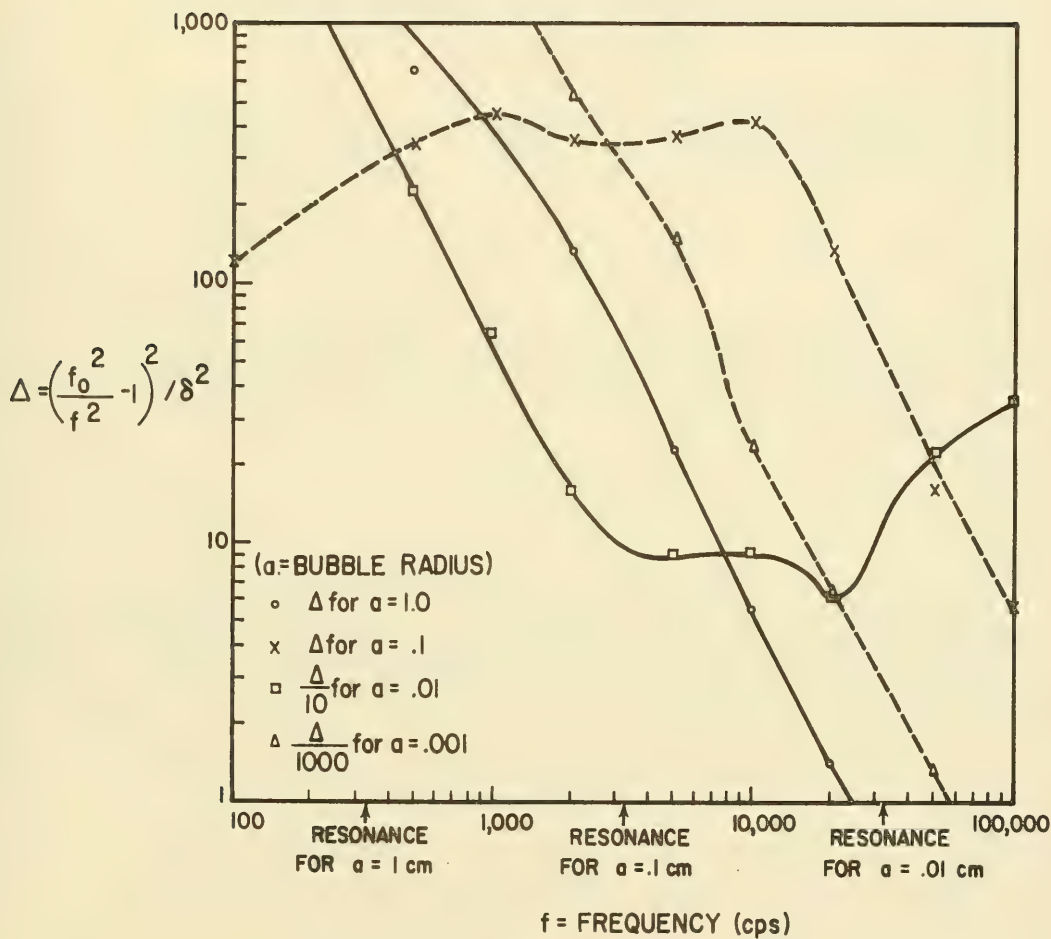


FIGURE III-10  $\Delta = \left( \frac{f_0^2}{f^2} - 1 \right)^2 / \delta^2$  AS A FUNCTION OF INCIDENT FREQUENCY FOR FOUR TYPICAL BUBBLE SIZES



The intensities of the incident and scattered sound are given by (see Equation III-6):

$$I_{\text{inc}} = \frac{|p_{\text{inc}}|^2}{2 \rho_0 c_0} \quad I_{\text{sc}} = \frac{|p_{\text{sc}}|^2}{2 \rho_0 c_0 r^2}$$

and the total scattered energy at the distance  $r$  is  $4 \pi r^2 I_{\text{sc}}$ . The scattering cross section  $\sigma_{\text{sc}}$  is defined by the expression

$$4 \pi r^2 I_{\text{sc}} = \sigma_{\text{sc}} I_{\text{inc}}$$

that is, it is the area such that the total incident energy crossing this area in a perpendicular direction is equal to the scattered energy. Then  $\sigma_{\text{sc}}$  is given by

$$\sigma_{\text{sc}} = \frac{4 \pi |p_{\text{sc}}|^2}{|p_{\text{inc}}|^2}$$

The scattering cross section does not provide all the information wanted in the case of an actual bubble, since the incident energy is reduced by both scattering and absorption. Let  $F_{\text{ex}}$  be the sum of these energies, i.e., the total energy extinguished from the incident wave. Then an extinction cross section can be defined analogously by

$$\sigma_{\text{ex}} I_{\text{inc}} = F_{\text{ex}}$$

The quantity  $F_{\text{ex}}$  is equal to the work done, per unit interval of time, on the bubble by the incident sound beam. Then, for a bubble of radius  $a$ , we have

$$F_{\text{ex}} = \overline{(\text{Re } p_{\text{inc}}(t)) (4 \pi a^2) (\text{Re } \frac{da}{dt})}$$

where  $p_{inc}$  is the pressure of the incident sound and the bar denotes the time average. The radial velocity of the air bubble  $u_r = \frac{da}{dt}$  satisfies (III-25), and using (III-26), we obtain:

$$i\omega \rho_o u_r = p_{sc,r} = p_{sc} \left( ik - \frac{1}{a} \right) \frac{e^{ika-i\omega t}}{a}$$

Determining  $u_r$  from this, calculating the time average, and dropping terms of order  $(ka)^2$ , we find:

$$F_{ex} = - \frac{p_{inc} \text{Im } p_{sc}}{\rho_o f}$$

This demonstrates our earlier statement that the imaginary part of  $p_{sc}$  determines the rate of energy transfer from the incident to the scattered wave. The extinction cross section now becomes:

$$\sigma_{ex} = \frac{2 c_o \text{Im } p_{sc}}{p_{inc} f}$$

Using the models for  $p_{sc}$  discussed before, we obtain the scattering and extinction cross sections shown in Table III-2. The scattering and extinction cross sections according to Model III for the four typical bubble sizes ( $a=1$  cm, 0.1 cm, 0.01 cm, and 0.001 cm) are shown in Figures III-11 and III-12. The resonant behavior of the bubbles is clearly demonstrated by the maxima of their cross sections. Below resonance the bubbles tend primarily to absorb energy, while above resonance the bubbles act principally as scatterers.

TABLE III-2

SCATTERING AND EXTINCTION CROSS SECTIONS OF AIR BUBBLES

	Model I	Model II	Model III
Scattering Cross Section $\sigma_{sc}$	$\left[ \frac{4\pi a^2}{1 - \left(\frac{w}{w_0}\right)^2} \right]^2 + \delta_I^2$	$\left[ \left(\frac{w_0}{w}\right)^2 - 1 \right]^2 + \delta_{II}^2$	$\left[ \left(\frac{w_0}{w}\right)^2 - 1 \right]^2 + \delta_{III}^2$
Extinction Cross Section $\sigma_{ex}$	$\frac{4\pi a^2 (\delta_I c_0 / wa)}{\left[ \left(1 - \frac{w}{w_0}\right)^2 \right]^2 + \delta_I^2} + \delta_I^2$	$\frac{4\pi a^2}{\left[ \left(\frac{w_0}{w}\right)^2 - 1 \right]^2 + \delta_{II}^2} + \delta_{II}^2$	$\frac{4\pi a^2 (\delta_{III} c_0 / wa)}{\left[ \left(\frac{w_0}{w}\right)^2 - 1 \right]^2 + \delta_{III}^2} + \delta_{III}^2$

Note:  $\delta_{II} c_0 / wa = 1$ , which explains the simple form of  $\sigma_{ex}$  for Model II.

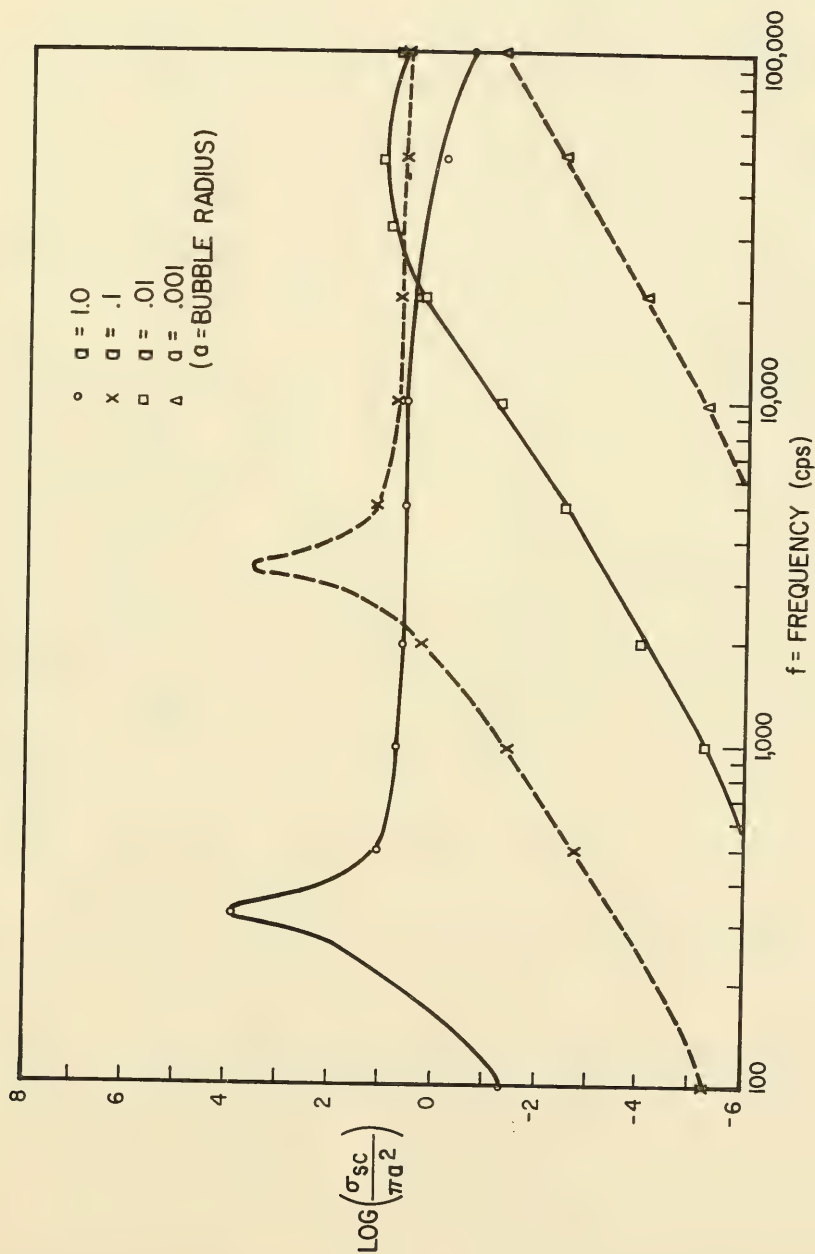


FIGURE III-11 RATIO OF SCATTERING CROSS SECTIONS TO GEOMETRIC CROSS SECTIONS

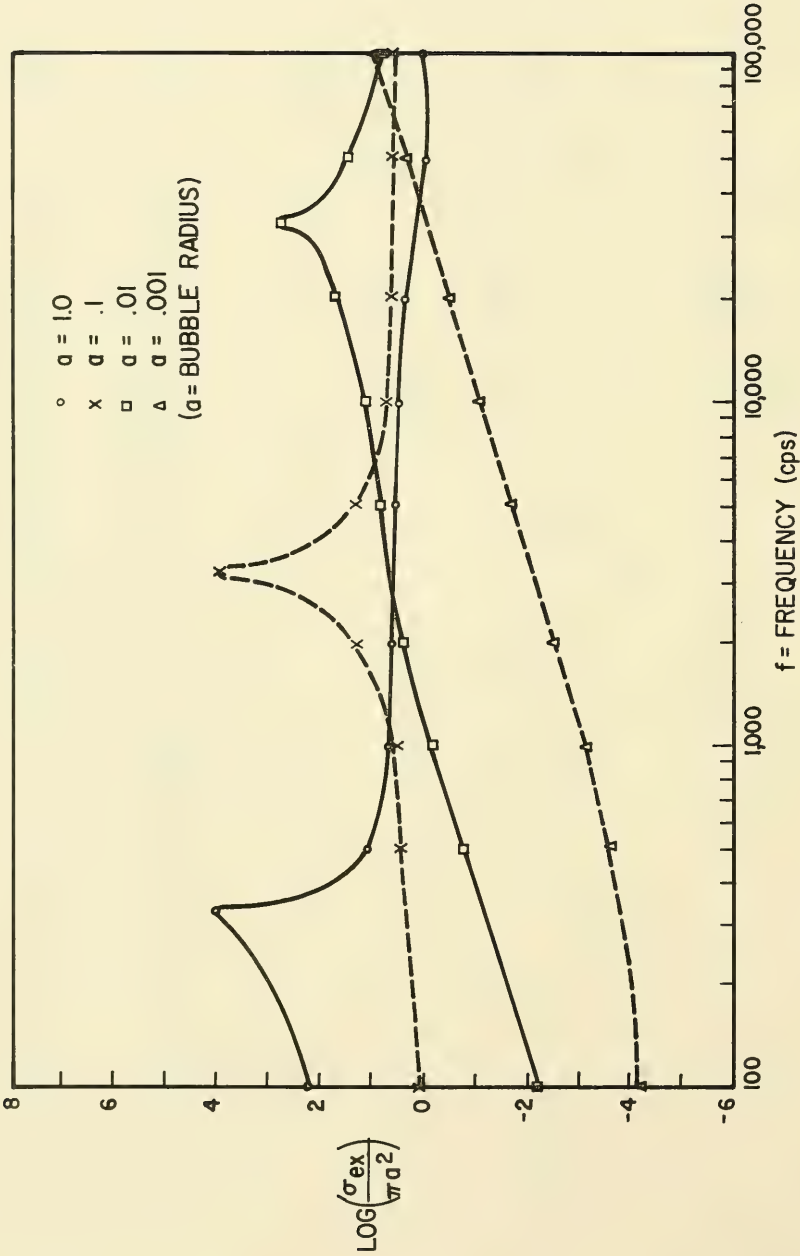


FIGURE III-12 RATIO OF EXTINCTION CROSS SECTIONS TO GEOMETRIC CROSS SECTIONS

### Multiple Scattering

In most regions of the ocean, the density of air bubbles is very low. Usually the spacing between air bubbles is so great that, when a sound wave passes through the medium, the scattered spherical wave from any one bubble is negligible compared to the sound field by the time the scattered wave reaches the bubbles nearest to it. In this situation, each bubble scatters the incident wave, and multiple scattering can be ignored. If there are  $n$  bubbles per unit volume, each with extinction cross section  $\sigma_e$ , the total extinction cross section per unit volume will be  $n\sigma_e$ . A sound wave progressing in the  $x$ -direction with intensity  $I(x)$  will be attenuated according to  $\frac{dI}{dx} = -n\sigma_e I$ ; therefore,  $I(x) = I(0)e^{-n\sigma_e x}$ . The scattered energy will be in the form of many incoherent spherical wavelets, and attenuation of the sound wave will be the dominant phenomenon.

Occasionally there are regions of relatively high air-bubble density, amounting to a fractional volume of air of perhaps up to  $10^{-3}$ . We have already mentioned certain regions of high air-bubble density such as fresh wakes, schools of fish with air bladders, or patches immediately under the ocean surface due to rain and spray. If the fractional volume of air is  $10^{-3}$ , the bubble spacing must average on the order of  $16a$  (where  $a$  is, as usual, the bubble radius). We have noted earlier that the sound frequency at which a bubble is resonant corresponds to a wave number  $k_0$  such that  $(k_0 a)^3 = 3gh^3 \approx 1.5 \times 10^{-4}$ , so that the resonant wavelength is approximately  $\lambda_0 \approx 500a$ . With a fractional volume of air of  $10^{-3}$ , we therefore find that a resonant wavelength measures approximately 30 bubble spacings. Under these circumstances, we may expect the sum of the amplitudes of the scattered wavelets arriving at a bubble from its nearest neighbors to be of the same order of magnitude as the wavelet the bubble scatters itself--for a bubble may have some 10 nearest neighbors, which are 10 to 20 bubble radii removed from it and all more or less in phase with it (since there are  $\pm 30$  bubble spacings to a wavelength). Near resonance, the amplitude of the scattered wave at the bubble surface  $\frac{1}{a} |p_{sc}|$  tends to be an order of magnitude greater than the amplitude  $|p_{inc}|$  of the "incident" wave. This may be seen from Figure III-9, which gives the damping constant at resonance. At resonance, we see from Table III-1 that  $\frac{1}{a} |p_{sc}| = |p_{inc}|/\delta$ . But, from Figure III-9, we see that  $\delta$  is typically between 0.01 and 0.2 for frequencies between 100 cps and 10,000 cps, which proves the above assertion.

In the immediate neighborhood of each bubble, therefore, the bubble's own scattered wave is of the same order of magnitude as the sum of the scattered waves received from neighboring bubbles, and an order of magnitude greater than the "incident" wave. However, since the bubbles and the bubble spacing are much smaller than a wavelength, we might expect the medium to exhibit some more or



less homogeneous cooperative behavior in transmitting (and attenuating) a sound wave. In other words, we might hope that the medium, viewed macroscopically, could sustain an over-all wave motion even though microscopically (i.e., on the scale of the individual bubbles) the local field would be anything but a simple attenuating plane wave.

Suppose, therefore, that plane waves of the form  $e^{ikx-i\omega t}$  could propagate in such a medium. The "wave number"  $k$  must now be complex; its real part corresponds to the phase velocity of the motion (which is not going to be  $c_0$ ), and its imaginary part gives the attenuation of the wave amplitude.

There should be a corresponding complex sound velocity  $c = \frac{\omega}{k}$ . How do we determine  $c$ ?

Consider an element of volume,  $V_0$ , which is fairly large compared to a bubble spacing but fairly small compared to a wavelength (say three bubble spacings as a typical dimension). Let  $\rho_0$ , which is the density of the water, also be the density of the mixture--the error will be very small when the fractional volume of air is approximately  $10^{-3}$ . Let the bubble density be  $n$  bubbles/cm<sup>3</sup>, so that there are  $N = nV_0$  bubbles in  $V_0$ . To begin with, let all bubbles have the same radius  $a$ ; later we shall study the case where there is a distribution of bubble sizes.

Suppose an (average) pressure wave is passing through the medium. The volume element  $V_0$  is sufficiently small that we may think of the (incident) overpressure as homogeneous throughout  $V_0$ , and represented by  $\Delta p(t) = \Delta p e^{-i\omega t}$ . As a result of this macroscopic sound wave, the volume of the element changes according to  $\Delta V(t) = \Delta V e^{-i\omega t}$  and its density according to  $\Delta \rho(t) = \Delta \rho e^{-i\omega t}$ . Conservation of mass of the element requires that  $\rho_0 V_0 = (\rho_0 + \Delta \rho)(V_0 + \Delta V)$  so that to first order

$$\Delta \rho = - \Delta V \left( \frac{\rho_0}{V_0} \right)$$

If the "applied" pressure  $\Delta p$  causes a density change  $\Delta \rho$ , the sound velocity in the mixture is given by:

$$c^2 = \frac{\Delta p}{\Delta \rho} = - \frac{\Delta p}{\Delta V} \left( \frac{V_0}{\rho_0} \right) \quad (\text{III-30})$$

The variations in the volume  $\Delta V$  consist of two parts--the change in water volume  $\Delta V_w$  and the change in the air volume  $\Delta V_a$ . Therefore,

$$\Delta V = \Delta V_w + \Delta V_a \quad (\text{III-31})$$

Let us examine  $\Delta V_a$  and see how it depends on  $\Delta p$ . Note that  $\Delta V_a$  is just the sum of the volume changes of each of the  $N = n V_o$  bubbles in  $V_o$ . Now, whereas the macroscopic picture is that of a sound wave,  $\Delta p(x,t) = \Delta p_o e^{ikx-i\omega t}$ , propagating through the mixed medium, the microscopic picture is quite different. As a result of  $\Delta p$ , each bubble is caused to pulsate. Suppose the internal pressure inside the bubble is caused to vary as  $\Delta p'(t) = \Delta p' e^{-i\omega t}$ , and suppose further that

this gives rise to a scattered wave,  $\Delta p(t) = \Delta p_{sc} \frac{e^{ik_o r}}{r} e^{-i\omega t}$  (where  $k_o = \frac{\omega}{c_o} =$  wave number in pure water and  $r$  is measured from the bubble center), in the

vicinity of each bubble. Near resonance, both  $\Delta p'$  and  $\frac{\Delta p_{sc}}{a}$  are much greater than  $\Delta p$ . However, we know from Table III-1 that  $\Delta p_{sc}$  is proportional to  $\Delta p$  according to:

$$\Delta p_{sc} = g(a) \Delta p \quad \text{where} \quad g(a) = \begin{cases} \left( \frac{a}{\left( \frac{\omega_o}{\omega} \right)^a - 1 - i\delta} \right) & \text{for models II, III} \\ \frac{a}{1 - \left( \frac{\omega}{\omega_o} \right)^a - i\delta} & \text{for model I} \end{cases} \quad (\text{III-32})$$

We also note from (III-29) that the internal pressure  $\Delta p'$  is proportional to the scattered pressure  $\frac{\Delta p_{sc}}{a}$ , and in fact near resonance almost equal to it:

$$\Delta p' = \Delta p_{sc} \frac{3 \gamma p_o}{\omega^2 \rho_o a^3} (1 - ika) e^{ika} = \frac{\Delta p_{sc}}{a} \left( \frac{\omega_o}{\omega} \right)^a (1 - ika) e^{ika} \quad (\text{III-29a})$$

Hence, if we substitute (III-32) in (III-29a) and ignore terms of order  $(ka)^2$ , we find that the internal pressure  $\Delta p'$  is proportional to  $\Delta p$ :

$$\Delta p' = \frac{3\gamma p_o g(a)}{\omega^2 \rho_o a^3} \Delta p = \left( \frac{\omega_o}{\omega} \right)^2 \frac{g(a)}{a} \Delta p \quad (\text{III-33})$$

Since we know the variation in internal pressure, we can calculate the variation in volume of each bubble. The undeformed bubble has a volume  $V_b = \frac{4}{3} \pi a^3$ ; when its internal pressure is changed adiabatically from  $p_o$  to  $p_o + \Delta p'$ , its volume must change so as to keep  $pV^\gamma$  constant, so that:

$$\Delta V_b = - \frac{V_b}{\gamma} \frac{\Delta p'}{p_o}$$

The total change in the volume of air  $\Delta V_a$  is therefore (using Equation III-33):

$$\Delta V_a = N \Delta V_b = - \frac{NV_b \Delta p'}{p_o \gamma} = - \frac{3g(a)NV_b}{\omega^2 \rho_o a^3} = - \frac{4\pi n V_o g(a)}{\omega^2 \rho_o} \Delta p \quad (\text{III-34})$$

We can now evaluate the complex velocity of propagation  $c$  according to (III-30). It is a little easier to compute its inverse:

$$c^{-2} = - \frac{\rho_o}{V_o} \frac{\Delta V}{\Delta p} = - \frac{\rho_o}{V_o} \frac{\Delta V_w}{\Delta p} - \frac{\rho_o}{V_o} \frac{\Delta V_a}{\Delta p}$$

The first of the two terms on the right is seen to be the inverse square of the sound velocity in pure water,  $c_o^{-2}$ ; the second term may be simplified by using (III-34). Therefore, we find

$$c^{-2} = c_o^{-2} + \frac{4\pi n g(a)}{\omega^2 a} \quad (\text{III-35})$$

This is the fundamental result for bubble-water mixtures with substantial bubble-bubble interaction: a sound wave in such a medium propagates with an effective velocity of propagation given by the real part of  $c$ , and an effective attenuation given by the imaginary part of  $k = \frac{\omega}{c}$ .

A few comments are in order about this result. First, the same result may be obtained by a somewhat more rigorous method which considers in detail the combined effect of the many scattered wavelets. The method, due to Foldy, is given in Appendix B. Second, several authors have obtained (III-35), and all use the form of  $g(a)$  which corresponds to Models II and III. Meyer and Skudrzyk derived a slightly different expression, which caused them to use the mechanical analog (Model I) form of  $g(a)$ . In their paper they use  $\frac{\Delta p_{sc}}{a}$  as the total pressure on the air bubble, instead of  $\Delta p'$ . We see from (III-29) that this would lead to a result which differs from ours by a factor  $\left(\frac{\omega_o}{\omega}\right)^2$ , and indeed they obtain  $c^{-2} = c_o^{-2} + \frac{4\pi n g(a)}{\omega_o^2}$  instead of (III-35). However, since they choose Model I for  $g(a)$ , they introduce a compensating factor of  $\left(\frac{\omega}{\omega_o}\right)^2$ , and their end result is therefore equivalent to that of other authors, provided their damping constant is properly interpreted.

Equation III-35 is easily modified to take into account a bubble population which consists of different size bubbles. Suppose there are  $n(a)da$  bubbles per unit volume each, with radius in the range between  $a$  and  $a+da$ . The contribution of this portion of the bubble population to the change in total air volume would be identical to that of (III-34) but with  $n$  replaced by  $n(a)da$ . The total change in air volume is then found by integrating over  $da$ , and this therefore modifies the final result for  $c^{-2}$  to:

$$c^{-2} = c_o^{-2} + \frac{4\pi}{\omega_o^2} \int da n(a) g(a) \quad (III-36)$$

From (III-35) or (III-36) we can compute the relative sound speed in the bubbly mixture as the real part of  $\frac{c_o}{c}$ , and the attenuation of the intensity (which is twice the attenuation of the pressure) as twice the imaginary part of  $\frac{\omega}{c}$ . In particular, we may write (III-35), using the Model III expression for  $g(c)$  as:

$$\begin{aligned}
 \left( \frac{c_o}{c} \right)^2 &= 1 + \frac{4\pi n c_o^2}{\omega^2} \frac{a}{\left( \frac{\omega_o}{\omega} \right)^2 - 1 - i\delta} \\
 &= 1 + \frac{4\pi n c_o^2 a}{\omega^2} \left\{ \frac{\left( \frac{\omega_o}{\omega} \right)^2 - 1 + i\delta}{\left[ \left( \frac{\omega_o}{\omega} \right)^2 - 1 \right]^2 + \delta^2} \right\} = 1 + x + i y
 \end{aligned}
 \tag{III-37}$$

A little algebra leads readily to:

$$\begin{aligned}
 \left[ \operatorname{Re} \left( \frac{c_o}{c} \right) \right]^2 &= \left[ \frac{c_o}{\text{mixture sound velocity}} \right]^2 \\
 &= \frac{1+x}{2} \left[ 1 \pm \sqrt{1 + \frac{y^2}{(1+x)^2}} \right]
 \end{aligned}
 \tag{III-38a}$$

$$\begin{aligned}
 \left[ 2I_m \left( \frac{\omega}{c} \right) \right]^2 &= \left[ \text{intensity attenuation} \right]^2 \\
 &= 2 \left( \frac{\omega}{c_o} \right)^2 (1+x) \left[ -1 \pm \sqrt{1 + \frac{y^2}{(1+x)^2}} \right]
 \end{aligned}
 \tag{III-38b}$$

We can compare these results with the limiting case of very low air bubble densities. This means that  $x$  and  $y$  are both much less than 1, so that (III-38b) yields:

$$\text{intensity attenuation} \simeq \frac{\omega}{c_o} y = \frac{4\pi n c_o a \delta / \omega}{\left[ \left( \frac{\omega_o}{\omega} \right)^2 - 1 \right]^2 + \delta^2}$$

From Table III-2 we note that this is precisely  $n\sigma_e$  (for either Model II or Model III), as we would expect.

### Experimental Evidence

The expressions for the phase velocity and attenuation are generally in good agreement with experiment. In particular, we have the following body of experiments:

(1) Meyer and Skudrzyk (Ref. III-29) calculated the theoretical attenuation for uniform bubble mixtures which were resonant at 12 kc and for a mixture having a uniform distribution of bubble sizes. These agreed qualitatively quite well with experimental results.

(2) Carstensen and Foldy (Ref. III-3) measured attenuation and reflection for a bubble screen in a lake. Screens of both constant and varying bubble sizes were used. The results agreed qualitatively with the theory. The mixtures were generally resonant at 15 kc.

(3) Laird and Kendig (Ref. III-19) measured attenuation in a bubble screen having various sizes of bubbles. Although the reported results appear to be in good agreement with the theory, the nature of the experiment was such that there may be considerable error in the results. The screen as a whole was resonant at 8 kc.

(4) Fox, Curley and Larson (Ref. III-9) measured phase velocities and attenuation for a bubble screen resonant at 60 kc. The results agreed quantitatively with the theory.

(5) Macpherson (Ref. III-26) measured attenuation for a very carefully controlled, almost idealized, bubble screen. The bubbles were all of the same size and were resonant at 30 kc. The results agreed very well with the theory.

(6) Silberman (Ref. III-37) measured attenuations and phase velocities for screens which were resonant in the range 1 kc to 10 kc. The results generally agreed well with the theory.

The net result is that the theory for propagation of sound through an air bubble-water mixture is well supported by experimental work. Deviations from the theory can usually be explained by experimental conditions or improper use of a parameter, such as the damping constant, in comparing the theory with measurements. The following gives details on the experimental work.



Meyer and Skudrzyk made certain calculations of the expected attenuation and phase velocities for sound passing through water interspersed with air bubbles. For their calculations they used a damping constant given by

$$\delta = \left[ 0.015 + 11 \times 10^{-6} f_0 \right] \frac{f_0}{f}$$

where  $f_0$  is the resonant frequency of the bubble. This expression is based on the experimental work of Meyer and Tamm; however it gives damping constants which are larger than those given by other theories and found in other work, as may be seen by comparison with Figure III-9. As a result, many of Meyer and Skudrzyk's theoretical attenuation figures may be too high.

Figure III-13a shows the theoretical sound damping (in db/cm) as a function of the frequency, for a screen of gas bubbles which are all roughly the same size and have a resonant frequency of 12 kc. The radii of the bubbles are approximately 0.026 cm. The parameter is the relative gas content (by volume), which, in this graph, ranges from  $10^{-6}$  to  $10^{-2}$ . The strongest damping takes place at the resonant frequency. The curves are symmetrical for small gas content and unsymmetrical for large; thus the higher frequencies are more strongly influenced. The maximum damping is 0.3 db/cm at a gas concentration of  $10^{-6}$  and 95 db/cm at  $10^{-2}$ . This means that for the first example approximately one air bubble occurs per  $100 \text{ cm}^3$ , while in the second case approximately 100 bubbles occur in  $1 \text{ cm}^3$ .

Figure III-13b shows the calculated phase velocity of the bubble-water mixture for three concentrations, with the bubbles resonant at 10 kc. The velocity in the bubble-free medium  $c_0$  was taken as 1400 meters/sec.

An experimental screen of fairly uniform bubbles was created by forcing air through a porous plate. The results of attenuation measurements for such screens are shown in Figure III-13c. A number of screens corresponding to different volume concentrations were generated by varying the input rate of air from 160 to 500 liters per hour. The resonant frequency of the bubbles appears to be approximately 15 kc. The measured curves for the various quantities agree qualitatively with the theoretical curve of Figure III-13a.

When the diameters of the gas bubbles are distributed over a sizable range, we must use the integral form of the theory. As a special case, Meyer and Skudrzyk consider a screen made up only of bubbles whose resonant frequencies lie between 10 kc and 100 kc, i.e., bubbles whose radius lies between 0.033 cm and 0.0033 cm. In this band, the volume concentration,  $v$ , of the bubbles was taken to be constant; thus, there are very few large bubbles, but very many small ones. Figure III-14 shows the sound damping under these conditions, as a function of frequency.

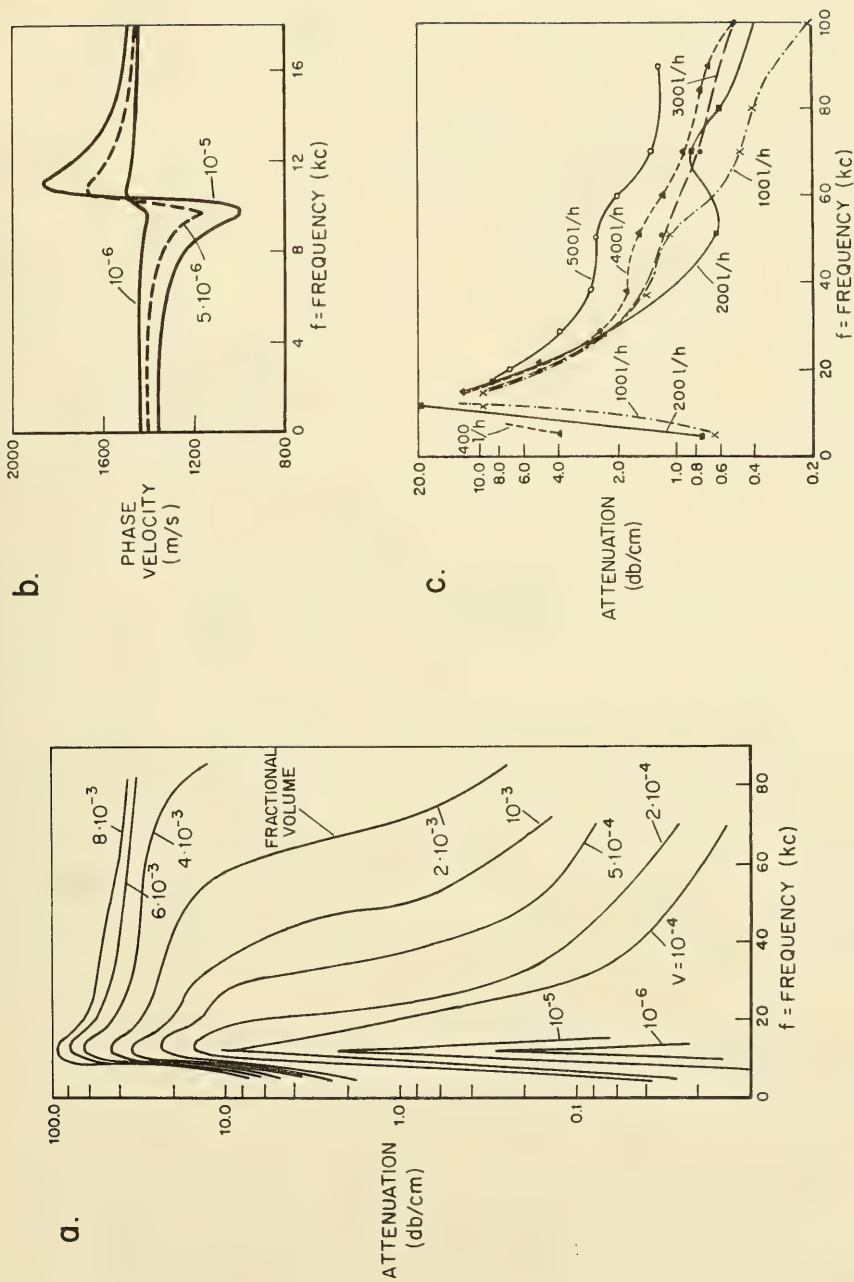


FIGURE III-13 ATTENUATION AND PHASE VELOCITY IN SCREENS WITH UNIFORM BUBBLE SIZES  
(AFTER MEYER AND SKUDRZYK)

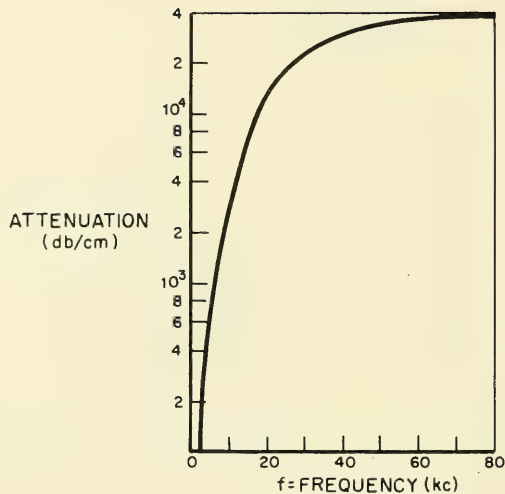


FIGURE III-14 THEORETICAL ATTENUATION THROUGH A BUBBLE SCREEN WITH A DISTRIBUTION OF BUBBLE SIZES (AFTER MEYER AND SKUDRZYK)

Figure III-15 illustrates examples of damping measured on screens generated by electrolysis. Physical observation showed immediately that, in this case, no uniform bubble mixture was present; rather, very small bubbles of different sizes arose, together with a few large bubbles. Comparison of the curves for Figures III-15a, b, and c, with Figure III-14 shows great similarity. In fact, it is possible in both figures to connect the measured points of a series of measurements for a fixed current density directly by a calculated curve, as shown for the curves in Figure III-15a and Figure III-15b for 60A and 15A respectively. The gas concentrations on which these calculations were based are  $4.8 \times 10^{-5}$  and  $9.2 \times 10^{-5}$ , very close to the concentrations expected from a study of the electrolytic process.

It should also be pointed out that in the electrolysis experiments Meyer and Skudrzyk used the damping constant for air, although measurements were actually made on hydrogen bubbles.

Carstensen and Foldy made a series of measurements on the attenuation of sound through a screen of bubbles and the amount of reflection from such a screen. The measurements were made under two classes of screen conditions: relatively few bubbles in the screen but all of essentially the same radius, and relatively large numbers of bubbles having a considerable range of radii. The device which produced the bubbles was suspended 10-1/2 feet below the surface of a lake and produced a

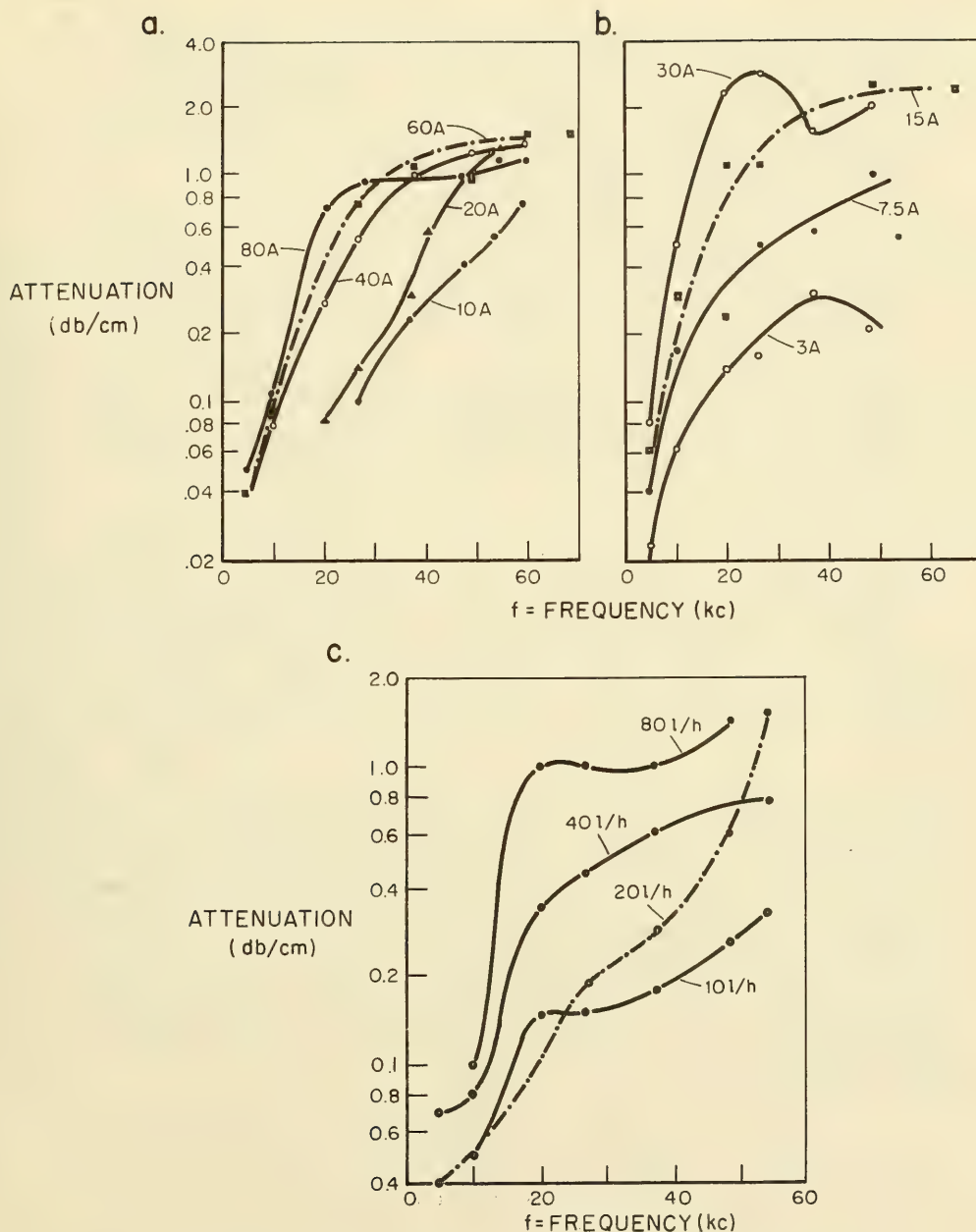


FIGURE III-15 OBSERVED ATTENUATION THROUGH BUBBLE SCREENS WITH A DISTRIBUTION OF BUBBLE SIZES (AFTER MEYER AND SKUDRZYK)

screen of bubbles having a cross section of about 17 inches by 3 - 6 inches extending various lengths in the vertical direction, depending on the experimental conditions. The incident waves were in a direction which made an angle of 35 degrees with the normal. A reflection and transmission hydrophone were placed on opposite sides of the screen in mirror image position; thus, reflection and transmission could be measured simultaneously.

Bubbles were allowed to rise either uniformly or in short pulses. In the latter case, differing rates of rise for different bubble sizes separated the pulse so that at any one time all the bubbles on the acoustic axis would have approximately the same radius. Bubble radii and rates of rise were measured by determining the resonance frequency and elapsed time from the time the pulse was released. This data was then used to determine distributions of bubble sizes and the amount of air entrained in bubbles for various screen conditions. Typical data is shown in Figure III-16. Note in particular the small amount of air in the bubbles and the smaller number of bubbles on the axis at any one time for the pulses relative to the continuous release.

The experimental data was compared with the theory. To obtain theoretical values for the reflection coefficient, it was necessary to consider specific wave forms. These were taken as configurational averages, in the sense of Foldy's theory. Except for reflection, only the coherent terms were considered. In order to simplify the expressions, several assumptions were made concerning bubble distribution and the complex propagation constant. The net result is that the expressions used to calculate theoretical results are several approximations removed from the already approximate expressions of Foldy's theory.

Very few experimental results are presented. Those that are given show a fairly good correspondence between theory and experiment for the screens of essentially uniform bubble size. For such screens, attenuations and reflections were measured at frequencies corresponding to the theoretical resonance frequency of the bubbles along the acoustic axis at the time the sound was transmitted. Figures III-17a and III-17b illustrate the results obtained, giving a comparison of the theoretical and observed values. An estimate for the probable error is indicated for the experimental points. Carstensen and Foldy remark that the agreement between observed and calculated values "must be considered highly satisfactory in view of the difficulties of measurement and the approximations made in the theory."

The results of measurements of attenuation and reflection for continuous-flow screens are illustrated in Figures III-17c and III-17d. In the case of attenuation, the maximum measurable attenuation, due to equipment limitations, is also shown. The theoretical and experimental agreement here is not very satisfactory. A partial explanation for the reflection results possibly lies in the approximation that the screen has sharp boundaries. In the experiments, there was



actually a fairly sharply defined core of larger bubbles in the middle with a gradually tapering distribution of smaller bubbles in the front and back. In the case of attenuation, the equipment limitations make a good comparison of theory and experiment difficult.

The Laird and Kendig experiments were designed to confirm, if possible, the very high attenuations predicted by Foldy's theory. In order to eliminate the effect of a reflected beam, both the projecting and receiving transducers were placed in the bubble field and measurements were made for various separations of the transducers. A bubbly medium with a 2- by 6- foot cross section was produced by forcing air through a taffeta screen located 12 feet below the surface of a lake.

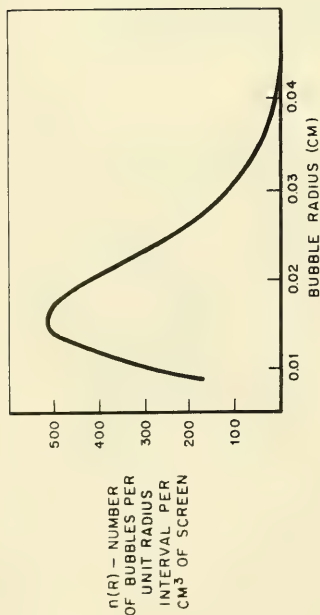
Measurements of the attenuation were made at frequencies ranging from 2 kc to 16 kc, and with the transducers separated by 1-1/2, 3, 4-1/2, and 6 inches. Figure III-18 illustrates the data obtained. The vertical lines represent maximum fluctuations and the horizontal mark is an estimated average. The random fluctuations in the bubble distribution caused the attenuation to vary by as much as 40 db over a 10 second interval.

For each frequency, the attenuation (in db per inch) was obtained by plotting the attenuation data for the various separations, with the separation distance along the x-axis and the attenuation (in db) along the y-axis. If the data lie along a straight line, then the attenuation follows an exponential law, and the slope of the line gives the attenuation in db per inch, which is then independent of the separation. Laird and Kendig remark that the data did not lie perfectly along a straight line and that a "certain amount of judgment" was used in fitting the straight lines.

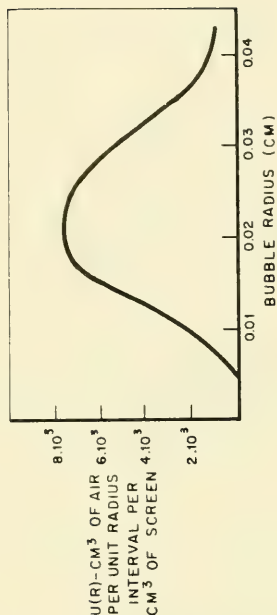
The data were analyzed in terms of Model III, by a procedure paralleling that of Carstensen and Foldy. Again, only the first coherent term was considered. The expected and observed attenuations are compared in Figure III-19.

The bubble screens contained many different bubble sizes; consequently it was necessary to use the integral representations for the complex propagation constant. The experimental data for bubble distribution,  $n(R)$ , and bubble volume ratio,  $u(R)$ , were well fitted by the distributions shown in Figure III-20. These give the modal value of the number of bubbles per  $\text{cm}^3$  as 0.89 and the bubble volume ratio  $4.5 \cdot 10^{-4}$ . The Poisson distributions were used in calculating the necessary integrals. Note that the resonant frequency of the bubbles corresponding to the maximum value of  $u(R)$  is 6 kc, while that for bubbles corresponding to the maximum of  $n(R)$  is 8.8 kc.

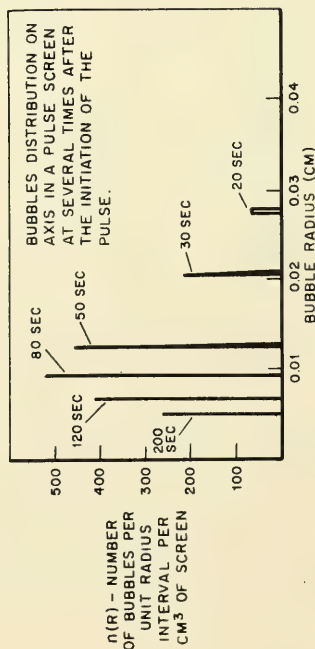




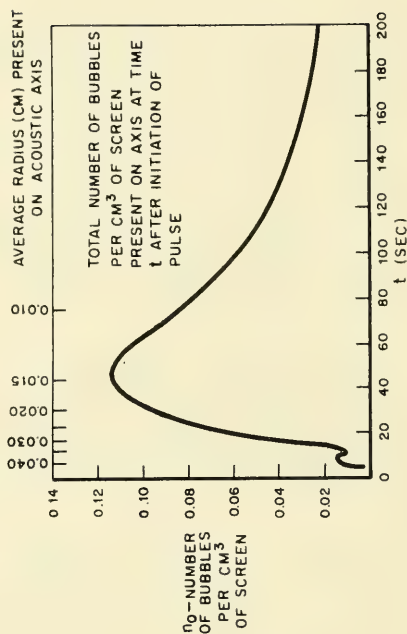
a. BUBBLE DENSITY IN CONTINUOUS-FLOW SCREEN.



b. AIR DENSITY IN CONTINUOUS-FLOW SCREEN CORRESPONDING TO BUBBLE DENSITY SHOWN IN "c".

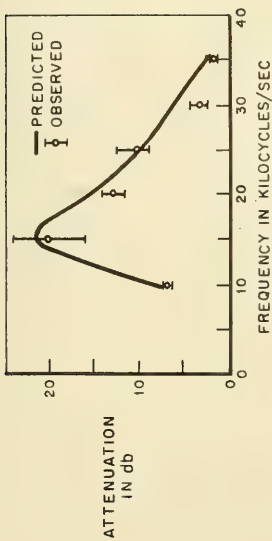


c. BUBBLE DENSITY IN PULSE SCREEN.

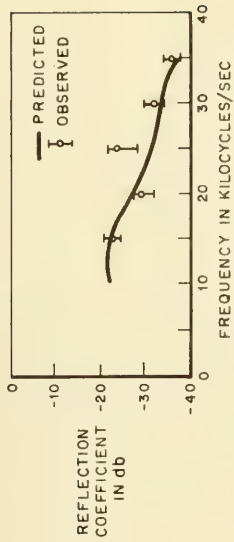


d. TOTAL NUMBER OF BUBBLES PER UNIT VOLUME IN PULSE SCREEN COMPUTED FROM DATA SHOWN IN "c".

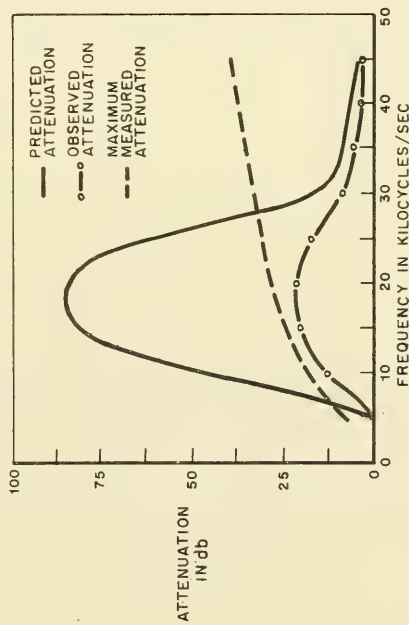
FIGURE III-16 STATISTICAL CHARACTERISTICS OF BUBBLE SIZES IN CONTINUOUS FLOW AND PULSED SCREENS (AFTER CARSTENSEN AND FOLDY)



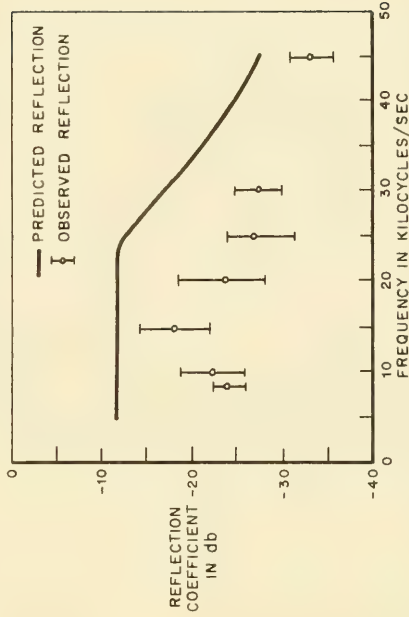
a. RESONANT ATTENUATION OF THE PULSE SCREEN  
(UNIFORM BUBBLE SIZE)



b. RESONANT REFLECTION OF THE PULSE SCREEN  
(UNIFORM BUBBLE SIZE)



c. ATTENUATION THROUGH CONTINUOUS-FLOW SCREEN



d. REFLECTION FROM CONTINUOUS-FLOW SCREEN

FIGURE III-17 ATTENUATION AND REFLECTION FROM PULSED AND CONTINUOUS FLOW BUBBLE SCREENS  
(AFTER CARSTENSEN AND FOLDY)

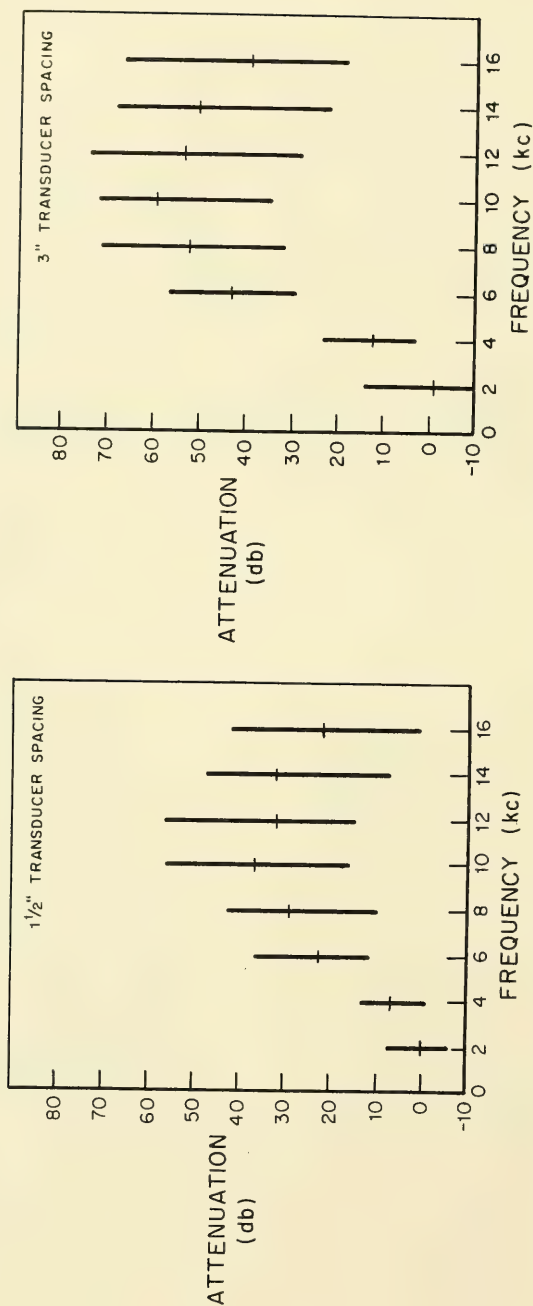


FIGURE III-18 TRANSMISSION MEASUREMENTS THROUGH CONTINUOUS FLOW SCREENS (AFTER LAIRD AND KENDIG)

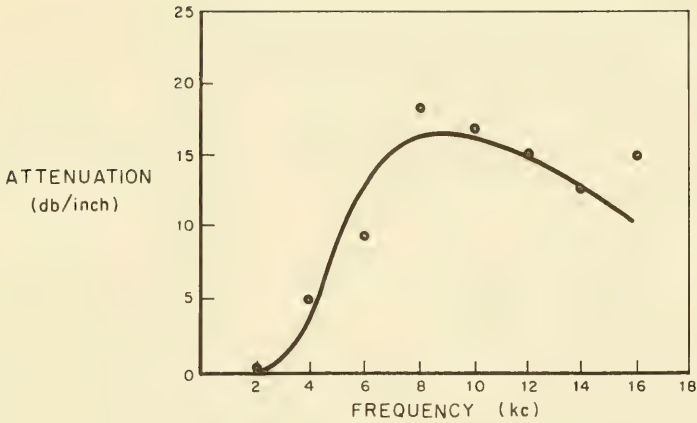


FIGURE III-19 THEORETICAL AND OBSERVED ATTENUATIONS (AFTER LAIRD AND KENDIG)

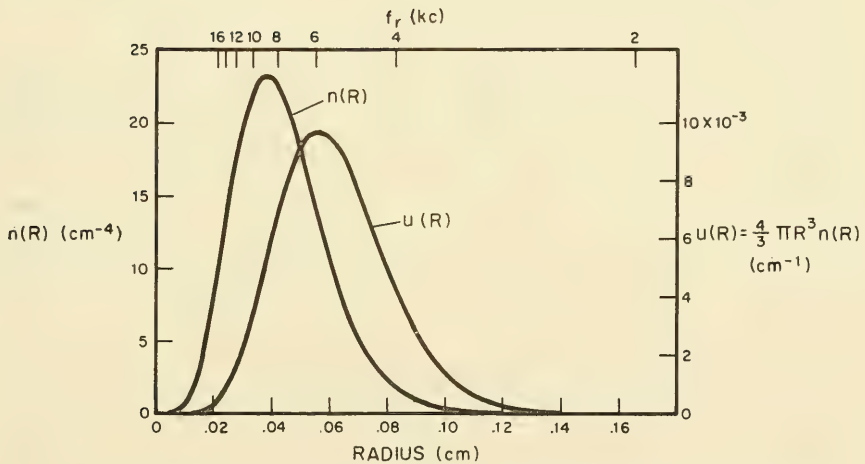


FIGURE III-20 DISTRIBUTION OF THE NUMBER OF BUBBLES AND FRACTIONAL VOLUME AS A FUNCTION OF BUBBLE RADIUS (AFTER LAIRD AND KENDIG)

The values of the damping constant used in these computations were those obtained by Carstensen and Foldy. Since no data was available for the damping constant at off-resonant frequencies it was assumed to depend only on the resonant frequency. In the light of other evidence, the damping constant used in these experiments seems high; however Laird and Kendig report that if at 12 kc  $\delta$  is assumed to be 0.06 instead of 0.12, the theoretical attenuation is increased by only 4%. Thus the attenuation is relatively insensitive to the damping constant.

Figure III-21 gives a plot of the computed values of the phase velocity. At low frequencies, this is about one-third that of bubble-free water, while at higher frequencies it approaches the velocity in bubble-free water. Some attempts were made to verify these phase velocities experimentally, but the wide fluctuations in phase and amplitude of the transmitted signal made this impossible. Measurements at frequencies above 50 kc were possible and showed that at these frequencies the phase velocity in bubbly water is "essentially the same" as that in bubble-free water.

Comparing Laird and Kendig's computed phase velocity with the calculations and measurements of Meyer and Skudrzyk and of Fox, Curley and Larson indicates that Laird and Kendig's peak phase velocity is much too high.

Fox, Curley, and Larson measured the behavior of the phase velocity and the absorption in bubbling water for various frequencies. A bubble screen was created by forcing air through a porcelain bacteriological filter. It was found that the large majority of the bubbles had radii in the range of  $0.012 \pm 0.004$  cm, and would, therefore, have resonant frequencies of approximately 60 kc. Figure III-22 shows a distribution of the air volume contained in bubbles of various sizes. The average volume was found to be  $(2 \pm 0.5) (10^{-4})$  cc of air per cc of water. In order to eliminate any boundary effects, the transducers were located in the bubble screen and separated by 2-1/2 cm.

In the analysis of the data, the damping constant  $\delta$  was taken as 0.5, although theoretically it should be 0.12. Such a large value of  $\delta$  was required in order to make the theoretical predictions correspond at all with experimental results.

The experiments are summarized in Figure III-23. The dashed lines represent the theoretical prediction when all bubbles are assumed to be of the same size, while the solid lines correspond to the integral forms of the theory and take into account the distribution of bubble sizes. The precision of phase velocity measurements is estimated to be within 5%, while the precision of attenuation experiments is within 2 db/cm. Each point represents an average reading.

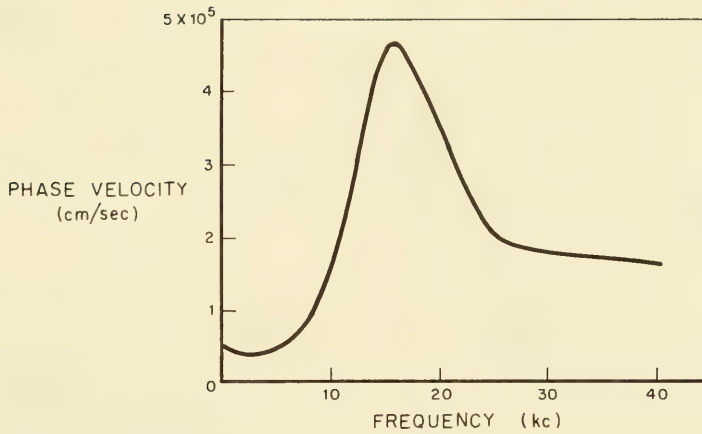


FIGURE III-21 THEORETICAL PHASE VELOCITY  
(AFTER LAIRD AND KENDIG)

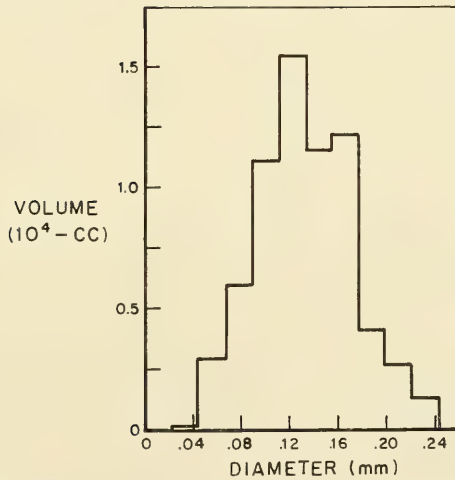
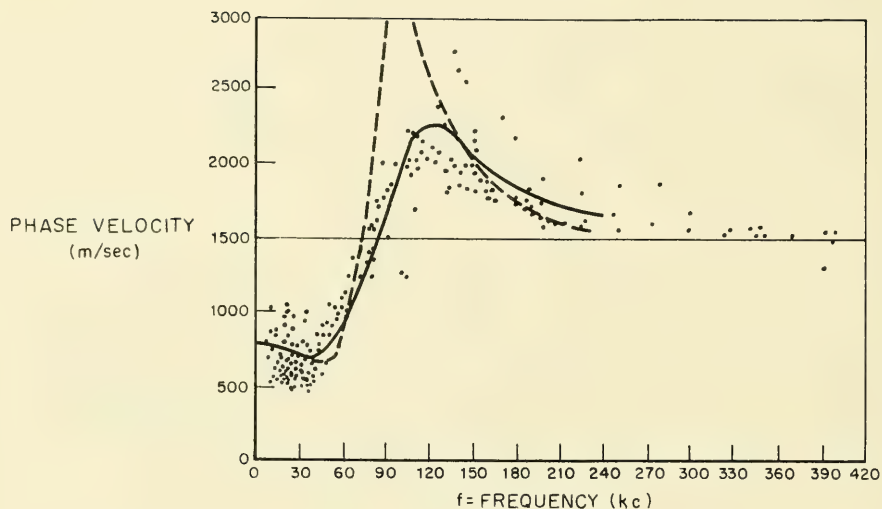
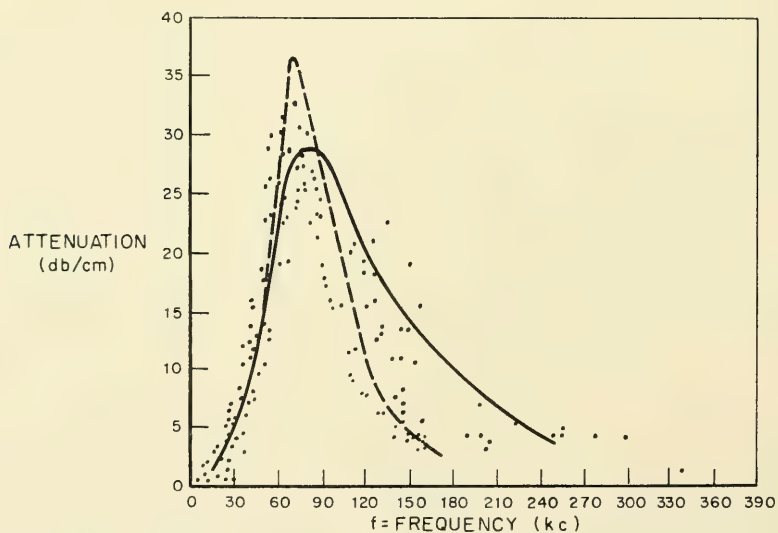


FIGURE III-22 DISTRIBUTION OF FRACTIONAL VOLUME  
FOR VARIOUS BUBBLE SIZES (AFTER FOX,  
CURLEY AND LARSON)





a. PLOT OF PHASE VELOCITY vs FREQUENCY SHOWING ALL OF THE RELIABLE DATA OBTAINED.



b. PLOT OF ABSORPTION vs FREQUENCY SHOWING ALL OF THE RELIABLE DATA OBTAINED.

FIGURE III-23 PHASE VELOCITY AND ATTENUATION THROUGH A SCREEN HAVING THE BUBBLE DISTRIBUTION OF FIGURE III-22 (AFTER FOX, CURLEY AND LARSON)

Macpherson's experiments involved measurements of reflection and attenuation through carefully controlled bubble screens having a large number of bubbles of uniform size and spacing. Bubbles were generated in a laboratory tank by electrolysis and had average radii of 0.008 to 0.025 cm, depending upon the electrode used. For any particular experiment, the standard deviation of the radius was approximately 7% of the mean. In a vertical plane, the screens had the form of one or more, essentially two-dimensional, slowly rising lattices. The lattice spacings ranged from about one bubble in  $10 \text{ cm}^2$  to 40 bubbles in  $10 \text{ cm}^2$ . Measurements were made for one-millisecond sound pulses with angles of incidence equal to  $0^\circ$  and  $45^\circ$ . The isonified area was  $15 \text{ cm}^2$ .

Theoretical values were calculated following the approach of Carstensen and Foldy. None of the incoherent terms were considered.

Figure III-24a shows the measurements and expected values of attenuation produced by a single bubble screen of approximately 4 bubbles per  $\text{cm}^2$ . As can be seen, the agreement with the theoretically predicted curves is good. The slight spread of the experimental points outside the theoretical curves is ascribed to the small nonuniformity of the bubbles. Similar results were obtained with other spacings. Macpherson measured the damping constant  $\delta$  at 30 kcps as  $0.080 \pm 0.003$ . This corresponds closely to the theoretical value of 0.082 and contrasts sharply with the poor agreement obtained by Carstensen and Foldy. Macpherson also mentions that the "frequency variation of  $\delta$  at resonance over the range 15-40 kc, and the off-resonant behavior were in close agreement with the theory."

For theoretical evaluations with more than one screen, it is assumed that the attenuation is strictly additive, with no interaction between the screens. This is justified by the fact that the spacing between screens is of the order of 4 cm, which corresponds to a wide spacing of bubbles and is analogous to the case in which the bubbles were widely spaced in the lattice. In this latter case, it was seen that the bubbles could be treated as independent scatterers, and by the same argument, the successive screens can be considered independently. Figure III-24c shows the result of placing two screens of slightly different bubble sizes one behind the other, separated by a distance of about 4 cm. As can be seen, the condition for no interaction is upheld inasmuch as the attenuation and phase shifts add algebraically. The steady state reflection measurements were made on screens similar to those used for transmission. The results for a screen of 4 bubbles per  $\text{cm}^2$  are shown in Figure III-25 and can be seen to agree very well with the theory.

To provide experimental justification for calculating the theoretical curves from the coherent term only, some measurements were made to show the presence of the incoherent wave system. It was possible to show that about 10 cm from a nearly resonant screen of 4 bubbles per  $\text{cm}^2$  the measured intensity of the incoherent component was of the order of magnitude given by the theory, namely about 12 db. Away from resonance or further away from the bubble screen, it was not possible to detect this component at all.

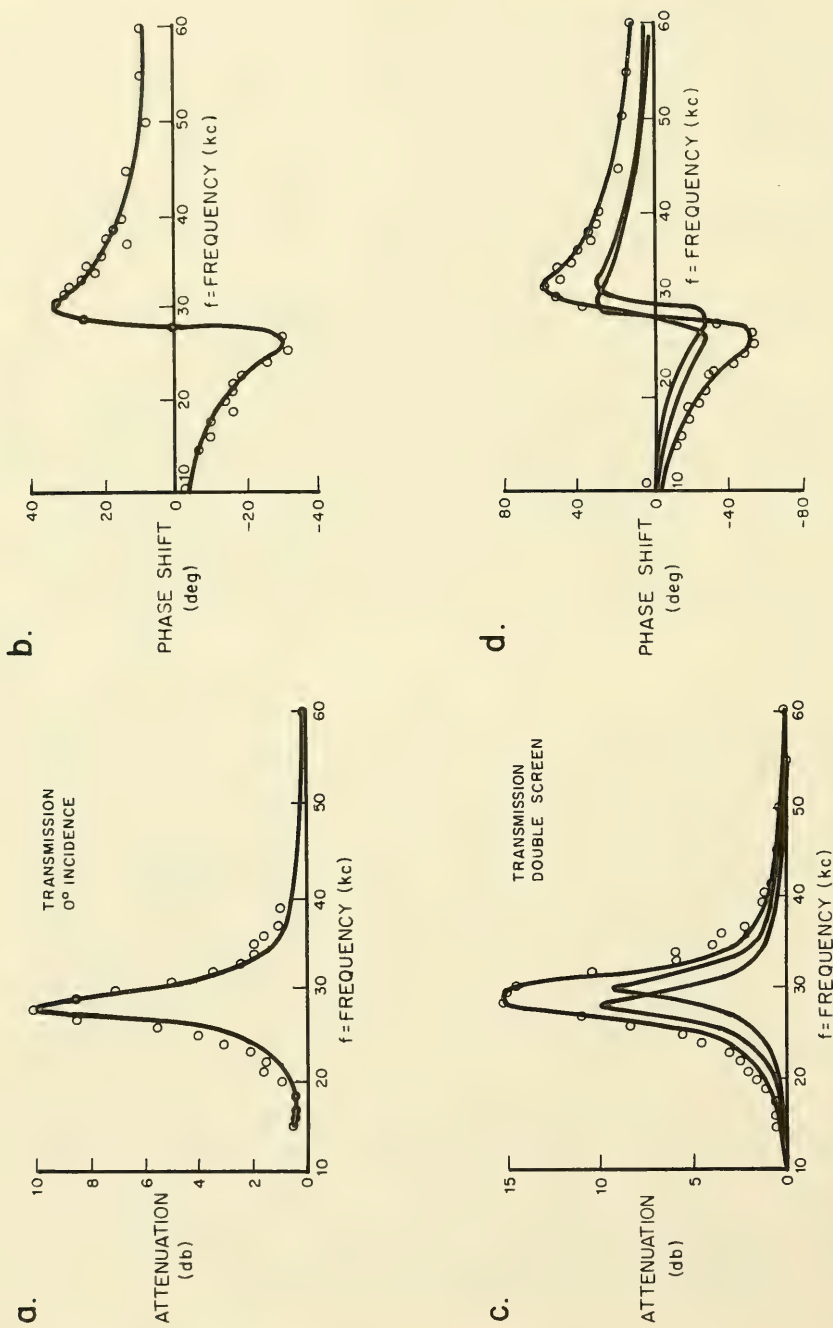


FIGURE III-24 ATTENUATION AND PHASE SHIFT THROUGH SINGLE AND DOUBLE LATTICE SCREENS AT NORMAL INCIDENCE

Silberman made measurements of phase velocity and attenuation for sound traveling through air bubble-water mixtures in vertical pipes. The pipes were made of steel with inside diameters of 2 and 3 inches and lengths of 8 and 6 feet, respectively. Because of the small pipe size and the frequencies used, the pipe diameter was less than half a wavelength; consequently the sound could be viewed as plane waves.

Two configurations of experimental equipment were used. In the first, the pipe was fastened to a base containing the sound generator, and bubbles were introduced by a tube through the base. In the second apparatus, the bottom of the tube was open, and the sound generator was supported independently. Bubbles were generated by a number of needle orifices positioned outside the tube. The entire apparatus was suspended in a water tank. Problems arising in bubble production were responsible for changing from the first apparatus to the second. With the first, there was considerable difficulty in obtaining bubbles of uniform size and spatial distribution.

Measurements were made by recording the pressure at various points along the tubes. For standing waves, the pressure at a point  $x$  is given by

$$p(x) = 2e^{-d\ell} \left[ \cosh^2 \alpha (\ell - x) - \cos^2 \frac{2\pi f}{c_0} (\ell - x) \right]^{1/2}$$

where

- $\alpha$  = attenuation constant
- $\ell$  = length of the column
- $f$  = frequency of the sound
- $c_0$  = velocity of sound

Using this equation and the pressure measurements, the experimental attenuation constant can be determined. Phase constants were determined by measuring the half wavelength distances between successive nodes or antinodes, and the phase velocity was calculated from the equation

$$c_0 = f \lambda$$

where  $\lambda$  is the measured wavelength. The effects of elasticity of the pipe wall and of viscosity were small enough to be neglected. Corrections were made to allow for the variation in hydrostatic pressure at various points along the tubes.

Typical velocity measurements obtained in one series of experiments are shown in Figure III-26. Bubble sizes for this series varied appreciably; however, no details are given. No information is given regarding the frequency, but since all velocities are less than that of sound in pure water, we can infer that the frequency was always less than the resonant frequency of any major fraction of the bubbles.

Comparisons are made with the predictions of the preceding theory and Wood's theory. The latter states that the velocity in a bubbly mixture is given by

$$\left( \frac{c_o}{c} \right)^2 = \left( 1 - v + \frac{v \rho_o c_o}{P_o} \right) \left( 1 - v + \frac{v \rho_o'}{\rho_o} \right)$$

where  $v$  is the volume of air per unit volume of mixture,  $\rho_o$  and  $\rho_o'$  are the density of the water and gas,  $c_o$  is the sound velocity in water, and  $P_o$  is the pressure (including atmospheric). The results agree well with both theories and indicate that:

(1) The phase velocity is relatively independent of the frequency when the incident frequency is less than the resonant frequency of a significant fraction of the bubbles.

(2) The phase velocity depends strongly on  $v$ , the fraction of air in the mixture, with the velocity  $c$  (in feet per second) being given roughly by

$$c = 100 (10v)^{1/2}$$

The results of more carefully controlled experiments are shown in Figure III-27. Here, phase velocity and attenuation are plotted as functions of frequency and are compared with theoretical values given by Equation III-38. The calculations were based on a single average bubble size ( $r$ ) and air concentration. No information on the variations in bubble size or air concentration was given. The figures are in order of decreasing concentration and decreasing bubble size. Each plotted point was obtained by averaging 2 to 14 separate determinations. Each experiment was made with a single bubble size, except for the experiment whose data are shown in Figure III-27d; this latter experiment was made with a mixture of two bubble sizes. Static pressure variation is accounted for by the separate theoretical curves for each mixture depth.

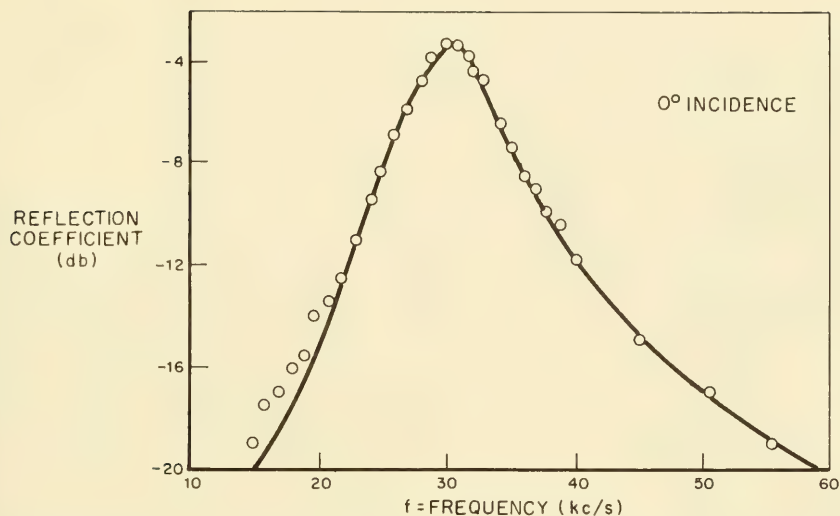


FIGURE III-25 REFLECTION OF NORMALLY INCIDENT SOUND FROM A SINGLE LATTICE SCREEN (AFTER MacPHERSON)

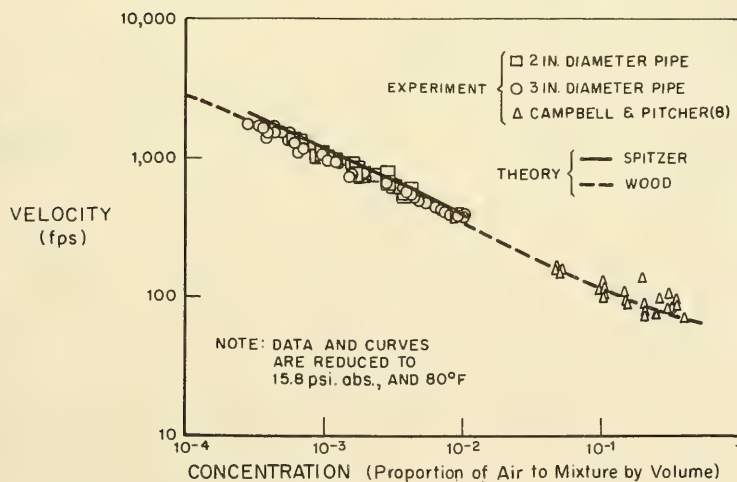


FIGURE III-26 PHASE VELOCITY IN AIR-WATER MIXTURES (AFTER SILBERMAN)



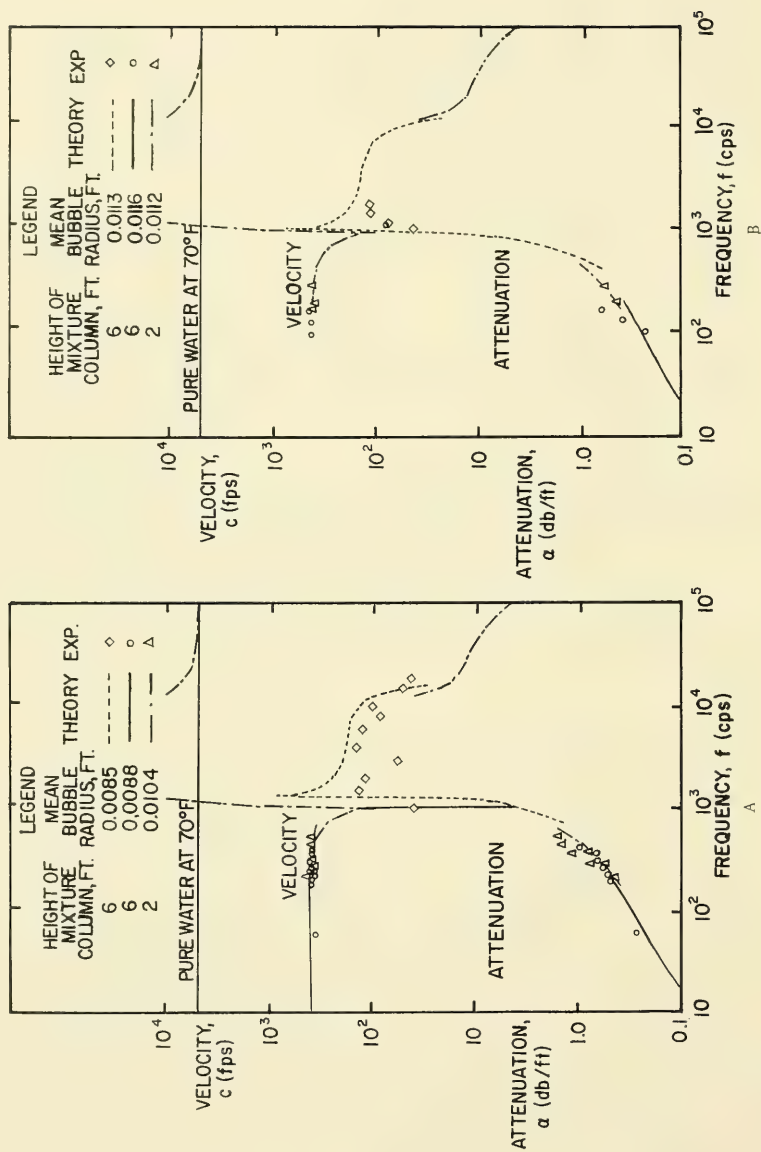


FIGURE III-27 PHASE VELOCITY AND ATTENUATION AS FUNCTIONS OF FREQUENCY AT VARIOUS CONCENTRATIONS AND BUBBLE SIZES

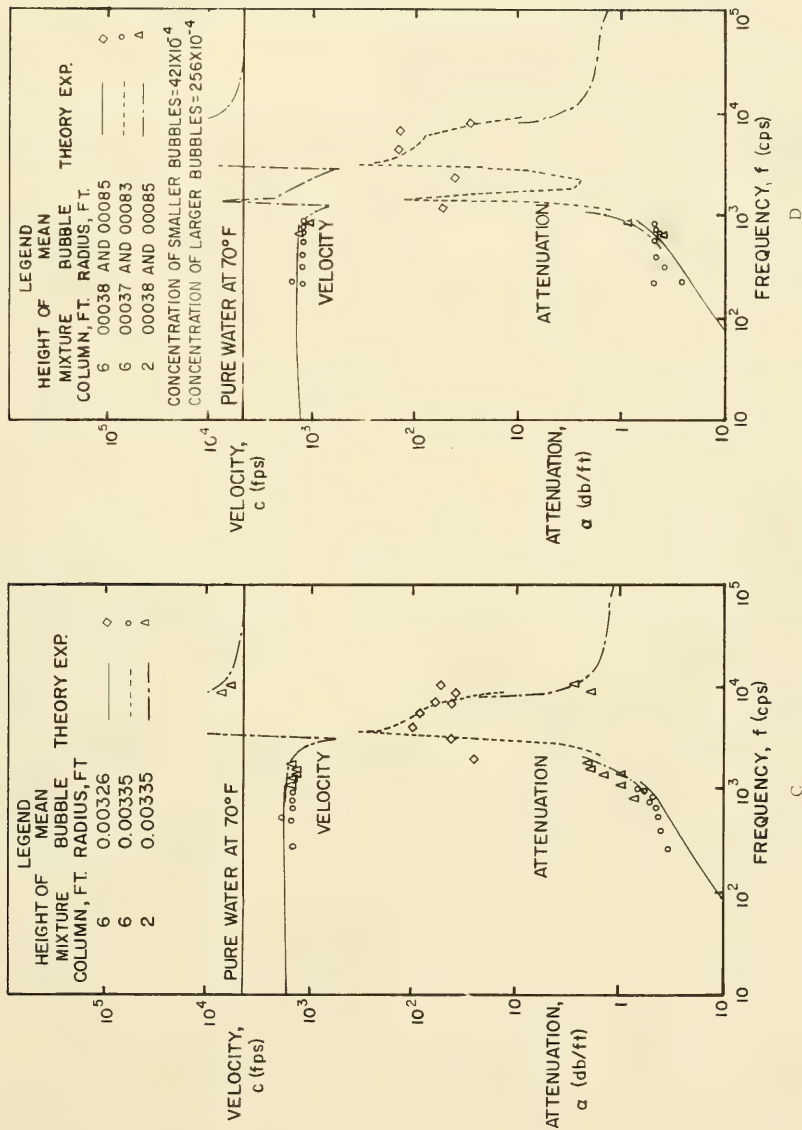
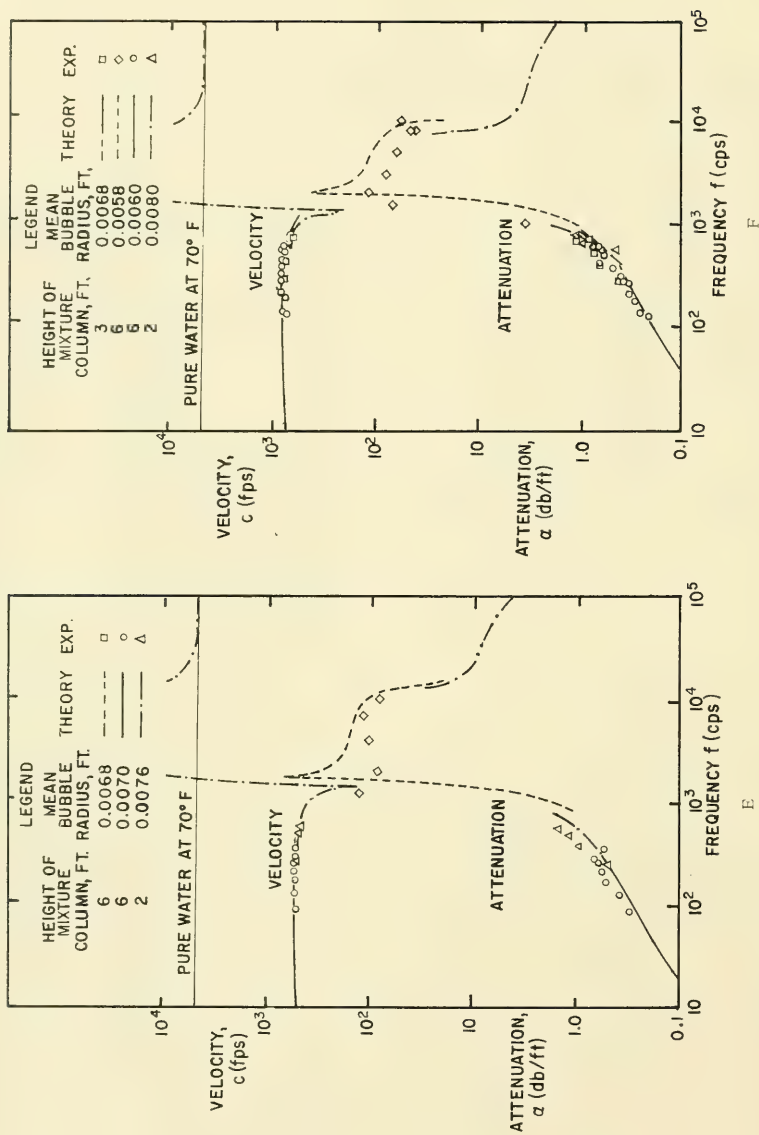


FIGURE III-27 CONTINUED



CONTINUED

FIGURE III-27

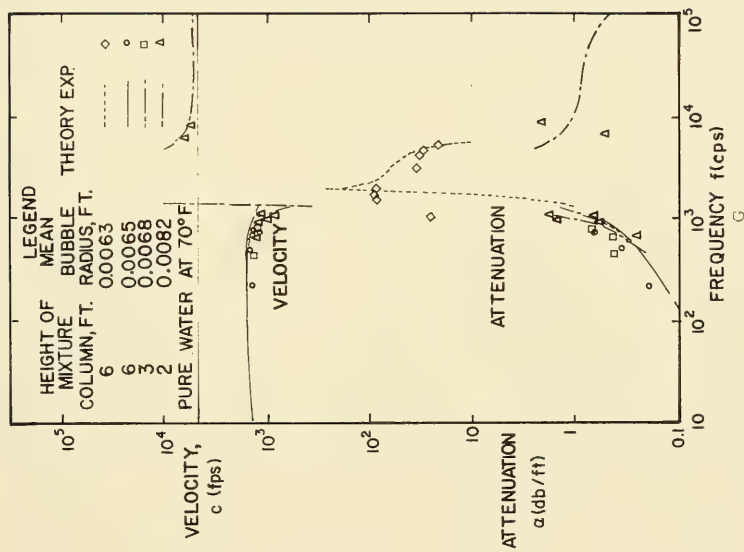


FIGURE III-27 CONTINUED

Most of the velocity measurements were confined to frequencies less than the resonant frequency for the air bubbles in the mixture, but some were also made at greater frequencies. (See Figures III-27c and III-27g.) The agreement between theory and experiment can be considered satisfactory. The results confirm the theoretical predictions that

1. as the incident frequency approaches the resonant frequency from below, the phase velocity decreases rapidly
2. for incident frequencies above resonance, the phase velocity is greater than in the bubble-free water.

Attenuation measurements did not always compare as satisfactorily with the theory as velocity measurements, but the theory certainly provides a useful estimate. The percentage discrepancy is considerably larger for frequencies at or above resonance than for lower frequencies, which might be overlooked because of the logarithmic scale. Some of this may be due to the equipment, which was not designed to handle such high attenuations. For frequencies below resonance, the attenuation measurements are generally a little larger than the theory predicts. Some of this was attributed to the noise level in the system.

### C. SCATTERING BY MARINE ORGANISMS

Scattering in the ocean is due in part to marine objects such as fish, plants and debris. The principal effect of these scatterers is to cause volume reverberation (i.e., back scattering) and attenuation of the propagating sound.

A convenient method of measuring such scattering is to radiate the sound in a succession of pulses, each of which is short compared with the interval between pulses. The transducer receives back-scattered energy between pulses which has come from scatterers farther and farther from the source as time-after-pulse increases. It is expected that, since the pulse of sound forms an expanding spherical shell of constant thickness, it will generally be scattered by many objects in the water and numerous scattered waves will arrive simultaneously at the receiver. The usual treatment is based on this assumption; that is, at any instant, scattering from many individual objects is superposed. It is convenient to define a scattering coefficient,  $m$ , of a unit volume, analogous to the back-scattering cross section of an individual scatterer.

The phenomenon of volume reverberation has been studied at great length. Considerable data have been amassed, which have been very well summarized by Urick and Pryce (Ref. III-41) and will not be presented here in detail.

Much of the work has been directed towards studying the variation of  $m$  with changes in volume and frequency. The nature of the data collected varies greatly from study to study, but usually the reverberation level is found to peak at certain frequencies. These peaks are believed to be caused by scattering from marine organisms. The data also show a gradual decrease in the volume scattering coefficient with increasing depth, except for a pronounced peak corresponding to depths in the range of 200m-400m. This has led to the discovery of the so-called deep scattering layer which is believed to consist of marine organisms.

To explain the experimental data, we must take recourse to the models of scattering from a fluid sphere or an air bubble treated earlier in this chapter. Admittedly most marine organisms are not exactly spherical, but for small scatterers ( $ka \ll 1$ ) shape is not too important, and for larger scatterers ( $ka \sim 1$ ) whose scattering is shape-dependent we still have no better guide.

The model based on a fluid sphere does not take into account the flexural properties of the skin or carapace of marine organisms. To consider the effect of this, Machlup (Ref. III-25) studied scattering from a spherical elastic shell containing a fluid. His theoretical results indicate that for incident wavelengths of the order of magnitude of the radius of the sphere, the behavior for thin shells is similar to that of the fluid sphere alone. For longer wavelengths, a correction may be computed, good to terms in the first power of the ratio of the thickness to the diameter of the shell.

These models, though they apply strictly to spheres, may be used as a qualitative guide for testing the properties of various possible sound scatterers. For instance, Hersey and Backus<sup>(1)</sup> cite work which points out that certain euphausiids contain a globule of oil which might account for the scattering observed from deep scattering layers. This oil was found to be 15% more compressible than water at the same depth. The globule has a radius of the order of  $10^{-3}$  m. Based on (III-15), its back-scattering cross section<sup>(2)</sup> would be of the order of  $2 \cdot 10^{-12} \text{ m}^2$  at 20 kc/sec. Based on the scattering or reverberation levels detected, this would require a population density of about  $10^4$  to  $10^5$  such scatterers per cubic meter. Such concentrations are extremely unlikely, and the euphausiids' oil globules are, therefore, a very improbable explanation of the deep scattering layer.

---

1. Hill, Ref. III-15

2. In this case half of the scattered energy is back scattered.



Another example is furnished by the swim-bladders of fish. A previous section of this report considered the scattering of sound by air bubbles. For a single bubble, the scattered intensity has a peak at the incident frequency  $f_o$  given by (III-22), which may be rewritten as

$$2\pi f_o = \frac{1}{a} \sqrt{\frac{3\gamma p_o}{\rho_o}} \quad (\text{III-39})$$

where  $a$  is the radius of the bubble,  $p_o$  the pressure on the bubble and  $\rho_o$  is the density of the water. The intensity of sound scattered in the ocean often has a pronounced peak at some particular frequency; thus, there is strong reason to believe that the scattering is caused by gas-bubble scatterers. Likely candidates are fishes having gas-filled swim-bladders. The swim-bladders are not generally spherical in shape, but nevertheless the properties of spherical bubble scatterers, as a function of hydrostatic pressure and bubble size, are a useful guide for speculation about the size of the fish and their behavior during migration in depth.

Suppose that the gas-filled swim-bladders are spherical in shape and behave acoustically like free bubbles. As the fish swims from a shallow to a deeper depth, its bubble is compressed and its buoyancy decreases. Consequently, it may take gas from solution in the water and increase the gas in its swim bladder to adjust its buoyancy on the way down. If it reacts to keep its swim-bladder the same size, then its resonant scattering frequency will vary as  $p^{1/2}$ . As it returns to shallow depth, it must then vent or absorb gas from the swim-bladder to maintain approximately neutral buoyancy. A second possibility is that the fish allows its bubble to compress and expand with descent and ascent. This implies that the fish can tolerate being heavy at maximum depth. Assuming constant temperature,

$\pi \frac{4}{3} a^3 p$  is a constant, hence  $1/a$  varies as  $p^{1/3}$ , from which we have

$$\frac{f}{f_r} = \left( \frac{p}{p_o} \right)^{5/6} \quad (\text{III-40})$$

since the density changes very slowly with depth. Generally, large migrations in depth amount to considerable changes in temperature as well. Almost everywhere the ocean temperature decreases with increasing depth below the isothermal layer. The effect of temperature on  $1/a$  is approximately as  $T^{-1/3}$ . Usually the temperature change will have the effect of reducing the frequency change by a small amount--of the order of 2% for a temperature change of 20°C.

The swim-bladders of bathypelagic fishes are not generally spherical but are more nearly prolate spheroids. Furthermore, they probably do not behave strictly as "free" bubbles but are constrained by the body of the fish. Scattering by a prolate spheroidal bubble can be shown to have a resonant frequency which varies as  $p^{1/3}$  if the bubble size and shape remain constant. If the gas content remains constant and the bubble is free to compress in all directions, then the resonant frequency varies as  $p^{5/6}$ , as for the spherical bubble. However, if the bubble is constrained so that it will not shorten its major diameter, but will compress by becoming "slimmer," then the resonant frequency varies very nearly as  $p$ . The latter possibility is likely, because the structure of the fish leaves it freer to compress in this way.

The above two possible modes of behavior for the swim-bladder require considerably different biological mechanisms. There is considerable controversy as to whether such behavior is anatomically at all possible, and if so, which, if either, exists in the types of marine organisms picked up in dragging operations in the deep scattering layer. Further details are given in Hill (Ref. III-15).

No experimental studies have been made of single specimens over a sufficiently great frequency range to permit the evaluation of simplified theoretical models. Some scattering cross sections have been reported by Albers (Ref. III-1). No frequencies are given, but presumably these are the resonant cross sections. The values given by Albers are

Shrimp (Palaemonetes)	$2.32 \cdot 10^{-8}$
Shrimp (Panaens)	$6.56 \cdot 10^{-5}$
Scup	$3.8 \cdot 10^{-4}$
Squid	$5.33 \cdot 10^{-4}$
Sea Bass	$4.4 \cdot 10^{-8}$

Hersey and Backus (Ref. III-15) have studied the relationship between peak sound scattering frequency and depth during the vertical migration of deep scattering layers. The relationship that would hold if the swim-bladder and its gas were responding passively to changes in ambient pressure (III-39) was observed during both a sunrise and sunset migration. This seems to imply that the gas content of the swim-bladder is kept constant, even though this causes the fish to be at neutral buoyancy only at one point of its depth range.

The relationship between variation in pressure and frequency of maximum scattered intensity that would be expected if the swim-bladder contents were being adjusted to maintain neutral buoyancy was observed only during sunset migration. Thus, it seems that some bathypelagic fish are able to absorb swim-bladder gas at a rate which would allow them to maintain neutral buoyancy during

an ascent of 200 meters in about one hour. It is probable (though not observed) that such an animal can effect the converse operation during a sunrise descent.

### Scattering by Many Organisms

Up to now we have considered only scattering by single marine organisms. We proceed to consider scattering by many organisms. The approach is more qualitative than in the case of air bubbles. A scattering or reverberation coefficient  $m$  is defined as the power scattered by a unit volume per unit intensity of an incident plane wave, with the scattering being equal in all directions. There is some physical evidence from dragging operations to indicate that the population density of scatterers causing volume reverberation is normally of the order of 10 - 15 per cubic meter, and may occasionally be as high as a few hundred scatterers per cubic meter. This is low enough so that interaction between scatterers, or multiple scattering, can be ignored. If there is no interaction between scatterers, then the volume reverberation coefficient,  $m$ , is simply the sum of the scattering cross sections of the scatterers in a unit volume.

Consider a transducer located at the center of a spherical coordinate system  $(r, \theta, \varphi)$  and assume that the energy emitted by the source per unit solid angle  $(\theta, \varphi)$  is described by  $F(\tau, \theta, \varphi)$ , where  $\tau$  is measured from the beginning of a pulse. The intensity of volume reverberation at the receiver at time  $t$  is related to  $m(r, \theta, \varphi)$ , the volume scattering coefficient of the medium, by

$$I(t) = \int_V \frac{F(\tau, \theta, \varphi)}{r^2} \cdot \frac{m(r, \theta, \varphi)b(\theta, \varphi)}{r^2} dV \quad (\text{III-41})$$

where  $b(\theta, \varphi)$  describes the directional properties of the transducer as a receiver and  $r = (c/2)(t - \tau)$ , where  $c$  is the velocity of sound in sea water.

The following assumptions are implicit in Equation III-41:

- The sound velocity in the medium is constant.
- The definition of  $m$  has the effect of averaging the contributions of individual scatterers.
- A volume element begins to scatter sound at the instant it is insonified and stops when the pulse has passed--i.e., there are no time lags or storage of energy in the scatterer.

- Scattering cross sections are small enough to neglect multiple scattering.
- The average reverberation intensity at the receiver is equal to the sum of the average intensities due to individual scatterers.
- The backward scattering coefficient is independent of the direction of incidence of the beam.

In general, one must solve or invert (III-41) to determine volume scattering coefficients from measured reverberation intensities.

Reverberation of a sinusoidal wave train radiated from a "search light" or piston-type transducer (i.e., a directional source having one radiation lobe, the main lobe, much stronger than all others) and received by the same transducer has been analyzed by UCDWR (Ref. III-39). The directional radiating and receiving properties of the transducer are considered to be identical, that is,  $F(\tau, \theta, \varphi)$  can be written  $F(\tau) b(\theta, \varphi)$ . Assuming a sinusoidal pulse of the form  $p_o \sin \omega \tau$ , we then have

$$F(\tau, \theta, \varphi) = \frac{p_o^2 \sin^2 2\pi(f\tau - r/\lambda)}{\rho c} 10^4 \quad (\text{III-42})$$

where  $p_o$  is the instantaneous pressure in dynes/cm<sup>2</sup> at a range  $r = 1$  meter. Assuming the transducer has axial symmetry, we have  $b(\theta, \varphi) = b(\theta)$ . If  $m$  is assumed to be independent of position

$$I(t) = \frac{4\pi \cdot 10^4}{ct^2} \frac{p_o^2}{2\rho c} r_o m \int_0^\pi b^2(\theta) d\theta \quad (\text{III-43})$$

Using the experimental data, this equation was solved for  $m$  to give peak values close to  $3 \cdot 10^{-7}$  at depths of about 400m in the frequency range 10-80 kc.

Machlup (Ref. III-15) has treated the problem of back scattering of the omnidirectional shock wave from a nearby explosion to both omnidirectional and searchlight receivers. Let  $F(\tau)$  represent the energy flux of the shock wave per unit solid angle. Assuming  $\tau \ll t$  so that  $r \approx ct/2$ , the  $r$  integration can be performed. The total energy in the shock wave can be written as

$$E = 4\pi \int_0^\infty F(\tau) d\tau \quad (\text{III-44})$$

Then (III-41) reduces to

$$I(t) = \frac{E_c}{4r^2} \int_0^\pi m(r \cos \theta) b(\theta) \sin \theta d\theta \quad (\text{III-45})$$

where  $r = ct/2$  and  $m(r \cos \theta) = m(r, \theta, \varphi)$  if we assume that the scattering properties are layered horizontally and choose the vertical direction as the polar axis. Machlup then assumed  $b(\theta) = \cos \theta$  and was able to carry through the analysis to solve for  $m$  in terms of  $I$  and the other parameters to obtain peak values of  $m$  ranging from  $10^{-8} \text{ m}^{-1}$  to  $10^{-9} \text{ m}^{-1}$ . Figure III-28 shows a graph of  $m$  versus depth, based on measurements of 15-kc components of the explosive sound. Further details, together with an excellent bibliography, are given by Hersey and Backus (Ref. III-15).

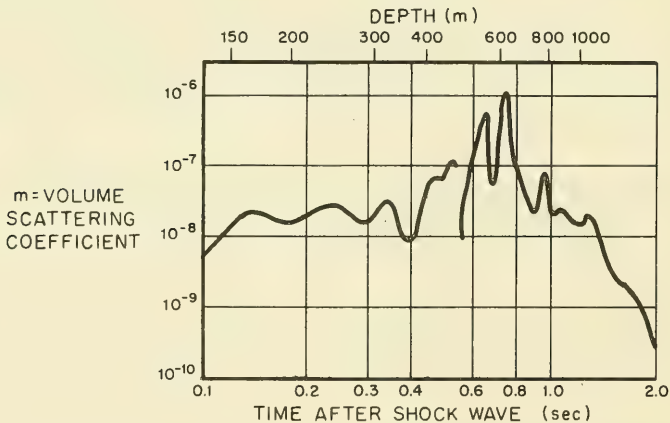


FIGURE III-28 VARIATION OF VOLUME SCATTERING CROSS SECTIONS (AFTER HERSEY AND BACKUS)

#### D. SCATTERING FROM THE SEA SURFACE

Scattering from the irregularities of the sea surface plays a dominant part in the propagation characteristics of the ocean. Unfortunately, however, a realistic description of the ocean surface makes the analysis of sound scattering



extremely difficult. The irregularities of the surface are typically of the same order of magnitude as the wavelength of the sound, i.e., between 15 cm and 15 m, and we have observed earlier for volume inhomogeneities that this is a bothersome range for analysis. In this range, scattering is highly directional, and dependent on the detailed shape of the scatterer. At the same time, the surface is constantly changing shape, and a realistic description must be stochastic in nature. Finally, the motion of the surface causes regions of turbulence just below the surface, and disturbances such as white caps or rain (spray) cause air bubbles in the surface layer. Reflection from this composite surface naturally defies an accurate analysis.

As a consequence, the work in this field divides sharply into two kinds: on the one hand, experimental work on scattering from the real ocean surface; on the other, theoretical analyses of scattering from an idealized surface (usually sinusoidally corrugated) supported by controlled experiments in pools. The one notable exception is the recent work by Marsh, et al. (Ref. III-27) which attempts to analyze scattering from a stochastic surface and compares in a very limited way its theoretical results with the experimental data obtained in the ocean.

The ocean experiments have been well summarized in review articles by Urlick and Pryce (Ref. III-40), and will therefore not be described here. Very little has been added since their survey in this area. Instead, we shall concentrate on giving some unity to the disjointed theoretical treatments, and hope that this will enhance understanding and stimulate the application of the present theory to explain scattering experiments from the actual ocean surface.

All authors attack essentially the same theoretical problem. Consider a plane wave\* in the water

$$p_{\text{inc}}(x,y,z,t) = p_{\text{inc}} e^{i k (\alpha x + \beta y + \gamma z) - i \omega t} \quad (\text{III-46a})$$

$$(\text{Note: } k = \frac{\omega}{c_0}, \alpha^2 + \beta^2 + \gamma^2 = 1)$$

---

\*The upward vertical direction is taken to point along the z-axis, and the sea surface is on the average parallel to the (x,y) plane. Because of the special significance of the z-direction, we shall employ (x,y,z) coordinates rather than  $(x_1, x_2, x_3)$ . The water lies below the surface, i.e.,  $z < S(x,y)$  denotes a point in the water. The z-component of the propagation vector of the incident wave points upward along the z-axis.



which is incident on the ocean surface

$$z = S(x, y) \quad (\text{III-46b})$$

The ocean surface supposedly changes shape only very slightly during one cycle of the incident sound wave, so that the motion of the surface may be ignored in the scattering analysis. The pressure distribution of the resulting scattered wave  $p_{sc}(x, y, z, t)$  must satisfy the wave equation. Furthermore, the total acoustic pressure  $p = p_{inc} + p_{sc}$  must satisfy an appropriate boundary condition on the surface  $S(x, y)$ . Because of the very poor impedance match between water and air, the boundary condition is approximated very closely\* by requiring the total overpressure at the surface to vanish, i.e., letting the surface be a pressure release and allowing no sound to be transmitted to the air. Finally,  $p_{sc}$  must be an "outgoing" wave, i.e., its energy must flow from the surface downward, and  $p_{sc}$  must remain finite as  $z \rightarrow -\infty$ . These three conditions

1.  $\nabla^2 p_{sc} = \frac{1}{c_o^2} \frac{\partial^2 p_{sc}}{\partial t^2}$
2.  $p_{inc} + p_{sc} = 0$  on  $z = S(x, y)$
3.  $p_{sc}$  is outgoing and remains finite (the so-called radiation condition).

completely define the theoretical problem. The question of interest is: how does  $p_{sc}$  depend on the characteristics of  $S(x, y)$ ?

---

\*This may be seen by studying reflection of a sound wave  $p_{inc} = e^{ik(\alpha x + \gamma z) - i\omega t}$  from a plane interface between water and air. We recall from Section III-B that the ratios of density and sound velocity for water and air are approximately

$$g = \frac{\rho'_o}{\rho_o} \approx 1.3 \times 10^{-3}, \quad h = \frac{c'_o}{c_o} \approx 0.2. \quad \text{The incident wave causes a reflected and a}$$

transmitted wave,  $p_{refl} = p_r e^{ik(\alpha x - \gamma z) - i\omega t}$  and  $p_{trans} = p_t e^{ik(\alpha' x - \gamma' z) - i\omega t}$ .

If we require the total pressure and normal velocity to be continuous at the inter-

face, we find readily that  $p_r = \frac{1 - gh \sqrt{\frac{1 - \alpha^2}{1 - h^2 \alpha^2}}}{1 + gh \sqrt{\frac{1 - \alpha^2}{1 - h^2 \alpha^2}}}$ . Since  $gh \approx 0.26 \times 10^{-3}$ , the

reflected wave has a pressure which lies between 99.948% and 100% of the incident pressure, depending on  $\alpha$ .

Most authors share the same general approach to the problem. They regard the scattered wave as a superposition of plane waves emanating from the surface and having the same frequency  $\omega$  as the incident wave. If they are to satisfy the wave equation, these plane waves must have the form:

$$p_{\text{plane}} = \phi e^{ik(\lambda x + \mu y + \nu z) - i\omega t} \quad \text{where } \lambda^2 + \mu^2 + \nu^2 = 1 \quad (\text{III-47})$$

In particular, for given  $\lambda$  and  $\mu$ , we must choose the root  $\nu$  such that the radiation condition is satisfied. This means that we desire:

$$\arg \nu = \arg \sqrt{1 - \lambda^2 - \mu^2} = \begin{cases} \pi \text{ (i.e., } \nu \text{ negative) if } \nu \text{ real} \\ \frac{3\pi}{2} \text{ (i.e., } \nu \text{ positive) if } \nu \text{ imaginary} \end{cases} \quad (\text{III-48})$$

The scattered wave is now written as a superposition of such plane waves:

$$p_{\text{sc}} = \iint_{-\infty}^{\infty} d\lambda d\mu \phi(\lambda, \mu) e^{ik(\lambda x + \mu y + z \sqrt{1 - \lambda^2 - \mu^2}) - i\omega t} \quad (\text{III-49})$$

Finally, we apply the boundary condition that the total pressure vanishes at the surface, and obtain an integral equation for  $\phi(\lambda, \mu)$ , given  $S(x, y)$ :

$$p_{\text{inc}} e^{ik(\alpha x + \beta y + \gamma S(x, y))} + \iint_{-\infty}^{\infty} d\lambda d\mu \phi(\lambda, \mu) e^{ik(\lambda x + \mu y + S(x, y) \sqrt{1 - \lambda^2 - \mu^2})} = 0 \quad (\text{III-50})$$

Different authors use different schemes for obtaining approximate solutions to (III-50). All are especially interested in the value of  $\phi(\alpha, \beta)$ , i.e., the strength of the scattered wave in the specularly reflected\* direction. Most authors confine themselves to sinusoidal surfaces, although their approaches are generally valid

---

\*The direction in which a plane wave is reflected by a plane interface.

for periodic surfaces and could therefore be used as well for the more or less cnoidal surfaces\* to be expected from the theory of propagation of surface waves. Marsh, however, obtains an approximate solution in terms of the correlation function (or equivalently the spectrum) of the surface.

### 1. Periodic Surfaces

When the surface  $S(x,y)$  is periodic, the scattered wave  $p_{sc}$  can be represented by the superposition of a countable number of plane reflected waves. In other words, the function  $\phi(\lambda, \mu)$  becomes discrete. This may be seen as follows.

For simplicity in the argument, let us restrict ourselves to a "corrugated" periodic surface, generated by straight line generators parallel to the  $y$ -axis and periodic with period  $\xi$  in the  $x$  direction. The geometry is illustrated in Figure III-29.

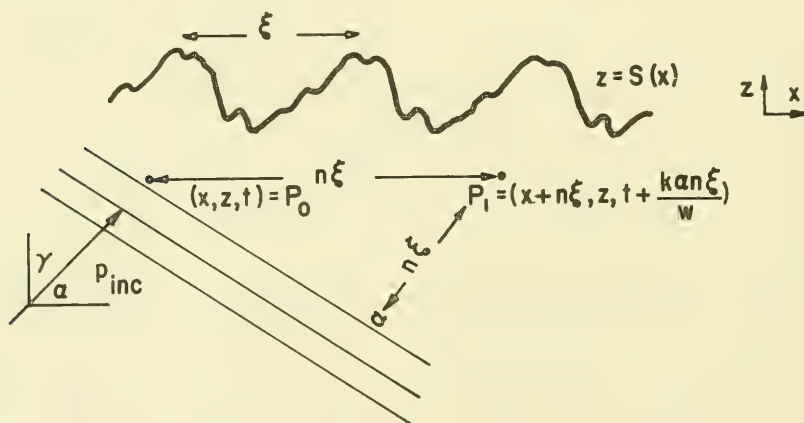


FIGURE III-29 SCHEMATIC DIAGRAM OF A PLANE WAVE INCIDENT ON A CORRUGATED SURFACE

If the plane wave

$$p_{inc}(x, z, t) = p_{inc} e^{ik(\alpha x + \gamma z) - i\omega t} \quad (\text{III-51})$$

is incident on this surface, it causes a scattered wave  $p_{sc}(x, z)e^{-i\omega t}$ .

\*J. J. Stoker, "Water Waves," Interscience Publishers 1957.

Suppose that we irradiate the surface instead with the retarded incident wave

$$p_{inc}^{(\tau)}(x, z, t) = p_{inc} e^{ik(\alpha x + \gamma z) - i\omega t + i\tau} = p_{inc}(x, z, t) e^{i\omega t} \quad (III-52)$$

In other words,  $p_{inc}$  is identical at the two space-time points  $P_0 = (x, z, t)$  and  $P_1 = (x + n\xi, z, t + \frac{k\alpha n\xi}{\omega})$ . The incident wave will produce a scattered wave which has also been retarded by  $\tau$ :

$$p_{sc}^{(\tau)}(x, z, t) = p_{sc}(x, z) e^{-i\omega t} e^{i\omega t} \quad (III-53)$$

Instead of shifting the time axis, we could consider a translation of the  $x$ -axis by an integral number of periods  $n\xi$ . This translates the surface into itself. The corresponding incident wave is

$$p_{inc}^{(n\xi)} = p_{inc} e^{ik(\alpha x + \alpha n\xi + \gamma z) - i\omega t} = p_{inc}(x, z, t) e^{ik\alpha n\xi} \quad (III-54)$$

and causes a scattered wave

$$p_{sc}^{(n\xi)} = p_{sc}(x + n\xi, z) e^{-i\omega t} \quad (III-55)$$

However, we note that  $p_{inc}^{(n\xi)}$  could equally well be regarded as a retarded version of  $p_{inc}$ , retarded by an amount  $\tau = k\alpha n\xi/\omega$ . The surface has remained the same, since  $S(x + n\xi) = S(x)$ , and so we expect that the scattered waves will be the same, i.e.,

$$p_{sc}^{(n\xi)} = p_{sc}(\tau = k\alpha n\xi/\omega) \quad (III-56)$$

We could alternatively have written (III-56) as:

$$p_{sc}(x, z, t) = p_{sc}(x + n\xi, z, t + k\alpha n\xi/\omega) \quad (\text{III-57})$$

Thus, the scattered wave is the same at  $P_0$  and  $P_1$ . Substituting (III-53) and (III-55) in (III-56), we find:

$$p_{sc}(x, z) e^{i\alpha k n \xi} = p_{sc}(x + n\xi, z) \quad (\text{III-58})$$

It follows that  $p_{sc}(x, z) e^{-i\alpha k x}$  must be a periodic function with period  $\xi$ ; therefore, it can be expanded in a Fourier series:

$$p_{sc}(x, z) e^{-i\alpha k x} = \sum_{n=-\infty}^{\infty} A_n(z) \left( \frac{2\pi i n x}{\xi} \right) \quad (\text{III-59})$$

However,  $p_{sc}(x, z)$  must satisfy the Helmholtz equation

$$\frac{\partial^2}{\partial x^2} p_{sc} + \frac{\partial^2}{\partial z^2} p_{sc} + k^2 p_{sc} = 0 \quad (\text{III-60})$$

and this permits us to solve for the functions  $A_n(z)$ . In fact, each of the terms,  $A_n(z) \left( \frac{2\pi i n x}{\xi} \right) e^{i\alpha k x}$ , must satisfy (III-60) separately, since the functions  $\left( \frac{2\pi i n x}{\xi} \right) e^{i\alpha k x}$  are linearly independent. Consequently,  $A_n(z)$  satisfies:

$$\frac{d^2}{dz^2} A_n(z) - k^2 \left[ \left( \alpha + \frac{2\pi n}{\xi k} \right)^2 - 1 \right] A_n(z) = 0 \quad (\text{III-61})$$

Let us introduce the sequence of direction cosines:

$$\alpha_n = \alpha + \frac{2\pi n}{\xi k}, \quad \gamma_n = (1 - \alpha_n^2)^{1/2} \quad (\text{III-62})$$

As stated in (III-42), the  $\gamma_n$  must be chosen so that

$$\gamma_n \leq 0 \text{ if } 1 - \alpha_n^2 \geq 0 \quad (\text{III-63})$$

$$\text{if } \gamma_n > 0 \text{ if } 1 - \alpha_n^2 < 0$$

Then

$$A_n(z) = A_n e^{ik\gamma_n z} \quad (\text{III-64})$$

The scattered wave may therefore be written as

$$p_{sc}(x, y) = \sum_{n=-\infty}^{\infty} A_n e^{ik(\alpha_n x + \gamma_n z)} \quad (\text{III-65})$$

The components corresponding to values of  $n$  for which  $1 - \alpha_n^2 \geq 0$  are plane waves propagating downward with direction cosines  $(\alpha_n, \gamma_n)$ . For  $n$  such that  $1 - \alpha_n^2 < 0$ , the corresponding component of scattering is a plane wave propagating in the  $x$  direction but with an amplitude decreasing exponentially as  $z$  decreases.

In order to solve the scattering problem in this setting, it remains to obtain the coefficients  $A_n$ . There are several ways of doing this, depending upon the approximations used and the assumptions concerning scattering in a neighborhood of the surface. One usually studies the sinusoidal surface

$$z = S(x) = h \cos px \quad (\text{III-66})$$

irradiated by an incident wave

$$p_{inc} = e^{ik(\alpha x + \gamma z)} \quad (\text{III-67})$$



The wavelength of the surface is  $\xi = \frac{2\pi}{p}$ , hence the direction cosines,  $\alpha_n$ , are given by

$$\alpha_n = \alpha + \frac{np}{k} \quad (\text{III-68})$$

Since this wave is travelling upward and the time dependence is given by  $e^{-i\omega t}$ , we must have  $\gamma \geq 0$ . The boundary condition which must be satisfied is

$$p_{\text{inc}}(x, S(x)) + p_{\text{sc}}(x, S(x)) = 0 \quad (\text{III-69})$$

An expression giving any particular coefficient  $A_t$  in terms of the others can be obtained by first factoring out the term  $e^{ik(\alpha x + \gamma_t z)}$  from the sum  $p_{\text{inc}} + p_{\text{sc}}$ . Then, on the surface  $z = h \cos px$ , the boundary condition gives

$$e^{ik(\gamma - \gamma_t)h \cos px} + \sum_{n=-\infty}^{\infty} A_n e^{[np + k(\gamma_n - \gamma_t)h \cos px]} = 0 \quad (\text{III-70})$$

Using the expansion

$$e^{i\theta \cos px} = \sum_{m=-\infty}^{\infty} i^m e^{impx} J_m(\theta) \quad (\text{III-71})$$

it can be shown that

$$i^t A_t = -J_0[(\gamma_t - \gamma)kh] = \sum_{\substack{n=-\infty \\ n \neq -t}}^{\infty} i^n A_n J_{n-t}[(\gamma_n - \gamma_t)kh] \quad (\text{III-72})$$

If  $kh$  is so small that all the terms involving a Bessel function of order greater than zero may be ignored, we obtain the so-called Rayleigh approximation

$$A_t = -(-i)^t J_0[(\gamma_t - \gamma)kh] \quad (\text{III-73})$$

A different approach to this same problem requiring a less strenuous assumption on the Bessel functions is used by La Casce and Tamarkin (Ref. III-18). If we factor out the term  $e^{ik\alpha x}$ , note at the same time that  $\gamma_0 = -\gamma$ , the boundary condition (III-69) becomes

$$A_0 + e^{2ik\gamma h \cos px} + \sum_{\substack{m=-\infty \\ m \neq 0}}^{\infty} A_m e^{impx + (\gamma_m + \gamma) h \cos px} = 0 \quad (\text{III-74})$$

Using (III-71), this may be written as

$$\sum_{n=-\infty}^{\infty} i^n e^{inpx} J_n(2k\gamma h) + A_0 + \sum_{n=-\infty}^{\infty} \left[ \sum_{\substack{m=-\infty \\ m \neq 0}}^{\infty} i^{n-m} A_m J_{n-m}[kh(\gamma_m + \gamma)] \right] e^{inpx} = 0 \quad (\text{III-75})$$

For  $n = 0, -1, 1$ , we have the following:

$n = 0$

$$J_0(2k\gamma h) + A_0 + iA_{-1}J_1[kh(\gamma_{-1} + \gamma)] + i^{-1}A_1J_{-1}[kh(\gamma_1 + \gamma)] \\ + \sum_{\substack{m=-\infty \\ |m| \geq 2}}^{\infty} i^{-m}A_mJ_m[kh(\gamma_m + \gamma)] = 0 \quad (\text{III-76a})$$

$n = 1$

$$iJ_1(2k\gamma h) + A_1J_0[kh(\gamma_1 + \gamma)] + i^3A_{-1}J_2[kh(\gamma_{-1} + \gamma)] \\ + \sum_{\substack{m=-\infty \\ |m| \geq 2}}^{\infty} i^{1-m}A_mJ_{-1-m}[kh(\gamma_m + \gamma)] = 0 \quad (\text{III-76b})$$

$$\underline{n = -1}$$

$$i J_{-1} (2k\gamma h) + i^{-2} A_1 J_{-2} [kh(\gamma_1 + \gamma)] + A_{-1} J_0 [kh(\gamma_{-1} + \gamma)] \\ + \sum_{\substack{m=-\infty \\ |m| \geq 2}}^{\infty} i^{1-m} A_m J_{1-m} [kh(\gamma_m + \gamma)] = 0 \quad (\text{III-76c})$$

Then La Casce and Tamarkin assume that  $kh$  is so small that Bessel functions of order greater than one (instead of zero as before) can be neglected. Furthermore, they assume that  $A_1$  is also very small. Then, from (III-76c) and (III-76a) one obtains the approximations

$$A_0 \approx -J_0 (2kh\gamma) - \frac{kh(\gamma_1 + \gamma)}{2} \quad (\text{III-77})$$

$$A_{-1} \approx -i J_1 (2kh\gamma)$$

These expressions for  $A_0$  and  $A_{-1}$  indicate an interaction between the specularly reflected and higher order components. For frequencies so low that  $\gamma_1$  is complex,  $A_0$  is given only by

$$A_0 \approx -J_0 (2kh\gamma) \quad (\text{III-78})$$

i.e., there is a cutoff frequency below which the specular magnitude is given simply by the Rayleigh approximation.

Heaps has determined values of the  $A_n$  under the assumption that  $A_n = 0$  for  $n$  such that  $\gamma_n$  is imaginary. This is equivalent to assuming that all the reflected radiation is in plane undamped waves. For any particular surface, Equation III-72 becomes a finite set of linear equations for the  $A_n$ , which may be solved by the usual methods.

Following an approach similar to that used to obtain the equations for the  $A_n$ , it can be shown that  $MS(|p|)$ , the mean square value of the total pressure  $p$  at the surface, is given by

$$MS|p| = \sum_{m=-\infty}^{\infty} |J_m[kh(\gamma_t - \gamma)]| + \sum_{n=-\infty}^{\infty} i^n A_n J_{n-t}[kh(\gamma_n - \gamma_t)]^2 \quad (\text{III-79})$$

Since  $p = 0$  on the surface, it follows that  $MS(|p|) = 0$ . The evaluating (III-79) with the values of  $A_n$  obtained from the finite set of linear equations shows the effect of neglecting the damped plane waves.

From (III-6), the intensity,  $I_z$ , in the  $z$  direction of a plane wave  $p = A e^{ik(\alpha x + \gamma z)}$  is given by  $I_z = \frac{\gamma}{2\rho_0 c_0} |A|^2$ . The difference between the energy incident on the surface and that reflected in plane undamped waves is therefore proportional to

$$E = \gamma - \sum_n |A_n|^2 \gamma_n \quad (\text{III-80})$$

where the summation is over  $n$  such that  $|\alpha + \frac{np}{k}| \leq 1$ . Then  $1 - \frac{E}{\gamma}$  is the fraction of the incident energy contained in the plane undamped waves and  $(E/\gamma)$  is the fraction absorbed.

Table III-3 gives the results of some calculations done by Heaps (Ref. III-13) for a surface of the form  $S(x) = h \cos px$  with  $h = 0.15$  cm and  $p = 3.08$   $\text{cm}^{-1}$ . The coefficients  $A_n$  were obtained from (III-72), where the summation is only over  $n$  such that  $|\alpha + \frac{np}{k}| \leq 1$ . The appearance of non-zero values of  $MS(|p|^2)$  is a consequence of neglecting terms in (III-72) involving larger values of  $n$ . The value of  $1 - E/\gamma$  gives the fraction of the incident energy reflected in plane undamped waves. The figures in parentheses are the corresponding quantities using the Rayleigh values for  $A_n$ .

From Table III-3a, it is apparent that at normal incidence ( $\theta=0^\circ$ ) the listed values of  $A_n$  satisfy the condition  $MS|p|^2 = 0$  (and so also the condition of zero surface pressure) much better than the Rayleigh values do and, in fact, account for about 90% of the incident energy, whereas the Rayleigh theory accounts for only 68% of the energy. Table III-3b suggests that, at an angle of incidence of  $40^\circ$ , there is little to choose between the two theories. In either case, an appreciable portion (10% or more) of the incident energy must be reflected in other than plane undamped waves.

TABLE III-3

REFLECTION COEFFICIENTS  $A_n$  FOR THE  
 SURFACE  $S(x) = 0.15 \cos 3.08x$  AND INCIDENT ANGLE  $\theta$

(a)

 $\theta = 0^\circ$ 

(Normal Incidence)

$kh$	0.5	0.924	1.25	1.5	1.75
$A_0$	-0.864	-0.363	0.019	0.240	0.376
$iA_1$	-0.442	-0.634	-0.576	-0.415	-0.188
$-A_2$		-0.275	-0.456	-0.557	-0.558
$-iA_3$				-0.241	-0.364
$MS p ^2$	0.0 (0.053)	0.019 (0.086)	0.037 (0.062)	0.0 (0.053)	0.023 (0.064)
$1-E/\gamma$	0.898 (0.664)	0.824 (0.677)	0.900 (0.686)	0.918 (0.684)	0.808 (0.683)

(b)

 $\theta = 40^\circ$ 

$A_0$	-0.840	-0.496	-0.198	-0.173	0.016
$-iA_{-1}$	0.354	0.520	0.520	0.514	0.326
$iA_1$				-0.650	-0.539
$-A_{-2}$		-0.268	-0.388	-0.461	-0.491
$iA_{-3}$		0.065	0.168	0.254	0.331
$A_{-4}$			-0.032	-0.083	-0.149
$-iA_{-5}$				0.009	0.036
$A_{-6}$					-0.002
$MS p ^2$	0.139 (0.138)	0.354 (0.357)	0.467 (0.479)	0.064 (0.095)	0.059 (0.167)
$1-E/\gamma$	0.860 (0.710)	0.683 (0.810)	0.610 (0.691)	0.885 (0.768)	0.740 (0.802)

Using the expressions (III-67) and (III-65) for  $p_{inc}$  and  $p_{sc}$ , together with (III-71), it can be shown that for a surface of the form  $S(x) = h \cos px$ , the boundary condition  $p_{inc} + p_{sc} = 0$  is also equivalent to

$$\sum_{n=-\infty}^{\infty} i^n A_{m-n} J_n(kh \gamma_{m-n}) = -(i)^m J_m(kh \gamma) \quad (\text{III-81})$$

Then, assuming  $A_n$  to be of the form  $A_n = \sum_t A_{n,t} (kh)^t$ , Heaps (Ref. III-14)

shows that  $A_{n,t}$  is given by

$$|t| \geq |n|$$

$$A_{n,t} = \frac{-(i\gamma)^t}{2^t \left[ \frac{1}{2}(t+n) \right]! \left[ \frac{1}{2}(t-n) \right]!} - \sum_{r=1}^t \sum_j \frac{(i\gamma_{n-j})^r A_{n-j, t-r}}{2^r \left[ \frac{1}{2}(r+j) \right]! \left[ \frac{1}{2}(r-j) \right]!} \quad (\text{III-82})$$

where  $j$  is such that  $|j| \leq r$ ,  $|n-j| \leq t-r$ , with  $r$  and  $j$  both even or odd. Neglecting  $(kh)^4$  and higher powers, this gives

$$A_0 = -1 + \frac{1}{2}(kh)^2 \gamma (\gamma_1 + \gamma_{-1})$$

$$A_{\pm 1} = i(kh \gamma) - i(kh)^3 \gamma \left[ \frac{1}{8} \gamma^3 + \frac{1}{4} (\gamma \gamma_1 + \gamma \gamma_{-1} + \gamma_{\pm 1} \gamma_{\pm 2}) - \frac{1}{4} \gamma_{\pm 1}^2 + \frac{1}{8} \gamma_{\mp 1} \right]$$

$$A_{\pm 2} = \frac{1}{2}(kh)^2 \gamma \gamma_{\pm 1} \quad (\text{III-83})$$

$$A_{\pm 3} = -i(kh)^3 \gamma \left[ \frac{1}{24} \gamma^3 \pm \frac{1}{8} \gamma_{\pm 1}^2 + \frac{1}{4} \gamma_{\pm 1} \gamma_{\pm 2} \right]$$

Heaps (Ref. III-14) also considered the problem of scattering from a sinusoidal surface when the incident wave is a spherical wave centered a finite distance  $d$  below the surface. The scattered wave is represented in the form

$$p_{sc} = k\gamma \frac{e^{ikr}}{r} \sum_{m=-\infty}^{\infty} B_m e^{ikd \gamma_m} \quad (\text{III-84})$$

When powers of  $(kh)^4$  and greater are neglected, the  $B_m$  are given by expressions similar to (III-83) except that instead of  $kh$ , the term  $h$  appears, and instead of  $\gamma_n$ , the terms



$$\beta_n = \left[ k^2 - (a - np)^2 - b^2 \right]^{\frac{1}{2}} \quad (\text{III-85})$$

appear, where  $a = k \sin \theta \cos \phi$  and  $b = k \sin \theta \sin \phi$ , and  $(r, \theta, \phi)$  are a system of spherical coordinates. No computations or experimental results are given.

Using this model, Heaps also obtains expressions for the intensity and average intensities of the resultant field.

The so-called Rayleigh approximation requires that the surface irregularities are small in comparison with the wavelength of the incident radiation. Brekhovskikh (Ref. III-18) has developed a theory which permits large irregularities, but assumes that at the irregular surface the sound field can be specified in terms of the laws of geometric acoustics. At each point on the surface, the sound field is assumed to be the same as if the reflection from that point were to occur from an infinite plane tangent to the surface at the specified point. In other words, the distribution of the scattered field over the surface is assumed to be that which could be expected on the basis of considering only one incident wave while neglecting secondary scattering from individual sectors of the surface. By specifying the field at the surface in this manner, it is possible to use the Green (or Helmholtz) formula to compute the field at points away from the surface.

Consider a surface of the form  $z = S(x)$  and an incident wave given by

$$p_{\text{inc}}(x, z) = e^{ik(\alpha x + \gamma z)} \quad (\text{III-86})$$

At the surface the scattered wave  $p_{\text{sc}}$  is given by the boundary condition:

$$p_{\text{inc}}[x, S(x)] + p_{\text{sc}}[x, S(x)] = 0.$$

Thus, we have

$$p_{\text{sc}}[x, S(x)] = -e^{ik[\alpha x + \gamma S(x)]} \quad (\text{III-87})$$

We also require  $\frac{\partial p_{\text{sc}}}{\partial n}$ , where the derivative is taken along the normal to the surface. Using the condition of locally specular reflection, this derivative is given on the surface by

$$\frac{\partial p_{\text{sc}}}{\partial n} = ik(\alpha a + \gamma c) e^{ik[\alpha x + \gamma S(x)]} \quad (\text{III-88})$$

where  $(a, c)$  are the direction cosines of the normal to the surface. Let  $\underline{r}_1 = [x_1, y_1, S(x_1)]$  be a point on the surface,  $\underline{r} = (x, y, z)$  be an arbitrary observation point, and  $\underline{k} = (k_x, k_y, k_z)$  be an arbitrary propagation vector. We use the relation

$$\frac{e^{i|\underline{k}| |\underline{r} - \underline{r}_1|}}{|\underline{r} - \underline{r}_1|} = \frac{i}{2\pi} \int_{-\infty}^{\infty} \int_{-\infty}^{\infty} e^{i \left[ k_x(x-x_1) + k_y(y-y_1) + k_z(z-S(x_1)) \right]} \frac{dk_x dk_y}{k_z} \quad (\text{III-89})$$

in the Helmholtz formula

$$p_{sc}(x, y, z) = \frac{1}{4\pi} \int_S \left\{ \frac{\partial p_{sc}}{\partial n} \left( \frac{e^{i|\underline{k}| |\underline{r} - \underline{r}_1|}}{|\underline{r} - \underline{r}_1|} \right) - p_{sc} \frac{\partial}{\partial n} \left( \frac{e^{i|\underline{k}| |\underline{r} - \underline{r}_1|}}{|\underline{r} - \underline{r}_1|} \right) \right\} ds \quad (\text{III-90})$$

and substitute (III-87) and (III-88) to yield:

$$p_{sc}(x, y, z) = -\frac{1}{4\pi} \int_S \int_{-\infty}^{\infty} \int_{-\infty}^{\infty} \frac{k}{2k_z} \left[ \frac{(\alpha - \alpha')a + (\gamma - \gamma')c}{c} \right] e^{i(k_x x + k_y y + k_z z)} \cdot e^{i(k\alpha - k_x + n\pi)x_1 - k_y y_1 + (k\gamma - k_z)S(x_1)} \frac{dk_x dk_y dx_1 dy_1}{2} \quad (\text{III-91})$$

where  $(\alpha', \beta', \gamma')$  are the direction cosines of  $\underline{r}' = \underline{r}_1$ . If the function  $S(x)$  describing the surface is periodic, with period  $\frac{2\pi}{p}$ , we can set

$$\frac{k}{2k_z} \left[ \frac{(\alpha - \alpha')a + (\gamma - \gamma')c}{c} \right] e^{i(k\gamma - k_z)S(x_1)} = \sum_{n=-\infty}^{\infty} A_n e^{inpx_1} \quad (\text{III-92})$$

Substituting this in (III-91) gives

$$p_{sc}(x, y, z) = -\frac{1}{4\pi^2} \sum_{n=-\infty}^{\infty} \int_S \int_{-\infty}^{\infty} \int_{-\infty}^{\infty} A_n e^{i(k_x x + k_y y + k_z z)} \cdot e^{i(k\alpha - k_x + n\pi)x_1 - k_y y_1} dx_1 dy_1 \frac{dk_x dk_y}{2} \quad (\text{III-93})$$

Then using the properties of the delta function, we obtain

$$p_{sc}(x, y, z) = \sum_{n=-\infty}^{\infty} A_n e^{ik(\alpha_n x + \gamma_n z)} \quad (\text{III-94})$$

with  $\alpha_n$  and  $\gamma_n$  given by (III-62). Thus, we obtain an expression giving  $p_{sc}$  as a sum of plane waves having the direction cosines obtained for general reflection from a periodic surface. In particular, suppose the surface is given by

$S(x) = h \cos px$ . Since  $e^{i\beta \cos px}$  is the generator for the Bessel function, cf (III-71), we can write (III-92) as a series in Bessel functions. Substituting this in (III-93), and after some analysis, we obtain the coefficients

$$A_n = \frac{(\alpha - \alpha_n)^2 + (\gamma - \gamma_n)^2}{2 \gamma_n (\gamma - \gamma_n)^2} J_n \left[ (\gamma - \gamma_n) kh \right] \quad (\text{III-95})$$

The basic limitation of this approach is associated with the shape of the uneven surface. The nature of the irregularities must be such that overshadowing does not occur, i.e., the surface should be locally flat. Overshadowing is assumed to occur when the angle of incidence is greater than the angle between the normal to the plane  $z=0$  and the tangent to the surface at the point of maximum slope. The larger the slope, the smaller must be the angle of incidence to prevent overshadowing. The criterion of local flatness, when applied to those portions of the surface with the least radius of curvature, can be shown to reduce to the inequality

$$\cos \alpha > \frac{1}{2} \frac{hp^2}{k} \quad (\text{III-96})$$

where  $\alpha$  is the angle of incidence.

We first discussed the Rayleigh formulation which was based on the assumption that  $kh \ll 1$ , where  $k$  is the wave number of the incident sound and  $h$  is the height of the surface roughness. The Brekhovskikh model just considered assumes that in a neighborhood of the surface the reflected sound follows the laws of geometric acoustics and behaves as though scattered from a plane tangent to the surface. Another formulation, due to Lysanov (Ref. III-22), is based on the assumption that the scattering surface satisfies the conditions

$$\frac{1}{2} \left( \frac{\partial S}{\partial x} \right)_{\max}^2 < < 1, \quad kh \left| \frac{\partial S}{\partial x} \right| < < 1 \quad (\text{III-97})$$

where the surface  $S$  is generated by lines parallel to the  $y$  axis and  $\left(\frac{\partial S}{\partial x}\right)_{\max}$  is the maximum value of the slope. The total field  $p = p_{\text{inc}} + p_{\text{sc}}$  at an arbitrary point  $(x, z)$  can be expressed in terms of the field and its normal derivative on the scattering surface, using Green's formula. For the two dimensional case, this is given by

$$p(x, z) = p_{\text{inc}}(x, z) + \frac{i}{4} \int_S \left\{ p \frac{\partial}{\partial n} H_0^{(1)}(kr_1) - H_0^{(2)}(kr_1) \frac{\partial p}{\partial n} \right\} ds \quad (\text{III-98})$$

where  $r_1$  is the distance between the point of observation  $(x, z)$  and the variable point  $(x_1, S(x_1))$  on the surface. The integration is along the curve obtained by cutting the uneven surface  $S(x)$  by the plane  $y = 0$ .

The boundary condition used in this model is the same as in the others, i.e.,  $p = 0$  for  $z = S(x)$ . Then, the scattered wave is given by

$$p_{\text{sc}} = -\frac{i}{4} \int H_0^{(1)}(kr_1) f(x_1) dx_1 \quad (\text{III-99a})$$

where

$$f(x_1) = \frac{dp}{dn} \frac{1}{n} \frac{1}{z} \quad \text{or} \quad \frac{1}{n} \frac{dp}{dn} \quad (\text{III-99b})$$

For this we must know  $f(x_1)$ . This is obtained by solving

$$p_{\text{inc}}(x_2, S(x_2)) = \frac{i}{4} \int H_0^{(1)}(kr_1) f(x_1) dx_1 \quad (\text{III-100})$$

where  $(x_2, S(x_2))$  is another arbitrary point on the surface, and  $r_1$  is the distance between  $(x_1, S(x_1))$  and  $(x_2, S(x_2))$ .

Using the approximation (III-97), (III-100) can be written as:

$$p_{\text{inc}}(x_2, S(x_2)) = \frac{i}{4} \int H_0^{(1)}(k|x_2 - x_1|) f(x_1) dx_1 \quad (\text{III-101})$$

In order to solve this expression for  $f(x_1)$  explicitly, suppose the incident wave is a plane wave of the form

$$p_{\text{inc}}(x, z) = e^{ik(\alpha x + \gamma z)} \quad (\text{III-102})$$

If the surface  $S(x)$  is periodic of height  $h$  and period  $\frac{2\pi}{p}$ ,  $e^{ik\gamma S(x)}$  may be expanded in the form

$$e^{ik\gamma S(x)} = \sum_{n=-\infty}^{\infty} B_n e^{inpx} \quad (\text{III-103})$$

Then  $p_{\text{inc}}(x_2, S(x_2))$  may be written as

$$p_{\text{inc}}(x_2, S(x_2)) = \sum_{n=-\infty}^{\infty} B_n e^{ik\alpha_n x} \quad (\text{III-104})$$

where  $\alpha_n = \alpha + \frac{np}{k}$ . Let  $\gamma_n = (1 - \alpha_n^2)^{\frac{1}{2}}$ . As in the previous cases, when  $\alpha_n > 1$ ,  $\gamma_n$  is chosen so that  $i\gamma_n > 0$ . Then, using (III-99b), we can obtain an expression for  $f(x_1)$ . Substituting this in (III-101), and after some analysis, we find that  $p_{\text{sc}}$  is given by

$$p_{\text{sc}}(x, z) = \sum_{n=-\infty}^{\infty} A_n e^{ik(\alpha_n x + \gamma_n z)} \quad (\text{III-105a})$$

where

$$A_n = \frac{1}{\gamma_n} \sum_{k=-\infty}^{\infty} B_{n-k} B_k \gamma_{n-k} \quad (\text{III-105b})$$

If  $S(x_2)$  is of the form  $S(x_2) = h \cos px_2$ , then  $B_n = (i)^n J_n(kh)$ , i.e.,  $B_n$  is of order  $(kh\gamma)^n$ . Neglecting terms of order greater than  $(kh\gamma)^2$  and assuming  $\gamma_{\pm 1} \approx \gamma$  (i.e.,  $k > 1$ ), we obtain

$$\begin{aligned} A_0 &\approx -1 + (kh\gamma)^2 \\ A_{\pm 1} &\approx i kh \gamma \\ A_{\pm 2} &\approx \frac{1}{2} (kh\gamma)^2 \end{aligned} \quad (\text{III-106})$$

The different approaches thus far described can be summarized as follows. The Rayleigh-La Casce and Tamarkin-Heaps approaches basically start with the scattered wave  $p_{sc}$  expressed as a sum of plane damped and undamped waves. The surface is assumed to be of the form  $S(x) = h \cos px$ . Using the condition that the total field must be zero at the boundary and employing the expansion (III-71), an infinite set of simultaneous equations is obtained for the coefficients  $A_n$ . Explicit solutions for the first few coefficients are calculated for small values of  $(kh)$ .

Brekhovskikh and Lysanov initially express  $p_{sc}$  in terms of a Helmholtz integral. Then, assuming periodicity of the surface, they also obtain an expression giving  $p_{sc}$  as the sum of plane waves. The coefficients  $A_n$  are obtained as explicit functions, i.e., they are not expressed as functions of each other. The Lysanov formulation gives the coefficients as an infinite series involving Bessel functions, while the Brekhovskikh approach expresses the coefficients in terms of a single Bessel function.

Parker (Ref. III-33) has approached the surface scattering problem by using the spectral representation of the scattered wave given in (III-49). Without the time dependence, this is

$$p_{sc} = \int_{-\infty}^{\infty} \int_{-\infty}^{\infty} \phi(\lambda, \mu) e^{ik(\lambda x + \mu y + \nu z)} d\lambda d\mu \quad (III-107)$$

where  $\lambda^2 + \mu^2 + \nu^2 = 1$  and  $\nu \geq 0$  if  $1 - \lambda^2 - \mu^2 \geq 0$  and  $\nu > 0$  otherwise, cf. (III-48). As in the other treatments, the incident wave is taken to be a plane wave of the form

$$p_{inc} = e^{ik(\alpha x + \gamma z)} \quad (III-108)$$

Then, the boundary condition that  $p_{inc} + p_{sc} = 0$  at the surface becomes an integral equation for  $\phi(\lambda, \mu)$ , as given in (III-50).

In his development, Parker works primarily with  $\Phi(x, y)$ , the Fourier transform of  $\phi(\lambda, \mu)$ . With  $z = S(x, y)$ , he first shows that

$$\lim_{S \rightarrow 0} \Phi(x, y) = \Phi_0(x, y) = -e^{ik\alpha x} \quad (III-109)$$



when the incident wave is given by (III-108). Then, a representation for  $\tilde{\Phi}$  is assumed which is of the form

$$\tilde{\Phi}(x, y) = \tilde{\Phi}_0(x, y) e^{iku(x, y)} \quad (\text{III-110})$$

where  $u(x, y)$  goes uniformly to zero as  $S(x, y)$  vanishes. After considerable analysis,  $u$  is found to be given by

$$u = \frac{2S(x, y)\gamma}{1 + S(x, y) \sum_{n=1}^{\infty} \left( S(x, y) \theta \frac{\partial}{\partial x} \right)^n \frac{1}{S(x, y)}} \quad (\text{III-111})$$

where  $\theta = \tan(\cos^{-1}\gamma)$  and  $\left( S(x, y) \theta \frac{\partial}{\partial x} \right)^n$  signifies that the operator  $S(x, y) \theta \frac{\partial}{\partial x}$  is to be applied  $n$  times. To obtain this result, it is assumed that certain terms can be neglected in solving a non-linear differential equation and that truncation of certain Taylor series expansions is permissible.

The spectrum  $\phi(\lambda, \mu)$  can then be written as

$$\phi(\lambda, \mu) = -\frac{1}{2\pi} \int_{-\infty}^{\infty} \int_{-\infty}^{\infty} e^{iku(x, y)} e^{ik[(\lambda - \alpha)x + \mu y]} dx dy \quad (\text{III-112})$$

If the surface  $S(x, y)$  can be expressed as a periodic function of  $x$ , with period

$\frac{2\pi}{p}$ , then  $u$  also will be periodic and can be written as

$$e^{iku(x)} = \sum_{n=-\infty}^{\infty} B_n e^{-inpx} \quad (\text{III-113a})$$

with

$$B_n = \frac{1}{2\pi} \int_{-\pi}^{\pi} e^{iku(x)} e^{-inpx} d(px) \quad (\text{III-113b})$$

Substituting (III-113) into (III-112) gives

$$\phi(\lambda, \mu) = -2\pi \delta(\mu) \sum_{n=-\infty}^{\infty} B_n \delta\left(\lambda - \alpha - \frac{np}{k}\right) \quad (\text{III-114})$$

which, when substituted into (III-107), gives

$$p_{sc}(x, z) = - \sum_{n=-\infty}^{\infty} B_n e^{ik(\alpha_n x + \gamma_n z)} \quad (\text{III-115a})$$

where

$$\alpha_n = + \frac{np}{k} \quad (\text{III-115b})$$

$$\gamma_n = \left(1 - \alpha_n^2\right)^{\frac{1}{2}}$$

with the usual conventions (III-48) on the sign of  $\gamma_n$ . This is exactly the type of expansion obtained in the other approaches dealing with periodic surfaces. The coefficients are given as the Fourier coefficients of the function  $e^{iku(x)}$ , as in (III-113).

Parker's development requires that  $S(x, y) \geq 0$ ; thus, a sinusoidal one dimensional surface may be given by

$$S(x) = h(1 - \cos px) \quad (\text{III-116})$$

Then, it turns out that

$$ku = c_o + \sum_{n=1}^{\infty} c_n \sin(np x + b_n) \quad (\text{III-117a})$$

where

$$c_n = \frac{2kh \gamma a_n}{\left[1 + (ph)^2 \theta^2\right]^{\frac{1}{2}}} \quad (\text{III-117b})$$

and  $\theta = \tan^{-1}(\gamma)$ . The quantities  $a_n$  and  $b_n$  are functions only of the parameter  $\text{ph } \theta$ . These functions are somewhat complicated and are given by Parker (Ref. III-33, pg. 680). If we assume  $\text{ph } \theta \leq 1$ , we need consider only the term for  $n=0, 1, 2$  in (III-117). Therefore

$$ku(x) = c_0 + c_1 \sin(px + b_1) + c_2 \sin(2px + b_2) \quad (\text{III-118})$$

Using (III-71),  $e^{iku}$  can be expanded as the product of two series of Bessel functions. Substituting this in (III-113b),  $B_0$  is given by

$$B_0 = \sum_{n=-\infty}^{\infty} J_{2n}(c_1) J_n(c_2) e^{-i(2b_1 - b_2)} \quad (\text{III-119})$$

Recall that in terms of our usual notation,  $B_0 = -A_0$ . Furthermore, for  $\text{ph } \theta \leq 1$ , it turns out that  $2b_1 - b_2 \approx -2\pi$ , and thus we have

$$A_0 = - \sum_{n=-\infty}^{\infty} J_{2n}(c_1) J_n(c_2) \quad (\text{III-120})$$

Since  $c_n$  is of the order of  $kh$ , it follows that for  $kh$  small enough ( $kh \ll 1$ ), we may ignore Bessel functions of order 2 or greater and therefore

$$A_0 \approx - J_0(c_1) J_0(c_2) \quad (\text{III-121})$$

This first coefficient is the only one for which Parker obtains even an approximate expression.

As mentioned earlier, no work seems to have been done in relating the above theories to scattering observed in the sea. However, laboratory experiments, with artificially constructed wave surfaces give at least qualitative support to the theories. La Casce and Tamarkin (Ref. III-18) used a corrugated cork surface floating on water to give the sinusoidal pressure release. Several surfaces were used, with the incident sound at 10 kc intervals over the range 80 kc - 300 kc and various angles of incidence. Leporskii (Ref. III-21) made similar measurements using a totally submerged thin glass foil as a reflecting surface.

In both cases, very close agreement was found between the theoretical and experimental scattering directions. La Casce measured these by noting the directions which corresponded to peaks in the reflected sound. He found the observed angle generally to be within  $2^\circ$  of the expected angle; only rarely was the difference as large as  $3^\circ$ . Leporskii, using a more precise technique, found even closer agreement. Leporskii's results are shown in Figure III-30, which compares the expected and experimental angles. The data reported is for incident sound with  $k \sim 1.7 \text{ mm}^{-1}$  (for several different scattering orders), and for surfaces with  $p \sim 0.41 \text{ mm}^{-1}$ ,  $h \sim 1.0 \text{ mm}$ . Figure III-30a refers to surfaces with sinusoidal corrugation, while Figure III-30b deals with sawtooth corrugations. (Other data of Leporskii relating to scattering directions is shown in Figures III-39 and III-41).

Figures III-31 through III-38 show some of La Casce and Tamarkin's experimental results and compare these with the various theories. The data is for the amplitudes  $A_0$  and  $A_{-1}$ . Two surfaces are considered, each of the form  $S(x) = h \cos px$ . Surface A has  $p = 3.12 \text{ cm}^{-1}$ ,  $h = 0.24 \text{ cm}$  while surface B has  $p = 3.08 \text{ cm}^{-1}$  and  $h = 0.15 \text{ cm}$ . Measurements were made at  $0^\circ$  and  $40^\circ$  angles of incidence. The order of presentation is as follows:

Figure	Component	Surface	Angle of Inc	Theoretical Models Compared*
III-31	$A_0$	A	$0^\circ$	1, 2, 3, 4
III-32	$A_0$	B	$0^\circ$	1, 2, 3, 4, 5
III-33	$A_0$	A	$40^\circ$	1, 2, 3, 4
III-34	$A_0$	B	$40^\circ$	1, 2, 3, 4, 5
III-35	$A_{-1}$	A	$0^\circ$	1, 2, 3
III-36	$A_{-1}$	B	$0^\circ$	1, 2, 3, 5
III-37	$A_{-1}$	A	$40^\circ$	1, 2, 3
III-38	$A_{-1}$	B	$40^\circ$	1, 2, 3, 5

\*1. Rayleigh

2. Rayleigh (La Casce)

3. Brekhovskikh

4. Parker

5. Heaps

The experimental data exhibit a peaking, or nodal, behavior. All of the theoretical models predict this fairly well, suggesting that the Bessel functions used in the models are appropriate for describing the scattering magnitude. All the models predict roughly the same behavior, and there is nothing

in the experimental data which indicates any one as being the most suitable. Heaps' approach, which neglects the damped waves, seems to give the best results. The poorest agreement occurs for the larger angle ( $40^\circ$ ) of incidence. In general, experimental results for surface B agree with the theoretical predictions better than those for surface A. This is to be expected; since B has a smaller value of  $h$ , the condition on  $(kh)$  and the slope will be better satisfied.

Leporskii has compared his experimental data with the predictions of the Brekhovskikh (Ref. III-21) and Lysanov (Ref. III-22) models. Since the surfaces and frequencies are quite different, the data cannot be compared directly with La Casce's. Furthermore, since results are presented for only a few frequencies, we cannot observe the variation in scattering amplitudes with changes in frequency, as shown in Figures III-39 through III-41. On the other hand, Leporskii's technique permits him to observe several of the scattering orders.

Figure III-39 illustrates the theoretical and experimental agreement for the Brekhovskikh model, with the dotted lines giving the theoretical values and the solid lines the experimental results. The dashed lines are the boundaries of the sectors within which the Brekhovskikh theory is claimed to be valid. The arrows pointing towards the center of the pattern show the direction of the incident wave; the arrows pointing away show the direction of specular scattering. As can be seen from the figure, the agreement is qualitatively good; however, in each case there is significant disagreement for the magnitude of some scattering order. The conditions of the theory were well satisfied in the experiment; hence some inadequacy apparently remains in the theoretical development.

Figures III-40 and III-41 compare the prediction of the Lysanov model with Leporskii's experimental results. Figure III-40 compares the magnitudes of the expected and observed amplitudes for various orders of scattering surfaces, frequencies and angles of incidence. Though not stated, the conditions are presumably the same as in the analysis of the Brekhovskikh model. Figure III-41 illustrates the scattering of various orders. As with the Brekhovskikh model, the agreement is qualitatively good; however, the scatter shown in Figure III-40 suggests that there may still be significant discrepancies between theoretical expectation and experimental observations.

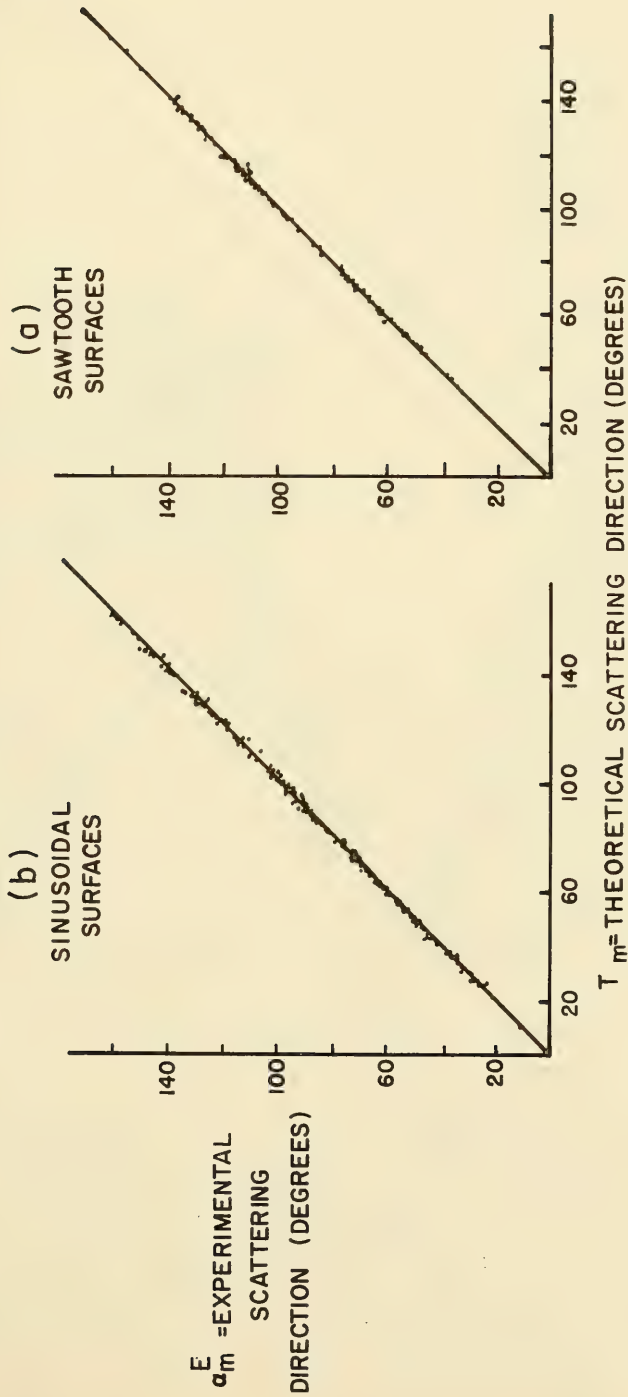


FIGURE III-30 THEORETICAL AND EXPERIMENTAL SCATTERING DIRECTIONS  
(AFTER LEPORSKII)



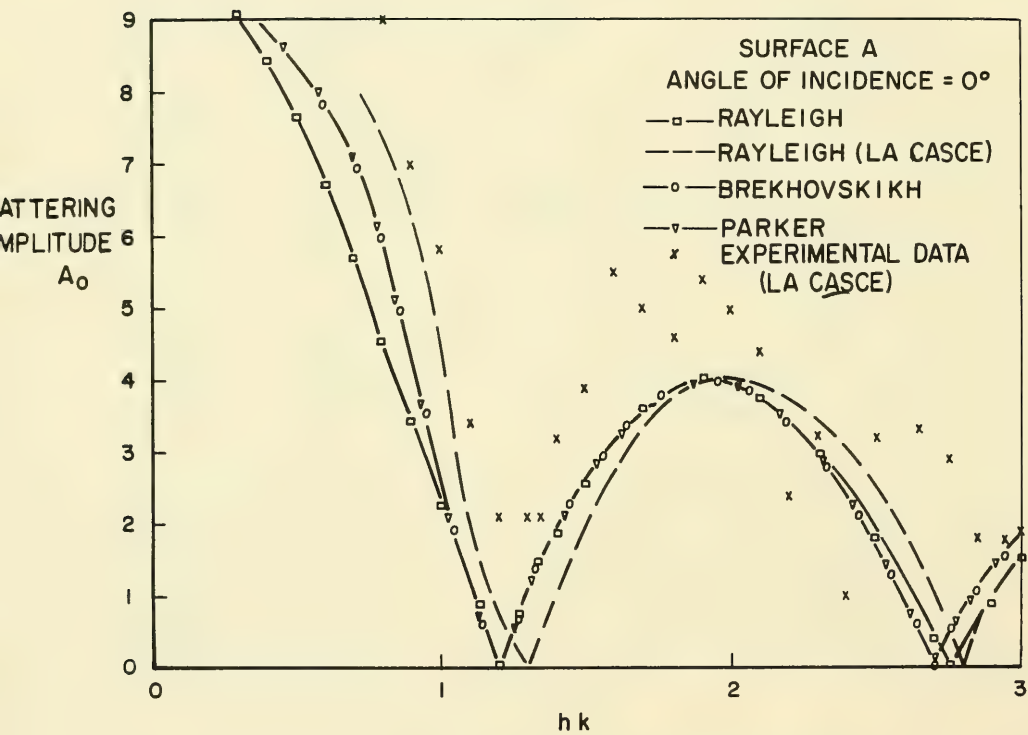


FIGURE III-31 EXPERIMENTAL AND THEORETICAL MAGNITUDES OF  $A_0$  FOR SURFACE A

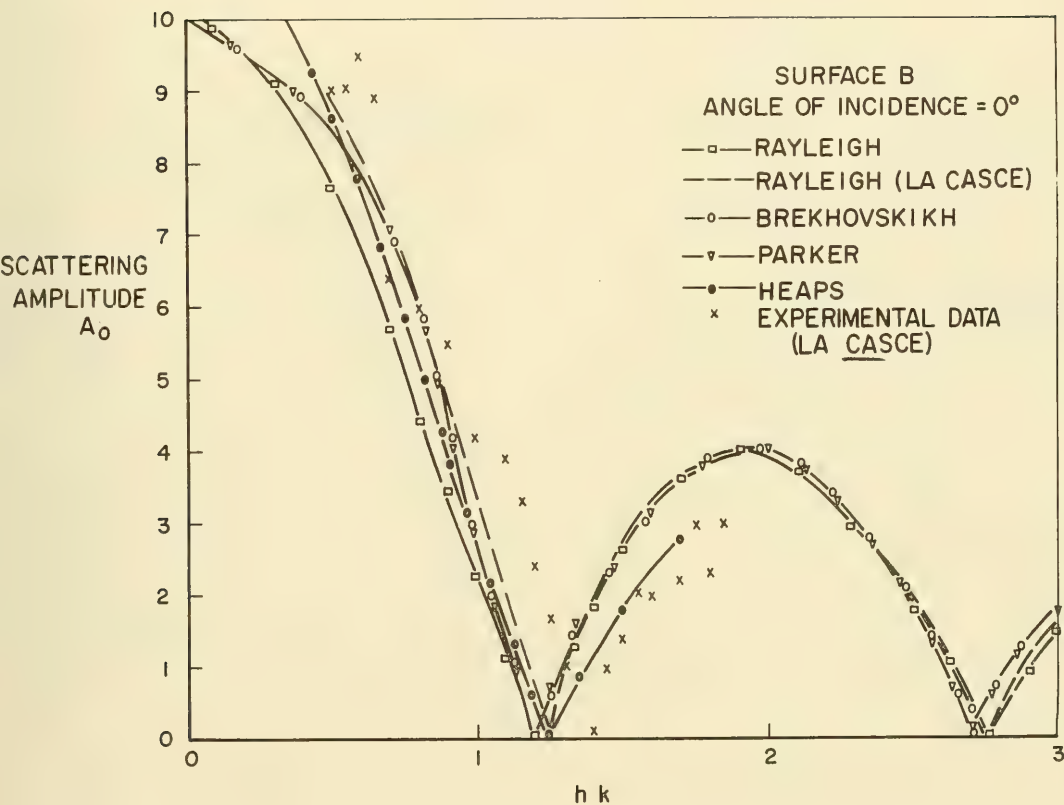


FIGURE III-32 EXPERIMENTAL AND THEORETICAL MAGNITUDES OF  $A_0$  FOR SURFACE B

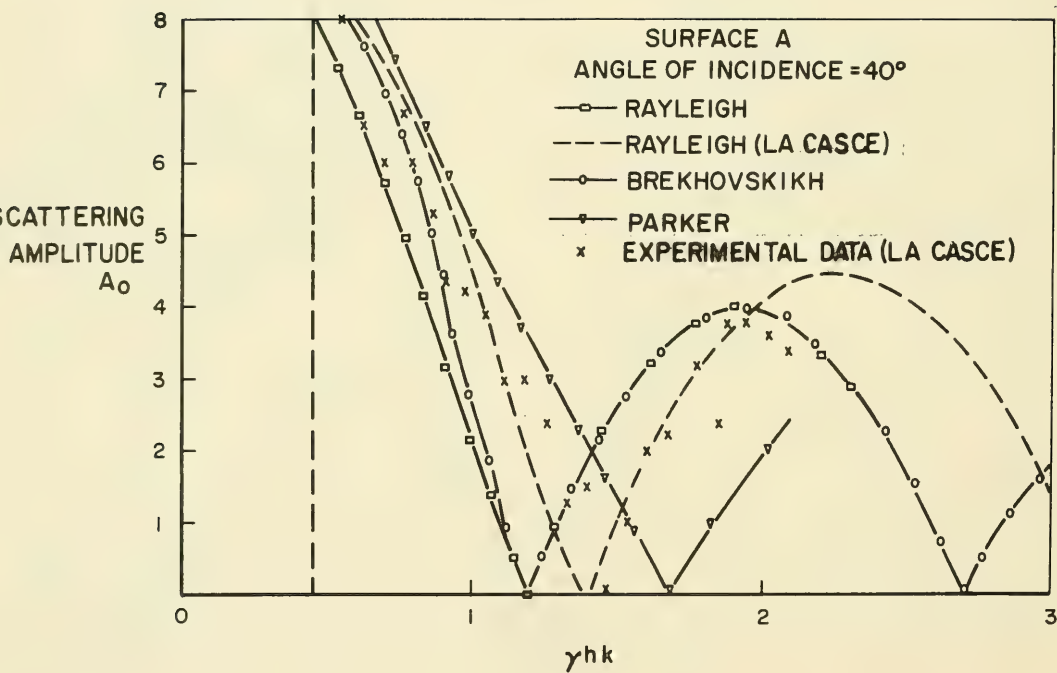


FIGURE III-33 EXPERIMENTAL AND THEORETICAL MAGNITUDES OF  $A_0$  FOR SURFACE A

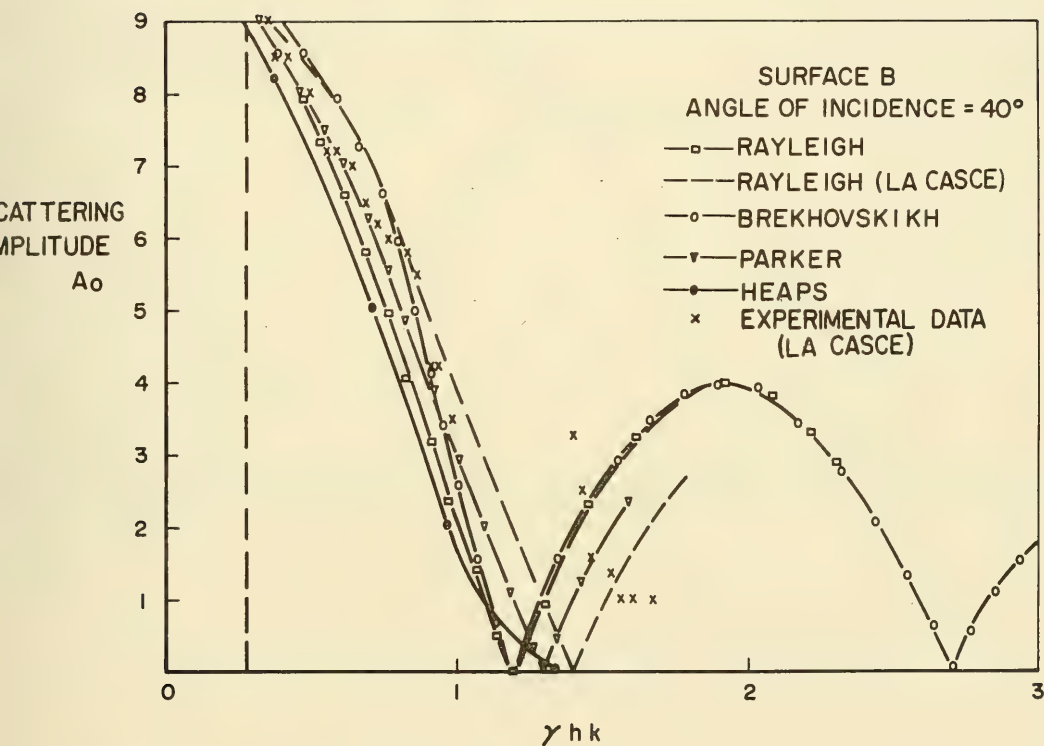


FIGURE III-34

EXPERIMENTAL AND THEORETICAL MAGNITUDES OF  $A_0$   
FOR SURFACE B

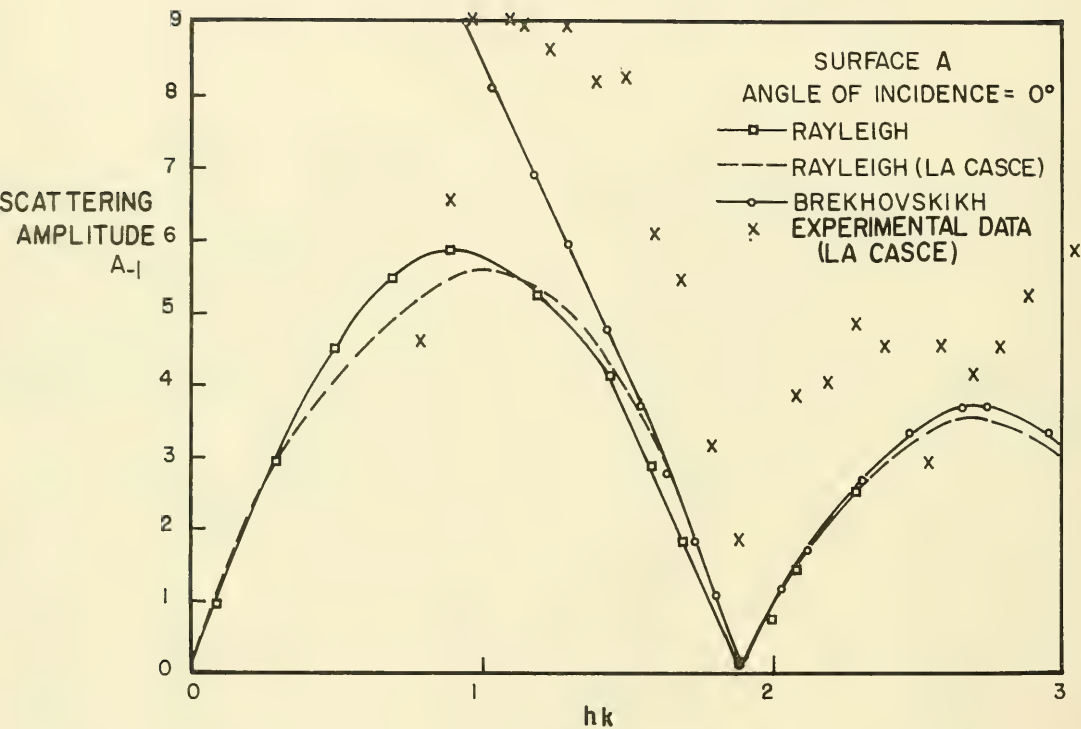


FIGURE III-35

EXPERIMENTAL AND THEORETICAL MAGNITUDES OF  $A_{-1}$  FOR SURFACE A

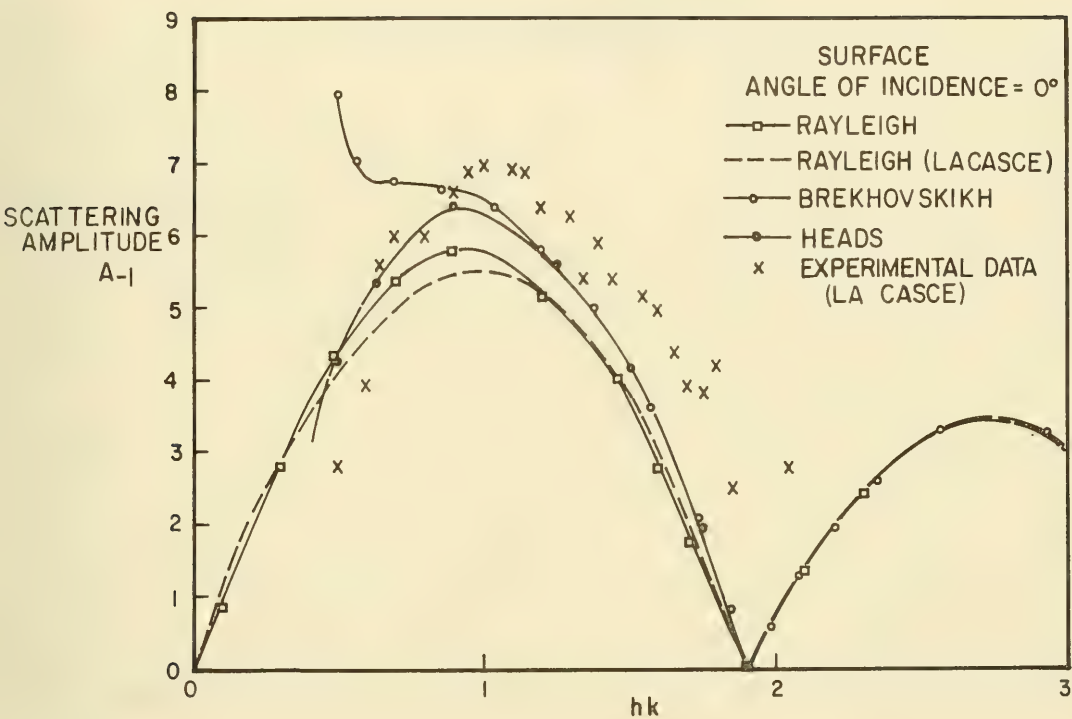


FIGURE III-36 EXPERIMENTAL AND THEORETICAL MAGNITUDES OF  $A_{-1}$  FOR SURFACE B



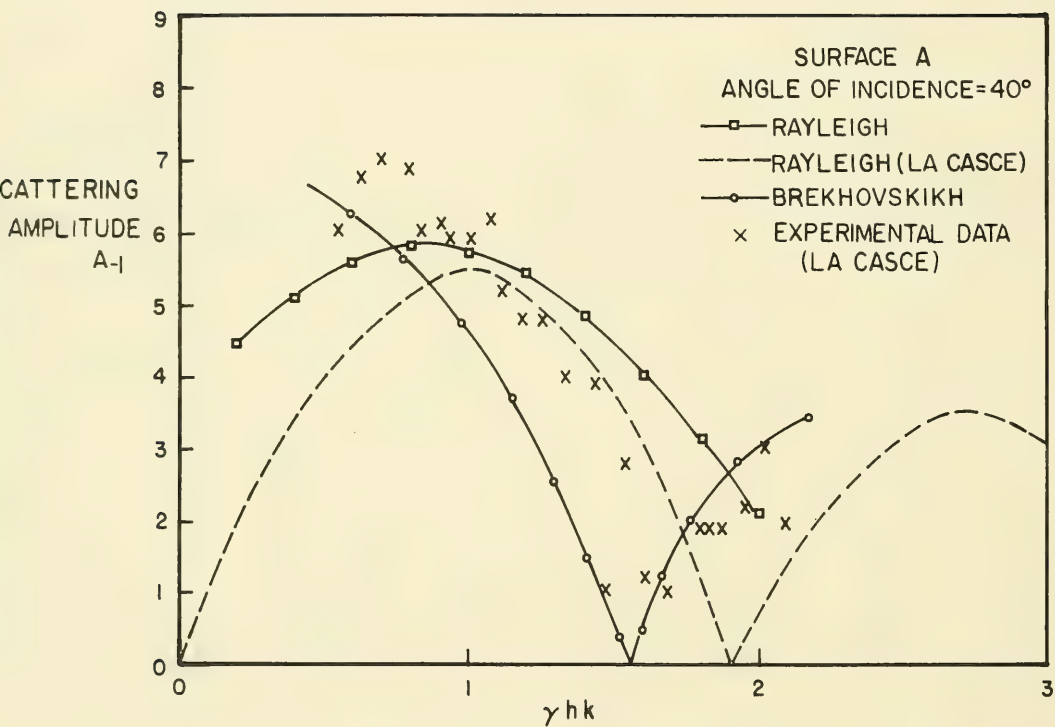


FIGURE III-37 EXPERIMENTAL AND THEORETICAL MAGNITUDES OF  $A_{-1}$  FOR SURFACE A

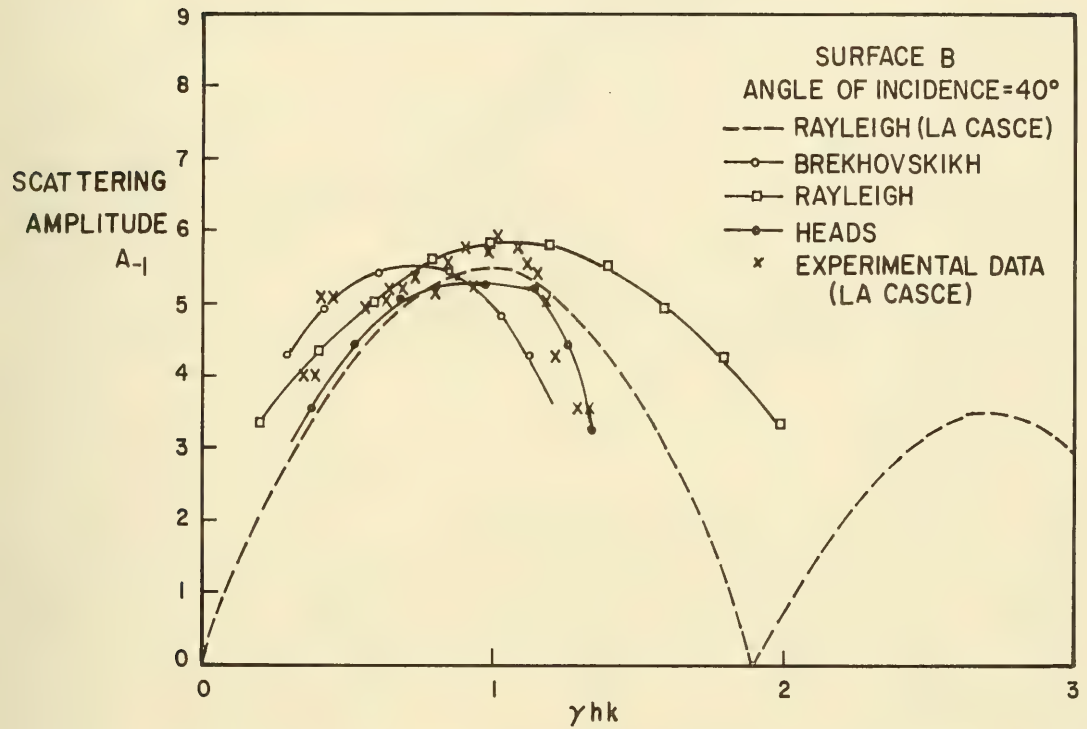


FIGURE III-38

EXPERIMENTAL AND THEORETICAL MAGNITUDES OF  
 $A_{-1}$  FOR SURFACE B

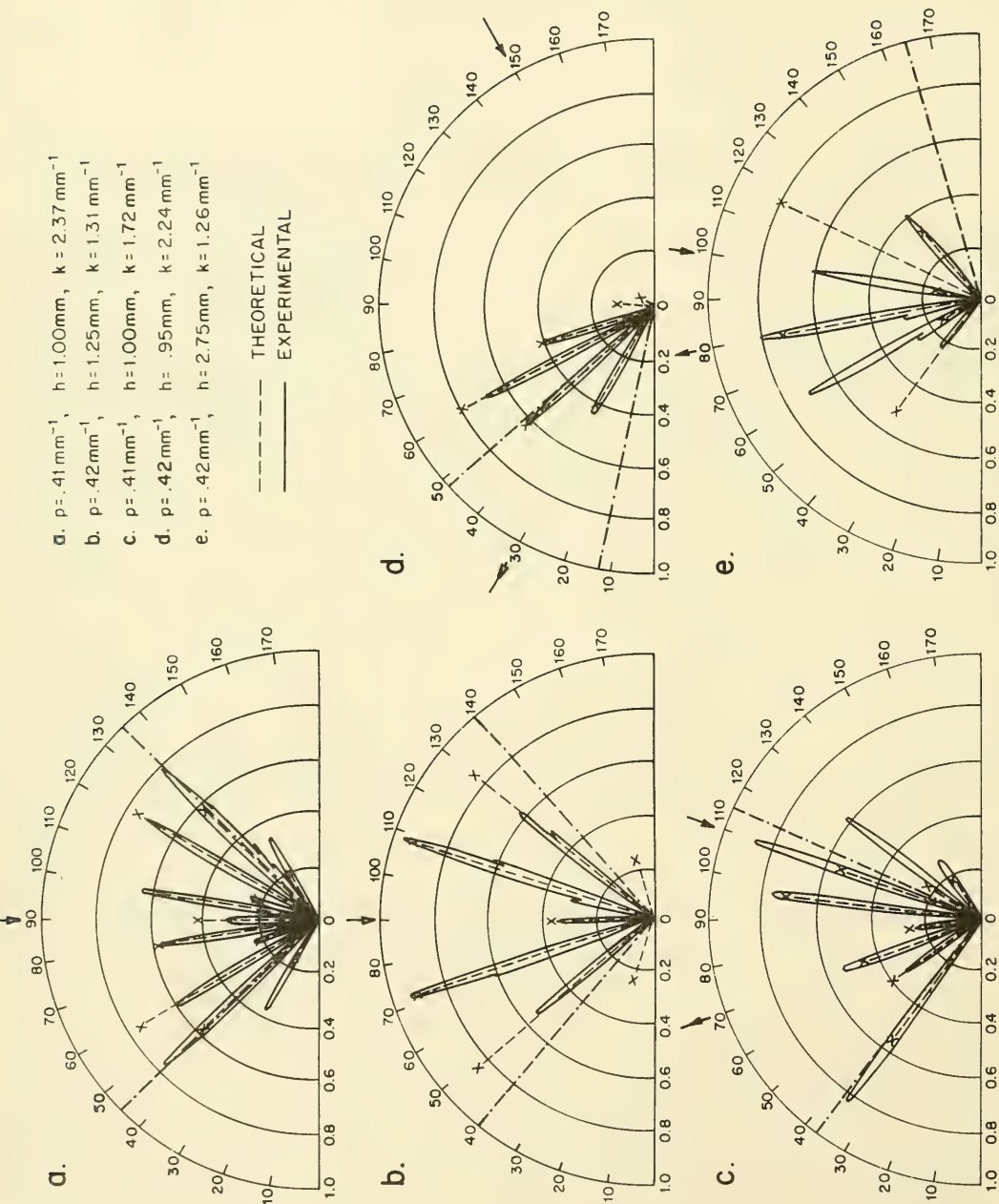


FIGURE III-39 COMPARISON OF THEORETICAL (BREKHOVSKIKH) AND EXPERIMENTAL SCATTERING PATTERNS (AFTER LEPORSKII)

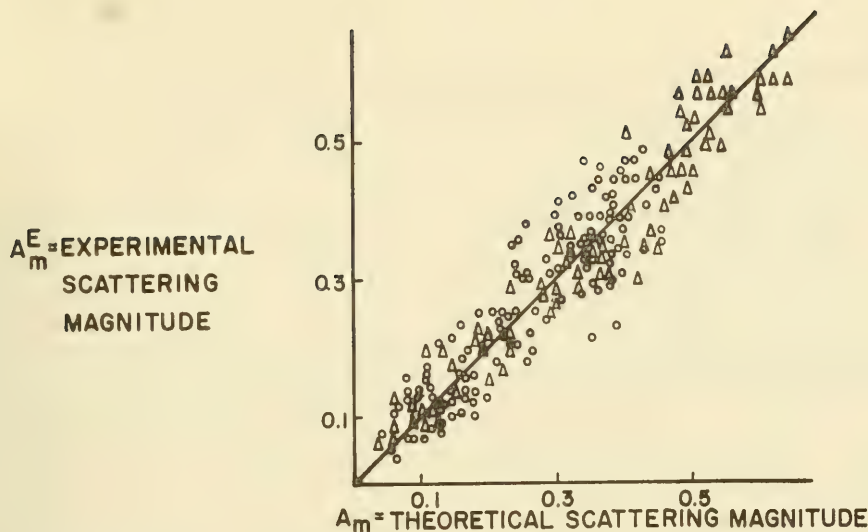


FIGURE III-40 COMPARISON OF THEORETICAL AND EXPERIMENTAL SCATTERING MAGNITUDES FOR THE LYANOV THEORY (AFTER LEPORSKII)

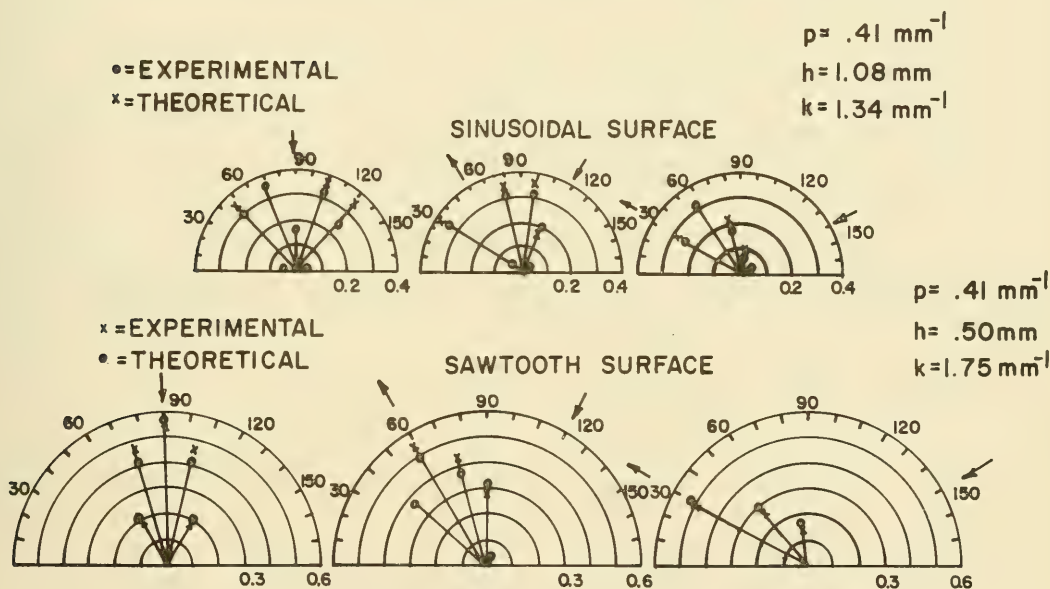


FIGURE III-41 THEORETICAL AND EXPERIMENTAL SCATTERING PATTERNS FOR THE LYANOV MODEL (AFTER LEPORSKII)

## 2. Stochastic Surfaces

The foregoing developments have all assumed that the sea surface possesses a definite functional description  $z = S(x, y)$ . This description was generally taken to be one-dimensional and periodic in nature; that is, the surface was generated by a family of lines parallel to one of the coordinate axes. In such a situation, the scattered wave resulting from a plane incident wave could be expressed as the sum of plane waves. To obtain the magnitude of the scattered plane waves, we studied the surface  $z = S(x) = h \cos px$ .

In reality, the sea surface is extremely complex and varying in time. Generally it is not locally periodic nor one dimensional, although it may be approximately so when considered from a macroscopic viewpoint. As mentioned earlier, there may also be inhomogeneities near the surface. Accordingly, any results based on a model such as  $S(x) = h \cos px$  can only be suggestive of the true scattering behavior.

Marsh, et al. (Ref. III-27) have approached the problem of scattering from the surface by using a spectral description of the sea. In particular, they use the Neumann-Pierson spectrum  $A^2(\omega)$ , where  $A^2(\omega) d\omega$  gives the contribution to the mean square wave height due to surface waves having frequencies between  $\omega$  and  $\omega + d\omega$ . The surface is furthermore assumed to be isotropic, i.e., the correlation of the surface height at two points depends only on the distance between them. This means that the surface waves have (on the average) no well defined direction. Using such a description of the surface, Marsh obtains an approximate expression for the intensity scattered in the specular direction. Since his treatment is a little obscure, and contains some numerical errors, we shall present it in some detail.

As in the other treatments, the incident wave is a plane wave, of the form

$$p_{\text{inc}}(x, y, z) = e^{ik(\alpha x + \beta y + \gamma z)} \quad (\text{III-122})$$

and the scattered wave is represented by

$$p_{\text{sc}}(x, y, z) = \int_{-\infty}^{\infty} \int_{-\infty}^{\infty} e^{ik(\lambda x + \mu y + \nu z)} \Phi(\lambda, \mu) d\lambda d\mu \quad (\text{III-123})$$

where  $\lambda, \mu, \nu$  are direction cosines satisfying (III-48).

Suppose that we have such a representation for the scattered wave, i.e., we have found a  $\hat{\Phi}(\lambda, \mu)$  such that (III-123) is true. Then

$$p'_{sc}(x, y) = p_{sc}(x, y, 0) = \int_{-\infty}^{\infty} \int_{-\infty}^{\infty} e^{-ik(\lambda x + \mu y)} \hat{\Phi}(\lambda, \mu) d\lambda d\mu \quad (\text{III-124})$$

gives the scattered wave in the plane  $z=0$ . (The coordinate axes are assumed to be oriented so that the plane  $z=0$  lies completely below the surface.) If we use the notation  $\hat{\Phi}$  to denote the Fourier transform of  $\Phi$ , then (III-124) also states that  $p'_{sc} = \hat{\Phi}$ .

The autocorrelation function of  $p'_{sc}$  is given by<sup>(1)</sup>

$$\Psi(x, y) = (p'_{sc} * p'_{sc})(x, y) = \int_{-\infty}^{\infty} \int_{-\infty}^{\infty} p_{sc}(\xi, \eta) \bar{p}_{sc}(\xi + x, \eta + y) d\xi d\eta \quad (\text{III-125})$$

Let  $\bigwedge(\lambda, \mu) = \hat{\Psi}(\lambda, \mu)$  be the Fourier transform of  $\Psi(x, y)$ , i.e.,

$$\bigwedge(\lambda, \mu) = \frac{1}{2\pi} \int_{-\infty}^{\infty} \int_{-\infty}^{\infty} e^{-i(\lambda x + \mu y)} \Psi(x, y) dx dy \quad (\text{III-126})$$

Since the Fourier transform of the autocorrelation function  $(p'_{sc} * p'_{sc})$  is the absolute square of the transform of  $p'_{sc}$ , it follows also that

$$\bigwedge(\lambda, \mu) = |\hat{p}'_{sc}(\lambda, \mu)|^2. \quad (\text{III-127})$$

---

1. We are using \* to denote the convolution of two functions, and a superscript bar to indicate complex conjugate.

However,  $p'_{sc} = \hat{\Phi}$ , hence  $\hat{p}'_{sc} = \hat{\Phi} = \Phi$ , and therefore

$$\wedge(\lambda, \mu) = |\Phi(\lambda, \mu)|^2. \quad (\text{III-128})$$

Consequently  $\wedge(\lambda, \mu)$  is the absolute square of the amplitude of the scattered wave traveling in the  $(\lambda, \mu, \nu)$  direction, and therefore,  $\wedge(\lambda, \mu)$  is proportional to the power scattered in the  $(\lambda, \mu, \nu)$  direction.

It is now necessary to obtain an expression for  $\Phi(\lambda, \mu)$ . We introduce the nondimensional coordinates  $\xi, \eta$  given by

$$kx = \xi, \quad ky = \eta \quad (\text{III-129})$$

Let the surface be described by  $S(x, y)$ . (The explicit form of this function will not be required.) In terms of these new variables, the surface can be described by the normalized function,  $\zeta(\xi, \eta)$ , such that:

$$kS(x, y) = \sigma \zeta(\xi, \eta) \quad (\text{III-130})$$

where  $\sigma = kh$  and  $h^2 = \langle S^2(x, y) \rangle$  denotes the mean square height of the surface. Then

$$p_{sc}[x, y, S(x, y)] = \int_{-\infty}^{\infty} \int_{-\infty}^{\infty} e^{i[\lambda \xi + \mu \eta + \nu \zeta(\xi, \eta)]} \Phi(\lambda, \mu) d\lambda d\mu \quad (\text{III-131})$$

As in the other developments, we have the boundary condition that

$$p_{inc}[x, y, S(x, y)] + p_{sc}[x, y, S(x, y)] = 0$$

Hence

$$e^{i[\alpha \xi + \beta \eta + \gamma \zeta(\xi, \eta)]} + \int_{-\infty}^{\infty} \int_{-\infty}^{\infty} e^{i[\lambda \xi + \mu \eta + \nu \zeta(\xi, \eta)]} \Phi(\lambda, \mu) d\lambda d\mu = 0 \quad (\text{III-132})$$



Let  $\Phi(\lambda, \mu)$  be expressed as a power series in  $\sigma$  in the form

$$\Phi(\lambda, \mu) = \sum_{n=0}^{\infty} \sigma^n \Phi_n(\lambda, \mu) \quad (\text{III-133})$$

Since (III-132) must be true for all  $\sigma$ , it then follows that

$$\frac{(-i\sigma \zeta(\xi, \eta))^m}{m!} e^{-i(\alpha \xi + \beta \eta)} + \sum_{n=0}^m \frac{[i \zeta(\xi, \eta)]^n}{n!} \int_{-\infty}^{\infty} \int_{-\infty}^{\infty} e^{-i(\lambda \xi + \beta \eta)} \vee^n \Phi_{m-n}(\lambda, \mu) d\lambda d\mu = 0 \quad (\text{III-134})$$

Solving this for  $\Phi_m(\lambda, \mu)$  for  $m=0, 1, 2$ , we have

$$\Phi_0(\lambda, \mu) = -\delta(\lambda - \alpha) \delta(\mu - \beta) \quad (\text{III-135a})$$

$$\Phi_1(\lambda, \mu) = 2i \vee \left[ \zeta(\xi, \eta) e^{-i(\alpha \xi + \beta \eta)} \right]^{-1} \quad (\text{III-135b})$$

$$\Phi_2(\lambda, \mu) = 2 \vee \left[ \zeta(\xi, \eta) \right]^{-1} * \left( \vee \left[ \zeta(\xi, \eta) e^{-i(\alpha \xi + \beta \eta)} \right]^{-1} \right) \quad (\text{III-135c})$$

where  $[f]^{-1}$  denotes the inverse Fourier transform of  $f$  and  $f * g$  denotes the convolution of  $f$  and  $g$ .

To see how these are obtained, we consider the solution for  $\Phi_2(\lambda, \mu)$ , assuming  $\Phi_0(\lambda, \mu)$  and  $\Phi_1(\lambda, \mu)$  have been obtained as given above. Then writing out (III-134) for  $m=2$ , we have

$$I_0 + I_1 + I_2 + I_3 = 0 \quad (\text{III-136a})$$

where

$$I_0 = \frac{[-i \vee \zeta(\xi, \eta)]^2}{2!} e^{-i(\alpha \xi + \beta \eta)} \quad (\text{III-136b})$$

$$I_1 = \frac{[i\zeta(\xi, \eta)]^2}{2!} \int_{-\infty}^{\infty} \int_{-\infty}^{\infty} e^{-i(\lambda\xi + \beta\eta)} \nu^2 \tilde{\Phi}_0(\lambda, \mu) d\lambda d\mu \quad (\text{III-136c})$$

$$I_2 = i\zeta(\xi, \eta) \int_{-\infty}^{\infty} \int_{-\infty}^{\infty} e^{-i(\lambda\xi + \mu\eta)} \nu \tilde{\Phi}_1(\lambda, \mu) d\lambda d\mu \quad (\text{III-136d})$$

$$I_3 = \int_{-\infty}^{\infty} \int_{-\infty}^{\infty} e^{-i(\lambda\xi + \mu\eta)} \tilde{\Phi}_2(\lambda, \mu) d\lambda d\mu \quad (\text{III-136e})$$

Substituting for  $\tilde{\Phi}_1(\lambda, \mu)$  in (III-136d), we have

$$I_2 = i\zeta(\xi, \eta) \left( \hat{\nu} * 2i\nu \left[ \zeta(\xi, \eta) e^{-i(\alpha\xi + \beta\eta)} \right]^{-1} \right) \quad (\text{III-137})$$

Substituting (III-135a) in (III-136c), and recalling that  $\lambda^2 + \mu^2 + \nu^2 = 1$ , we see that  $I_0 + I_1 = 0$ . Then  $I_2 + I_3 = 0$ , and  $-I_2$  is the Fourier transform of  $\tilde{\Phi}_2(\lambda, \mu)$ . From this we have

$$\begin{aligned} \tilde{\Phi}_2(\lambda, \mu) &= \left[ -I_2 \right]^{-1} \\ &= +2\nu \left[ \zeta(\xi, \eta) \right]^{-1} * \left( \nu \left[ \zeta(\xi, \eta) e^{-i(\alpha\xi + \beta\eta)} \right]^{-1} \right) \end{aligned} \quad (\text{III-138})$$

The first three terms  $\tilde{\Phi}_0$ ,  $\tilde{\Phi}_1$ ,  $\tilde{\Phi}_2$  must be considered to obtain the lowest order correction to the intensity in the specular direction. With  $\tilde{\Phi} = \tilde{\Phi}_0 + \sigma \tilde{\Phi}_1 + \sigma^2 \tilde{\Phi}_2 + \dots$ , the component  $\tilde{\Phi}_0$  is associated with the specular direction and  $\tilde{\Phi}_1$  with the non-specular direction. The energy in the non-specular wave must come from the incident wave and be  $\approx \sigma^2 \tilde{\Phi}_1^2 + \dots$ ; hence, the energy in the specular direction must be  $\approx 1 - \sigma^2 \tilde{\Phi}_1^2 + \dots$  (where the incident plane wave has unit amplitude). Consequently, there cannot be a correction of order  $\sigma$  to the specular term, for this would require an energy correction of order  $\sigma$  -- since  $[1 - O(\sigma)]^2 = 1 - 2[O(\sigma)] + O(\sigma^2)$ .

For the rest of the analysis, it is assumed that all terms involving a factor  $\sigma^n$ , where  $n \geq 3$ , may be ignored. It is difficult to determine whether this assumption is warranted; however, if the  $m = 2$  specular correction is small compared to the  $m = 0$  component, we might have confidence in the adequacy of 3 terms. The wave number  $k$  is given by  $k = 2\pi f/c$  where  $c = 150,000$  cm/sec is the speed of sound in water. For  $f = 1000$  cps and small waves ( $h = 100$  cm), we have  $\sigma \approx 4$ . We will have  $\sigma > 1$  whenever  $fh > 50,000$ , which happens for most sea states and sound frequencies of interest. Thus we see that this truncation is valid only when the magnitudes of the  $\Phi_n(\lambda, \mu)$  decay rather rapidly--e.g., exponentially.

Using this truncated form for  $\Phi$ , the amplitude of the scattered wave in the plane  $z = 0$ , is

$$\begin{aligned} p'_{sc}(\xi, \eta) &= \int_{-\infty}^{\infty} \int_{-\infty}^{\infty} e^{-i(\lambda\xi + \mu\eta)} \Phi(\lambda, \mu) d\lambda d\mu \\ &= e^{-i(\alpha\xi + \beta\eta)} + 2i\gamma\sigma\zeta(\xi, \eta)e^{-i(\alpha\xi + \beta\eta)} \end{aligned} \quad (\text{III-139})$$

$$-2\gamma\sigma^2\zeta(\xi, \eta) \left[ \hat{\nu}(\xi, \eta) * \left[ \zeta(\xi, \eta) e^{-i(\alpha\xi + \beta\eta)} \right] \right]$$

where  $\hat{\nu}$  is the Fourier transform of  $\nu$ . The autocorrelation function  $\Psi(\xi, \eta)$  of  $p'_{sc}(\xi, \eta)$  is given by

$$\begin{aligned} \Psi(\xi, \eta) &= e^{-i(\alpha\xi + \beta\eta)} \left[ 1 + 4\gamma^2\sigma^2 Z(\xi, \eta) \right. \\ &\quad \left. - 4\gamma\sigma^2 \int_{-\infty}^{\infty} \int_{-\infty}^{\infty} \nu(\lambda, \mu) \hat{Z}(\lambda, \mu) d\lambda d\mu \right] \end{aligned} \quad (\text{III-140})$$

where  $Z(\xi, \eta)$  is the autocorrelation function of  $\zeta(\xi, \eta)$  and  $\hat{Z}$  is the Fourier transform of  $Z$ . The Fourier transform of  $\Psi(\xi, \eta)$  then gives  $\Lambda(\lambda, \mu)$ , the intensity, as

$$\begin{aligned} \Lambda(\lambda, \mu) = & \left[ 1 - 4 \gamma \sigma^2 \int_{-\infty}^{\infty} \int_{-\infty}^{\infty} v(\ell, m) \hat{Z}(\ell - \alpha, m - \beta) d\ell dm \right] \delta(\lambda - \alpha) \delta(\mu - \beta) \\ & + 4 \gamma^2 \sigma^2 \hat{Z}(\lambda - \alpha, \mu - \beta). \end{aligned} \quad (\text{III-141})$$

The term  $4 \gamma^2 \sigma^2 \hat{Z}(\lambda - \alpha, \mu - \beta)$  gives the intensity of the nonspecular waves, while

$$\Omega_{\text{spec}} = 1 - 4 \gamma \sigma^2 \int_{-\infty}^{\infty} \int_{-\infty}^{\infty} v(\ell, m) \hat{Z}(\ell - \alpha, m - \beta) d\ell dm \quad (\text{III-142})$$

gives the intensity in the specular direction, where  $\ell^2 + m^2 + v^2 = 1$ . We will now concentrate on an analysis of this latter term.

Marsh, et al. describes the surface by using the Neumann-Pierson energy spectrum

$$A^2(\omega) = \frac{c}{\omega^6} e^{-\left(\frac{2g^2}{\omega^2 s^2}\right)} \text{cm}^2 \text{sec} \quad (\text{III-143})$$

where

$$c = 4.8 (10^4) \text{cm}^2 \text{sec}^{-5}$$

$$g = \text{acceleration due to gravity} = 980 \text{cm sec}^{-2}$$

$$s = \text{wind speed in cm sec}^{-1}$$

$$\omega = \text{angular frequency in rad. sec}^{-1}$$

Using the assumed isotropy of the surface they find that  $Z(r)$ , the normalized autocorrelation function of the surface, is given by

$$Z(r) = \frac{\pi}{2h^2} \int_0^{\infty} J_0\left(\frac{\omega^2 r}{g}\right) A^2(\omega) d\omega \quad (\text{III-144})$$

where  $h^2$  is the mean square wave height,  $J_0$  is the zero order Bessel function of the first kind, and  $r'^2 = \xi^2 + \eta^2$ . Marsh also shows that  $\hat{Z}(\ell, m)$  can be written as

$$\hat{Z}(\ell, m) = \frac{1}{2\pi} \int_0^\infty Z(r') J_0 \left[ r' (1 - v^2)^{\frac{1}{2}} \right] r' dr' \quad (\text{III-145})$$

Substituting (III-145) for  $\hat{Z}(\ell, m)$  in (III-142), and (III-144) for  $Z(r')$ , gives

$$\Omega_{\text{spec}} = 1 - \frac{v \sigma^2}{h^2} \int_0^\infty \int_{-1}^1 \int_{-(1-m^2)^{\frac{1}{2}}}^{(1-m^2)^{\frac{1}{2}}} \int_0^\infty v(\ell, m) J_0 \left( \frac{w^2 r'}{kg} \right) \cdot A^2(w) J_0 \left\{ r' \left[ 1 - v^2 (\ell - \alpha, m - \beta) \right]^{\frac{1}{2}} \right\} r' dw d\ell dm dr' \quad (\text{III-146})$$

Making the change in variable  $t = \frac{w^2}{kg}$  and using the identity

$$\int_0^\infty q dq \int_0^\infty F(t) J_0(qt) J_0(qp) t dt = F(p) \quad (\text{III-147a})$$

with the correspondence

$$F(t) = \frac{A^2 \left[ (kgt)^{\frac{1}{2}} \right]}{t^{3/2}}$$

$$q = r' \quad (\text{III-147b})$$

$$p = \left\{ 1 - \left[ v(\ell - \alpha, m - \beta) \right]^2 \right\}^{\frac{1}{2}}$$

one obtains

$$\Omega_{\text{spec}} = 1 - \frac{v k^{5/2} g^{1/2}}{2} \int_{-1}^1 \int_{-(1-m^2)^{\frac{1}{2}}}^{(1-m^2)^{\frac{1}{2}}} v(\ell, m) \frac{A^2 \left[ (k g p)^{\frac{1}{2}} \right]}{p^{3/2}} d\ell dm. \quad (\text{III-148})$$

Note that  $p$  is a function of  $\ell$  and  $m$ . Using the change of variables

$$\begin{aligned}\alpha &= (1 - \gamma^2)^{\frac{1}{2}} \cos \theta \\ \beta &= (1 - \gamma^2)^{\frac{1}{2}} \sin \theta \\ \ell &= (1 - \nu^2)^{\frac{1}{2}} \cos (\theta + \phi) \\ m &= (1 - \nu^2)^{\frac{1}{2}} \sin (\theta + \phi)\end{aligned}\quad (\text{III-149})$$

we obtain

$$\Omega_{\text{spec}} = 1 - \frac{\nu k^{5/2} g^{\frac{1}{2}}}{2} \int_0^1 \int_0^{2\pi} \frac{\nu^2 A^2 [(kgw)^{\frac{1}{2}}]}{w^{3/2}} d\nu d\theta \quad (\text{III-150a})$$

where

$$w^2 = 2 - \nu^2 - \gamma^2 - 2 \left[ (1 - \gamma^2) (1 - \nu^2) \right]^{\frac{1}{2}} \cos \theta \quad (\text{III-150b})$$

Using the substitution

$$a = \frac{ks^2}{2g} \quad (\text{III-151})$$

the Neumann-Pierson sea surface spectrum can be written as

$$A^2(w) = A^2 \left[ (kgw)^{\frac{1}{2}} \right] = \frac{c}{k^3 g^3 w^3} e^{-\frac{1}{aw}} \quad (\text{III-152})$$

Therefore,

$$\Omega_{\text{spec}} = 1 - \frac{sc\gamma}{2q^3 (2a)^{\frac{1}{2}}} \int_0^1 \int_0^{2\pi} \nu^2 w^{-3/2} e^{-\frac{1}{aw}} d\nu d\theta \quad (\text{III-153})$$

where, we recall,

$g$  = acceleration due to gravity =  $980 \text{ cm sec}^{-2}$

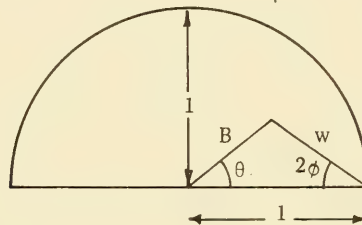
$c$  = a constant =  $4.8 (10^4) \text{ cm}^2 \text{ sec}^{-5}$

$s$  = wind speed in  $\text{cm sec}^{-1}$

Let  $I$  denote the integral in (III-153). Since  $w(-\theta) = w(\theta)$ ,  $I$  can be written as

$$I = \int_0^1 \int_0^\pi v w^{-\gamma/2} e^{-\frac{1}{aw}} d\theta (v dv) \quad (\text{III-154})$$

In evaluating the integral analytically, we assume  $\gamma = 0$  in the expression for  $w$ . This corresponds to a grazing angle of incidence for the incident sound. Letting  $B^2 = 1 - \gamma^2$ , we then have  $w^2 = 1 + B^2 - 2B \cos \theta$ . With  $(B, \theta)$  as the variables of integration, we have the domain illustrated below.



Then  $B^2 = 1 + w^2 - 2w \cos 2\theta$  and so  $v^2 = 2w - w^2 - 4w \sin^2 \phi$ . Writing the integral  $I$  in terms of the variables  $w$  and  $\phi$ , the element of area  $v dv d\theta$  becomes  $w dw d(2\phi)$ . For any particular value of  $w$ ,  $\phi$  can range from 0 to  $\phi_0$  such that  $1 = 1 + w^2 - 2w \cos 2\theta$ , i.e., to  $\phi_0$  such that  $\sin \phi_0 = (2-R)/4$ . In terms of these variables and limits,  $I$  becomes\*

$$I = 4 \int_0^2 \int_0^{\phi_0} v w^{-\gamma/2} e^{-\frac{1}{aw}} d\phi dw \quad (\text{III-155})$$

---

\*Marsh reports  $I = \int_0^2 \int_0^{\phi_0} v w^{-\gamma/2} e^{-\frac{1}{aw}} d\phi dw$ . Apparently a factor of 2 was

omitted in reducing the range of the original variable  $\theta$  or in changing the variable of integration.



After some analysis, which requires that  $a \gg 1$ , Marsh obtains\*

$$I = 3.38a^2 - 1.86a \quad (\text{III-156})$$

Recall that  $a = ks^2/2g$ , where  $s$  is the wind speed. With an incident frequency of  $f_{\text{kc}}$  kilocycles and a wind speed of  $S_{\text{knots}}$  in knots,  $a$  is given by

$$a = 0.05 f_{\text{kc}} S_{\text{knots}}^2 \quad (\text{III-157})$$

For a typical condition of 2 kc sound and 10 knot winds, we have  $a = 10$ , which satisfies the necessary condition that  $a \gg 1$ .

With the value of  $I$  given in (III-156), the expression for  $\Omega_{\text{spec}}$ , the intensity of the scattered sound in the specular direction, becomes,

$$\Omega_{\text{spec}} = 1 - \frac{sc\gamma}{2g^3(2a)^{\frac{1}{2}}} (3.38 a^2 - 1.86a) \quad (\text{III-158})$$

This expression can be written in terms of the variables  $H$  and  $b$ , where  $H$  is the average trough to crest wave height in feet,  $b = fH$ , (and  $f$  is the frequency of the incident sound in kilocycles). We require the following relations for the sea's behavior:

$$(h_{\text{feet}})^2 = 2.42 \cdot 10^{-6} (S_{\text{knots}})^5 \quad (\text{III-159})$$

$$H = 1.77h$$

Neglecting the term  $1.86a$  ( $a^2$  is large compared to  $a$ , since  $a \gg 1$ ) and substituting (III-159) in (III-158), we have<sup>(1)</sup>

$$\Omega_{\text{spec}} = 1 - 0.528 b^{3/2} H^{1/10} \gamma \quad (\text{III-160})$$

\*The expression for  $I$  given in (III-156) is two times that reported by Marsh.

This results from the error mentioned in the preceding footnote.

(1) Marsh reports  $\Omega_{\text{spec}} = 1 - 0.485 b^{3/2} H^{1/10} \gamma$ . Part of the difference is accounted for by the factor of 2 omitted in evaluating  $I$ : this is partly compensated for by a second arithmetic error by Marsh. Though not stated explicitly, Marsh presumably also drops the linear term in  $I$ , for otherwise another term, with different exponents for the variables, would appear in the expression for  $\Omega_{\text{spec}}$ .

In the analytical evaluation of  $I$ ,  $\gamma$  was taken to be zero. Careful numerical evaluation<sup>(2)</sup> of  $I$  shows that for large  $a$  ( $a \gg 1$ ),  $\gamma$  can have an appreciable effect on the value of  $I$ . Table III-4 shows the value of  $I$  obtained by numerical methods, and the analytical approximation for  $\gamma = 0$  over a broad range of  $a$ . The generally close agreement illustrates the accuracy of the analytical approximations.

TABLE III-4

COMPARISON OF NUMERICAL AND ANALYTICAL INTEGRATION OF  $I$   
AT  $\gamma = 0$

<u>a</u>	<u>I</u> <u>Numerical</u>	<u>I</u> <u>Analytical</u> <u>Approximation</u>
0.1	0.0002	-0.152
0.5	0.302	-0.087
1.0	2.01	1.52
2.0	10.43	9.8
5.0	76.73	75.2
10.0	321.54	319.40
50.0	8395	8357
100.0	33742	33614

Figure III-42 shows the effect of a nonzero value of  $\gamma$  in the evaluation of  $I$ . Let  $I_0(a)$  denote the value of  $I$  for  $\gamma = 0$ . Then, for nonzero  $\gamma$ ,  $I(a)$  can be given by

$$I(a) = \delta(a, \gamma) I_0(a) \quad (\text{III-161})$$

For certain  $\gamma$ , the values of  $\delta(a, \gamma)$  are plotted in Figure III-42. As an example of the effect of a nonzero value of  $\gamma$ , suppose  $\gamma = 0.2$ . This corresponds to an angle of incidence of  $11.5^\circ$ . At  $a = 10$  (typical sea conditions), the true value of  $I$  is 483, which is 50% more than the value obtained assuming  $\gamma = 0$  when evaluating the integral.

(2) Unpublished work by R. F. Meyer and L. Lawrence.

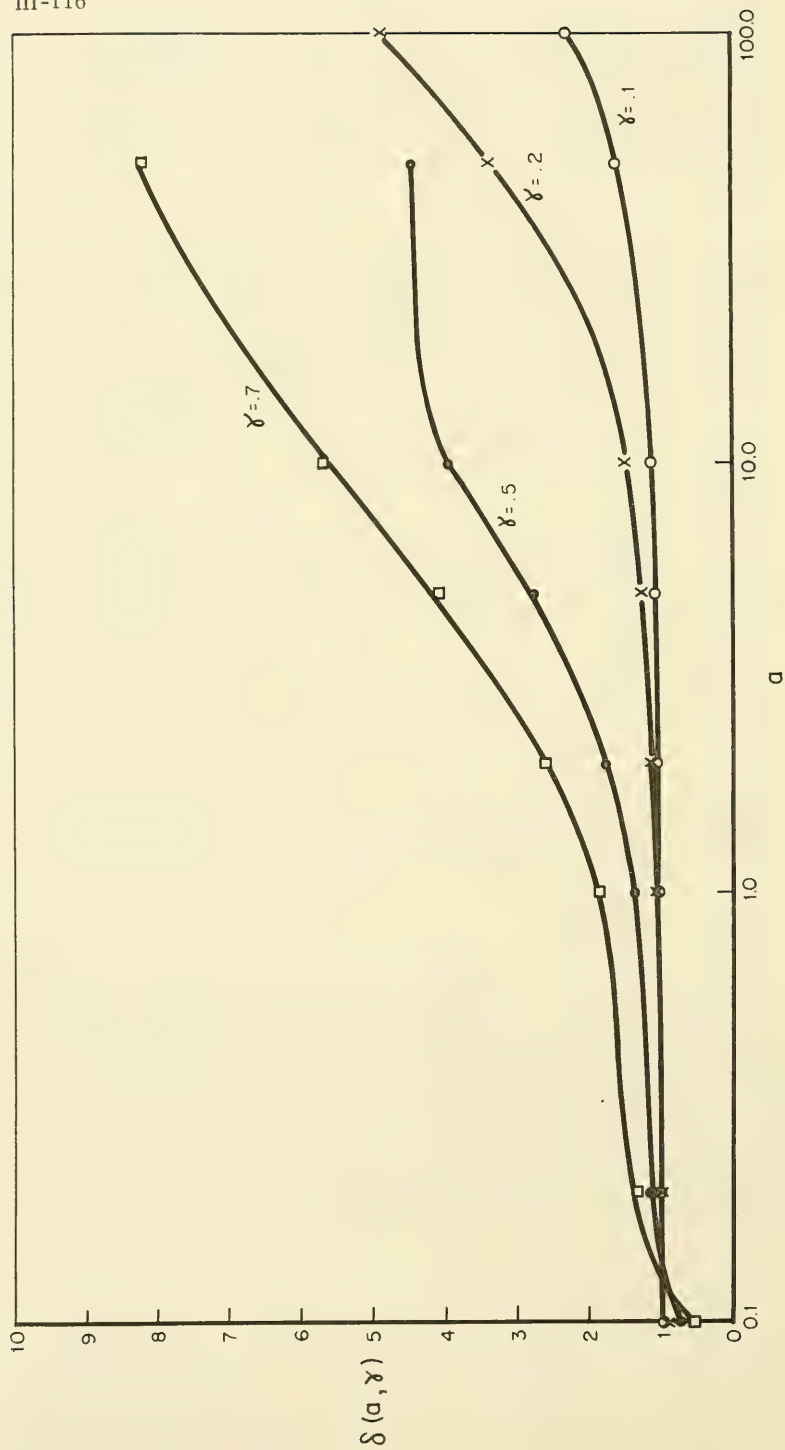


FIGURE III-42 RATIO OF I AT  $\gamma \neq 0$  TO I AT  $\gamma = 0$

It may be well at this point to restate the assumptions used in this development.

(1) The development giving the general expression for the scattered intensity depended upon:

- (a) The representation of the scattered wave as an integral sum of plane waves.
- (b) The existence of a convergent expansion in powers of  $(kh)$  for  $\tilde{\Phi}$ , the weighting function in the foregoing integral sum.
- (c) The applicability of certain Fourier inversion theorems.
- (d) A description of the sea surface as a single-valued function of position in a plane parallel to and below the surface. This precludes certain curling conditions in ocean waves.

The operator representation and theorems from generalized harmonic analysis used by Marsh are not needed for the further developments. The entire development is formalistic in nature, consisting of the manipulation of formulas on functions to which they may or may not be applicable. No attempt is made to ascertain the applicability of these operations, either by physical arguments or analytical considerations.

(2) In applications, the sea surface is assumed to be isotropic--i.e., no particular direction to the waves--and the sea surface spectrum is given by the Neumann-Pierson model

$$A^2(w) = \frac{c}{w^5} e^{-2g^2/w^2 s^2} \quad (\text{III-161})$$

where  $c$  is a constant (not the velocity of sound). This expression is needed to obtain the autocorrelation function of the sea surface.

(3) In applications, it is assumed that in the power series expression for  $\tilde{\Phi}(\lambda, \mu)$ ,

$$\sum_{m=0}^{\infty} \sigma_m^{\tilde{\Phi}}(\lambda, \mu) \quad (\text{III-162})$$

terms for  $m \geq 3$  can be ignored. This appears to be somewhat doubtful, and Marsh offers no substantiating arguments. For frequencies and wave heights of interest,  $\sigma$  is often larger than one. Furthermore, nothing is mentioned about the behavior of the  $\Phi_m(\lambda, \mu)$ . Since these involve inverse transforms of the function describing the sea surface, they may have large values for certain  $\lambda$  and  $\mu$ . In summary, we cannot rely on the bounded or decaying nature of the  $\Phi_m(\lambda, \mu)$  or small values of  $\sigma$  to assure the legitimacy of truncating the series after the first three terms.

(4) In the reduction of certain integrals, it is assumed that

$$a = (ks^2/2q) = (0.0564)(f_{kc})(s_{\text{knots}})^2 \quad (\text{III-163})$$

is "large." Marsh's analysis, as presented, does not indicate how large this should be. He does assume later that  $a^2$  is large relative to  $a$  (an order of magnitude or more). For one kilocycle sound, we need a wind speed of 15 knots or more for this to be so. This in turn requires  $\sigma$  to be larger than one, making assumption (3) questionable.

(5) The mean square surface height,  $h^2$ , is related to the wind speed by

$$(h_{\text{feet}})^2 = 2.42 \cdot 10^{-6} (s_{\text{knots}})^5 \quad (\text{III-164})$$

and the average trough to crest wave height,  $H$ , is related to  $h$  by

$$H = 1.77h \quad (\text{III-165})$$

Marsh applies the foregoing analysis to the case of a wave field which can be viewed as the composition of a finite number of rays with substantially plane wave fronts which impinge on the surface and undergo scattering. The medium is assumed to be an isothermal surface layer of depth  $L$ . The limiting ray for a surface source and receiver is denoted by  $\Gamma_0$ , with  $\Gamma_i$  denoting the other rays which are reflected from the surface. The diagram below illustrates the situation.

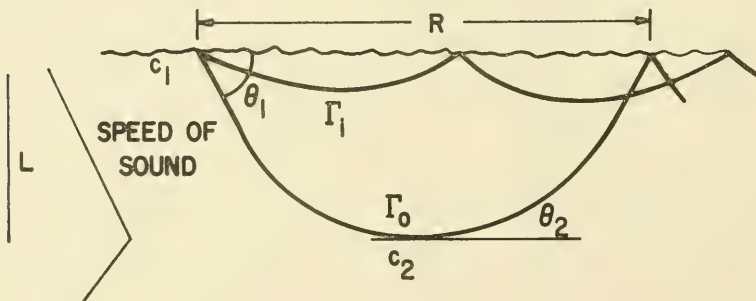


FIGURE III-43 SKETCH OF LIMITING SOUND RAY BENDING

If the sound waves make several surface contacts, it is clear that the only significant propagated mode is that involving the specularly reflected waves. The nonspecular components are incoherent, undergoing three-dimensional scattering.

Let  $J_i$  be the intensity of the ray,  $\Gamma_i$ , at some point just prior to a reflection, and  $J_i'$  the intensity of the specularly reflected ray just after reflection. Then  $J_i' = J_i \Omega_{\text{spec}}$ . The total field is the sum of all terms  $J_i$  which correspond to rays reaching a given point by specular reflection. Marsh asserts that it has been well established that a reasonable account of scattering losses can be obtained by considering only the limiting ray. In this, the losses attributed to scattering are partitioned equally over the number of surface contacts made by the limiting ray.

In terms of the above diagram, we have for the limiting ray,

$$\frac{\cos \theta_2}{\cos \theta_1} = \frac{c_2}{c_1} = \frac{c_1 + GL}{c_1} = 1 + \frac{GL}{c_1} \quad (\text{III-166})$$

where

$c_2$  = speed of sound at the depth  $L$

$c_1$  = speed of sound at the surface

$G$  = increase in the speed of sound due to the pressure increase, per unit distance.

Then

$$\cos \theta \approx 1 - \frac{GL}{c_1} \quad (\text{III-167})$$

and so

$$\theta_1 \approx \left( \frac{2GL}{c_1} \right)^{\frac{1}{2}} \quad (\text{III-168})$$

Using  $c_1 \approx 5000 \text{ ft sec}^{-1}$  and  $G = 0.018 \text{ sec}^{-1}$ , we have

$$\gamma = \sin \theta_1 \approx \theta_1 \approx 2.7 \cdot 10^{-3} L^{\frac{1}{2}} \quad (\text{III-169})$$

For the limiting ray  $\Gamma_0$  the transmission loss (in db per bounce) due to scattering is given by

$$\alpha_s = 10 \log \frac{J_0}{J'_0} \quad (\text{III-170})$$

Using the above value of  $\gamma$ , we have\*

$$\alpha_s = -10 \log \left[ 1 - 0.00143 b^{3/2} H^{1/10} L^{1/2} \right] \quad (\text{III-171})$$

The factor  $H^{1/10}$  varies only a little over a large range of possible sea states. The term  $L^{1/2}$  is also relatively insensitive, compared to the factor  $b^{3/2}$ . Using typical values of  $L = 200$  ft and  $H = 3$  ft, we have

$$\alpha_s = -10 \log \left[ 1 - 0.0226 b^{3/2} \right] \quad (\text{III-172})$$

Considering the extreme values of  $H = 6$  ft,  $L = 300$  ft at one end, and  $H = 2$  ft,  $L = 100$  ft at the other, we obtain

$$\alpha_s = -10 \log \left[ 1 - 0.0297 b^{3/2} \right] \quad (\text{III-173a})$$

and

$$\alpha_s = -10 \log \left[ 1 - 0.0153 b^{3/2} \right] \quad (\text{III-173b})$$

respectively.

Recapitulating the basis of the last part of this development, we assumed that:

- (1) Sound is traveling in an isothermal layer for which the velocity gradient (due to increasing pressure) is  $0.018 \text{ sec}^{-1}$ .
- (2) Only the sound in the limiting ray is considered.
- (3) For (III-172), which is used in most of the later material, the depth,  $L$ , of the layer is taken as 200 ft and the average trough to crest wave height,  $H$ , as 3 ft. The sensitivity of this is shown by (III-173a) and (III-173b), which give analogous expressions for  $H = 6$  ft,  $L = 300$  ft. for one extreme and  $H = 2$  ft,  $L = 100$  ft. for the other.

---

\*This differs from  $\alpha_s = -10 \log \left[ 1 - 0.0013 b^{3/2} H^{1/10} L^{1/2} \right]$  as reported by Marsh because of the different coefficient (0.528 instead of 0.485) in the expression for  $\Omega$  spec.



Figure III-44 graphs the above expressions for the surface loss per bounce. The experimental data points are taken from (Ref. III-27). Marsh comments that although the scatter is considerable, it is not surprisingly so, and that the over-all fit is good. As pointed out before, Marsh's original result apparently has several numerical errors. Using the corrected form, we obtain somewhat higher theoretical estimates. These tend to provide a better fit to the experimental values.

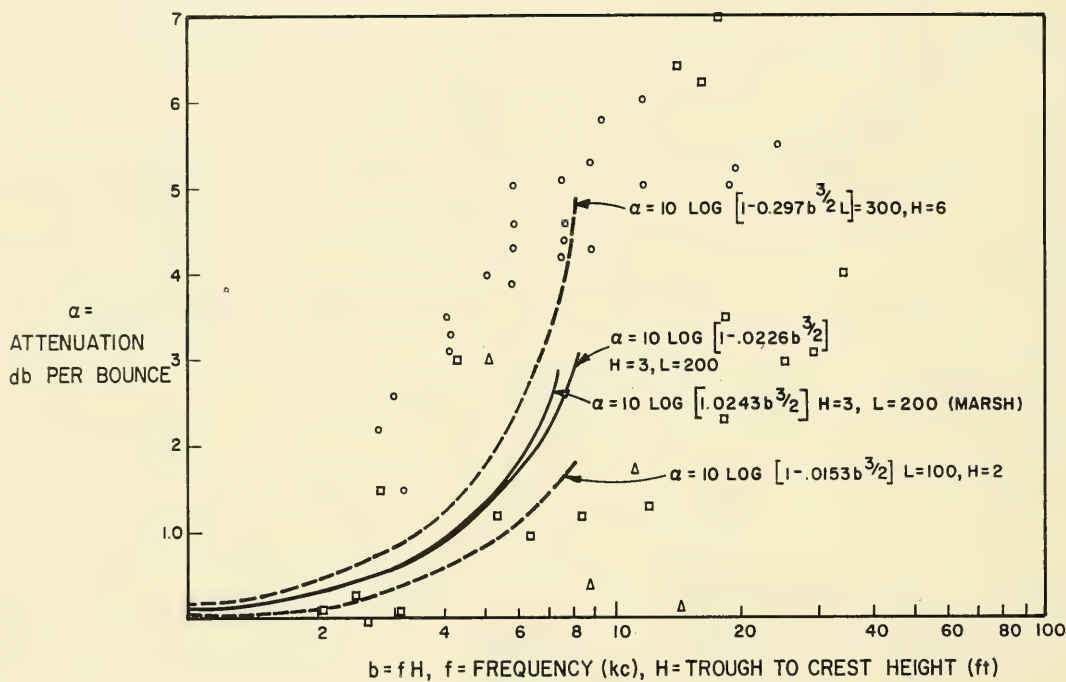


FIGURE III-44 SEA SURFACE SCATTERING LOSS IN SPECULAR DIRECTION  
FOR EMITTING RAY IN ISOTHERMAL LAYER

#### IV. WEAK INHOMOGENEITIES

The properties of the ocean medium, as encountered by a sound wave passing through it, are constantly varying even in the absence of the strong inhomogeneities discussed in the previous chapter. The pressure, salinity, and temperature exhibit small variations both in the horizontal plane and in the vertical direction. The variations in the vertical direction tend to exhibit a layer structure, whereas the horizontal variations are more in the nature of random patches. In this chapter we shall examine the effect of these inhomogeneities on the propagation of sound waves.

##### A. THE WAVE EQUATION FOR AN INHOMOGENEOUS MEDIUM

The derivation of the acoustic wave equation appropriate for an ocean medium with slightly varying properties has been dealt with in considerable detail by previous authors, including a report in the present series.<sup>1</sup> The variations in pressure, salinity, temperature, and gravitational field introduce a number of corresponding additional terms beyond those appearing in the ordinary wave equation for a homogeneous medium. An analysis of the order of magnitude of the different additional terms under actual ocean conditions indicates that the dominant effect for the analysis of sound propagation comes from the spatial variations of the velocity of sound  $c$  caused by the variations in temperature and salinity. The magnitude of this effect exceeds the effects of spatial variations in density by at least a factor of 10. For our purposes, therefore, it will be adequate to confine ourselves to a wave equation with a slightly varying velocity of sound:

$$\frac{1}{c^2} \frac{\partial^2 p}{\partial t^2} = \nabla^2 p \quad (\text{IV-1})$$

The velocity of sound,  $c$ , is a slightly varying function of position and time. Let  $c_0$  be a typical average value of the sound velocity in the spatial region in which we wish to study acoustic wave propagation. We may then introduce the local index of refraction of the medium,  $n$ , as the ratio of the average sound velocity to the local sound velocity:

$$n(\underline{x}, t) = \frac{c_0}{c(\underline{x}, t)} = 1 + v(\underline{x}, t) \quad (\text{IV-2})$$

---

1. Arthur D. Little, Inc., Ref. IV-4, Part A, Section 1-14  
Chernov, Ref. IV-2, Part II, Chapters III and IV

Note that we are using the vector notation  $\underline{x} = (x_1, x_2, x_3)$  to indicate position coordinates of a point. We shall also have occasion to denote the length of the vector  $\underline{x}$  by  $|\underline{x}| = x$  (see Appendix C - Notation). The variation in the index of refraction is supposed to be extremely small:

$$|\nu| \ll 1 \quad (\text{IV-3})$$

Typical values of the variations in the index of refraction for the ocean are of the order of magnitude of  $10^{-4}$  or less.

The problems of practical interest are of two kinds:

(a) An incoming plane, spherical, or cylindrical wave hits a region of inhomogeneities and is scattered.

(b) A source of acoustic waves is situated inside an inhomogeneous region, and the waves emitted by the source are distorted by the inhomogeneities.

For sufficiently small regions of space, these problems can be attacked by a formal perturbation theory using the magnitude of the variations in the index of refraction as the parameter of smallness. We may write the index of refraction as unity plus a very small multiple of a function of space and time:

$$n(\underline{x}, t) = 1 + \nu(\underline{x}, t) = 1 + \epsilon \mu(\underline{x}, t) \quad (\text{IV-4})$$

where

$$\epsilon \ll 1, \quad |\mu| \sim 1 \quad (\text{IV-5})$$

We can now consider a family of problems depending on the parameter  $\epsilon$ . For  $\epsilon = 0$ , the solution to the problem is just the corresponding solution for the homogeneous medium. If the pressure distribution is an analytic function of  $\epsilon$  near  $\epsilon = 0$ , we may expand the pressure in a formal power series in the parameter of smallness:

$$p = p^{(0)} + \epsilon p^{(1)} + \epsilon^2 p^{(2)} + \dots \quad (\text{IV-6})$$

In this case, the wave equation (IV-1) becomes:

$$\nabla^2 (p^{(0)} + \epsilon p^{(1)} + \dots) = (1 + \epsilon \mu)^2 \frac{1}{c_0^2} \frac{\partial^2}{\partial t^2} (p^{(0)} + \epsilon p^{(1)} + \dots) \quad (\text{IV-7})$$

By collecting terms of the same order in  $\epsilon$  in (IV-7), we find a hierarchy of equations for the successively higher-order terms in the power series for the pressure:

$$\nabla^2 p^{(0)} = \frac{1}{c_o^2} \frac{\partial^2 p^{(0)}}{\partial t^2} \quad (\text{IV-8a})$$

$$\nabla^2 p^{(1)} = \frac{1}{c_o^2} \frac{\partial^2 p^{(1)}}{\partial t^2} + \frac{2\mu}{c_o^2} \frac{\partial^2 p^{(0)}}{\partial t^2} \quad (\text{IV-8b})$$

The first of these equations has as its solution the pressure distribution in the homogeneous medium. The equation for the first order correction is also a wave equation, but with a nonzero inhomogeneous term. This term shows how, to first order, the inhomogeneities of the medium interact with the unperturbed pressure distribution and thus act as sources of secondary waves.

In all the problems of interest, we shall be concerned with a pressure distribution that has harmonic time dependence:

$$p(\underline{x}, t) = p(\underline{x}) e^{-i\omega t} \quad (\text{IV-9})$$

Also, we shall usually be concerned with either a plane or spherical incoming wave:

$$\begin{aligned} p^{(0)}(\underline{x}) &= A_o e^{ik \cdot \underline{x}} && (\text{plane wave}) \\ p^{(0)}(\underline{x}) &= A_o \frac{e^{ikx}}{x} && (\text{spherical wave}) \end{aligned} \quad (\text{IV-10})$$

$$(\text{Note that } x = |\underline{x}| \text{ and } k = |k| = \frac{\omega}{c_o})$$

In either case, the equation governing the first order correction term to the pressure satisfies a Helmholtz equation with a distributed source function:\*

$$\nabla^2 p^{(1)} + k^2 p^{(1)} = -2\mu k^2 p^{(0)} \quad (\text{IV-11})$$

---

\*Since the temporal variations in the index of refraction occur very slowly compared to the time required for the acoustic wave to pass by a typical inhomogeneity, we may regard  $\mu(\underline{x}, t)$  as constant during the passage time.

The incoming (zero- order) wave, therefore, provides the energy to generate a source distribution for the first-order wave. We shall see later that this corresponds to a single scattering approximation, in the sense of Chapter II. In other words, the power series expansion in terms of a slight correction to the index of refraction not only approximates the quadratic expression for the index of refraction in (IV-7), but also removes higher orders of scattering from the first-order approximation.

The solution to (IV-11) is given (see Appendix A) by the integral:

$$\epsilon p^{(1)}(\underline{x}) = -\frac{2k^2\epsilon}{4\pi} \int_V d\underline{\xi} \, \upsilon(\underline{\xi}) p^{(0)}(\underline{\xi}) \frac{e^{ikr}}{r} \quad (\text{IV-12})$$

The geometry required to explain the nomenclature of (IV-12) is shown in Figure IV-1. A scattering element at  $\underline{\xi}$  acts as a secondary source emitting a spherical wave to an observer at  $\underline{x}$ . The volume of the scattering element is denoted by  $d\underline{\xi} = d\xi_1 d\xi_2 d\xi_3$  in rectangular coordinates. The integral in (IV-12) runs over the entire portion of space containing inhomogeneities (i.e., that portion of space for which  $\upsilon \neq 0$ ). The vector running from the scattering element to the observer is called  $\underline{r} = \underline{x} - \underline{\xi}$ .

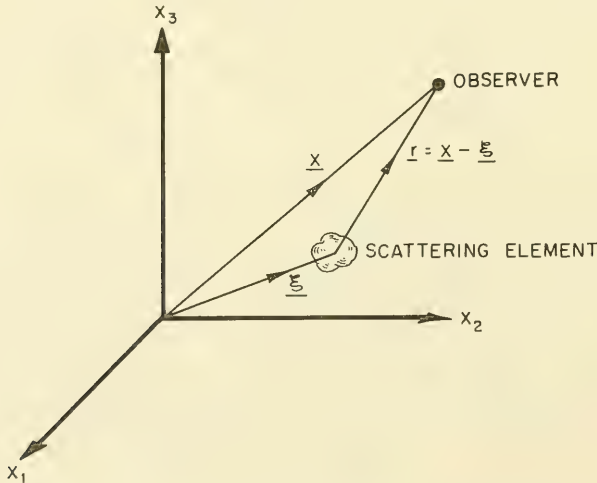


FIGURE IV-1 THE GEOMETRY OF SCATTERING

We may see that this corresponds to a single scattering approximation by following a different procedure yielding the same result. If we introduce the harmonic time dependence of  $p$  (IV-9) into the wave equation (IV-7), we can make the approximation:

$$\nabla^2 p + k^2 p = - (2 \epsilon \mu + \epsilon^2 \mu^2) k^2 p \simeq -2 \epsilon \mu k^2 p \quad (\text{IV-13})$$

This approximation involves only the assumption of weak inhomogeneities, i.e.,  $\epsilon \ll 1$ . We may integrate (IV-13) to give an integral equation for the pressure distribution:

$$p(\underline{x}) = p^{(0)}(\underline{x}) - \frac{2 \epsilon k^2}{4\pi} \int_V d\underline{\xi} \mu(\underline{\xi}) p(\underline{\xi}) \frac{e^{ikr}}{r} \quad (\text{IV-14})$$

This solution is obtained by the following reasoning. When  $\mu = 0$ , the desired homogeneous solution to (IV-13) is the original incoming wave  $p^{(0)}$ . The inhomogeneous (or scattered) portion of the solution is obtained by regarding the right side of (IV-13) as a source function emitting spherical waves of the appropriate strength. The distinction between (IV-12) and (IV-14) is that (IV-14) contains the unknown function  $p$  under the scattering integral rather than the known incident field  $p^{(0)}$ . As usual, the solution for (IV-14) may be obtained by successive iteration starting with an initial guess. If we use  $p^{(0)}$  as the initial approximation, one iteration of (IV-14) will then yield (IV-12) as the single scattered pressure. It is clear that the single scattering approximation will be valid only as long as the twice-scattered power is small compared to the once-scattered power. In fact, one would expect the single scattering approximation to hold only when the single scattered power is small compared to the incident wave. For the actual conditions encountered, we shall show later that the single scattering approximation is adequate as long as the radius of the scattering region ( $R$ ) satisfies:

$$R < \frac{10,000}{f^2} \text{ km.} \quad (\text{IV-15})$$

where the radius of the scattering region is to be measured in kilometers and  $f$  denotes the frequency of the sound in kilocycles. In most practical cases, we do not exceed this region. For sufficiently high frequencies, e.g., frequencies above the 10 kilocycle range, we may be interested in propagation through regions of inhomogeneities greater than those permitted by (IV-15). For example, according to the above, the single scattering approximation for sonar at a frequency of 40 kc is certainly invalid at ranges in excess of 7 km. We shall therefore want to develop an approximation scheme which is more uniformly valid, in the sense that



the first-order correction term giving the first approximation to the scattered pressure remains a good approximation also for large distances of propagation.\* This is done as follows: In a medium without inhomogeneities, the waves of interest (plane, spherical, cylindrical) may be represented in terms of their amplitude and phase by:

$$p_o(\underline{x}) = A_o(\underline{x}) e^{iS_o(\underline{x})} = e^{i\ell n A_o + iS_o} = e^{i\psi_o(\underline{x})} \quad (\text{IV-16a})$$

where

$$\psi_o(\underline{x}) = S_o(\underline{x}) - i \ell n A_o(\underline{x}) \quad (\text{IV-16b})$$

The functions  $A_o$  and  $S_o$  are both real functions representing, respectively, the amplitude and phase of the wave as a function of position. We observe that a surface on which  $S_o$  is constant is a surface of constant phase; such a surface can be regarded as a wave front for our purposes. If a source of wave motion, which would have resulted in a pressure distribution (IV-16a) in a homogeneous medium, is placed in an inhomogeneous medium, the resulting wave will have the same general form but will differ in detail. The resulting wave can always be represented as:

$$p(\underline{x}) = A(\underline{x}) e^{iS(\underline{x})} = e^{i\psi(\underline{x})} \quad (\text{IV-17a})$$

where

$$\psi(\underline{x}) = S(\underline{x}) - i \ell n A(\underline{x}) \quad (\text{IV-17b})$$

The function  $\psi$  represents the complex phase of the wave and will turn out to be very useful in the analysis. We can always represent the complex phase of the perturbed wave in terms of the complex phase function of the original homogeneous wave plus a perturbation term:

$$\psi = \psi_o + \psi_1 \quad (\text{IV-18})$$

The perturbation  $\psi_1$  is now not necessarily small compared to  $\psi_o$ . In other words, we permit the inhomogeneous wave to have a large difference in amplitude and phase from the unperturbed homogeneous wave. To compare this approach with the approach used for very small perturbations, we observe that if  $\psi_1$  is small:

$$P = e^{i\psi_o} e^{i\psi_1} = p_o (1 + i \psi_1 + \dots) \quad (\text{IV-19})$$

---

\* Chernov - Chapter V, Section 16.

For small perturbations, we may therefore identify the correction term of (IV-6) with the corresponding term of (IV-19), which yields:

$$\epsilon p^{(1)} = i p_0 \psi_1 \quad (\text{IV-20})$$

When the perturbations are indeed small, the approximation theory about to be developed should go over into the small perturbation theory according to the relation (IV-20).

From (IV-18) we conclude that:

$$\psi_1 = \psi - \psi_0 = (S - S_0) - i \ell_n \frac{A}{A_0} \quad (\text{IV-21})$$

We may, therefore, identify the changes in phase and logarithm, i.e., amplitude due to the inhomogeneities of the medium:

$$\Delta S = (S - S_0) = \text{Re } \psi_1 \quad (\text{IV-22a})$$

$$\Delta \ell_n A = \ell_n \frac{A}{A_0} = \text{Im } \psi_1 \quad (\text{IV-22b})$$

The wave in the inhomogeneous medium must satisfy the wave equation (IV-1), and if we introduce harmonic time dependence (IV-9) and the definition of the index of refraction (IV-2), we obtain the wave equation for the pressure:

$$(\nabla^2 + n^2 k^2) p = 0 \quad (\text{IV-23})$$

The complex phase function must, therefore, satisfy an equation which is obtained by substituting (IV-17a) in (IV-23). After a little manipulation, we find that  $\psi$  is governed by:

$$i \nabla^2 \psi - (\nabla \psi)^2 + n^2 k^2 = 0 \quad (\text{IV-24})$$

Since  $p_0$  is the solution of the wave equation with an index of refraction of unity, the complex phase function  $\psi_0$  must satisfy equation (IV-24) with  $n = 1$ :

$$i \nabla^2 \psi_0 - (\nabla \psi_0)^2 + k^2 = 0 \quad (\text{IV-25})$$

If we substitute (IV-18) in (IV-24) and make use of (IV-25), we obtain an equation for the correction to the complex phase function  $\psi_1$ :

$$i \nabla^2 \psi_1 - (\nabla \psi_1)^2 - 2(\nabla \psi_0 \cdot \nabla \psi_1) + (n^2 - 1)k^2 = 0 \quad (\text{IV-26})$$

From this equation, we would like to eliminate those terms which we can legitimately regard as being of second-order importance even if  $\psi_1$  itself is not necessarily small compared to unity. To this end, we shall make two approximations.

1. Since the variations of the index of refraction are small, we may certainly make the approximation:

$$n^2 - 1 = v(2 + v) \sim 2v \quad (\text{IV-27})$$

If we make this approximation, we are dropping a term  $v^2 k^2$  from (IV-26), and we are, therefore, making explicitly the assumption:

$$v < 2 \quad (\text{IV-28})$$

It is clear that this approximation is always permissible if the inhomogeneities are indeed weak. The approximation corresponds entirely to the one made in (IV-13) and does not restrict us to the small scattering approximation which we wish to avoid.

2. If we want to remove those terms from (IV-26) which would be of second order if  $\psi_1$  were small, we must also remove the square of the gradient of  $\psi_1$ , i.e.,  $(\nabla \psi_1)^2$ . This entails the assumption that the size of the gradient is comparable in order of magnitude to the term just neglected above:

$$(\nabla \psi_1)^2 \sim v^2 k^2 \quad (\text{IV-29})$$

Because of (IV-28), this assumption is tantamount to the condition on the gradient of  $\psi_1$ :

$$|\nabla \psi_1| < 2k \quad (\text{IV-30})$$

Let us examine the physical meaning of (IV-30). If the magnitude of the gradient of the complex phase function is to be sufficiently small, both its real part and its imaginary part must be small enough to satisfy (IV-30). In other words:

$$\left| \nabla \epsilon_n \frac{A}{A_0} \right| < 2k, \text{ or since } k = \frac{2\pi}{\lambda}, \text{ we require that}$$

$$\lambda \left| \nabla \epsilon_n \frac{A}{A_0} \right| < 4\pi \quad (\text{IV-31a})$$

$$|\nabla (S - S_0)| < 2k \quad (\text{IV-31b})$$

The last expression in (IV-31a) may be interpreted as follows: the gradient of the logarithm of the relative amplitude is a measure of the rate of change of the relative logarithmic amplitude with distance. If this is multiplied by the wavelength of the undisturbed wave, we obtain a measure of the change of the relative logarithmic amplitude over one wavelength. The change in the relative logarithmic amplitude encountered in going one wavelength must, therefore, be small compared to  $4\pi$ . This condition is always satisfied for any of the typical wavelengths and scattering strengths encountered in the ocean.

The condition (IV-31b) is considerably more restrictive. To understand its implications, we observe that the surfaces  $S_0(\underline{x}) = \text{constant}$  and  $S(\underline{x}) = \text{constant}$  are the wave fronts, respectively, of the undisturbed and the perturbed waves. The gradient vectors  $\nabla S_0$  and  $\nabla S$  will point in the direction of wave propagation in both cases. The magnitudes of  $\nabla S$  and  $\nabla S_0$  must be of the order of magnitude of the wave number  $k$ , since  $S$  and  $S_0$  are the local phases of the waves, and since the phase changes by an amount  $2\pi$  in going one wavelength, i.e.,  $\frac{\Delta S}{\Delta x} \sim \frac{2\pi}{\lambda} = k$ . The meaning of (IV-31b) is, therefore, that the difference between two unit vectors pointing in the direction of propagation of the undisturbed and perturbed wave must be very small compared to 2, even though the phase and the amplitude of the two waves may differ greatly.

If we make these two approximations and remove the corresponding terms from (IV-26) we find that the correction to the complex phase  $\psi_1$  is governed by:

$$2 \psi k^2 + i \nabla^2 \psi_1 - 2 (\nabla \psi_0 \cdot \nabla \psi_1) = 0 \quad (\text{IV-32})$$

We may reduce this to the ordinary inhomogeneous wave equation by introducing the function  $W$  according to:

$$\psi_1 = e^{-i\psi_0} W = \frac{W}{p_0} \quad (\text{IV-33})$$

If we substitute (IV-33) into (IV-32) and use (IV-25) to simplify the expression, we obtain:

$$\nabla^2 W + k^2 W = 2i \psi k^2 p_0 \quad (\text{IV-34})$$

In the homogeneous case (i.e.,  $\psi = 0$ ), we know that the appropriate solution of (IV-34) is  $W = 0$ , since in that case we desire that  $\psi_1 = 0$ . We are, therefore, only interested in the inhomogeneous solution to (IV-34) which, subject to the condition of giving an outgoing wave, must be:

$$W(\underline{x}) = 2k^2 i \int_V d\underline{\xi} \frac{e^{ikr}}{r} \psi(\underline{\xi}) p_0(\underline{\xi}) \quad (\text{IV-35})$$

The relevant vectors are those shown in Figure IV-1, and  $\underline{r}$  is again the vector connecting the scattering element and the point of observation. We now obtain the correction to the complex phase by substituting the above expression for  $W$  in (IV-33):

$$\psi_1(\underline{x}) = \frac{2k^2 i}{4\pi} \int_V d\underline{\xi} \frac{e^{ikr}}{r} \cup(\underline{\xi}) \frac{p_o(\underline{\xi})}{p_o(\underline{x})} \quad (\text{IV-36})$$

First of all, we observe that for small values of  $\psi_1$ , (IV-36) and (IV-12) do indeed correspond according to the correspondence principle given in (IV-20). Second, we note that the integral to be evaluated either in the small perturbation theory in (IV-12) or in the "smooth" perturbation theory leading to (IV-36) is essentially the same. What differs is the interpretation of the integral.

In the small perturbation theory, the integral essentially represents the first order correction of the pressure as a result of the inhomogeneity. In the more uniformly valid approximation, the integral corresponds, loosely speaking, to the correction to the complex phase resulting from the inhomogeneity. Depending on the situation, we shall avail ourselves of either interpretation. In much of the later work of this chapter, however, we shall be concerned with integrals of this type and therefore introduce the symbol  $p_1$  to connote the integral:

$$p_1(\underline{x}) = \varepsilon p^{(1)}(\underline{x}) = ip_o(\underline{x}) \psi_1(\underline{x}) = -\frac{2k^2}{4\pi} \int_V d\underline{\xi} \frac{e^{ikr}}{r} \cup(\underline{\xi}) p_o(\underline{\xi}) \quad (\text{IV-37})$$

## B. SCATTERING FROM AN ISOLATED INHOMOGENEITY

The micro-structure of the ocean consists of a multitude of weak inhomogeneities of every size and shape. The statistical description of the inhomogeneities encountered in the actual ocean medium will be studied in the next section. In the present section we shall confine ourselves to the diffraction of a plane wave by a single inhomogeneity (of the refractive index) in an otherwise entirely homogeneous ocean. In particular, we wish to determine the far field of the scattered wave and to gain some insight into the dependence of the far field on the characteristics of the scattering inhomogeneities and the frequency of the incoming plane wave.

To simplify the geometry of the problem, we shall locate the scattering inhomogeneity so as to include the origin of the coordinate system. The incoming plane wave of unit amplitude is taken to propagate in the positive  $x_1$  direction (see Figure IV-2).

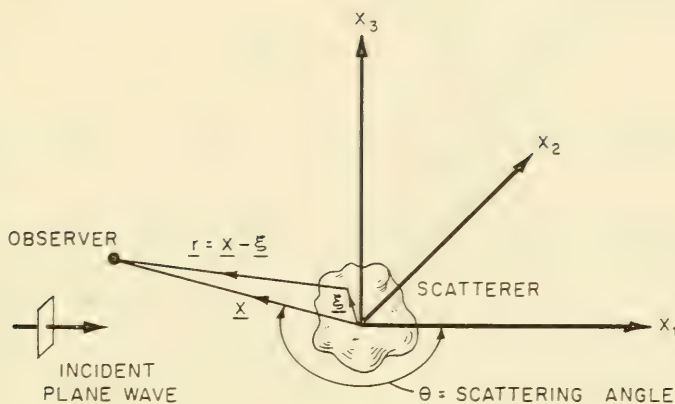


FIGURE IV-2 SCATTERING COORDINATES

If we drop the time dependence  $e^{-i\omega t}$  (see IV-9), the incoming plane wave is represented by:

$$p_0(\underline{x}) = e^{ikx_1} \quad (\text{IV-38})$$

The inhomogeneity is represented by a distribution  $v(\underline{\xi}) \ll 1$  which is the deviation from unity of the index of refraction. The scattering integral to be evaluated is therefore obtained by substituting the incoming plane wave (IV-38) into the scattering integral (IV-37):

$$p_1(\underline{x}) = -\frac{2k^2}{4\pi} \int_V d\underline{\xi} \frac{e^{ik(r+\xi_1)}}{r} v(\underline{\xi}) \quad (\text{IV-39})$$

To evaluate this integral in the far field (i.e., at a distance from the inhomogeneity which is large compared to the characteristic size of the inhomogeneity), we must approximate the distance  $r$  which is given by:

$$r = |\underline{x} - \underline{\xi}| = (x^2 + \xi^2 - 2\underline{x} \cdot \underline{\xi})^{\frac{1}{2}} = x \left( 1 + \frac{\xi^2}{x^2} - 2\frac{\underline{x}}{x} \cdot \frac{\underline{\xi}}{x} \right)^{\frac{1}{2}} \quad (\text{IV-40})$$



We note that the vector  $\frac{\underline{x}}{x}$  is a unit vector in the  $\underline{x}$  direction, i.e., pointed from the origin at the observer. For the far field, the magnitude of the vector  $\underline{\xi}$  must be small compared to  $x$ . In other words:

$$\frac{\xi}{x} \ll 1 \quad (\text{IV-41})$$

We may, therefore, approximate  $r$ , as given in (IV-40), to first order in  $\frac{\xi}{x}$  by:

$$r \simeq x \left[ 1 - \left( \frac{\underline{x}}{x} \right) \cdot \frac{\underline{\xi}}{x} \right] = x - \left( \frac{\underline{x}}{x} \right) \cdot \underline{\xi} \quad (\text{IV-42})$$

In order to obtain an approximation to (IV-39) which is correct to the zeroth order of  $\frac{\xi}{x}$ , we must approximate the exponent  $(r + \xi_1)$  of (IV-39) in a fashion which is accurate to first order in  $\frac{\xi}{x}$ , but we may use the zeroth order approximation  $r \sim x$  to approximate the denominator in (IV-39). The first order approximation to the exponent to (IV-39) may be rearranged by introducing a unit vector  $\underline{e}^{(1)}$  pointed in the  $x_1$  direction. In that case we may, using (IV-42), approximate the distance  $r + \xi_1$  by:

$$r = \xi_1 \simeq x - \underline{\xi} \cdot \left( \frac{-\underline{x}}{x} - \underline{e}^{(1)} \right) = x - \underline{\xi} \cdot \underline{d} \quad (\text{IV-43})$$

In the above, we found it convenient to introduce a vector  $\underline{d}$  which is the difference between a unit vector pointing at the observer and a unit vector pointing in the  $x_1$  direction:

$$\underline{d} = \frac{\underline{x}}{x} - \underline{e}^{(1)} \quad (\text{IV-44a})$$

Recall that the  $x_1$  direction is the direction of propagation of the incident wave so that  $\underline{d}$  represents a measure of the difference between the observer position and the forward direction of scattering. If we introduce the angle  $\theta$  as the angle between the observer direction  $\underline{x}$  and the  $x_1$  direction (see Figure III-2), we may write the length of the vector  $\underline{d}$  as:

$$d = |\underline{d}| = \left( 2 - 2 \frac{\underline{x}}{x} \cdot \underline{e}^{(1)} \right)^{\frac{1}{2}} = \left[ 2 (1 - \cos \theta) \right]^{\frac{1}{2}} = \sin \frac{\theta}{2} \quad (\text{IV-44b})$$



We now introduce the approximation (IV-43) into the scattering integral (IV-39) and obtain for the far field the expression:

$$p_1(\underline{x}) \approx -\frac{2k^2 e^{ikx}}{4\pi x} \int_V d\underline{\xi} e^{-ikd\underline{\xi}} v(\underline{\xi}) \quad (\text{IV-45})$$

Equation (IV-45) leads to the following observations:

1. The scattered pressure field has the nature of a spherically spreading wave with a multiplicative directivity pattern which depends on the angle  $\theta$ . In particular, the forward direction of scattering the vector  $\underline{d}$  is zero, and the pressure is given by:

$$p_1(x_1) = -\frac{2k^2 e^{ikx_1}}{4\pi x_1} \int_V d\underline{\xi} v(\underline{\xi}) = -\frac{S e^{ikx_1}}{x_1} \quad (\text{IV-46a})$$

In this equation, we have introduced the parameter  $S$  as the forward scattering strength of the inhomogeneity. We note that the forward scattering strength is proportional to the square of the frequency and to the total volume integral of the correction to the index of refraction. The pressure distribution in the far field in any direction may now be written in terms of a directivity pattern as:

$$p_1(\underline{x}) = S D(\theta, \phi) \frac{e^{ikx}}{x} \quad (\text{IV-46b})$$

Here we have introduced  $D(\theta, \phi)$ , the directivity pattern of the scattering,\* which corresponds to the ratio of the integrals in (IV-45) and (IV-46b).

2. We recognize the integral in (IV-45) to be the Fourier transform of the refractive index  $v(\underline{\xi})$  evaluated at a wave number vector  $k\underline{d}$  which has a magnitude  $2k \sin \frac{\theta}{2}$ . The Fourier transform of  $v(\underline{\xi})$ , e.g.,  $N(\underline{\chi})$ , represents the amplitude of the decomposition of  $v(\underline{\xi})$  into waves with wave-number vector  $\underline{\chi}$ ; in other words, it is the spectrum of  $v(\underline{\xi})$ . If the spectrum  $N(\underline{\chi})$  is large in vicinity of  $\underline{\chi}$ , it corresponds to an inhomogeneity with a substantial Fourier component of wave-number  $\underline{\chi}$ . Equation IV-45 tells us that the scattered field will be large for a scattering angle  $\theta$  such that the spectrum  $N(\underline{\chi})$  is large at  $\chi = 2k \sin \frac{\theta}{2}$ . If the spectrum of  $v(\underline{\xi})$  is large only for values of  $\chi$  much less than  $k$ , it is clear that the substantial portion of the scattered field will be confined to a small angle  $\theta \sim \frac{\chi}{k}$ . In other words, inhomogeneities which

---

\*  $\theta$  and  $\phi$  are the polar and azimuthal angle of a spherical coordinate system,  $\underline{x} = (x, \theta, \phi)$  with  $x_1$  as polar axis.

are very large compared to the wave length of the incoming sound, and whose index of refraction changes very smoothly, will scatter the sound in the forward direction in a narrow cone. This means that a large and smooth scatterer will cause a collimated beam of scattered pressure. Conversely, if the spectrum of  $v(\xi)$  is substantial for values of  $\chi$  of the same order as or larger than  $k$ , the scattering will essentially be omnidirectional.

3. It is instructive to examine the above in some detail for a spherically symmetric pattern:

$$v(\underline{\xi}) = v(\xi) \quad (\text{IV-47})$$

To evaluate (IV-45) in this case, it is convenient to introduce a spherical coordinate system for the vector  $\underline{\xi}$  using the vector  $\underline{d}$  as the polar axis,  $\underline{\xi} = (\xi, \theta_o, \phi_o)$ . In this coordinate system,

$$\underline{\xi} \cdot \underline{d} = \xi d \cos \theta_o = 2 \xi \sin \frac{\theta}{2} \cos \theta_o \quad (\text{IV-48})$$

(IV-45), therefore, becomes:

$$\begin{aligned} p_1(\underline{x}) &= -\frac{2k^2 e^{ikx}}{4\pi x} \int_0^\infty d\xi \int_0^\pi d\theta_o \int_0^{2\pi} d\phi_o \xi^2 \sin \theta_o v(\xi) e^{-2ik\xi \sin \frac{\theta}{2} \cos \theta_o} \\ &= -\frac{2k^2 e^{ikx}}{\Gamma x} \int_0^\infty d\xi \xi \sin(\Gamma \xi) v(\xi) \end{aligned} \quad (\text{IV-49})$$

where we have performed the  $\theta_o$  and  $\phi_o$  integrations and introduced  $\Gamma$  according to:

$$\Gamma = 2k \sin \frac{\theta}{2} \quad (\text{IV-49a})$$

In this case, the directivity pattern defined above becomes a function of  $\theta$  (or equivalently of  $\Gamma$ ) alone. We recall that the meaning of the directivity pattern is the ratio of the scattering integral  $p_1$  at a point  $\underline{x}$  divided by the value of  $p_1$  at a point located at the same distance  $x$  in the forward direction. For the spherically symmetric case, the directivity pattern is given by:

$$D(\theta) = \frac{\int_0^\infty d\xi \xi \sin(\Gamma \xi) v(\xi)}{\int_0^\infty d\xi \xi^2 v(\xi)} \quad (\text{IV-50})$$

If the scatterer is very small compared to  $\frac{1}{k}$ , the quantity  $\Gamma \xi$  will be much less than unity for any  $\xi$  located inside the scatterer.<sup>k</sup> We note that  $\frac{\sin \Gamma \xi}{\Gamma \xi} \sim 1$  for  $\Gamma \xi \ll 1$ ; thus, in this case, the directivity pattern becomes approximately 1 in all directions. Such a very small scatterer, which causes essentially isotropic scattering, is called a classical or Rayleigh scatterer, and bears out our earlier conclusions that very small scatterers will in general produce omnidirectional scattering. We find very large scatterers producing a collimated beam.

The scattering strengths and directivity patterns for a few typical spherically symmetric scatters are listed in Table IV-1. The directivity patterns are also shown graphically in Figure IV-3 on a decibel scale. We observe from Figure IV-3 that the directivity pattern,  $D(\theta)$ , drops by about a factor of 10 (20db) as  $\Gamma a$  is increased from zero to about 4. There is some variation, depending on the details of the refractive index distribution, but all directivity patterns drop a factor of 10 between  $\Gamma a = 0$  and a value of  $\Gamma a$  greater than  $2\frac{1}{2}$  and smaller than  $6\frac{1}{2}$ . We may, therefore, conclude that the principal scattered energy for a large scatterer ( $ka \gg 1$ ) is confined to an angle for which:

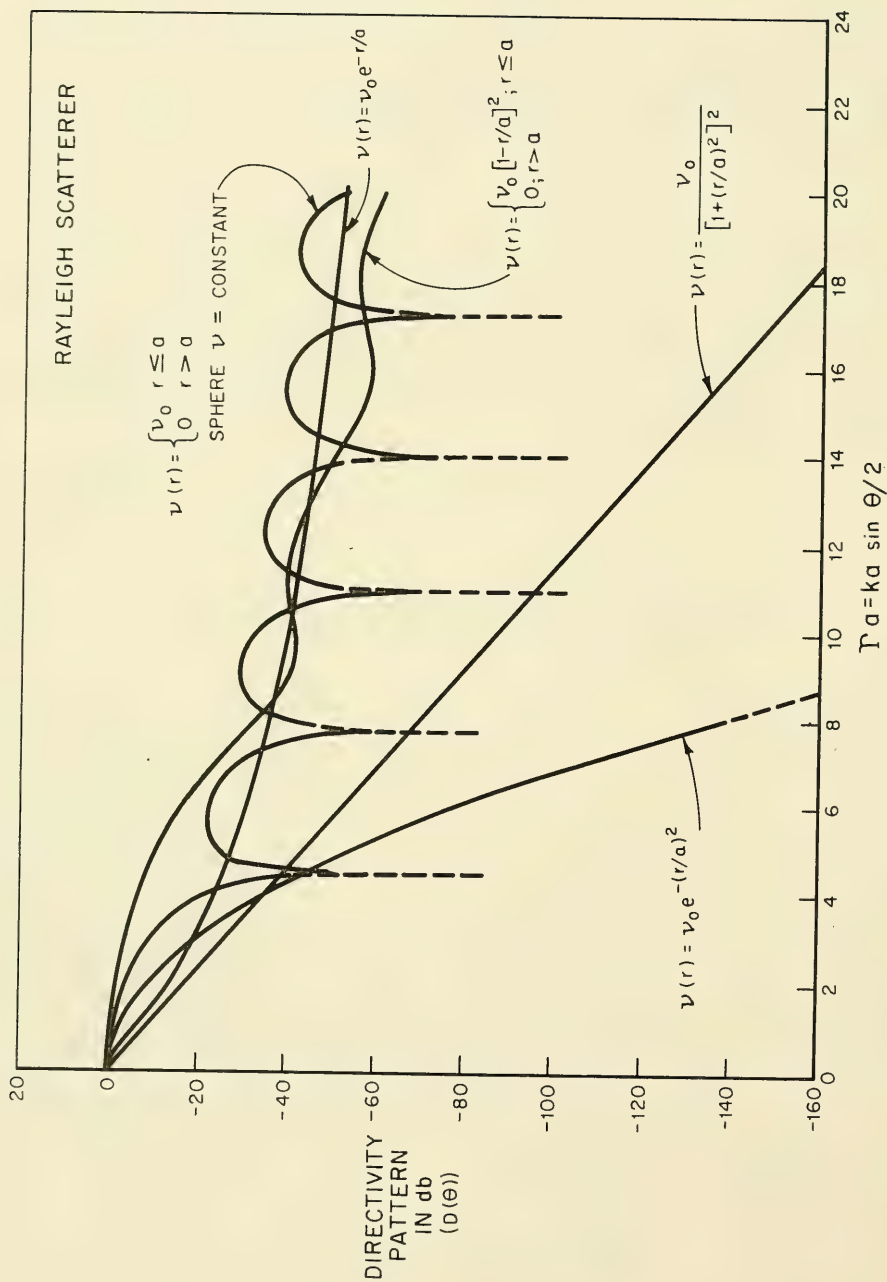
$$\Gamma a = 2k a \sin \frac{\theta}{2} < 4, \text{ or equivalently } \theta < \frac{4}{ka} \quad (\text{IV-51})$$

TABLE IV-1 (after Skudrzyk)

SCATTERING STRENGTHS AND DIRECTIVITY PATTERNS  
OF SPHERICALLY SYMMETRIC SCATTERERS

Deviation of Index of Refraction (Inhomogeneity) $v(\xi)$	Scattering Strength $S$	Directivity Pattern $D(\theta)$	Remarks
$v(\xi) = \begin{cases} v_0 & \text{for } \xi < a \\ 0 & \text{for } \xi > a \end{cases}$	$\frac{2}{3} k^2 a^3 v_0$	$3 \frac{(\sin \Gamma a - \Gamma a \cos \Gamma a)}{(\Gamma a)^3}$	spherical scatterer with constant sound velocity
$v(\xi) = v_0 e^{-\xi/a}$	$4k^2 a^3 v_0$	$\frac{1}{1 + \Gamma^2 a^2}$	exponentially decaying inhomogeneity
$v(\xi) = \begin{cases} v_0 (1 - \frac{\xi}{a})^2 & \text{for } \xi < a \\ 0 & \text{for } \xi > a \end{cases}$	$\frac{k^2 a^3 v_0}{15}$	$30 \frac{(4 - 6 \frac{\sin \Gamma a}{a} + 2 \cos \Gamma a)}{(\Gamma a)^4}$	parabolically decaying inhomogeneity
$v(\xi) = \frac{v_0}{(1 + (\xi/a)^2)^2}$	$\frac{\pi}{2} k^2 a^3 v_0$	$e^{-\Gamma a}$	inhomogeneity decaying as $(\xi/a)^{-4}$
$v(\xi) = v_0 e^{-(\xi/a)^2}$	$\frac{\sqrt{\pi}}{2} k^2 a^3 v_0$	$e^{-\Gamma^2 a^2/4}$	Gaussian inhomogeneity

Note:  $\Gamma = 2k \sin \frac{\theta}{2}$ .

FIGURE IV-3 DIRECTIONALITY PATTERN AS A FUNCTION OF  $\Gamma_a$  (AFTER SKUDRZYK)

### C. THE WEAK INHOMOGENEITIES OF THE OCEAN

The temperature distribution of the ocean exhibits a layered structure in the vertical direction. This structure is largely the result of the energy input due to weather conditions at the surface of the ocean (such as heat radiation of the sun and evaporation) and the heat conduction of the water. The detail of the layered structure changes with the time of day and with the seasons. A typical pattern of variation during the course of a day is shown in Figure IV-4. The figure shows, for several times of day, the temperature distribution as a function of depth, expressed in terms of a characteristic length scale which is the square root of the product of the diffusivity of the heat conduction and the length of a day. The resulting curves are seen to produce a surface layer of the order of 200 feet in which the temperature fluctuates substantially with the time of day, and in which the temperature gradients are negative during part of the day. These reverse gradients cause an unstable configuration which results in turbulent mixing. As a consequence, the macroscopic structure of the uppermost layer of the ocean has an isothermal character, although under examination in detail it will exhibit innumerable patches of various sizes which result from the turbulent mixing process. This top layer (of the order of magnitude of a few hundred feet) is called the isothermal layer, although it is isothermal only in the large. Below the isothermal layer, there is a region, called the thermocline, in which the temperature gradient is practically constant.

In addition to the instabilities occurring relatively near the surface of the ocean, turbulence is caused by large scale internal waves and currents. In all cases, the effect of the turbulence is to break up the systematic layered structure of the ocean into a random, patchy structure.

The resulting micro-structure of the temperature gives rise to a corresponding micro-structure of the index of refraction, which is the principal type of random inhomogeneity affecting wave propagation.

The general range of sizes of the patches to be encountered may be obtained from the following considerations. The largest patches to be encountered at a depth  $h$  below the surface should be those resulting directly from the original layered structure, and can therefore be expected to be patches extending between the ocean surface and the depth of  $2h$ . If these largest patches are more or less spherical, we would expect their diameters to be of the order of  $2h$ . The smallest patches, on the other hand, would be determined by the heat conductivity of the water. To quote Batchelor, who has investigated theoretically the statistical properties of the microthermal structure: "The dominant feature of the action of the turbulent motion on the temperature distribution is a continual reduction of the length-scale of temperature variations ... The continual increase in the magnitude of temperature gradients due to random convection will ultimately be checked by the

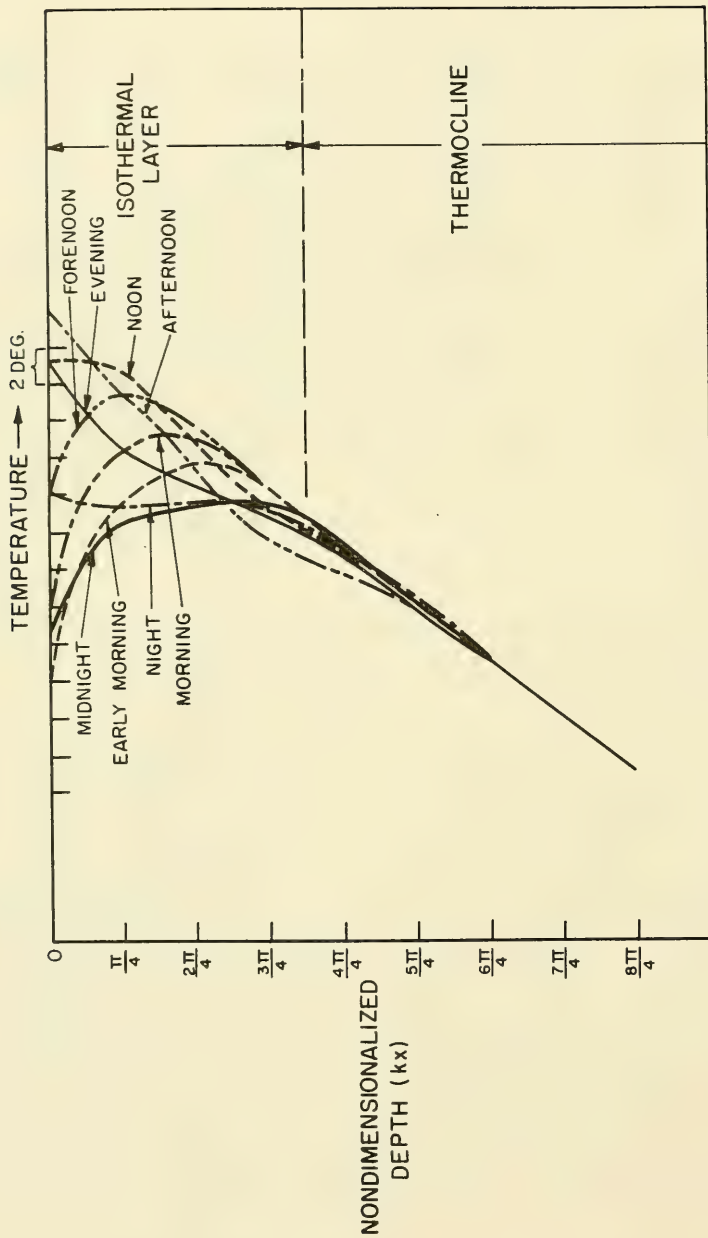


FIGURE IV-4 COMPUTED DAILY VARIATIONS OF THE MEAN TEMPERATURE OF THE SEA  
(AFTER SKUDRZYK)



smoothing action of thermal conduction, and no further refinement of the temperature distribution can occur; in this way, a length-scale characterizing the smallest temperature 'eddies' is determined."

Some recordings of the microthermal variations at various depths are shown in Figure IV-5.

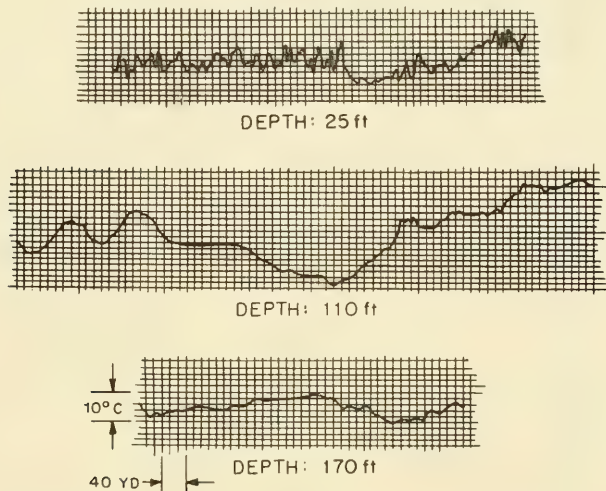


FIGURE IV-5      MICROTHERMAL VARIATIONS AT  
VARIOUS DEPTHS (AFTER URICK  
AND SEARFOSS)

The scale and amplitude of the dominant fluctuations are seen to be substantially greater at a depth of 110 ft than at a depth of 25 ft, as would be expected by the above argument; in fact, a dominant patch diameter of the order of twice the depth seems to be in general agreement with the recordings shown. Note that at a depth of 170 ft the amplitude of the patches appears to have decreased somewhat, indicating that the microthermal structure is again more uniform. The dominant patch diameter has been plotted versus the depth for a fair number of such recordings, and the resulting plot is shown in Figure IV-6. The outer scale of the patches is seen to agree quite well with two times the depth of the observation.



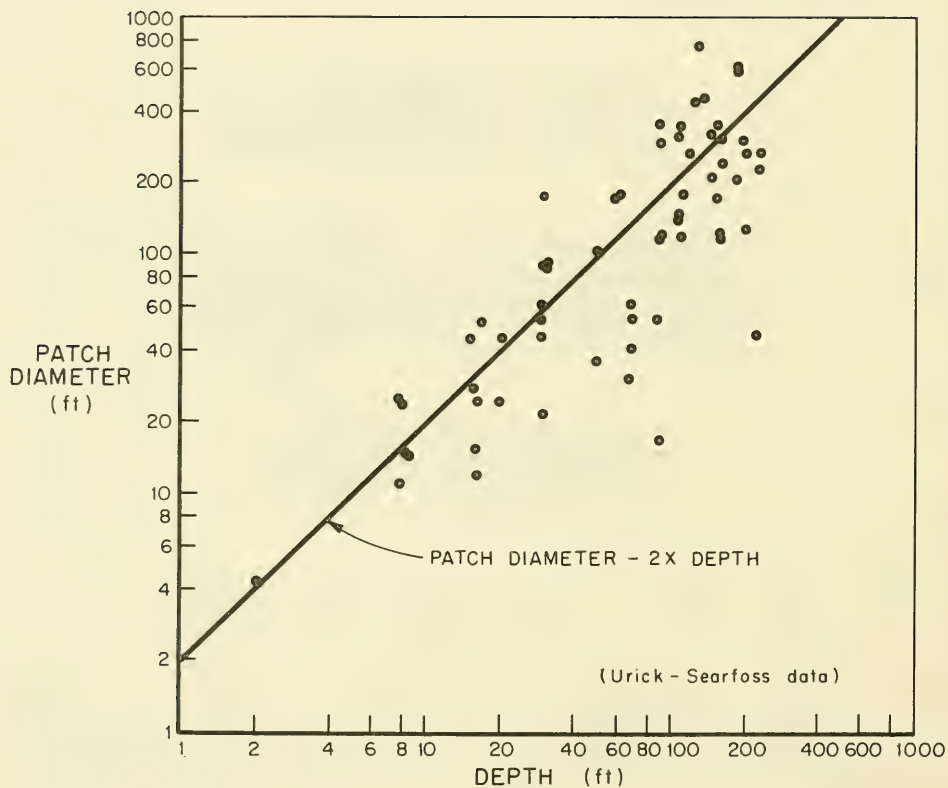


FIGURE IV-6 PATCH DIAMETER VS DEPTH (AFTER SKUDRZYK)

The micro-structure of the ocean changes with time. The rate of change is very slow compared to the passage of an acoustic wave, but the change can be expected to be substantial over a period of the order of minutes, and unrecognizable over a period of hours. We desire, therefore, a statistical description of this micro-structure. Clearly, the most we can hope for would be the joint probability density of the values of the index of refraction at sets of points in the ocean. Some measurements have been made of the probability distribution of the temperature differential between pairs of points in the ocean. Two such measurements are shown in Figure IV-7 and indicate that the temperature difference between two fixed points in the ocean tends to have a normal distribution.

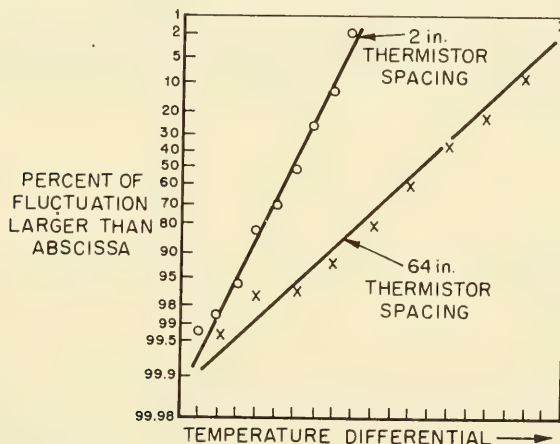


FIGURE IV-7 PROBABILITY DISTRIBUTION OF TWO-POINT TEMPERATURE DIFFERENCE

It is very likely, therefore, that the joint probability density function of the index of refraction is multivariate normal. In most applications, the principal characteristic of the index of refraction  $\nu(\underline{x})$  required is the so-called structure function:

$$B_{\nu}(\underline{x}, \underline{r}) = \left\langle \left( \nu(\underline{x}) - \nu(\underline{x} + \underline{r}) \right)^2 \right\rangle_{\text{ensemble or time}} \quad (\text{IV-52})$$

This function measures the mean square difference of the index of refraction at two fixed points. The mean must be taken over the ensemble of different micro-structures which occur in the course of time. The structure function is, therefore, in general a function of the coordinates of the two points involved, or as in (IV-52), a function of the position of one of the points and of the vector connecting the two points. Note further that the subscript  $\nu$  on the structure function indicates that this is the structure function of the index of refraction. Later in this chapter, it will be desirable to deal with the statistical properties of the fields of turbulent velocity ( $u$ ) or of the field of convected temperature ( $T$ ). The current discussion is equally applicable to the  $u$  and  $T$  fields. The field being considered will always be indicated as the subscript of the structure function, correlation function, spectrum, etc.

The micro-structure of the ocean is clearly not stationary in space. In other words, the structure function of (IV-52) can certainly be expected to depend on the depth of the observation  $x_3$ . However, the structure function will usually be stationary in the horizontal plane. For a particular depth, we may therefore write:

$$B_{\nu}(\underline{x}, \underline{r}) = B_{\nu}(x_3, \underline{r}) \quad (\text{IV-52a})$$

If, for reasons of convenience, we desire to ignore the dependence of the structure function on the depth of the observations, we shall simply suppress the  $x_3$  dependence and write  $B_{\nu}(\underline{r})$ .

The structure function is also not isotropic, in that the mean square fluctuations in the vertical direction may be expected to be somewhat different from those in the horizontal direction. Thus, if we introduce cylindrical coordinates for the vector  $\underline{r}$  ( $\underline{r} = (r, \theta, r_3)$ ), the structure function may be expected to depend both on  $r$  and on  $r_3$ . This is another way of stating that the patches, instead of being spherical on the average, may have a tendency to be lenticular. In general, therefore, the structure function depends on the three variables  $x_3$ ,  $r$ , and  $r_3$ :

$$B_{\nu}(\underline{x}, \underline{r}) = B_{\nu}(x_3, r, r_3) \quad (\text{IV-52b})$$

Unfortunately, not enough is known about the vertical anisotropy and nonstationarity of the micro-structure. From the little calculation that has been done, it is pretty clear that their effect on scattering is substantial. However, we shall usually ignore both effects and deal with a structure function  $B_{\nu}(r)$  which depends on the distance of the two points alone.

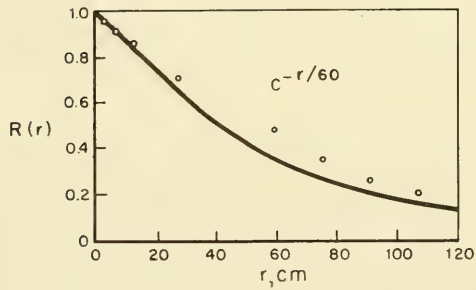
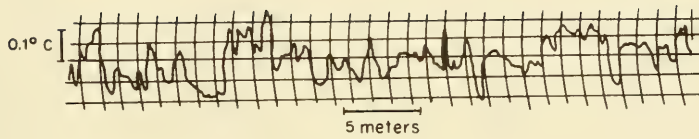


FIGURE IV-8 TEMPERATURE FLUCTUATIONS AND ASSOCIATED CORRELATION FUNCTION (AFTER LIEBERMANN)

If the fluctuations of the index of refraction are stationary, we can introduce the usual correlation function:

$$R_{\nu}(\underline{r}) = \frac{\langle \nu(\underline{x}) \nu(\underline{x} + \underline{r}) \rangle}{\langle \nu(\underline{x})^2 \rangle} \quad (\text{IV-53})$$

The correlation function is related to the structure function according to:

$$B_{\nu}(\underline{r}) = \langle \left( \nu(\underline{x}) - \nu(\underline{x} + \underline{r}) \right)^2 \rangle = 2 \langle \nu^2 \rangle \left( 1 - R_{\nu}(\underline{r}) \right) \quad (\text{IV-54})$$

We note that the mean square fluctuation of the index of refraction is independent of position in the stationary case; thus, we may just write  $\langle \nu^2 \rangle$ .

The original experimental studies of the correlation of the temperature fluctuations in the ocean were made around 1948 by Urick and Searfoss, and were followed in 1951 by further experiments by Liebermann. Some of Urick and Searfoss' temperature recordings have already been presented in Figure IV-5. In Figure IV-8 we present a temperature recording near the surface made by Liebermann, together with its corresponding correlation function. The points of Figure IV-8 suggest that the use of an exponential correlation function may be quite appropriate for correlation distances between a few centimeters and a few meters:

$$R_{\nu}(r) = e^{-r/a} \quad (\text{IV-55})$$

Because of the heat conductivity of the water, the use of an exponential correlation function is certainly not appropriate for very small correlation distances, i.e., a few centimeters or less. We shall see later that the slope of the correlation function must go to zero as  $r$  approaches zero if the microstructure is to be continuous; clearly the thermal conductivity will prevent any discontinuity in the temperature from occurring. Whenever the fine structure of the patches is important (i.e., in the range below a few centimeters), it may be preferable to use a Gaussian form of the correlation function:

$$R_{\nu}(r) = e^{-r^2/a^2} \quad (\text{IV-56})$$

Both (IV-55) and (IV-56) are strictly empirical correlation functions, but both have been used extensively in the literature. Neither reflect the turbulent mechanisms which generate the thermal micro-structure of the ocean, and it was not until the last five years that attempts have been made to base the scattering calculations on a correlation function which does reflect the physical mechanisms responsible for the ocean micro-structure.

A substantial amount of effort has been devoted during the past 10 years to the statistical investigation of turbulence, aimed both at representing the turbulent velocity field and at describing the resulting micro-structure of the distribution of the temperature and of the index of refraction. We shall merely sketch the principal conclusions from this research; two excellent surveys with considerably greater detail may be found in the book by Tatarski (Part I) and in the paper by Batchelor.

To describe the micro-structure resulting from turbulence, it is convenient to use a spectral representation of the fields involved. Consider the representation of the covariance function of the index of refraction in a stationary medium in terms of its Fourier transform:

$$\langle v(\underline{x})v(\underline{x} + \underline{r}) \rangle = \langle v^2 \rangle R_v(\underline{r}) = \iiint_{-\infty}^{\infty} d\underline{k} e^{i \underline{k} \cdot \underline{r}} S_v(\underline{k}) \quad (\text{IV-57a})$$

The function  $S_v$  is the Fourier transform of the covariance function, and it indicates the amplitude of each spectral component present in the covariance function. The spectrum itself is therefore given by:

$$S_v(\underline{k}) = \iiint_{-\infty}^{\infty} d\underline{r} e^{-i \underline{k} \cdot \underline{r}} R_v(\underline{r}) \frac{\langle v^2 \rangle}{(2\pi)^3} \quad (\text{IV-57b})$$

The above merely reflects the Fourier transform theorem. If the turbulence is isotropic, i.e., the correlation function depends on the distance  $r$  alone, the spectrum  $S_v(k)$  will also be isotropic, i.e., depend only on the magnitude of the wave number  $(k)$ . To show this, we introduce spherical coordinates for the vector  $\underline{r}$  in (IV-57b) using  $\underline{k}$  as the polar axis of the coordinate system:

$$\underline{r} = (r, \theta, \phi) \text{ such that } \underline{k} \cdot \underline{r} = k r \cos \theta \quad (\text{IV-58})$$

The element of volume in the integral now becomes  $d\underline{r} = 2\pi r^2 \sin \theta dr d\theta$ , and (IV-57b) may be rewritten as:

$$S_v(\underline{k}) = \int_0^{\infty} dr \int_0^{\pi} \frac{d\theta}{(2\pi)^2} r^2 \sin \theta e^{-i k r \cos \theta} R_v(r) \langle v^2 \rangle \quad (\text{IV-59})$$

We observe that the spectrum in the isotropic case indeed depends only on  $(k)$ . The integration over  $\theta$  can be performed and yields:

$$S_U(k) = \frac{1}{4\pi k^2} \left[ 2 \int_0^{\infty} \frac{dr}{\pi} (kr) \sin(kr) R_U(r) \langle v^2 \rangle \right] = \frac{E_U(k)}{4\pi k^2} \quad (\text{IV-60})$$

In the above, we have defined a function  $E_U$  which is very closely related to the spectrum  $S_U$  and which, in fact, has the property that:

$$S_U(k) dk = S_U(k) (4\pi k^2) dk = E_U(k) dk \quad (\text{IV-60a})$$

In other words, if we wish, in the isotropic case, to deal with a spectrum relative to a wave number interval rather than relative to a wave number volume element (as we must in the nonisotropic case) we should use  $E_U$  as the isotropic spectrum. Henceforth, whenever we refer to the spectrum under conditions of isotropy, we shall always mean  $E_U$ , defined according to

$$E_U(k) = 2 \int_0^{\infty} \frac{dr}{\pi} (kr) \sin(kr) R_U(r) \langle v^2 \rangle \quad (\text{IV-61a})$$

The inverse relation to the above may be found by using a spherical coordinate system to permit the integration of (IV-57a); proceeding in a manner entirely analogous to the above, we obtain:

$$\langle v^2 \rangle R_U(r) = \int_0^{\infty} dk \frac{\sin(kr)}{kr} E_U(k) \quad (\text{IV-61b})$$

A number of generally valid statements may be deduced from this pair of transforms relating the spectrum and the covariance function. We expect the correlation function essentially to vanish for values of  $r$  greater than some large distance  $R$ . Similarly, we expect the spectrum ( $E_U$ ) to be cut off at some high frequency ( $K$ ) corresponding to spatial gradients so steep that the heat conductivity of the water will destroy them. In other words, both the correlation function and the spectrum exhibit cutoffs at large distances and large wave numbers, respectively. Consider now (IV-61a) for wave numbers much less than  $\frac{1}{R}$ , i.e., wave numbers corresponding to spatial wave lengths greater than the maximum correlation distance. It follows that in this case  $(kr)$  will always be much less than 1, and the sine in (IV-61a) may be approximated by its argument. Thus, we find that near  $k = 0$  the spectrum has the form:

$$E_U(k) \approx \frac{2k^2 \langle v^2 \rangle}{\pi} \int_0^{\infty} dr r^2 R(r) \quad (\text{IV-62})$$



In other words, the spectrum vanishes quadratically near  $k = 0$ , and the range for which this quadratic behavior is appropriate is somewhat less than  $\frac{1}{R}$ .

Because of the definition of the correlation function (IV-53), the value of the correlation function for zero correlation distance will be unity. It follows from (IV-61b) that the mean square fluctuation of the index of refraction is just the total area under the spectrum:

$$\langle v^2 \rangle = \int_0^{\infty} dk E_v(k) \quad (\text{IV-63})$$

Just as we were able above to find the behavior for the spectrum for small values of  $k$  based on the known behavior of the correlation function for large values of  $r$ , so we may also determine the behavior of the correlation function for small values of  $r$  from the known behavior of the spectrum for values of  $k$  larger than  $K$ . In fact, for any correlation distance  $r$  substantially less than  $\frac{1}{K}$ , we may approximate (IV-61b) as follows:

$$\langle v^2 \rangle R_v(r) \approx \int_0^{\infty} dk \left( 1 - \frac{(kr)^2}{6} \dots \right) E_v(k) = \langle v^2 \rangle - \frac{r^2}{6} \int_0^{\infty} dk k^2 E_v(k) \quad (\text{IV-64})$$

We observe that the expansion of the correlation function near  $r = 0$  does not contain a term proportional to  $r$ , which substantiates our earlier assertion that an exponential correlation function cannot possibly be applicable for very small values of  $r$ , the correlation distance, if there is a cutoff frequency of the spectrum due to conduction. We may also obtain the structure function for very small values of  $r$  through the substitution of (IV-64) in (IV-54):

$$B_v(r) = 2 \langle v^2 \rangle \left[ 1 - R_v(r) \right] \sim r^2 \quad (\text{IV-64a})$$

For small values of  $r$ , the structure function therefore behaves like  $r^2$ .

The above argument will hold equally well for the spectrum and structure function of the turbulent velocity ( $u$ ) or of the temperature distribution ( $T$ ). To find the spectrum in the intermediate range of wave numbers, we must appeal to Kolmogoroff's general theory of turbulence as described, for example, in Tatarski. We shall content ourselves with a general dimensional argument providing some justification for the final results.

Consider a fluid which is maintained by some means or other in an unstable state, i.e., a state which results in the occurrence of turbulence. Suppose that an external source of energy provides a power  $P$  per unit mass of the medium.

The dimensions of  $P$  are power per unit mass =  $\frac{m l^2}{t^3} \cdot \frac{1}{m} = \frac{l^2}{t^3}$ . We suspect the existence of a spectrum of the velocity of the turbulent motion which is pretty universal, i.e., a spectrum which, at least for a substantial portion of the frequency, is independent of the details of the energy source and independent of the detailed properties of the medium, but subject only to the condition that turbulence is maintained. The resulting spectrum  $E_u(k)$  can, if it is to be universal, depend only on the variables  $k$  and  $P$ :

$$E_u = E(P, k) \quad (IV-65)$$

The dimensions of  $k$  are  $\frac{1}{l}$ . The dimensions of the spectrum  $E_u$  are  $\frac{l^3}{t^2}$ , as may be seen from the definition of a spectrum as in (IV-64), with the realization that for the velocity spectrum the mean square velocity fluctuations  $\langle u^2 \rangle$  must be used instead of  $\langle v^2 \rangle$ . There is clearly no dimensionless combination of  $P$  and  $k$ , and we are, therefore, looking for a combination of  $P$  and  $k$  which is dimensionally consistent with  $E_u$ :

$$E_u \sim P^m k^n \quad \text{or} \quad \frac{l^3}{t^2} \sim \frac{l^{2m-n}}{t^{3m}} \quad (IV-66)$$

It follows at once that  $m = 2/3$  and  $n = -5/3$ , and in the range of interest, the spectrum must be of the form:

$$E_u \sim P^{2/3} k^{-5/3} \quad (IV-67)$$

The above is the Kolmogoroff law of turbulence, stating that for ranges in which a universal law of turbulence is applicable, the spectrum must decrease as the  $5/3$  power of the wave number. Clearly, the above law can only be expected to be valid for values of the wave number below the viscous cutoff. In other words, for turbulent eddies so small that the viscosity of the medium becomes important, the spectrum will in general also depend on the viscosity, and the above dimensional argument will no longer be applicable. Suppose that the eddy size for which this occurs is  $l_{\text{visc}}$ ; we shall call this the inner scale of the turbulence and would expect the Kolmogoroff spectrum for the velocity to be valid for wave numbers less than  $\frac{2\pi}{l_{\text{visc}}}$ .

We desire the spectra of the fluctuations of the temperature and the index of refraction rather than of the velocity field. It turns out, however, that one may again expect a range of frequencies for which a universal spectrum decaying like the  $-5/3$  power of the frequency is applicable:

$$E_{\nu} \sim k^{-5/3} \quad \left( \frac{2\pi}{L} < k < \frac{2\pi}{\ell_{\text{cond}}} \right) \quad (\text{IV-68})$$

The meaning of  $\ell_{\text{cond}}$  and  $L$  is the following:

In the case of sea water, the heat conduction cutoff of the spectrum occurs at lower wave numbers than the viscous cutoff; in other words, the viscosity of the water can support smaller eddies than the thermal conductivity. The range of validity of (IV-68) is therefore cutoff at the high wave number end by the scale determined by heat conduction. At low wave numbers, i.e., for large patches, we would certainly not expect a universal law of turbulence for patch diameters of the order of magnitude of the layer thickness of the originally layered structure which was broken up by the turbulence. The outer scale  $L$  of the thermal micro-structure will therefore be of the order of twice\* the diameter of the largest patches, which has been shown earlier (see Figure IV-6) to have a diameter of the order of twice the depth. We would, therefore, expect the outer structure  $L$  to be of the order of four times the depth. For wave lengths of the order of magnitude of the largest patches, the details of the original layered structure become important. We show in Figure IV-9 the general shape of spectrum that is to be expected. For very small wave numbers, the spectrum starts at zero and increases quadratically. For slightly larger wave numbers, the spectrum is more or less flat, going through a maximum corresponding to the dominant patches resulting directly from the breaking up of the original layers. For the intermediate range of wave numbers, corresponding to wave lengths between the depth of the measurement and a few centimeters, the spectrum obeys the Kolmogoroff law. Finally, for very large wave numbers in the conduction range, the spectrum decreases very rapidly.

We may also obtain the structure function corresponding to the Kolmogoroff spectrum. According to (IV-54) and (IV-61b), the structure function is given by:

$$B_{\nu}(r) = 2 \langle v^2 \rangle \left[ 1 - R_{\nu}(r) \right] = 2 \int_0^{\infty} dk \left( 1 - \frac{\sin kr}{kr} \right) E(k) \quad (\text{IV-69})$$

---

\*"twice" because  $L$  is a full wavelength, containing both a patch with  $v > 0$  and a patch with  $v < 0$ .

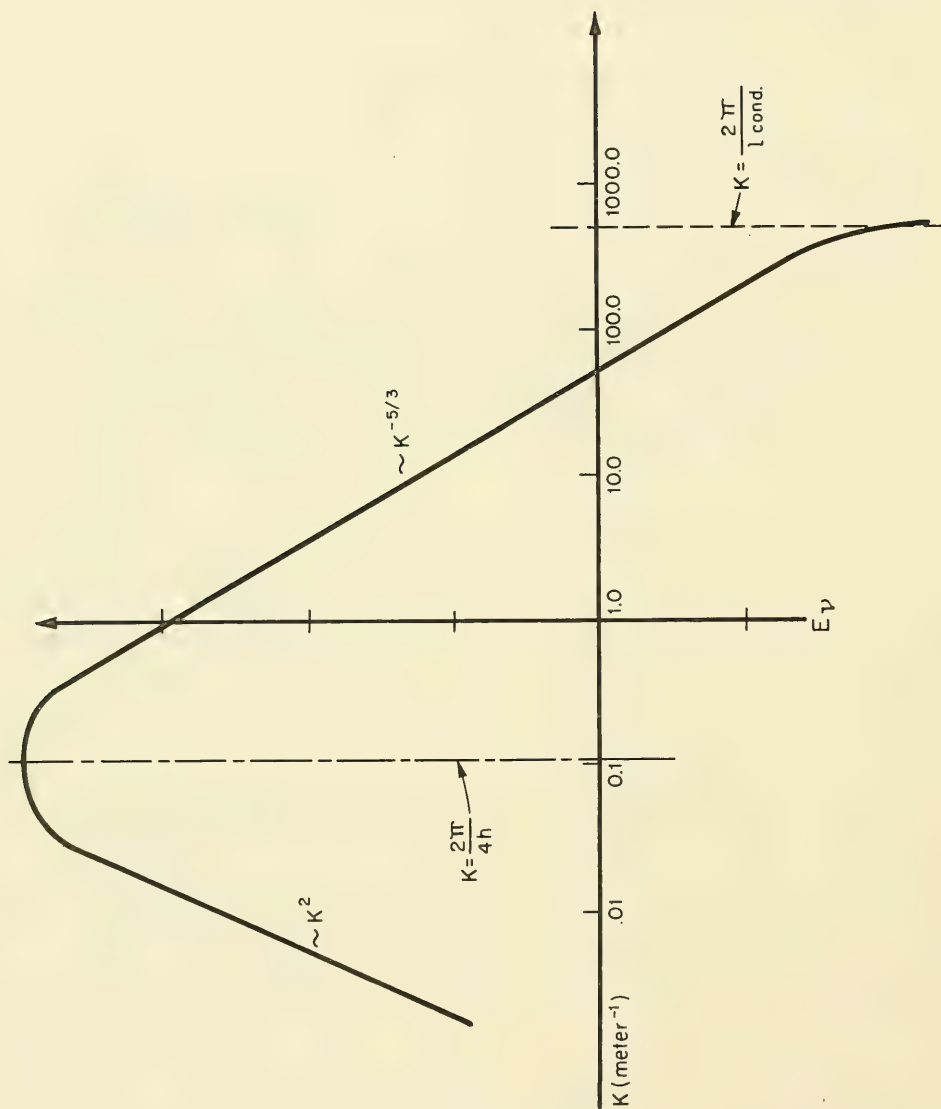


FIGURE IV-9 SCHEMATIC REPRESENTATION OF PHYSICALLY REALISTIC SPECTRUM (LOG-LOG SCALE)

For intermediate values of the correlation distance, i.e.,  $\ell_{\text{cond}} \ll r \ll L$ , the main contribution of the integral will come from the part of the spectrum in the range  $\frac{2\pi}{L} < k < \frac{2\pi}{\ell_{\text{cond}}}$  so that:

$$B_{\text{v}}(r) \approx 2 \int_{2\pi/L}^{2\pi/\ell_{\text{cond}}} dk \left(1 - \frac{\sin kr}{kr}\right) k^{-5/3} = r^{2/3} \int_{2\pi r/L}^{2\pi r/\ell_{\text{cond}}} d\xi \left(1 - \frac{\sin \xi}{\xi}\right) \xi^{-5/3} \approx r^{2/3} \int_0^{\infty} d\xi \left(1 - \frac{\sin \xi}{\xi}\right) \xi^{-5/3} \quad (\text{where } \xi = kr) \quad (\text{IV-70})$$

For the Kolmogoroff law, the structure function behaves as the 2/3 power of the distance of separation. Figure IV-10 shows a number of measured structure functions for the thermal fluctuations, which appear to substantiate the 2/3 power law in the intermediate range.

For purposes of calculation, and in the absence of better experimental information, we shall make use of a fairly bold approximation to the spectrum of the index of refraction as shown in Figure IV-9, an approximation of the form:

$$E_{\text{v}}(k) \approx \begin{cases} 0 & \text{for } k < \epsilon \\ E_0 & \text{for } \epsilon < k < k_0 \\ E_0 \left(\frac{k_0}{k}\right)^{5/3} & \text{for } k > k_0 \end{cases} \quad (\text{IV-71})$$

In other words, above some wave number  $k_0$  we shall use the Kolmogoroff spectrum. Usually there will be no need to introduce the conduction cutoff at very high frequencies. For wave numbers below  $k_0$ , we shall assume the spectrum to be flat, down to some very small wave number  $\epsilon$  corresponding to the largest patch size to be expected. The spectrum is assumed to vanish below  $\epsilon$ . We may usually take the order of magnitude of  $\epsilon$  to be a factor of 10 smaller than  $k_0$ . Based on the spectrum (IV-71), we would, therefore, expect a mean square fluctuation of the refractive index, see (IV-63):

$$\langle v^2 \rangle = \int_0^{\infty} E(k) dk \approx E_0 k_0 + \frac{3}{2} E_0 k_0 = 2.5 E_0 k_0 \quad (\text{IV-72})$$

We can, therefore, eliminate  $E_0$  from (IV-71) and write the spectrum strictly in terms of the mean square fluctuation and the critical wave number  $k_0$ .

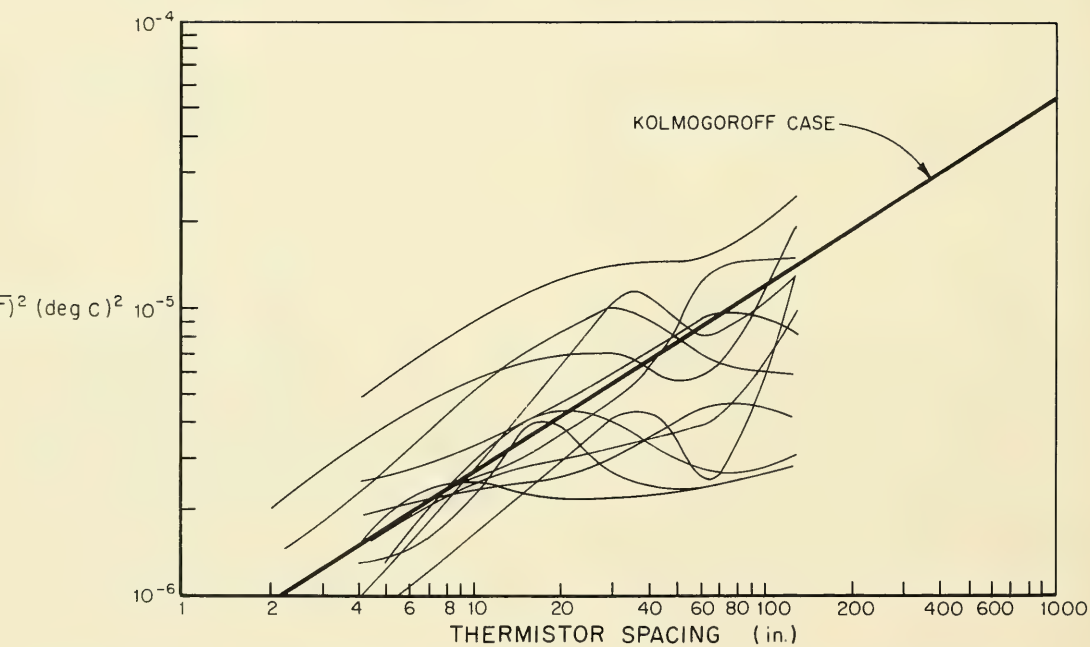


FIGURE IV-10 HORIZONTAL TEMPERATURE STRUCTURE FUNCTIONS AS MEASURED IN THE SEA

Ignoring the very low wave number range, we obtain the form of the Kolmogoroff spectrum which we shall henceforth use:

$$E(k) = \frac{0.4 \langle v^3 \rangle}{k_0} \begin{cases} 1 & \text{for } k < k_0 \\ \left(\frac{k_0}{k}\right)^{5/3} & \text{for } k > k_0 \end{cases} \quad (\text{IV-73})$$

In Figure IV-11, we show a number of actual measured correlation functions, including the fairly long range portion of the correlation function, as compared with a correlation function of the Kolmogoroff type. The general qualitative agreement seems to be very good, certainly much better than the exponential or Gaussian approximation, which turns out to be an appropriate approximation only for relatively small values of the correlation distance. As we shall see in the next section, the low wave number (large wavelength) portion of the spectrum is very important in most scattering calculations.

To summarize the results of this section, we present below a table of the three correlation functions, and their associated spectra, that have been used as various degrees of approximation of the micro-structure of the index of refraction.

TABLE IV-2

OCEAN MICRO-STRUCTURE CORRELATION FUNCTIONS  
AND ASSOCIATED SPECTRA

Correlation Function $R_v(r)$	Spectrum $E_v(k)$	Remarks
$e^{-r/a}$	$\frac{4 \langle v^2 \rangle a}{\pi} \frac{(ka)^2}{(1+(ka)^2)^2}$	Exponential
$e^{-r^2/a^2}$	$\frac{2a \langle v^2 \rangle}{\sqrt{\pi}} \left(\frac{ka}{2}\right)^2 e^{-\left(\frac{ka}{2}\right)^2}$	Gaussian
See Figure IV-11c	$0.4 \frac{\langle v^3 \rangle}{k_0} \begin{cases} 1 & \text{for } k < k_0 \\ (k_0/k)^{5/3} & \text{for } k > k_0 \end{cases}$	Kolmogoroff



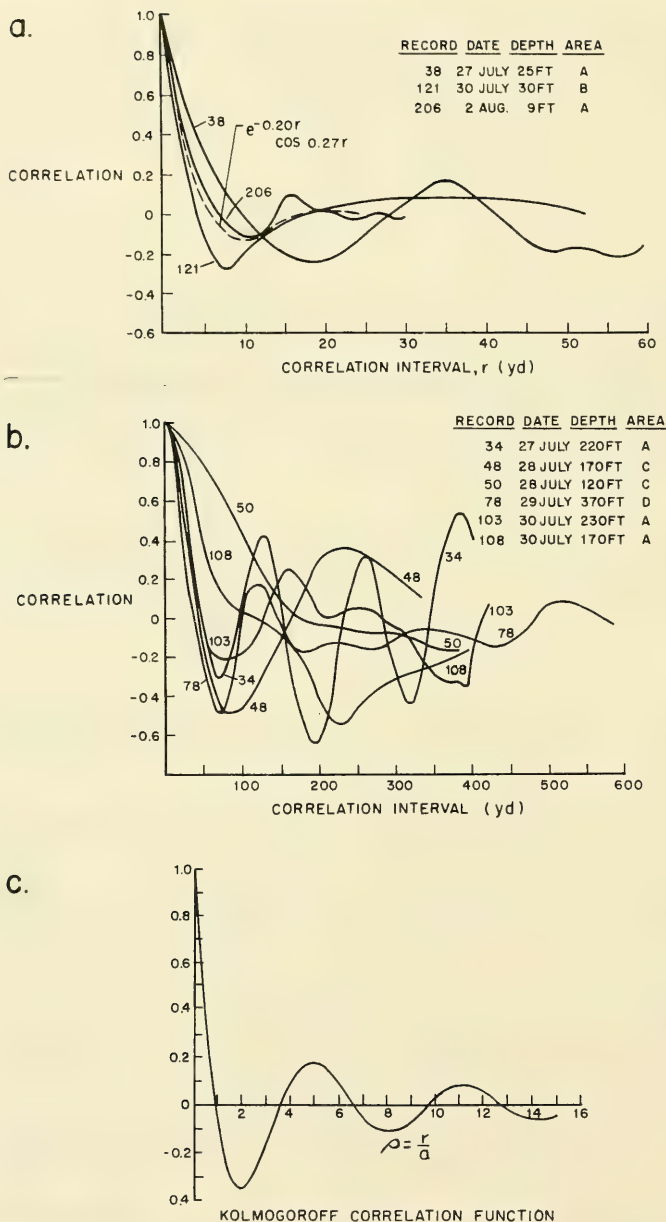


FIGURE IV-11

COMPARISON OF EXPERIMENTAL CORRELATION FUNCTIONS WITH A CORRELATION FUNCTION CORRESPONDING TO A KOLMOGOROFF SPECTRUM

#### D. SIGNAL FLUCTUATION AND CORRELATION RESULTING FROM THE OCEAN MICRO-STRUCTURE

We now have at our disposal the tools required to examine the statistical properties of the pressure fluctuations of a sound wave propagating through an inhomogeneous medium. As a first step, we consider the distribution of scattered power from a relatively small region of inhomogeneities at a distance large compared to the size of the region. The geometry of the situation has already been shown in Figure IV-2 for the individual scatterer, and we need merely replace the individual scatterer by a region of scatterers to make this figure applicable to the present discussion. We found in our analysis of the geometry of Figure IV-2 an expression for the first order scattered pressure which was:

$$p_1(\underline{x}) \approx - \frac{2k^2 e^{ikx}}{4\pi x} \int_V d\underline{\xi} e^{-ik\underline{d} \cdot \underline{\xi}} v(\underline{\xi}) \quad (\text{IV-45})$$

We recall the meaning of the vector  $\underline{d}$  to be the difference between the unit vector directed at the observer and the unit vector in the positive  $x_1$  direction, i.e., the direction of propagation of the incident sound. The magnitude of the vector  $\underline{d}$  was shown earlier to be  $d = 2 \sin \theta/2$ , where  $\theta$  is the scattering angle separating the direction of the observer from the direction of propagation.

The volume  $V$  is to be regarded as large compared to any single inhomogeneity, but small compared to the distance between the region and the observer. If we consider an ensemble of scattering volumes differing from each other in their micro-structure but all characteristic of the micro-structures which might be encountered in sequence over a long period of time, we would like to know the statistical properties of the scattered pressure  $p_1$  averaged over such an ensemble. Since the average of the refractive index  $<v(\underline{\xi})>$  over the ensemble must be zero, it is clear that the average fluctuation of the pressure must also vanish ( $<p_1> = 0$ ). We would like to compute the variance of the fluctuations of the pressure, which is analogous to computing the distribution of scattered power:

$$<|p_1|^2> = \frac{k^4}{(2\pi)^2 x^2} \int_V d\underline{\xi}^{(1)} \int_V d\underline{\xi}^{(2)} e^{-ik\underline{d} \cdot (\underline{\xi}^{(1)} - \underline{\xi}^{(2)})} <v(\underline{\xi}^{(1)}) v(\underline{\xi}^{(2)})> \quad (\text{IV-74})$$

$$= \frac{k^4}{(2\pi)^2 x^2} \iint_V d\underline{\xi}^{(1)} d\underline{\xi}^{(2)} e^{-ik\underline{d} \cdot (\underline{\xi}^{(1)} - \underline{\xi}^{(2)})} <v^2> R_V(\underline{\xi}^{(1)} - \underline{\xi}^{(2)})$$

To obtain (IV-74), we multiply  $p_1$ , as given in (IV-45), by its complex conjugate and average over the ensemble of different micro-structures, making use of the correlation function of the refractive index (IV-53). We may simplify (IV-74) by introducing the difference coordinates  $\underline{\xi} = \underline{\xi}^{(1)} - \underline{\xi}^{(2)}$ , since the integrand depends only on these coordinates. Let us retain  $\underline{\xi}^{(1)}$  as the other coordinate of integration. The only problem is then to determine the volume of integration for the  $\underline{\xi}$  coordinate. We realize, however, that because the volume  $V$  is much larger than the "correlation volume" of the correlation function  $R_U$ , the integration over  $\underline{\xi}$  may just as well be taken over all of space. Making these substitutions in (IV-74), we obtain:

$$\langle |p_1|^2 \rangle \approx \frac{k^4}{(2\pi)^2 x^2} \left( \int_V d \cdot \underline{\xi}^{(1)} \right) \int_{-\infty}^{\infty} d \cdot \underline{\xi} e^{-ikd \cdot \underline{\xi}} \langle U^2 \rangle R_U(\underline{\xi}) \quad (\text{IV-75})$$

The first integral in (IV-75) is seen to be the volume of the scattering region  $V$ . The second integral is the spectrum of the refractive index refined in (IV-57b). We therefore obtain for the scattered power the following very simple relation involving the spatial spectrum of the fluctuations of the refractive index:

$$\langle |p_1|^2 \rangle = \frac{2\pi k^4 V}{x^2} S_U(kd) \quad (\text{IV-76})$$

The scattered power is seen to be proportional to the volume of the scattering region; thus, the power scattered by two adjacent volumes must be added to give the power scattered by the two volumes combined. For the far field, therefore, the power scattered from two different volumes, each large compared to an individual inhomogeneity, is uncorrelated, as asserted in Chapter II.

When the scattering volume is isotropic, we may use the isotropic spectrum  $E_U$  as defined in (IV-60). Since the magnitude of the vector  $\underline{d}$  is  $2 \sin \theta/2$ , the angular distribution of the scattered power is given by:

$$\langle |p_1|^2 \rangle = \frac{k^4 V}{2x^2} \frac{E_U(2k \sin \theta/2)}{(2k \sin \theta/2)^2} \quad (\text{IV-77})$$

For practical purposes, we can select the spectrum corresponding to the exponential Gaussian, or Kolmogoroff correlation function from Table IV-2 and substitute in (IV-77). We observe that the directivity of the scattered power in the far field scattered by a volume with a statistically distributed index of refraction is exactly the same as the directivity resulting from scattering by a single inhomogeneity with a determinate distribution of the refractive index equal to the correlation function.

(IV-77) shows that the larger patches of the inhomogeneities are important in determining the forward scattering properties, whereas patches of the order of half the wavelength of the incoming sound dominate in determining the back scattering.

The total power scattered by a unit volume of scattering inhomogeneities may be obtained by integrating (IV-77) over the surface of a semisphere:

$$P_{\text{forward}} = 2\pi \int_0^{\pi/2} d\theta \, x^2 \langle |p_1(x_1\theta)|^2 \rangle \sin\theta = \pi k^4 \int_0^{\pi/2} d\theta \, \sin\theta \frac{E_v(2k \sin \theta/2)}{(2k \sin \theta/2)^2} \quad (\text{IV-78})$$

Because of the trigonometric identity  $\cos \theta = 1 - 2 \sin^2 \theta/2$ , we can write the differential  $\sin \theta \, d\theta$  as  $2 \, d \sin^2 \theta/2$ . We therefore introduce the new variable  $y = (2k \sin \theta/2)^2$  in (IV-78) and obtain a very simple expression for the total power scattered forward by unit volume of scatterer:

$$P_{\text{forward}} = \frac{\pi}{2} k^2 \int_0^{2k^2} dy \frac{E_v(\sqrt{y})}{y} \quad (\text{IV-79})$$

Consider now a plane wave incident on an infinitely extended slab of scatterers, the slab having unit thickness. A moment's reflection will make clear that (IV-79) must also be the total scattered power received per unit of surface at any point behind the slab. If the slab has a thickness  $L$ , the total scattered power will be:

$$P_{\text{sc}} = \frac{\pi}{2} k^2 L \int_0^{2k^2} dy \frac{E_v(\sqrt{y})}{y} \quad (\text{IV-80})$$

since we may simply add the scattered power from each of the individual slabs of unit thickness. Thus, an observer, embedded at a range  $L$  from the surface of an inhomogeneous half-space will find that (IV-80) determines the scattered power which he receives from forward scattering of the intervening medium if a plane sound wave is normally incident on the inhomogeneous half-space. With the use of Table IV-2, we may work out the details of (IV-80) for the case of an exponential and a Gaussian correlation function. These are presented in (IV-81).

$$\text{Exponential: } P_{sc} = 2 \langle v^2 \rangle a^3 k^2 L \int_0^{2k^2} \frac{dy}{(1+a^2 y)^2} = \frac{4 \langle v^2 \rangle a^3 k^4 L}{1+2a^2 k^2} \quad (\text{IV-81a})$$

$$\text{Gaussian: } P_{sc} = \sqrt{\pi} k^2 L \frac{a^3}{4} \langle v^2 \rangle \int_0^{2k^2} dy e^{-\frac{ya^2}{4}} = \sqrt{\pi} k^2 L a \langle v^2 \rangle \left( 1 - e^{-\frac{k^2 a^2}{2}} \right) \quad (\text{IV-81b})$$

We may take the high and low frequency limits of these expressions to obtain the approximate expressions for the scattered power shown in Table IV-3. These are seen to agree with the qualitative discussion of Chapter II. Furthermore, the exact expressions for the entire frequency range in (IV-81) permit us to examine the range of validity of the high and low frequency approximations. Thus, Table IV-3 also shows ranges of frequency for which the approximation can be tolerated. In this context, we have chosen a relative error of approximately 1/3 as the maximum allowable error for the approximation to be applicable. It should be emphasized that all of these results are good only for the far field where the geometric approximations leading to (IV-45) are valid. Furthermore, the scattering volume must not be too large if the single scattering approximation under which all of this was devised is to remain tenable. In other words, the range  $L$  must be sufficiently small that the scattered powers shown in Table IV-3 are small compared to unity.

TABLE IV-3

THEORETICAL SCATTERING FOR TWO TYPES OF  
CORRELATION FUNCTION

	$ka \gg 1$ (high freq.)	$ka \ll 1$ (low freq.)
Exponential	$P_{sc} \approx 2ak^2 \langle v^2 \rangle L$ applicable when $ka > 1$	$P_{sc} \approx 4a^3 k^4 \langle v^2 \rangle L$ applicable when $ka < \frac{1}{2}$
Gaussian	$P_{sc} \approx \sqrt{\pi} ak^2 \langle v^2 \rangle L$ applicable when $ka > 2$	$P_{sc} \approx \frac{\sqrt{\pi}}{2} a^3 k^4 \langle v^2 \rangle L$



For the high frequency case, this yields the condition (IV-15) which has been used earlier without justification. To obtain order of magnitude estimates of the quantities involved, we may assume a typical value for  $\langle v^2 \rangle$  in the ocean to be of the order of  $5 \times 10^{-9}$ . A typical value of the patch radius  $a$  is of the order of 1 to 10 meters, depending on the depth of the measurement. The results of Table IV-3 were obtained for the first time by Mintzer in 1953 for the case of a spherically spreading wave in a medium with a Gaussian correlation function. Mintzer compared the behavior of the scattered power as linearly depending on the range with experimental data obtained by Sheehy. (See Figure IV-12.) The coefficient of variance (the square root of the mean square power) is seen to behave very much more as the square root of the range than as the three-halves power of the range which would have been predicted by ray acoustics. The above arguments do not give us the near field, which is important at high frequencies when the focusing range can be quite large. Also, the measurements under actual ocean conditions are usually not measurements of the scattered pressure by itself but rather of the total pressure, i.e., of the sum of scattered and incident pressures, which are not normally in phase. The measurements usually recorded by instruments are either proportional to the square of the amplitude of the local pressure or else measurements of the phase of the pressure. Let us first consider, therefore, the type of results required to estimate the mean square fluctuations of the amplitude and the phase of the total acoustic pressure at a point in the medium. It is appropriate to perform the analysis on the basis of the "smooth" method of approximation rather than the method of "small" perturbations, since the fluctuations can be large. We recall from (IV-16a), (IV-19) and (IV-36) that the incident pressure, the total pressure, and the correction to the complex phase may be expressed as follows:

$$p_o(\underline{x}) = A_o(\underline{x}) e^{iS_o(\underline{x})} \quad (\text{IV-16a})$$

$$p(\underline{x}) = p_o(\underline{x}) e^{i\psi_1} \quad (\text{IV-19})$$

$$\psi_1(\underline{x}) = \frac{2k^2 i}{4\pi} \int_V d\underline{\xi} \frac{e^{ikr}}{r} v(\underline{\xi}) \frac{p_o(\underline{\xi})}{p_o(\underline{x})} = S_1 - iB_1 \quad (\text{IV-36})$$

In the above version of (IV-36), we have defined the quantities  $S_1$  and  $B_1$  as the real and the negative imaginary parts of  $\psi_1$ , respectively. We note here that their physical meaning, according to (IV-22a) and (IV-22b), is that of the fluctuation of the phase and of the logarithmic amplitude, respectively. The phase angle of the total pressure is therefore given by:

$$S(\underline{x}) = \text{Arg}(p(\underline{x})) = S_o(\underline{x}) + S_1(\underline{x}) = S_o(\underline{x}) + \text{Re} \psi_1(\underline{x}) \quad (\text{IV-82})$$

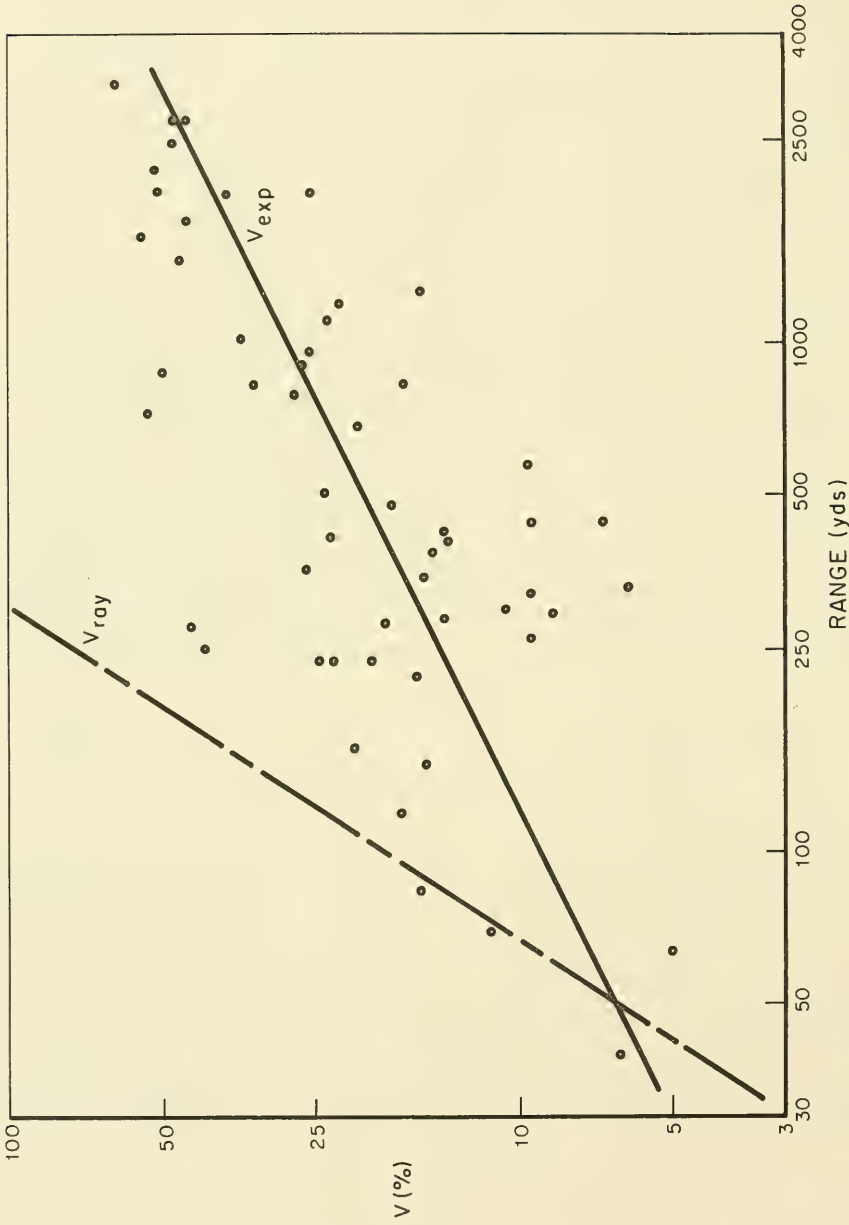


FIGURE IV-12 COEFFICIENT OF VARIATION AS A FUNCTION OF RANGE



It is clear from the above that the expected value of the phase will be just the phase of the incident wave  $S_0$ . The variance of the phase is therefore given by  $\langle S_1^2 \rangle$ , and this is one of the averages which we must calculate.

We are also interested in the variance of the amplitude of the total pressure. The literature is full of erroneous derivations\* of the variance, and we shall therefore take some time to develop an expression which has somewhat wider applicability.

Since (IV-36) shows the fluctuation of the complex phase to be the sum of a large number of independent contributions (independent if we divide the volume  $V$  into a number of sub-volumes each of which are still large compared to a single patch), we would expect, according to the central limit theorem, both the real and the imaginary part of  $\psi_1$  to obey a normal distribution. In fact, we have pretty good evidence (see Figure IV-7) that  $\psi$  itself is already normally distributed, which would even make the invocation of the central limit theorem unnecessary.  $S_1$  and  $B_1$  therefore obey a multivariate normal distribution with a characteristic function which is:

$$\chi_{(\sigma, \beta)} = \langle e^{i\sigma S_1 + i\beta B_1} \rangle = e^{-\frac{1}{2}(\sigma, \beta) \begin{pmatrix} \langle S_1^2 \rangle & \langle S_1 B_1 \rangle \\ \langle S_1 B_1 \rangle & \langle B_1^2 \rangle \end{pmatrix} \begin{pmatrix} \sigma \\ \beta \end{pmatrix}} \quad (\text{IV-83})$$

The computation of any averages involving the total pressure or its amplitude is much facilitated by the use of this characteristic function. We observe that the amplitude of the pressure is given by

$$A(\underline{x}) = |p(\underline{x})| = A_0(\underline{x}) e^{B_1(\underline{x})} \quad (\text{IV-84})$$

Averaging this expression over the ensemble, we obtain:

$$\langle A \rangle = A_0 \langle e^{B_1(\underline{x})} \rangle = A_0 \chi(0, -i) = A_0 e^{\frac{1}{2} \langle B_1^2 \rangle} \quad (\text{IV-85})$$

---

\*The common practice is to regard the total amplitude as very little different from the amplitude of the incident wave, expand the total amplitude to first order in the small quantity, and then square it to obtain the square of the amplitude. Taking the average, the first order term drops out and there remains the second order term. This second order term is incorrect, since it does not include the product of the zeroth and second order terms of the original expression of the total amplitude.

We note that the expected value of the amplitude is now no longer the amplitude of the incident wave but rather a slightly larger number. Note also that the logarithm of the amplitude fluctuation  $B_1$  is normally distributed, so that the amplitude itself, as given by (IV-84), should be expected to have a log normal distribution.

The mean square value of the amplitude can be obtained similarly by averaging the square of (IV-84):

$$\langle A^2 \rangle = A_0^2 \langle e^{2B_1(x)} \rangle = A_0^2 \int_0^\infty (0, -2i) = A_0^2 e^{2\langle B_1^2 \rangle} \quad (\text{IV-86})$$

We therefore obtain for the square of the coefficient of variation of the amplitude the expression:

$$V_a^2 = \frac{\langle |p|^2 \rangle - \langle |p| \rangle^2}{\langle |p| \rangle^2} = e^{\langle B_1^2 \rangle} - 1 \approx \langle B_1^2 \rangle \quad (\text{IV-87})$$

We had earlier computed the coefficient of variation for the entire field  $p$  for the interference range. Using the present scheme, the average of the total field is given by:

$$\langle p \rangle = p_0 \langle e^{iS_1 + B_1} \rangle = p_0 \int_0^\infty (1, -i) = p_0 e^{-\frac{1}{2}(\langle S_1^2 \rangle - \langle B_1^2 \rangle - 2i\langle S_1 B_1 \rangle)} \quad (\text{IV-88})$$

Similarly, the coefficient of variation becomes:

$$V_p^2 = \frac{\langle |p|^2 \rangle - \langle |p| \rangle^2}{\langle |p| \rangle^2} = e^{(\langle B_1^2 \rangle + \langle S_1^2 \rangle)} - 1 \approx \langle B_1^2 \rangle + \langle S_1^2 \rangle \quad (\text{IV-89})$$

As we show later, the mean square fluctuations of  $S_1$  and  $B_1$  become equal in the far field, and this explains, see (IV-88), why the magnitude of the total pressure became equal to the amplitude of the incident wave. It is clear from the above that we should like to evaluate the following averages over the ensemble:

$$\langle B_1^2 \rangle = \langle (\text{Im } \psi_1)^2 \rangle, \quad \langle S_1^2 \rangle = \langle (\text{Re } \psi_1)^2 \rangle, \quad \langle S_1 B_1 \rangle = -\langle \text{Re } \psi_1 \text{ Im } \psi_1 \rangle \quad (\text{IV-90})$$

We could just substitute the real and imaginary parts of  $\psi_1$  as given by (IV-36), but would find that the resulting integrals are very difficult to evaluate. In the high frequency ( $ka \gg 1$ ) case, a general evaluation of the integrals has been performed, and may be found in Chernov (Ref. IV-2, following p.66) where he considers rigorously the problem of a plane wave incident on an inhomogeneous half-space as shown in Figure II-3. The significant approximation to be made in the high frequency case is the result of the high directivity of the scattering from any small scattering volume. The signal received by an observer located at a point  $\underline{x}$  (see Figure IV-13) comes principally from those scatterers which are located in a narrow cone with the observer at its apex. The distance between an element of scattering volume and the observer may therefore be approximated according to:

$$r = \sqrt{(x_1 - \xi_1)^2 + \rho^2} \approx (x_1 - \xi_1) + \frac{1}{2} \frac{\rho^2}{x_1 - \xi_1} + \dots \quad (\text{IV-91})$$

where  $\rho^2 = (x_2 - \xi_2)^2 + (x_3 - \xi_3)^2$

The definition of  $\rho$  may be seen from Figure IV-13. If we substitute this approximation in (IV-36) and take the real and imaginary parts we obtain

$$S_1 = \frac{k^2}{2\pi} \int_0^{x_1} d\xi_1 \int_{-\infty}^{\infty} d\xi_2 \int_{-\infty}^{\infty} d\xi_3 \frac{\sin \left[ k \rho^2 / 2 (x_1 - \xi_1) \right]}{x_1 - \xi_1} \cup (\underline{\xi}) \quad (\text{IV-92a})$$

$$B_1 = \frac{k^2}{2\pi} \int_0^{x_1} d\xi_1 \int_{-\infty}^{\infty} d\xi_2 \int_{-\infty}^{\infty} d\xi_3 \frac{\cos \left[ k \rho^2 / 2 (x_1 - \xi_1) \right]}{x_1 - \xi_1} \cup (\underline{\xi}) \quad (\text{IV-92b})$$

These expressions can be used to obtain the averages given in (IV-90) in a fairly simple form. Since all averages involve taking an average of the product of the index of refraction at two different points, all of these averages will ultimately be in terms of the correlation function describing the inhomogeneity of the medium. The computation of the averages remain a formidable exercise in integration, and may also be found in Chernov. The resulting integrals can be approximated depending on whether the observer distance  $L$  is in the focusing or in the interference range. In other words, the nature of the approximation depends on whether the wave parameter  $D = \frac{4L}{ka^2}$  is much less or much greater than unity. Following Chernov, we

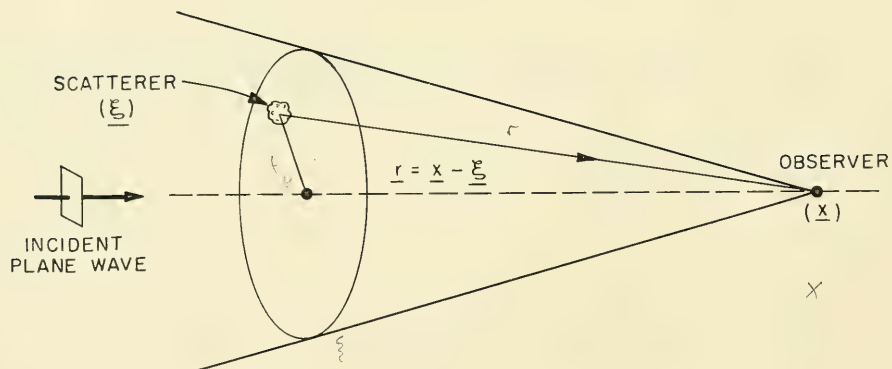


FIGURE IV-13      GEOMETRY FOR HIGH FREQUENCY SCATTERING

obtain the results shown in Table IV-4 for the mean square values of the phase and the amplitude. We note that amplitude and phase fluctuations become equal in the interference range. We also observe that the coefficient of variation of the amplitude in the focusing range behaves as the three-halves power of the range. This is just the result to be expected for ray acoustics and was already hinted at in Chapter II. It is possible in a similar fashion to evaluate the cross correlation between the phase and amplitude fluctuations at a given point,  $\langle B_1 S_1 \rangle$ . It is more interesting, however, to evaluate the cross correlation coefficient between the logarithmic amplitude and the phase:

$$R_{bs} = \frac{\langle B_1 S_1 \rangle}{\sqrt{\langle B_1^2 \rangle \langle S_1^2 \rangle}} \quad (\text{IV-93})$$

Chernov shows that for a Gaussian correlation function this cross correlation coefficient becomes, in the two extreme ranges:

$$R_{bs} \approx 0.6 \quad \text{for } D \ll 1 \quad (\text{focusing range}) \quad (\text{IV-94a})$$

$$R_{bs} \approx \frac{\log D}{D} \quad \text{for } D \ll 1 \quad (\text{interference range}) \quad (\text{IV-94b})$$

TABLE IV-4

THEORETICAL AMPLITUDE AND PHASE FLUCTUATIONS

	$D \gg 1$ (Interference Range)	$D \ll 1$ (Focusing Range)
$\langle S_1^2 \rangle$	$\langle v^2 \rangle k^2 L \int_0^\infty R(r) dr$	$2 \langle v^2 \rangle k^2 L \int_0^\infty R(r) dr$
$\langle B_1^2 \rangle$	$\langle v^2 \rangle k^2 L \int_0^\infty R(r) dr$	$\frac{1}{6} \langle v^2 \rangle L^3 \int_0^\infty \nabla^2 \nabla^2 R(r) dr$

The phase and the amplitude fluctuations at a point are therefore essentially uncorrelated for ranges of propagation long compared to the focusing distance of the inhomogeneities. On the other hand, they are quite strongly correlated inside the focusing range.

We can also calculate the cross correlation of the amplitude or the phase at two distinct points in space. Chernov computes some typical correlation distances (i.e., distances over which the correlation is appreciable) for two receiving points. We must distinguish between two points located relative to each other in the longitudinal direction of wave propagation and two points located transversely, i.e., in a constant phase plane of the incident plane wave. We find that a typical distance of longitudinal correlation is of the order of magnitude of the focusing range, which is approximately  $ka^2$ .

Longitudinal correlation can therefore extend over appreciable distances. In the transverse direction, however, the correlation distance of the single fluctuations is of the same order of magnitude as the correlation of the refractive index, i.e., of the order of magnitude of  $a$ . Figures IV-14 and IV-15 show some transverse correlation functions of the phase and the amplitude computed by Chernov on the basis of a Gaussian correlation function of the index of refraction. These quantitative conclusions about signal correlation appear to be borne out by experimental evidence such as that shown in Figure IV-16 (after Skudrzyk).

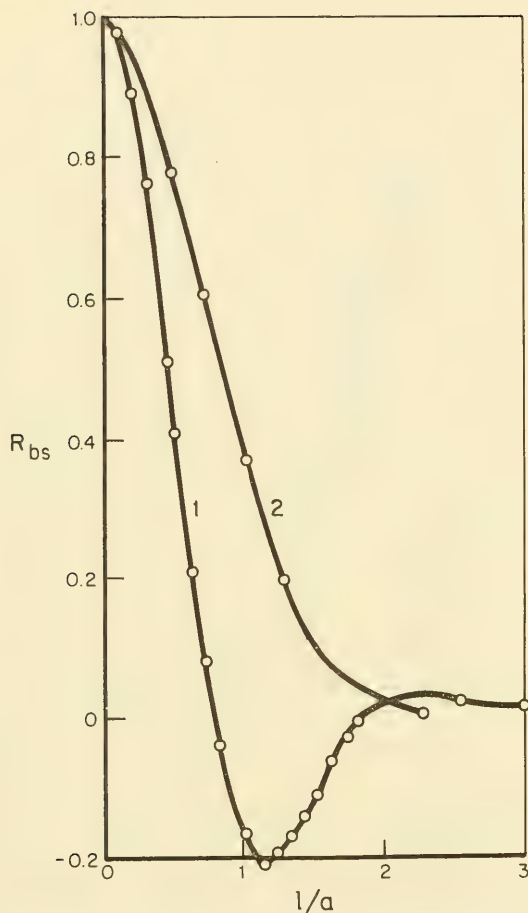


FIGURE IV-14 THE TRANSVERSE AUTOCORRELATION FOR THE CASE OF SMALL  $D$  ( $D \ll 1$ ): 1. The autocorrelation coefficient of the amplitude fluctuations; 2. The autocorrelation coefficient of the phase fluctuations, identical with the autocorrelation coefficient of the refractive index fluctuations. (After Chernov)



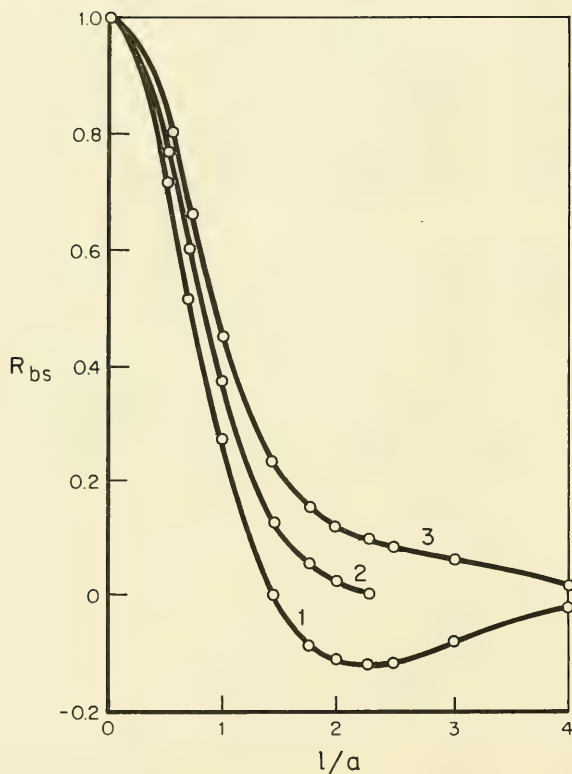


FIGURE IV-15 THE TRANSVERSE AUTOCORRELATION FOR THE CASE OF LARGE  $D$  ( $D = 10$ ): 1. The autocorrelation coefficient of the amplitude fluctuations; 2. The autocorrelation coefficient of the refractive index fluctuations; 3. The autocorrelation of the phase fluctuations. (After Chernov)

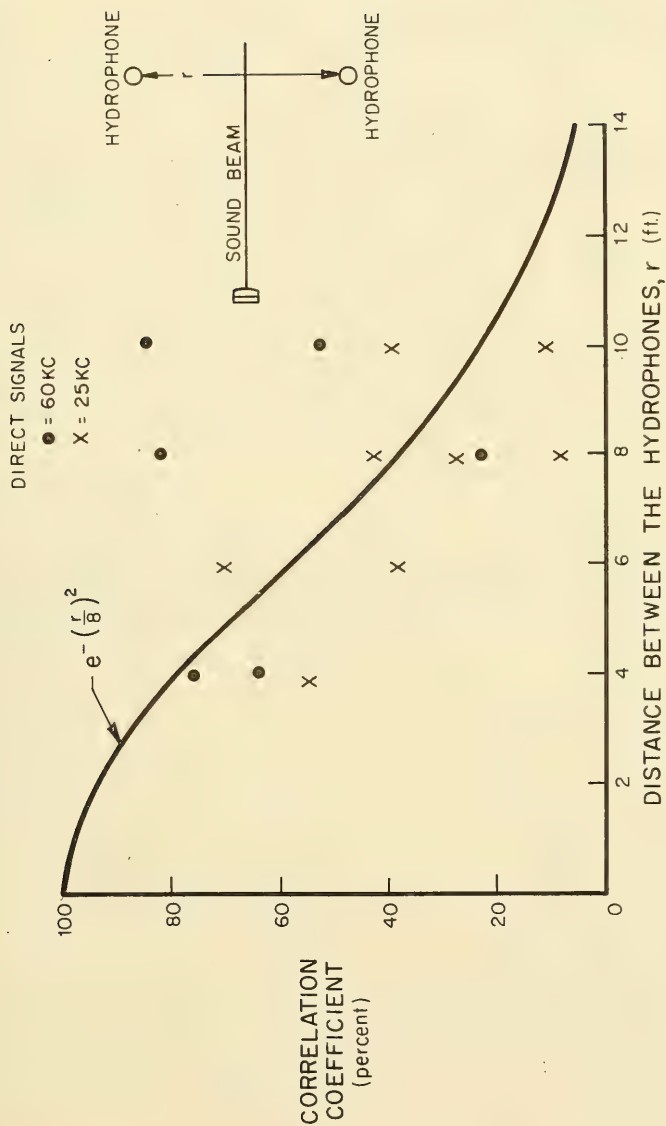


FIGURE IV-16 CORRELATION COEFFICIENT AS A FUNCTION OF THE DISTANCE BETWEEN THE HYDROPHONES



## APPENDIX A

### SOME SOLUTIONS OF THE WAVE EQUATION

We shall summarize here some well known facts about the solutions of the scalar wave equation:

$$\nabla^2 \varphi + k^2 \varphi = 0 \quad (\text{A-1})$$

The time dependence  $e^{-i\omega t}$  is suppressed. If we wish a spherically symmetric solution, (A-1) becomes:

$$\frac{1}{r^2} \frac{\partial}{\partial r} r^2 \frac{\partial}{\partial r} \varphi + k^2 \varphi = 0 \quad (\text{A-2})$$

It is readily seen that both  $\frac{e^{ikr}}{r}$  and  $\frac{e^{-ikr}}{r}$  satisfy (A-2), and if the suppressed time dependence is  $e^{-i\omega t}$ , the outgoing wave is given by:

$$\varphi = \frac{e^{ikr}}{r} \quad (\text{A-3})$$

At the origin, this wave function blows up, and  $\nabla^2 \varphi$  is ill-defined. In fact, we must resort to the definition of the divergence as a limiting ratio of flux to volume to evaluate  $\nabla^2 \varphi$  at the origin. Given any vector function  $\underline{v}(\underline{r})$ , the divergence is usually defined as:

$$\text{div } \underline{v} = \nabla \cdot \underline{v} = \lim_{\tau \rightarrow 0} \frac{1}{\tau} \oint_{\sigma} \underline{v} \cdot \underline{n} \, d\sigma \quad (\text{A-4})$$

where:

$\tau$  = small volume element containing the point at which  $\text{div } \underline{v}$  is to be computed

$\sigma$  = surface enclosing  $\tau$

$\underline{n}$  = local normal to  $\sigma$

Hence, for  $\nabla^2 \varphi$ , we substitute  $\underline{v} = \text{grad } \varphi = \nabla \varphi$  in (A-4) and obtain:

$$\nabla^2 \varphi = \lim_{\tau \rightarrow 0} \frac{1}{\tau} \oint \frac{\partial \varphi}{\partial n} \, d\sigma \quad (\text{A-5})$$

Take  $\tau$  to be a small sphere with radius  $\epsilon$  about the origin. Then the normal derivative is the radial derivative  $\frac{\partial \varphi}{\partial r}$ , and this is constant over the surface of the sphere:

$$\begin{aligned}\nabla^2 \varphi &= \lim_{\epsilon \rightarrow 0} \frac{3}{4\pi\epsilon^3} (4\pi\epsilon^2) \left[ \frac{\partial \varphi}{\partial r} \right]_{r=\epsilon} = \lim_{\epsilon \rightarrow 0} \frac{3}{\epsilon} \frac{e^{ik\epsilon}}{\epsilon^2} (-1 + ik\epsilon) \\ &= \lim_{\epsilon \rightarrow 0} \frac{3e^{ik\epsilon}}{4\pi\epsilon^3} [-4\pi + 4\pi ik\epsilon] \quad (A-6)\end{aligned}$$

Hence  $\nabla^2 \varphi$  blows up at the origin as  $\frac{-4\pi}{\tau}$ , and the limiting volume integral of  $\nabla^2 \varphi$  over a small sphere about the origin will remain finite:

$$\lim_{\tau \rightarrow 0} \int_{\tau} d\tau \nabla^2 \varphi \rightarrow -4\pi \quad (A-7)$$

Note that the volume integral of  $k^2 \varphi$  over  $\tau$  does approach zero, even though  $\varphi$  itself blows up. As a result,  $\varphi$  as given in (A-3) does not satisfy (A-1) at the origin, but satisfies the modified problem:

$$\nabla^2 \varphi + k^2 \varphi = -4\pi \delta(\mathbf{r}) \quad (A-8)$$

where  $\delta(\mathbf{r})$  is zero everywhere, except at the origin where it becomes infinite in such a way that  $\int_{\tau} d\tau \delta(\mathbf{r}) = 1$ . Such a function has the property that  $\int_{\tau} d\tau f(\mathbf{r}) \delta(\mathbf{r}) = f(\mathbf{o})$  for any  $f$ .

If the singularity is at a point  $\mathbf{r}'$  rather than at the origin, a shift of origin will show that:

$$\psi(\underline{\mathbf{r}}, \underline{\mathbf{r}}') = \frac{e^{ik|\underline{\mathbf{r}} - \underline{\mathbf{r}}'|}}{4\pi|\underline{\mathbf{r}} - \underline{\mathbf{r}}'|} \quad (A-9)$$

satisfies:

$$\nabla^2 \psi + k^2 \psi = -\delta(\underline{\mathbf{r}} - \underline{\mathbf{r}}') \quad (A-10)$$

The function given in (A-9) is known as the Green's function and permits solution of both the homogeneous and inhomogeneous wave equations through the use of Green's theorem. We shall, therefore, discuss briefly:

1. Green's theorem
2. the general solution to the homogeneous wave equation
3. the general solution to the inhomogeneous wave equation.

### 1. Green's Theorem

It follows from the definition of the divergence that, for any volume  $V$  bounded by a surface  $S$  with local normal  $\underline{n}$ , the volume integral of the divergence of a vector function  $\underline{v}$  is related to the outward flux by:

$$\int_V \text{div } \underline{v} \, dV = \int_S \underline{v} \cdot \underline{n} \, dS \quad (\text{A-11})$$

Suppose the vector function is given in terms of two arbitrary scalar functions  $\varphi$  and  $\psi$  according to:

$$\underline{v} = \varphi \nabla \psi - \psi \nabla \varphi \quad (\text{A-12})$$

Application of (A-11) then yields:

$$\int_V \nabla \cdot (\varphi \nabla \psi - \psi \nabla \varphi) \, dV = \int_S (\varphi \nabla \psi - \psi \nabla \varphi) \cdot \underline{n} \, dS$$

Both sides may be simplified to yield Green's theorem:

$$\int_V (\varphi \nabla^2 \psi - \psi \nabla^2 \varphi) \, dV = \int_S \left( \varphi \frac{\partial \psi}{\partial n} - \psi \frac{\partial \varphi}{\partial n} \right) \, dS \quad (\text{A-13})$$

## 2. Solution to Homogeneous Wave Equation

Let  $\varphi$  be a solution to the homogeneous scalar wave equation (A-1) everywhere in some volume  $V$ , bounded by a surface  $S$ . Let  $\psi$  be the solution (A-9) of the inhomogeneous equation (A-10). In summary:

$$\begin{aligned}\nabla^2 \varphi + k^2 \varphi &= 0 \\ \nabla^2 \psi + k^2 \psi &= -\delta(\underline{r} - \underline{r}') \text{ where } \psi = \frac{e^{ik|\underline{r} - \underline{r}'|}}{4\pi|\underline{r} - \underline{r}'|}\end{aligned}$$

Multiply the first of these equations by  $\psi$ , the second by  $\varphi$ , and subtract:

$$\psi \nabla^2 \varphi - \varphi \nabla^2 \psi = \varphi \delta(\underline{r} - \underline{r}')$$

Integrate both sides over the volume  $V$ . The left side can be changed to a surface integral by Green's theorem. The right side simply selects  $\varphi$  at the point  $\underline{r}'$ , so we obtain:

$$\varphi(\underline{r}') = \int_S \left[ \psi(\underline{r}, \underline{r}') \frac{\partial \varphi(\underline{r})}{\partial n} - \varphi(\underline{r}) \frac{\partial \psi(\underline{r}, \underline{r}')}{\partial n} \right] dS \quad (\text{A-14})$$

This is the Helmholtz formula, which gives the value of the wave function inside a closed surface in terms of a distribution of simple and dipole sources on the surface.

## 3. Solution to the Inhomogeneous Wave Equation

If  $\varphi$  is a solution of the inhomogeneous scalar wave equation

$$\nabla^2 \varphi + k^2 \varphi = f(\underline{r}) \quad (\text{A-15})$$

we can again use the same Green's function  $\psi(\underline{r}, \underline{r}')$  which satisfies

$$\nabla^2 \psi + k^2 \psi = \delta(\underline{r} - \underline{r}') \quad (\text{A-9})$$

to obtain a solution. Again we multiply (A-15) by  $\psi$ , (A-9) by  $\varphi$ , subtract, integrate over a volume  $V$ , and apply Green's theorem. This yields:

$$\varphi(\underline{r}') = \int_S \left[ \psi(\underline{r}, \underline{r}') \frac{\partial \varphi(\underline{r})}{\partial n} - \varphi(\underline{r}) \frac{\partial \psi(\underline{r}, \underline{r}')}{\partial n} \right] dS - \int dV f(\underline{r}) \psi(\underline{r}, \underline{r}') \quad (\text{A-16})$$

Thus we see that  $\varphi$  consists of a solution to the homogeneous wave equation plus a particular solution to the inhomogeneous equation. This particular solution has the form of a volume distribution of simple sources.



## APPENDIX B

### THE MULTIPLE SCATTERING OF WAVES

The following development, due to Foldy\*, deals with scattering of an incident wave by a random distribution of scatterers. The treatment is in terms of general wave theory. The scatterers may be arbitrary in number and character, except that the scattered wave is assumed to be spherical and with an amplitude proportional to that of the wave exciting the scatterer. The constant of proportionality is assumed to be specified completely by the frequency and a single parameter of the scatterer, denoted by  $s$ .

If we have a collection of  $N$  scatterers and are given for each its position,  $\underline{r}_1, \dots, \underline{r}_N$ , and its scattering properties as specified by  $s_1, \dots, s_N$ , then we shall say that we have a particular configuration of the scatterers. The ensemble of configurations in which we are interested may be described by a probability distribution function  $P(\underline{r}_1, \dots, \underline{r}_N, s_1, \dots, s_N)$  so that  $P(\underline{r}_1, \dots, \underline{r}_N, s_1, \dots, s_N) d\underline{r}_1 \dots d\underline{r}_N ds_1 \dots ds_N$  represents the probability of finding the scatterers in a configuration in which the first scatterer lies in an element of volume  $d\underline{r}_1$  about the point  $\underline{r}_1$  and has a scattering parameter lying between  $s_1$  and  $s_1 + ds_1$ , and so on for the other scatterers. The average of a physical quantity over the ensemble of configurations is called a configurational average. Thus, for a function  $f(\underline{r}_1, \dots, \underline{r}_N, s_1, \dots, s_N)$ , the configurational average is

$$\langle f \rangle = \int_V \int_V \dots \int_V f(\underline{r}_1, \dots, \underline{r}_N, s_1, \dots, s_N) P(\underline{r}_1, \dots, \underline{r}_N, s_1, \dots, s_N) d\underline{r}_1 \dots d\underline{r}_N ds_1 \dots ds_N \quad (\text{B-1})$$

Subscripts will be used to indicate when the integration over one or more of the scatterers is to be omitted; thus  $\langle f \rangle_j$  indicates that the integration over  $\underline{r}_j$  and  $s_j$  is to be omitted. In the following we will also assume that the scatterers in an ensemble are independent of each other with respect to position and scattering parameter. In this case,  $P$  can be written as  $(1/N)^N n(\underline{r}_1, s_1) n(\underline{r}_2, s_2) \dots n(\underline{r}_N, s_N)$ , where  $n(\underline{r}, s) ds$  is the average number of scatterers per unit volume in the neighborhood of the point  $\underline{r}$  having scattering parameters lying between  $s$  and  $s + ds$ .

We will then consider the steady state scattering of waves of a single frequency  $\omega$ , so that the value of the scalar wave function at the point  $\underline{r}$  and time  $t$  can be represented as  $p(\underline{r})e^{-i\omega t}$ . In the absence of scatterers,  $p(\underline{r})$  will satisfy the wave equation  $\nabla^2 p + k_0^2 p = 0$ , where  $k_0 = (\omega/c_0)$  and  $c_0$  is the wave velocity in the scatterer-free medium. The scatterers are assumed to behave as point scatterers, scattering spherically symmetrical waves; thus in the neighborhood of the  $j$ -th scatterer the wave function will behave like  $B_j E(\underline{r}, \underline{r}_j)$ , where

---

\*L. L. Foldy (Ref. III-8).

$$E(\underline{r}, \underline{r}_j) = \frac{e^{+ik_0 |\underline{r} - \underline{r}_j|}}{|\underline{r} - \underline{r}_j|} \quad (B-2)$$

and  $B_j$  is a complex number. The external field acting on the  $j$ -th scatterer is defined as

$$p^j(\underline{r}) = p(\underline{r}) - B_j E(\underline{r}, \underline{r}_j) \quad (B-3)$$

The scattering properties of the scatterers are furthermore assumed to be characterized by the relationship  $B_j = g(s_j, \omega) p^j(\underline{r}_j)$ , making the strength of the scattered wave proportional to the external field acting on it. The value  $g(s_j, \omega)$  will be referred to as the scattering coefficient for the  $j$ -th scatterer and will be abbreviated to  $g_j$ . All the models for pulsating air bubbles suspended in water satisfy this condition. For the adopted model (Model III)

$$B = \frac{p_{inc}^a}{\left(\frac{\omega_0}{\omega}\right)^2 - 1 - i \delta(a, \omega)}$$

where  $\omega_0$  and  $\delta(a, \omega)$  are functions only of the bubble radius  $a$ , the frequency of the incident sound  $\omega$ , and various parameters of the gas in the bubble and the surrounding medium. Then the bubble radius is the scattering parameter and

$$g(a) = \frac{a}{\left(\frac{\omega_0}{\omega}\right)^2 - 1 - i \delta(a, \omega)}$$

The basic problem is then the following: Given the function  $g(s, \omega)$ , the distribution function  $n(\underline{r}, s)$  for the scatters and the wave function  $p_o(\underline{r})$  which is present in the medium in the absence of the scatterers, find  $\langle p(\underline{r}) \rangle$ , the configurational average of  $p(\underline{r})$ , in the presence of scatterers.

Consider a particular configuration of scatterers. Then

$$p(\underline{r}) = p_o(\underline{r}) + \sum_j B_j E(\underline{r}, \underline{r}_j) \quad , \quad p^j(\underline{r}) = p_o(\underline{r}) + \sum_{j'(\neq j)} B_{j'} E(\underline{r}, \underline{r}_{j'}) \quad (B-4)$$

represent the total field and the incident field on the  $j$ -th scatterer. Substituting the relationship  $B_j = g_j p^j(\underline{r}_j)$  in the above gives

$$p(\underline{r}) = p_o(\underline{r}) + \sum_j g_j p^j(\underline{r}_j) E(\underline{r}, \underline{r}_j) \quad (B-5)$$

$$p(\underline{r}_j) = p_o(\underline{r}_j) + \sum_{j'(\neq j)} g_{j'} p^{j'}(\underline{r}_{j'}) E(\underline{r}_j, \underline{r}_{j'}) \quad (\text{B-6})$$

These represent the fundamental equations of multiple scattering. The direct method would then consist of solving the set of simultaneous linear equations (B-6) for the  $p^j(\underline{r}_j)$  and substituting these in (B-5), thus giving  $p(\underline{r})$  as a function of the positions and scattering parameters of the scatterers. Then taking the configurational average of this quantity would give the desired results. Unfortunately, it is not possible to carry this procedure through because of the complexity of the integration. The alternative method used by Foldy involves finding equations satisfied by  $\langle p(\underline{r}) \rangle$  and then solving these equations for the desired averaged quantities.

Taking the configurational average of both sides of (B-5), we have

$$\begin{aligned} \langle p(\underline{r}) \rangle &= \langle p(\underline{r}) \rangle = \sum_j \iint_V g_j \langle p^j(\underline{r}_j) \rangle_j E(\underline{r}, \underline{r}_j) \frac{n(\underline{r}_j, s_j)}{N} ds_j d\mathbf{r}_j \quad (\text{B-7}) \\ &= p_o(\underline{r}) + \int_V G(\underline{r}) \langle p^j(\underline{r}_j) \rangle_j E(\underline{r}, \underline{r}_j) d\mathbf{r}_j \end{aligned}$$

where

$$G(\underline{r}) = \int_V g(s, \omega) n(\underline{r}, s) ds \quad (\text{B-8})$$

The quantity  $\langle p^j(\underline{r}_j) \rangle_j$  represents the external field acting on the  $j$ -th scatterer averaged over all possible configurations of all the other scatterers. The only rigorous way of evaluating it seems to be to solve the set of equations (B-6); substituting these in (B-7) and carrying out the necessary integrations would then give  $\langle p(\underline{r}) \rangle$ . As stated before, this does not appear to be feasible. Thus, we resort to approximating  $\langle p^j(\underline{r}_j) \rangle_j$  by the average field which would exist at  $\underline{r}_j$  if the  $j$ -th scatterer were not present. This last quantity differs from  $\langle p(\underline{r}_j) \rangle$  only by a term of order  $1/N$ . Thus, if  $N$  is large, we may substitute  $\langle p(\underline{r}_j) \rangle$  for  $\langle p^j(\underline{r}_j) \rangle_j$  in (B-7), obtaining the integral equation

$$\langle p(\underline{r}) \rangle \approx p_o(\underline{r}) + \int_V G(\underline{r}') \langle p(\underline{r}') \rangle E(\underline{r}, \underline{r}') d\mathbf{r}' \quad (\text{B-9})$$

Consider now the operator  $\nabla^2 + k_0^2$  and note that  $(\nabla^2 + k_0^2) E(\underline{r}, \underline{r}') = 4 \pi \delta(\underline{r} - \underline{r}')$ . Applying this operator to both sides of (B-9) gives

$$\nabla^2 \langle p(\underline{r}) \rangle + k_0^2 \langle p(\underline{r}) \rangle = -4 \pi G(\underline{r}) \langle p(\underline{r}) \rangle \quad (\text{B-10})$$

With  $k^2(\underline{r}) = k_0^2 + 4 \pi G(\underline{r})$ , we see that  $\nabla^2 \langle p(\underline{r}) \rangle + k^2(\underline{r}) \langle p(\underline{r}) \rangle = 0$ , and so  $\langle p(\underline{r}) \rangle$  satisfies the wave equation in a "continuous medium" in which the velocity of propagation depends upon the scattering coefficients and density of the scatterers and is, in general, a function of position. This is an important result, which gives the same characterization for propagation as obtained by considering the complex compressibility of a bubbly medium.

The problem of finding  $\langle p(\underline{r}) \rangle$  has thus been transformed to solving a boundary value problem for the wave equation, where the boundary conditions depend on  $G(\underline{r})$ . If  $G(\underline{r})$  is everywhere continuous and approaches a constant value or zero at infinity, then the boundary conditions are that  $\langle p(\underline{r}) \rangle - p_0(\underline{r})$  be everywhere continuous, have a continuous gradient, and at infinity, represent outward traveling waves. It should be noted that, in principle, it is possible to solve the integral equation (B-9) directly by using the Liouville-Neumann method of successive approximation. Repeatedly substituting for  $\langle p(\underline{r}) \rangle$  we have

$$\langle p(\underline{r}) \rangle = p_0(\underline{r}) + \sum_{m=1} p_m(\underline{r}), \text{ where } p_m(\underline{r}) = \int_V g(\underline{r}') p_{m-1}(\underline{r}') E(\underline{r}, \underline{r}') d\underline{r}' \quad (\text{B-11})$$

This also gives the desired solution, if the series converges uniformly.

In order to interpret these results, it is useful to consider the case of a single scatterer (the following discussion does not rely on any approximations). In this case the wave function becomes

$$p(\underline{r}) = p_0(\underline{r}) + g_1 p_0(\underline{r}_1) E(\underline{r}, \underline{r}_1) \quad (\text{B-12})$$

which is the sum of the incident wave and the spherical scattered wave. Consider a plane incident wave

$$p_0(\underline{r}) = A e^{i \underline{k}_0 \cdot \underline{r}} \quad (\text{B-13})$$

Then

$$p_{sc}(\underline{r}) = g_1 p_0(\underline{r}_1) E(\underline{r}, \underline{r}_1) \quad (\text{B-14})$$

represents the scattered wave.

Integrating its flux,  $p_{sc}^* \nabla p_{sc} - p_{sc} \nabla p_{sc}^*$  over a sphere of area  $A$  centered about  $\underline{r}_1$ , we find that the total flux is

$$4\pi i k_0 |g_1|^2 A^2 \quad (B-15)$$

Dividing this by  $i k_0 A^2$ , the flux per unit area normal to  $\underline{k}_0$  in the incident wave, we obtain the scattering cross section

$$\sigma_{sc} = 4\pi |g_1|^2. \quad (B-16)$$

Integrating the flux per unit area caused by both incident and scattered waves over the same sphere, gives

$$4\pi i k_0 |g_1|^2 A^2 + 4\pi (g_1 - g_1^*) A^2 \quad (B-17)$$

The negative of this quantity represents the net inward flux. Dividing this by the incident flux per unit area gives the absorption cross section

$$\sigma_{ab} = -4\pi |g_1|^2 - \frac{4\pi \text{Im}(g_1)}{k_0} \quad (B-18)$$

Expressed in terms of the cross section, the scattering coefficient  $g_1$  is

$$g_1 = \left( \frac{\sigma}{4\pi} - \frac{k_0^2 \sigma_e}{16\pi^2} \right)^{1/2} - \frac{i k_0 \sigma_{ex}}{4\pi} \quad (B-19)$$

where  $\sigma_{ex} = \sigma_{ab} + \sigma_{sc}$  is the extinction cross section. The scattering cross section per unit volume,  $S_{sc}(\underline{r})$ , is given by

$$S_{sc}(\underline{r}) = \int \sigma_{sc}(s) n(\underline{r}, s) ds = 4\pi \int |g(s)|^2 n(\underline{r}, s) ds. \quad (B-20)$$

Similarly the extinction cross section per unit volume is

$$S_{ex}(\underline{r}) = \int \sigma_{ex}(s) n(\underline{r}, s) ds = -\frac{4\pi}{k_0} \int \text{Im} [g(s)] n(\underline{r}, s) ds = -\frac{4\pi}{k_0} \text{Im} G(\underline{r}). \quad (B-21)$$



## APPENDIX C

### NOTATION

The Cartesian coordinate system is usually designated by  $(x_1, x_2, x_3)$ , and the resulting position vector  $\underline{x}$  has length  $x$ . Occasionally, especially if one coordinate direction has particular significance, we use the coordinates  $(x, y, z)$ , designate the position vector by  $\underline{r}$  and its length by  $r$ . Differentiation with respect to a spatial coordinate is designated either by comma (tensor notation) or by explicit differentiation signs, e.g.:

$$\frac{\partial p}{\partial x} = \frac{\partial p}{\partial x_3} = p_{,3}$$

Repeated subscripts should be summed over, in the usual tensor notation fashion. If  $\underline{u} = (u_1, u_2, u_3) = (u_x, u_y, u_z)$  is the velocity field, its divergence is given by:

$$\text{div } \underline{u} = \nabla \cdot \underline{u} = u_{i,i} = u_{1,1} + u_{2,2} + u_{3,3} = \frac{\partial u_x}{\partial x} + \frac{\partial u_y}{\partial y} + \frac{\partial u_z}{\partial z}$$

When there can be no confusion, differentiation with respect to time is occasionally indicated as a subscript  $t$ :

$$\frac{\partial p}{\partial t} = p_{,t} = p_t$$

The same might be done for differentiation with respect to  $x$ ,  $y$  or  $z$ , e.g., the one-dimensional wave equation:

$$\frac{\partial^2 p}{\partial x^2} = \frac{1}{c_o^2} \frac{\partial^2 p}{\partial t^2} \text{ becomes } p_{xx} = \frac{1}{c_o^2} p_{tt}$$





# BIBLIOGRAPHY

## CHAPTER III: SCATTERING BY STRONG INHOMOGENEITIES

- III-1      Albers, Vernon M., Underwater Acoustics Handbook (Penn. State Univ. Press, 1960).
- III-2      Anderson, V. C., Sound Scattering From a Fluid Sphere, J. Acoust. Soc. Am., v. 22 (1950) no. 4, pp 426-431.
- III-3      Carstensen, E. L. and Foldy, L. L., Propagation of Sound Through a Liquid Containing Bubbles, J. Acoust. Soc. Am., v. 19 (1947) no. 3, pp 481-501.
- III-4      Devin, C., Jr., Survey of Thermal, Radiation and Viscous Damping of Pulsating Air Bubbles in Water, J. Acoust. Soc. Am., v. 31 (1959) no. 12, pp 1654-1667.
- III-5      Eckart, C., The Scattering of Sound From the Sea Surface, J. Acoust. Soc. Am., v. 25 (1953) no. 3, pp 566-570.
- III-6      Exner, M. L., Messung der Dämpfung Pulsierender Luftblasen in Wasser, Acustica, v. 1 (1951), pp 25-33.
- III-7      Exner, M. L. and Hampe, W., Experimental Determination of the Damping of Pulsating Air Bubbles in Water, Acustica, v. 3 (1953), pp 67-72.
- III-8      Foldy, L. L., The Multiple Scattering of Waves, Phys. Rev., v. 67 (1945) no. 3, 4, pp 107-119.
- III-9      Fox, F. E., Curley, S. R. and Larson, G. S., Phase Velocity and Absorption Measurements in Water Containing Air Bubbles, J. Acoust. Soc. Am., v. 27 (1955) no. 3, pp 534-539.
- III-10     Glotov, V. P., Kolobaev, P. A. and Neuimin, G. G., Investigation of the Scattering of Sound by Bubbles Generated by an Artificial Wind in Sea Water and the Statistical Distribution of Bubble Sizes, Soviet Physics - Acoustics, v. 7 (1962) no. 4, pp 341-345.
- III-11     Grasyuk, D. S., Scattering of Sound Waves on the Uneven Surface of an Elastic Body, Soviet Physics - Acoustics, v. 6 (1960) no. 1, pp 30-33.

- III-12 Gulin, E. P., Amplitude and Phase Fluctuations of a Sound Wave Reflected from a Statistically Uneven Surface, Soviet Physics - Acoustics, v. 8, no. 2, pp 135-140.
- III-13 Heaps, H. S., Nonspecular Reflection of Sound from a Sinusoidal Surface, Journal of the Acoustical Society of America, v. 27 (1955) no. 4, pp 698-705.
- III-14 Heaps, H. S., Reflection of Plane Waves of Sound from a Sinusoidal Surface, Journal of Applied Physics, v. 28 (1957) no. 7, pp 815-818.
- III-15 Hill, M. N. (gen. ed.), The Sea (ch. 13, Sound Scattering by Marine Organisms, by Hersey, J. B. and Backus, R. H.), Interscience Publishers, 1962.
- III-16 Hsieh, D. Y. and Plesset, M. S., On the Propagation of Sound in a Liquid Containing Gas Bubbles, The Physics of Fluids, v. 4 (1961) no. 8, pp 970-975.
- III-17 Isakovich, M. A., The Scattering and Radiation of Waves by Statistically Inhomogeneous and Statistically Oscillating Surfaces, Soviet Physics - Acoustics, v. 2 (1956) no. 2, pp 149-153.
- III-18 La Casce, E. O., Jr., Tamarkin, P., Underwater Sound Reflection from a Corrugated Surface, Journal of Applied Physics, v. 27 (1956) no. 2, pp 138-148.
- III-19 Laird, D. T. and Kendig, P. M., Attenuation of Sound in Water Containing Air Bubbles, J. Acoust. Soc. Am., v. 24 (1952) no. 1, pp 29-32.
- III-20 Lauer, H., Über die Thermische Dämpfung von Blasen Verschiedener Gase in Wasser, Acustica, v. 1 (1959), pp 12-24.
- III-21 Leporskii, A. N., Experimental Investigation of Diffraction of Acoustic Waves by Periodic Structures, Soviet Physics - Acoustics, v. 1 (1955) no. 1, pp 50-59.
- III-21a Leporskii, A. N., Scattering of Sound Waves by Sinusoidal and Saw-Tooth Surfaces, Soviet Physics - Acoustics, v. 2 (1956) no. 2, pp 185-189.
- III-22 Lysanov, Iu. P., On the Scattering of Sound by a Nonuniform Surface, Soviet Physics - Acoustics, v. 4 (1958) no. 1, pp 45-49.

- III-23      Lysanov, Iu. P., One Approximate Solution for the Problem of the Scattering of Acoustic Waves by an Uneven Surface, Soviet Physics - Acoustics, v. 2 (1956) no. 2, pp 190-197.
- III-24      Lysanov, Iu. P., Theory of the Scattering of Waves at Periodically Uneven Surfaces, Soviet Physics - Acoustics, v. 4 (1958) no. 1, pp 1-10.
- III-25      Machlup, S., A Theoretical Model for Sound Scattering by Marine Crustaceans, J. Acoust. Soc. Am., v. 24 (1952) no. 3, pp 290-293.
- III-26      MacPherson, J. D., The Effect of Gas Bubbles on Sound Propagation in Water, Proc. Physical Society (British), v. 70 (1957) Part 1, pp 85-92
- III-27      Marsh, H. W., Exact Solution of Wave Scattering by Irregular Surface, J. Acoust. Soc. Am., v. 33 (1961) no. 3, pp 330-333.
- III-27a      Marsh, H. W., Schulkin, M., Kneale, S. G., Scattering of Underwater Sound by the Sea Surface, J. Acoust. Soc. Am., v. 33 (1961) no. 3, pp 334-340.
- III-27b      Marsh, H. W. and Schulkin, Scattering of Underwater Sound by the Sea Surface, Journal of Underwater Acoustics, v. 11 (1961) no. 1, pp 111-114. (Confidential)
- III-28      Meecham, W. C., Variational Method for the Calculation of the Distribution of Energy from a Periodic Surface I, Journal of Applied Physics, v. 27 (1956) no. 4, pp 361-367.
- III-29      Meyer, E. and Skudrzyk, E., Über die Akustischen Eigenschaften von Gasblasenschleiern in Wasser, Akust. Beih., v. 3 (1953), pp 434-440.
- III-30      Meyer, E. and Tamm, K., Eigenschwingung und Dämpfung von Gasblasen in Flüssigkeiten, Akustische Zeitschrift, v. 3 (1939), pp 145-152.
- III-31      Miles, J. W., On Nonspecular Reflection at a Rough Surface, J. Acoust. Soc. Am., v. 26 (1954) no. 2, pp 191-199.
- III-32      Mintzer, David, Discussion of the Paper by C. Eckart on Sea Surface Scattering, J. Acoust. Soc. Am., v. 25 (1953) no. 5, p 1015.
- III-33      Parker, J. G., Reflection of Plane Sound Waves from an Irregular Surface, J. Acoust. Soc. Am., v. 28 (1956) no. 4, pp 672-680.

- III-34 Parker, J. G., Reflection of Plane Sound Waves from a Sinusoidal Surface, J. Acoust. Soc. Am., v. 29 (1957) no. 3, pp 377-380.
- III-35 Physics of Sound in the Sea (Div. 6, v. 8, NDRC Summary Technical Reports), Part IV, "Acoustic Properties of Wakes," Research Analysis Group, Committee on Undersea Warfare, National Research Council.
- III-36 Plesset, M. S. and Hsieh, D. Y., Theory of Gas Bubble Dynamics in Oscillating Pressure Fields, The Physics of Fluids, v. 3 (1960) no. 6, pp 882-892.
- III-37 Silberman, E., Sound Velocity and Attenuation in Bubbly Mixtures Measured in Standing Wave Tubes, J. Acoust. Soc. Am., v. 29 (1957) no. 8, pp 925-933.
- III-38 Spitzer, L., Jr., Acoustic Properties of Gas Bubbles in a Liquid, NDRC Report No. 6.1-Sr 20-918, July 15, 1943.
- III-39 Univ. Calif. Div. War Research, Volume Reverberation: Scattering and Attenuation vs. Frequency, Rept. U50, pp 1-13 (1943); Stratification of Sound Scatterers in the Ocean, Rept. M397, pp 1-13 (1946); Forward Scattering From the Deep Scattering Layer, Rept. M445, pp 1-10 (1946).
- III-40 Urlick, R. J. and Pryce, A. W., A Summary of Underwater Acoustic Data, Part IV, Reverberation, Office of Naval Research, February 1954. (Confidential)
- III-40a Reverberation, An addendum to Part IV of the Summary of Underwater Acoustic Data. U. S. Navy Journal of Underwater Acoustics, v. 10 (1960) no. 1, pp 23-33. (Confidential)
- III-41 Urlick, R. J. and Pryce, A. W., A Summary of Underwater Acoustic Data, Part II, Target Strength, ONR.
- III-41a Target Strength, An addendum to Part II of the Summary of Underwater Acoustic Data. U. S. Navy Journal of Underwater Acoustics, v. 10 (1960) no. 1, pp 63-74. (Confidential)
- III-42 Urusovskii, I. A., Sound Scattering by a Sinusoidally Uneven Surface Characterized by Normal Acoustic Conductivity, Soviet Physics - Acoustics, v. 5 (1960) no. 3, pp 362-369.

## BIBLIOGRAPHY

### CHAPTER IV: SCATTERING FROM WEAK INHOMOGENEITIES

- IV-1      Bergmann, P. G., Propagation of Radiation in a Medium with Random Inhomogeneities, Phys. Rev., v. 70 (1946) no. 7/8, pp 486-492.
- IV-2      Chernov, L. A., Wave Propagation in a Random Medium, McGraw-Hill, 1960.
- IV-3      Liebermann, L. J., The Effect of Temperature Inhomogeneities in the Ocean on the Propagation of Sound, J. Acoust. Soc. Am., v. 23 (1951) no. 9, pp 563-570.
- IV-4      Arthur D. Little, Inc., Project Trident, "Analytical Background of Computational Methods for Underwater Sound Propagation," Technical Report 1230662, Bureau of Ships, NObsr-81564, 1962.
- IV-5      Mintzer, D., Wave Propagation in a Randomly Inhomogeneous Medium, I, J. Acoust. Soc. Am., v. 25 (1953) no. 5, pp 921-927.  
Mintzer, D., Wave Propagation in a Randomly Inhomogeneous Medium, II, J. Acoust. Soc. Am., v. 25 (1953) no. 6, pp 1107-1112.  
Mintzer, D., Wave Propagation in a Randomly Inhomogeneous Medium, III, J. Acoust. Soc. Am., v. 26 (1954) no. 2, pp 186-190.
- IV-6      Potter, D. S. and Murphy, S. R. On Wave Propagation in a Random Inhomogeneous Medium, J. Acoust. Soc. Am., v. 29 (1957) no. 2, pp 197-198.
- IV-7      Sheehy, M. J., Transmission of 24kc Underwater Sound From a Deep Source, J. Acoust. Soc. Am., v. 22 (1950) no. 1, pp 24-29.
- IV-8      Skudrzyk, E. J., "The Scattering of Sound in an Inhomogeneous Medium," ORL report NOrd 16597-63, 1960. Also as "Thermal Microstructure in the Sea and Its Contributions to Sound Level Fluctuations" in Underwater Acoustics ed. V. M. Albers, Plenum Press, N. Y., 1963.
- IV-9      Tatarski, V. I., Wave Propagation in a Turbulent Medium, McGraw-Hill, 1961.
- IV-10     Urlick, R. J. and Searfoss, C. W., "The Microthermal Structure of the Ocean Near Key West, Florida," Part I, Naval Research Laboratory Report No. S-3392, 1948 - Part II, Naval Research Laboratory Report No. S-3444, 1949.





PROJECT TRIDENT TECHNICAL REPORTSReport No.

1011260	COLOSSUS I, December, 1960 (C)
1021260	THEORETICAL INVESTIGATION OF CROSS-FIX PROBLEMS AND CORRELATION EFFECTS, December, 1960 (C)
1031260	THE SUBMARINE AS A SURVEILLANCE PLATFORM, December, 1960 (S)
1041260	Title Classified, December, 1960 (S)
1051260	AIRBORNE JEZEABEL, December, 1960 (S)
1061260	SURFACE-SHIP SONARS IN OCEAN-AREA SURVEILLANCE, December, 1960 (S)
1071260	Title Classified, December, 1960 (S)
1080361	LOW-POWER ENERGY SOURCES, March, 1961 (C)
1090561	SOLUS, May, 1961 (C)
1100561	NONACOUSTIC METHODS FOR SUBMARINE DETECTION, May, 1961 (S)
1110561	ARTEMIS, May, 1961 (S)
1120561	COLOSSUS II, May, 1961 (S)
1130961	RELIABILITY OF UNATTENDED ELECTRONICS EQUIPMENT, September, 1961 (U)
1141061	NUTMEG, October, 1961 (S)
1150162	DEEP JULIE, January, 1962 (S)
1160262	METHODS FOR ANALYZING THE PERFORMANCE OF DIS- TRIBUTED FIELDS OF DETECTORS, February, 1962 (C)
1170262	MAGNETIC ANOMALY DETECTORS IN FIXED SHALLOW WATER BARRIERS, February, 1962 (S)

Report No.

1180262	ELECTRICAL CONDUCTIVITY, COMPRESSIBILITY, AND VISCOSITY OF AQUEOUS ELECTROLYTIC SOLUTIONS, February, 1962 (U)
1190462	A FEASIBILITY STUDY OF THE PASSIVE DETECTION OF QUIET SUBMARINES, April, 1962 (S)
1200562	Title Classified, May, 1962 (S)
1210562	RADIATED NOISE CHARACTERISTICS OF DIESEL-ELECTRIC SUBMARINES, May, 1962 (S)
1220562	DIRECTIVE RECEIVING ARRAYS, May, 1962 (C)
1230662	ANALYTICAL BACKGROUNDS OF COMPUTATIONAL METHODS FOR UNDERWATER SOUND PROPAGATION, June, 1962 (U)
1240762	MARINE CORROSION AND FOULING, July, 1962 (U)
1250862	SURVEY ON AMBIENT SEA NOISE, August, 1962 (C)
1260862	DEEP SUBMERSIBLE WORK VEHICLES, August, 1962 (C)
1270862	THE EFFECT OF PRESSURE ON THE ELECTRICAL CONDUCTIVITY OF SEA WATER, August, 1962 (U)
1281262	ENGINEERING PROPERTIES OF MARINE SEDIMENTS, December, 1962 (U)
1291262	AN INTRODUCTION TO MODULATION, CODING, INFORMATION THEORY, AND DETECTION, December, 1962 (U)
1300363	SPHERICAL DIRECTIVE ARRAYS: A PRELIMINARY STUDY, March, 1963 (U)
1310363	ESTIMATES OF SUBMARINE TARGET STRENGTH, March, 1963 (C)
1320363	PHYSICAL CHEMISTRY IN THE OCEAN DEPTHS: THE EFFECT OF PRESSURE ON IONIC TRANSPORT PROCESSES AND EQUILIBRIA, March, 1963 (U)

Report No.

1330563	SUBMARINE CABLES AND REPEATERS, May, 1963 (C)
1340663	APPLICATION OF ADAPTIVE SAMPLING STRATEGIES TO THE PLANNING OF SURVEYS, June, 1963 (U)
1350663	CURRENT OPTICAL DATA PROCESSING TECHNIQUES IN ASW SYSTEMS, June, 1963 (S)
1370863	STRESS ANALYSIS OF SHIP - SUSPENDED HEAVILY LOADED CABLES FOR DEEP UNDERWATER EMPLACEMENTS, August, 1963 (U)



DISTRIBUTION LISTNo. of Copies

10	Bureau of Ships, Code 370 Department of the Navy Washington 25, D. C.
10	Chief of Naval Operations (OP-71) Department of the Navy Washington 25, D. C.
4	Commanding Officer and Director U. S. Navy Underwater Sound Laboratory Fort Trumbull, New London, Conn. ATTN: Mr. H. E. Nash
2	Office of Naval Research, Code 400X Department of the Navy Washington 25, D. C.
2	Director U. S. Naval Research Laboratory Washington 25, D. C. ATTN: Dr. H. Saxton
2	Chief, Bureau of Naval Weapons Department of the Navy Washington 25, D. C. ATTN: Mr. I. H. Gatzke
2	Commanding Officer U. S. Naval Air Development Center Johnsville, Pa. ATTN: Mr. R. I. Mason
2	Commanding Officer and Director U. S. Navy Electronics Laboratory San Diego 52, California ATTN: Dr. D. A. Wilson

No. of Copies

2	Commander, Antisubmarine Warfare Force U. S. Pacific Fleet Navy No. 128, c/o FPO San Francisco, California
1	Marine Physical Laboratory of the Scripps Institution of Oceanography San Diego 52, California
1	Technical Library (Code P80962) U. S. Naval Ordnance Test Station Pasadena Annex 3202 East Foothill Blvd. Pasadena 8, California
1	Officer in Charge U. S. Naval Oceanographic Unit Building #1, Treasure Island San Francisco 30, California
1	Commander Oceanographic System Atlantic Norfolk 11, Virginia
1	Commander, Antisubmarine Warfare Force U. S. Atlantic Fleet Norfolk 11, Virginia
1	Commanding Officer U. S. Navy Underwater Sound Laboratory Research Detachment Navy No. 138, c/o FPO New York, N. Y. ATTN: Dr. W. A. VonWinkle
1	Hudson Laboratories P. O. Box 239 Dobbs Ferry, N. Y. ATTN: Dr. R. A. Frosch

No. of Copies

1	President Naval War College Newport, Rhode Island
1	Commander Destroyer Development Group Two U. S. Atlantic Fleet Newport, Rhode Island
1	Director of Research Institute of Naval Studies 185 Alewife Brook Parkway Cambridge 38, Mass.
5	Defense Documentation Center Cameron Station Alexandria 12, Virginia

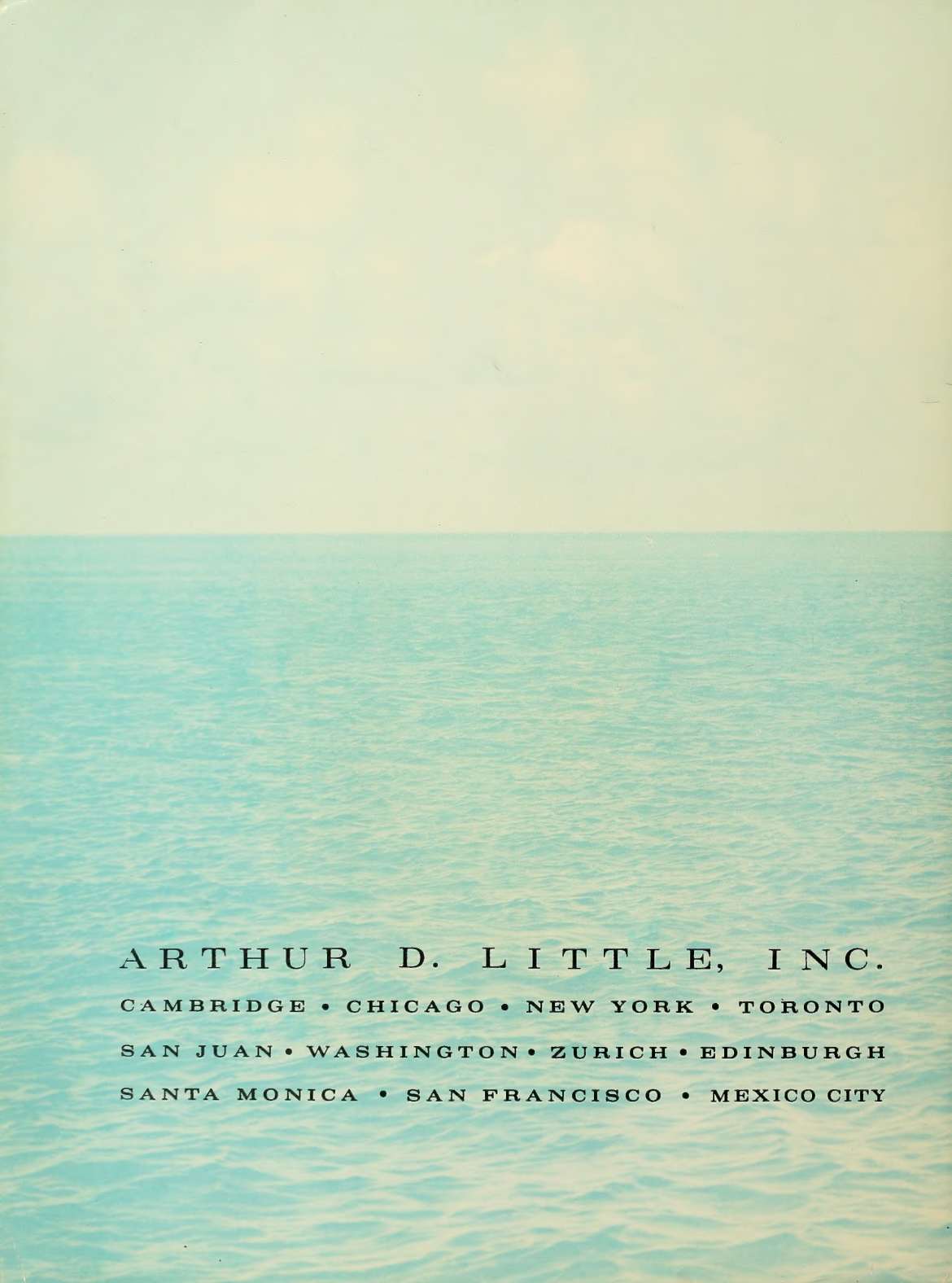




<p>A.D. _____ Accession No. _____</p> <p>Arthur D. Little, Inc., Cambridge 40, Massachusetts</p> <p>ACOUSTIC SCATTERING IN THE OCEAN</p> <p>(Project Trident Technical Report 1360863) August 1963. pp. xv + 221, Illustrations 67, Tables 8 (Contract N0bsr-81564)</p> <p>This report summarizes the existing knowledge regarding acoustic scattering by small inhomogeneities in the ocean. The report is divided into two parts, which treat respectively the scattering by strong (e.g., air bubbles, marine organisms, or the surface) inhomogeneities and weak (small fluctuations in the index of refraction) inhomogeneities. The theoretical discussion is, wherever possible, compared with experimental results.</p>	<p>UNCLASSIFIED</p>	<p>A.D. _____ Accession No. _____</p> <p>Arthur D. Little, Inc., Cambridge 40, Massachusetts</p> <p>ACOUSTIC SCATTERING IN THE OCEAN</p> <p>(Project Trident Technical Report 1360863) August 1963. pp. xv + 221, Illustrations 67, Tables 8 (Contract N0bsr-81564)</p> <p>This report summarizes the existing knowledge regarding acoustic scattering by small inhomogeneities in the ocean. The report is divided into two parts, which treat respectively the scattering by strong (e.g., air bubbles, marine organisms, or the surface) inhomogeneities and weak (small fluctuations in the index of refraction) inhomogeneities. The theoretical discussion is, wherever possible, compared with experimental results.</p>	<p>UNCLASSIFIED</p>
<p>A.D. _____ Accession No. _____</p> <p>Arthur D. Little, Inc., Cambridge 40, Massachusetts</p> <p>ACOUSTIC SCATTERING IN THE OCEAN</p> <p>(Project Trident Technical Report 1360863) August 1963. pp. xv + 221, Illustrations 67, Tables 8 (Contract N0bsr-81564)</p> <p>This report summarizes the existing knowledge regarding acoustic scattering by small inhomogeneities in the ocean. The report is divided into two parts, which treat respectively the scattering by strong (e.g., air bubbles, marine organisms, or the surface) inhomogeneities and weak (small fluctuations in the index of refraction) inhomogeneities. The theoretical discussion is, wherever possible, compared with experimental results.</p>	<p>UNCLASSIFIED</p>	<p>A.D. _____ Accession No. _____</p> <p>Arthur D. Little, Inc., Cambridge 40, Massachusetts</p> <p>ACOUSTIC SCATTERING IN THE OCEAN</p> <p>(Project Trident Technical Report 1360863) August 1963. pp. xv + 221, Illustrations 67, Tables 8 (Contract N0bsr-81564)</p> <p>This report summarizes the existing knowledge regarding acoustic scattering by small inhomogeneities in the ocean. The report is divided into two parts, which treat respectively the scattering by strong (e.g., air bubbles, marine organisms, or the surface) inhomogeneities and weak (small fluctuations in the index of refraction) inhomogeneities. The theoretical discussion is, wherever possible, compared with experimental results.</p>	<p>UNCLASSIFIED</p>



ARTHUR D. LITTLE, INC.  
PROJECT TRIDENT LIBRARY



ARTHUR D. LITTLE, INC.

CAMBRIDGE • CHICAGO • NEW YORK • TORONTO

SAN JUAN • WASHINGTON • ZURICH • EDINBURGH

SANTA MONICA • SAN FRANCISCO • MEXICO CITY